

APPLICATION OF HIGH-PRESSURE PHASE BEHAVIOR TO OPTIMIZE THE PLATINUM CATALYZED SELECTIVE OXIDATION OF 2-PROPANOL IN "SUPERCRITICAL" CARBON DIOXIDE

Roger Gläser^a, Jörg Williardt^a, David Bush^b,
and Charles A. Eckert^b

^a Institute of Chemical Technology
University of Stuttgart
D-70550 Stuttgart
Germany

^b School of Chemical Engineering
Georgia Institute of Technology
778 Atlantic Drive
Atlanta, GA 30332-0100
USA

Introduction

A promising utilization of the greenhouse gas carbon dioxide is its application as an environmentally benign, non-toxic and abundantly available reaction medium for organic synthesis at conditions above its critical point ($T_c = 31.1\text{ }^\circ\text{C}$, $p_c = 73.8\text{ bar}$).¹ Supercritical carbon dioxide exhibits unique solvent properties between those of typical liquids or gases that can be sensitively tuned by pressure and temperature. The use of supercritical carbon dioxide is particularly attractive as a solvent for selective oxidation reactions. Not only is carbon dioxide chemically inert and non-flammable, but it is miscible with both oxygen (or air) and organic reactants over a very broad range of compositions and reaction conditions. Therefore, limitations of oxygen mass transfer as often encountered in conventional liquid-phase oxidations can be eliminated by operating in a "supercritical", single-phase region. To capitalize on this advantage, the experimental conditions for existence of the single-phase region of a given reaction system have to be accurately known.² In spite of its utmost importance, this issue of high-pressure phase behavior is often not sufficiently addressed in studies of reactions at "supercritical" conditions.

An example where the beneficial properties of "supercritical" carbon dioxide as a reaction medium have been successfully applied is the selective oxidation of secondary alcohols with molecular oxygen to ketones over supported noble metal catalysts.^{3,4} Conventionally, this conversion is conducted in aqueous solution of the alcohol and, in many cases, the reaction rate is restricted by oxygen transport from the gas into the liquid reaction phase.^{5,6}

In the present study, we report on the peculiarities and the prediction of the high-pressure phase behavior of the multi-component reaction mixture related to the oxidative dehydrogenation of 2-propanol (IPOH) with molecular oxygen to acetone (AC) and water in "supercritical" carbon dioxide. The results of these predictions are then applied to choose reaction conditions for experimentally investigating the conversion over a carbon-supported platinum catalyst in a single, homogeneous phase.

Experimental

Phase Behavior. Calculations of the phase behavior were based on the Patel-Teja equation-of-state.⁷ Interaction parameters (k_{ij}) were fit to binary vapor-liquid equilibria (VLE) data from the literature and were used to predict the multi-component phase equilibria. It should be stressed that the term "supercritical" in its strict sense refers to

single components only, and is used here for the multi-component mixture in quotation marks as suggested previously.⁸

Materials. 2-Propanol (Fluka, puriss. p.a., over molecular sieve), 1,4-dioxane (Merck, p.a., ACS reagent) and carbon dioxide (Air Products, 99.995 %) were used as received. A carbon-supported platinum catalyst (5 Pt/C, 5 wt.-% Pt, precious metal surface $14.5\text{ m}^2/\text{g}$, specific surface area $1000\text{ m}^2/\text{g}$) available from Chempur was applied in the oxidation reactions.

Catalytic Experiments. The catalytic conversions were carried out at $40\text{ }^\circ\text{C}$ in a 100 ml batch reactor equipped with a magnetic stirrer (1000 min^{-1}) and a heating jacket. Prior to the experiments, the catalyst was placed in the reactor and dried in vacuum. After adding carbon dioxide, liquid 1,4-dioxane and 2-propanol were introduced into the reactor by means of an injection loop. 1,4-Dioxane (DO) served as an internal standard for closing the mass balance. The mixture was heated to reaction temperature and further carbon dioxide was added, if necessary. The reaction was started by adding oxygen to the reaction vessel to the desired reaction pressure. To monitor the progress of the reaction a small amount of the reaction mixture was continuously removed, expanded to ambient pressure through heated tubing and a needle valve and periodically analyzed by temperature-programmed capillary gas chromatography. *Generally, care must be exercised in carrying out oxidation experiments, especially at increased reactant concentrations.*

Results and Discussion

The VLE curves for the four-component reaction system IPOH/ $\text{O}_2/\text{CO}_2/\text{DO}$, have been calculated at fixed molar ratios of oxygen to carbon dioxide for the temperature of $40\text{ }^\circ\text{C}$. This temperature was chosen for the experiments due to its proximity to the critical temperature of pure CO_2 and to demonstrate the feasibility of selective alcohol oxidations at mild conditions. As depicted in **Figure 1**, the single-phase region for the reaction system is reached at pressures above the equilibrium line indicated for each O_2/CO_2 molar ratio. As expected, a higher pressure is needed to reach the single phase when the oxygen to carbon dioxide ratio is increased.

In **Figure 2**, the oxygen mole fraction is presented at a constant oxygen to carbon dioxide molar ratio of 5.3 %. The addition of carbon dioxide allows for high concentrations of oxygen in the liquid or the "supercritical" phase without going to high partial pressures of oxygen.

It is noteworthy, that, although the reactant concentration were quite low, the presence of 1,4-dioxane which was added to the

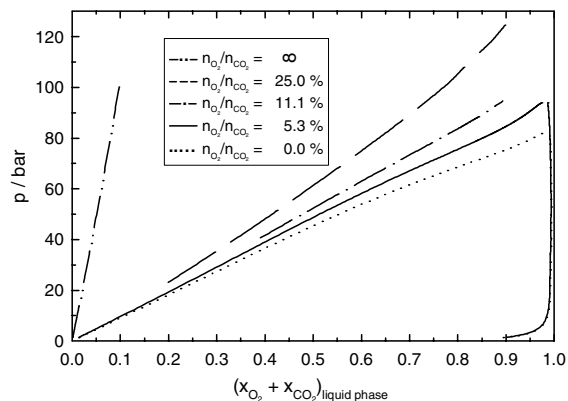


Figure 1. Vapor-liquid equilibrium of the oxygen/carbon dioxide/IPOH/DO mixture at $40\text{ }^\circ\text{C}$ for different oxygen/carbon dioxide mole fractions.

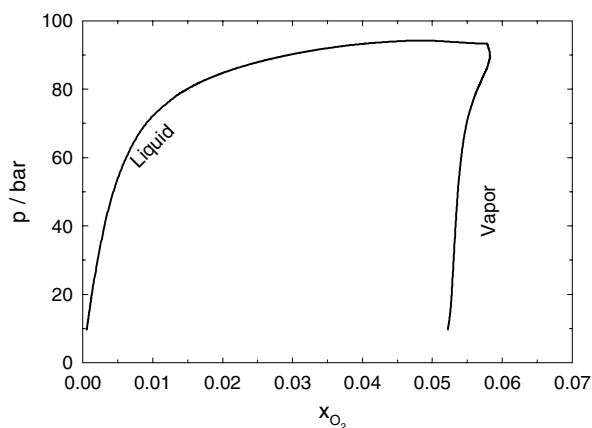


Figure 2. Oxygen mole fraction in the two-phase region for a fixed O_2/CO_2 molar ratio of 5.3 % at 40 °C.

mixture as an internal analytical standard in a comparable amount as the alcohol, decreases the pressure required for single-phase operation compared to the system containing oxygen, 2-propanol and carbon dioxide only. This is perhaps due to $CO_2/1,4$ -dioxane interactions, which exhibit negative deviations from Raoult's law in the binary mixture.

Pertinent results of the catalytic conversion of 2-propanol over 5 Pt/C with oxygen at 150 bar, i.e., sufficiently above the one corresponding to the VLE, are displayed in **Figure 3**. In all cases, acetone was the only detectable oxidation product indicating the high selectivity of the reaction at the mild reaction temperature. Within the single-phase region, the initial amount of 2-propanol relative to the catalyst mass could be increased above 6 mmol / 125 mg, a typical value for the reaction in aqueous solution where catalyst deactivation was observed.⁶ While no catalyst deactivation occurs at a fourfold increase of the IPOH/catalyst ratio, the conversion remains incomplete when eight times the initial amount of 2-propanol was present in the reactor. Nevertheless, and although the initial reaction rate r_0 was lower for the increased IPOH/catalyst ratios, a considerably higher amount of reactant could be converted with the same amount of catalyst in the high-pressure reaction medium.

To assess the influence of the oxygen mole fraction on the catalytic conversion, increasing amounts of oxygen were added to the

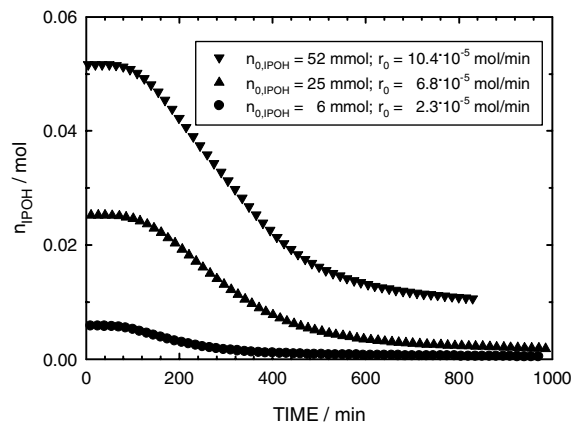


Figure 3. Conversion of increasing amounts of 2-propanol with molecular oxygen over 5 Pt/C in "supercritical" carbon dioxide ($x_{O_2} = 2.8$ %, $p_{O_2,CO_2} = 150$ bar, $m_{cat} = 125$ mg, r_0 : initial reaction rate).

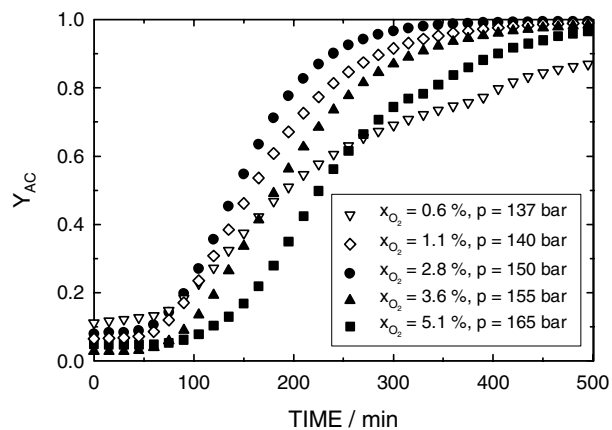


Figure 4. Influence of oxygen mole fraction on the acetone yield in the 2-propanol conversion with molecular oxygen over 5 Pt/C ($p_{O_2,CO_2} = 135$ bar, $n_{O_2,IPOH} = 13$ mmol, $m_{cat} = 250$ mg).

same mixture of the catalyst, carbon dioxide, 2-propanol and the standard 1,4-dioxane. It is observed, that the rate of acetone formation increases with the oxygen mole fraction from 0.6 (substoichiometric with respect to IPOH) to 2.8 % and, for higher oxygen concentrations, decreases again (**Figure 4**). This finding is in accordance with results reported by Jenzer et al.³ and can be rationalized by poisoning of the platinum surface due to partial over-oxidation. Although increasing oxygen mole fractions shift the VLE line to higher pressures (**Figure 1**), the reaction pressure in these experiments may be assumed to be high enough to avoid the occurrence of two separate phases.

In summary, the prediction of multi-component high-pressure phase behavior is helpful to devise reaction conditions for carrying out catalytic oxidation reactions in a single phase with "supercritical" carbon dioxide as a reaction medium. So far, only the initial reactant mixture has been considered. Further research will therefore be directed towards incorporating the changes in the compositions of the reaction mixture due to the consumption of the reactants and formation of the products into the phase behavior predictions. These changes are especially important for oxidation reactions, since highly polar and hydrogen-bonding products, such as acids or water, are among the products, and these will have a pronounced effect on the phase behavior, especially when the reactant concentrations and the conversion levels are high.

Acknowledgment

R.G. acknowledges a stipend from the Dr. Leni Schöninger foundation and Prof. Dr.-Ing. J. Weitkamp for generous support.

References

1. Kaupp, G., *Angew. Chem., Int. Ed. Engl.*, **1993**, *33*, 1452-1455.
2. McHugh, M.A., Subramaniam, B., *Ind. Eng. Chem. Proc. Des. Dev.*, **1986**, *25*, 1-12.
3. Jenzer, G., Sueur, D., Mallat, T., Baiker, A., *Chem. Commun.*, **2000**, 2247-2248.
4. Steele, A.M., Zhu, J. Tsang, S.C., *Catal. Lett.*, **2001**, *73*, 9-13.
5. Kluytmans, J.H.J., Markusse, A.P., Kuster, B.F.M., Marin, G.B., Schouten, J.C., *Catal. Today*, **2000**, *57*, 143-155.
6. Nicoletti, J.W., Whitesides, G.M., *J. Phys. Chem.*, **1989**, *93*, 759-767.
7. Patel, N.C., Teja, A.S., *Chem. Eng. Sci.*, **1982**, *37*, 463-473.
8. Jenzer, G., Mallat, T., Baiker, A., *Catal. Lett.*, **2001**, *73*, 5-8.

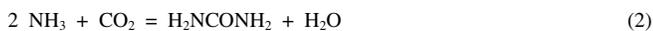
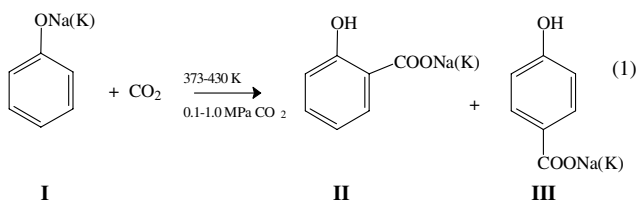
BRIDGING NATURAL FACTS WITH INDUSTRIAL PROCESSES FOR CARBON DIOXIDE UTILIZATION: METAL ENZYMES AND TRANSITION METAL SYSTEMS

Michele Aresta and Angela Dibenedetto

University of Bari and METEA Research Center
Department of Chemistry, Campus Universitario, 70126 - Bari, Italy,
fax +39 080 544 2083, e-mail:aresta@metea.uniba.it

Introduction

The direct use of carbon dioxide in the carboxylation of organic substrates finds a quite extensive application in Nature,¹ while only few processes based on carbon dioxide are industrially exploited: the Kolbe-Schmitt reaction² (Eq.1) and the synthesis of urea³ (Eq.2), that are known since more than one century, and the recent carboxylation of epoxide.



IV

Also, carbon dioxide is the electron acceptor in metabolic paths characteristic of anaerobic microorganisms, methanogens and acetogens⁴ among others. Their enzymatic reaction mechanism shows in some cases a surprising similarity with chemical processes.

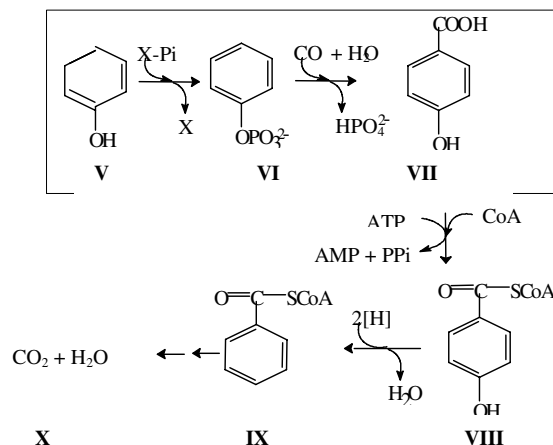
The conversion of organic compounds into methane requires a complex metabolic food chain⁵ as the biomass undergoes several steps (depolymerization, acidogenesis, acetate formation, methanogenesis, methanation of CO₂) that opens new perspectives for the development of biotechnologies and environmental friendly innovative synthetic methodologies based on carbon dioxide.^{1,6}

Results and Discussion

Biotechnological carboxylation of phenol

The Kolbe-Schmitt reaction (Eq.1) is industrially used since long time for the synthesis of 2-OH-benzoic acid and 4-OH-benzoic acid but the selectivity and yield are not completely mastered. However, it is highly wished to dispose of a selective process working under mild conditions.

We have found that the pathway for phenol degradation follows the route, quite usual in Nature, of "increasing the complexity of the molecule for its easier degradation".⁷ In fact, as shown in Scheme 1, phenol (V) is first phosphorylated (VI), then carboxylated to 4-OH-benzoic acid (VII), which is converted into the active form 4-OH-benzoyl-CoA (VIII) subsequently, dehydroxylated to benzoyl-CoA (IX), the active form of benzoic acid. The latter is eventually converted into CO₂ and H₂O (X).



Scheme 1. Phenol biodegradation pathway by *Thauera aromatica*

The carboxylase enzyme responsible for the carboxylation of phenol is Mn(II) dependent^{6,8} and affords very selectively the 4-OH-benzoic acid isomer, a compound that finds application in material science. We have developed a biotechnological synthesis of it, solving, thus, the problem of purity. The enzyme was supported on low-melting agar on which it has a life from several days to weeks.

A recent modification of this system makes use of a membrane for the separation of the reaction space where the enzyme is kept, from the space where the reaction product is extracted.

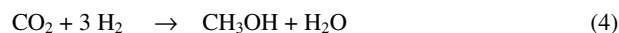
Such first application of the Phenol carboxylase enzyme for the functionalisation of organic substrates, is clean and affords an interesting turnover number of ca. 16 000.

CO₂ reduction to CO and the synthesis of acetic acid.

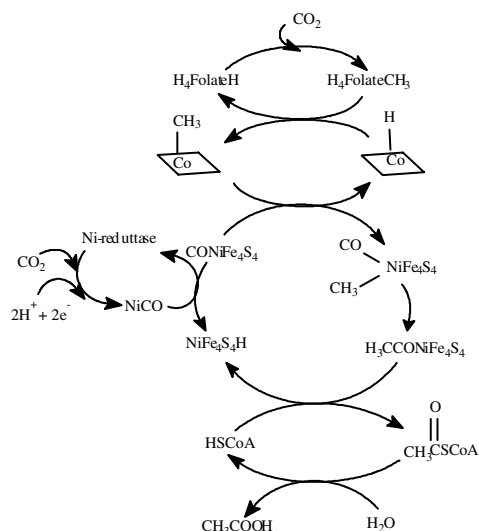
The reduction of CO₂ to CO (Eq.3) is the first step in the bacterial production of acetic acid from CO₂.



It recalls the "reverse gas shift reaction" occurring in industrial CO₂ reduction with H₂, that is believed to take place in the synthesis of methanol from CO₂. (Eq. 4)

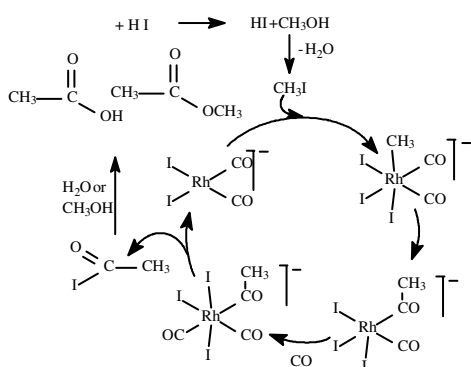


In bacteria, the CO₂ reduction is mediated by the enzyme CODH (Carbon monoxide dehydrogenase), that contains both Ni and Fe. Once formed, CO is coupled with a methyl group generated from CO₂ (Scheme 2) with the intervention of the tetrahydrofolate enzyme.



Scheme 2. Cycle of CODH

Such coupling generates the acetyl-moiety, $\text{CH}_3\text{-CO-}$ that generates acetic acid. It is amazing the similarity of the bacterial synthesis of acetic acid with the industrial Monsanto process. (Scheme 3)



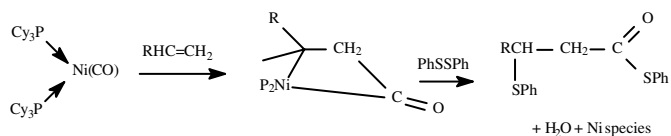
Scheme 3. Monsanto process

For a long time, Ni has been considered to be, in the enzymatic system, the metal center binding CO and probably catalysing the CO_2 reduction.⁹ It has been proposed that CO is bound to Fe, where the acetyl moiety is generated.¹⁰

Chemical model systems indicate that both Ni^{11} and Fe^{12} complexes are able to bind carbon dioxide. Concerning the CO_2 reduction to CO, at the present time only evidence that the Ni complex $(\text{PCy}_3)_2\text{Ni}(\text{CO}_2)$ (**XI**) catalyses the CO_2 reduction reaction in the presence of proton and electron donors has been collected.¹³ The fluxional behaviour of the carbon dioxide moiety co-ordinated to the metal has been unambiguously established in the case of **XI**, for which the limit forms and the rotational free energy barrier have been determined ($\Delta G^\ddagger = 39.6 \text{ kcal/mol}$).¹⁴

XI in toluene, under dinitrogen atmosphere, reacts with several Brønsted acids, under electron transfer conditions with formation of the carbonyl-bound species $(\text{PCy}_3)_2\text{Ni}(\text{CO})_2$ (**XII**) isolated from the reaction mixture as thermodynamic products, while $(\text{PCy}_3)_2\text{Ni}(\text{CO})$ (**XIII**) is a kinetic product.

The so formed CO is able to react with one olefin and Ph-SS-Ph to afford a thioacetyl moiety, fully mimicking the bacterial process (Scheme 4).



Scheme 4. Biomimetic synthesis of thioesters

These findings prompted us to propose the alternative acetyl formation based on Ni (Scheme 2).

The influence of Fe, Co, Ni on the production of methane

We have studied the influence of the concentration of Ni, Fe, Co on the methanation of fermentable vegetables and found that they influence at different extent the H_2 production, the CO_2 reduction to methane and, thus, the CH_4/CO_2 ratio that may reach quite high values (more than 4.5). This finding suggests that the natural biogas composition may have been influenced by the nature of the rocks that constitute the walls of the reservoirs. The presence of Ni, Fe, Co ions may have made available the metal ions to the bacterial pool for a better biogas quality.

Acknowledgement. The financial support by MURST (Project no. 9803026360) is gratefully

References

- (1) Aresta, M. and Forti, G. (Eds), in *Carbon Dioxide as a Source of Carbon*, Elsevier Publ. **1987**; Aresta, M. and Schloss, J. V. (Eds), in *Enzymatic and Model Reaction for Carbon Dioxide Carboxylation and Reduction Reactions*, Elsevier Publ. **1990**.
- (2) Kolbe, H., Lautemann, E. *Ann.* **1869**, 113, 125; Ota, K. *Bull. Chem. Soc. Jpn.*, **1974**, 47, 2343.
- (3) Fumasoni, S.; Pochetti, F.; Roberti, G. *Ger. Offen.* **1974**, 2,318,327, C.A., 80, 14593j; Fromm, D.; Luetzow, D. *Chem. Unserer Zeit*, **1979**, 13, 78.
- (4) Wood, H.G., Ragsdale, S.W., Pezacka, E. *Biochem. Int.* **1986**, 12, 421; Ragsdale, S.W., Wood, H.G., Morton, T.A., Ljungdahl, L.G., Der Vartanian D.V. in *The bioinorganic chemistry of Nickel*, VHC, New York, **1988**, 311.
- (5) Zehnder, A. J. B., In *Water pollution Microbiology*, **1978**, vol. 2, John Wiley & Sons, Inc., New York; Zeikus, J. G. In *Microbes and Their Natural Environments*, Slater, J. H. and Whittenbury J. W. Eds., **1983**, Cambridge University Press, London; Schink, B. In *Environmental Microbiology of Anaerobes* **1983**, Zehnder, A. J. B. Ed., Wiley, New York.
- (6) Lack, A., Fuchs, G. Aresta, M., Tommasi, I., *Eur. J. Biochem.* **1991**, 197, 473.
- (7) Platen, H., Schink, B. *Arch Microbiol.* **1987**, 149, 136; Schnell, S., Bak, F., Pfennig, N. *Arch. Microbiol.* **1989**, 152, 556.
- (8) Aresta, M., Tommasi I., Dileo C., Dibenedetto A., Narracci, M., Ziolkowski J., Jezierski A. *Canad. J. Chem.* **2001**, In press.
- (9) Cramer, S.P., Eidsness, M.K., Pan, W.-H., Morton, T.A., Ragsdale, S.W., DerVartanian, D.V., Ljungdahl, L.G., Scott, R.A. *Inorg. Chem.*, **1987**, 26, 2477.
- (10) Qui, D., Kumar, M. Ragsdale S.W., Spiro, T.G. *Science* **1994**, 264, 817; Kumar, M., Lu, W.-P., Ragsdale, S.W. *Biochemistry*, **1994**, 33, 9769.
- (11) Aresta, M., Nobile, C.F., Albano, V.G., Forni, E., Manassero, M. *J. C. S. Chem. Comm.*, **1975**, 636.
- (12) Karsh, H.H. *Chem. Ber.*, **1977**, 110, 2213; Komiyama, S., Kasuga, N., Hirano, M., Fukuoka, A. *J. Chem. Soc. Chem. Commun.*, **1994**, 1115.
- (13) Aresta, M., Quaranta, E., Tommasi, I. *J. Chem Soc. Chem. Commun.*, **1988**, 450; Aresta, M., Tommasi, I., Giannoccaro, P., Quaranta, E., Fragale, C. *Inorg. Chim. Acta*, **1998**, 272, 38.
- (14) Aresta, M., Quaranta, E., Tommasi, I., Gobetto, R., *Inorg. Chem.* **1992**, 31, pp. 4286-4290; Jegat, C., Fouassier, M., Tranquille, M., Mascetti, J., Tommasi, I., Aresta, M., Ingold, F., Dedieu, A. *Inorg. Chem.*, **1993**, 32, 1279.

CARBON DIOXIDE AS A SOLVENT FOR POLYMERIZATION AND CROSS COUPLING REACTIONS

A. B. Holmes*, T. R. Early, R. S. Gordon, L. M. Stamp

Melville Laboratory for Polymer Synthesis, University of Cambridge,
Pembroke Street, Cambridge, CB2 3RA UK

R. E. Shute

Astra Zeneca, Mereside, Alderley Park, Macclesfield,
Cheshire SK10 4TG

I. F. McConvey

Astra Zeneca Process Research, Silk Business Park,
Macclesfield, Cheshire SK10 4NA

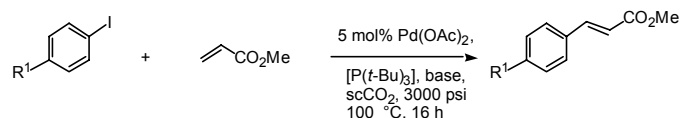
Introduction

Modern organic synthesis has entered a phase in which there is a desire to achieve rapid parallel reactions. Obviously this places more demands on the use of volatile organic solvents. There is therefore an increasing interest in using readily available carbon dioxide (for example from the combustion of fossil fuels) as an alternative solvent. There have been several significant recent reviews on the use of carbon dioxide as a solvent for organic synthesis.¹⁻³

In this paper we describe the applications of supercritical carbon dioxide (scCO₂) as a solvent for various organometallic cross coupling reactions. In particular we focus on the Heck⁴ and Suzuki⁵ cross coupling reactions which have emerged as some of the most powerful methods of forming a bond between sp² carbon atoms. We⁶ and Tumas⁷ had previously demonstrated the first palladium-mediated examples of these reactions in scCO₂, using perfluorinated phosphines to solubilize the palladium(0) complexes in the solvent medium. Subsequently Rayner found that certain commercially available non-fluorinated ligands were moderately reactive in the presence of trifluoroacetate counterion.⁸ Arai used phase transfer catalysis,⁹ and most recently Bannwarth obtained promising results in a Stille coupling with triphenylphosphine as ligand, although the results were still inferior to those in which the phosphine carried fluorinated chains.¹⁰

Results and Discussion

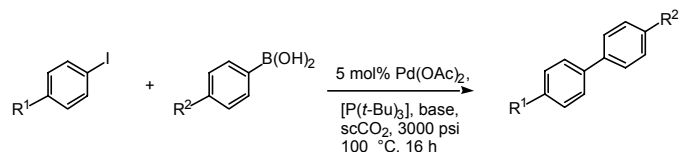
Cross Coupling Reactions. We have now found that tri-*tert*-butylphosphine [P(*t*-Bu)₃] in the presence of palladium(II) acetate is a very effective catalyst for Heck and Suzuki reactions in scCO₂, thus dispensing completely with the need for fluorinated solubilizing groups.¹¹ The ligand [P(*t*-Bu)₃] has been popularized by Fu and colleagues^{12,13} as a very powerful partner in catalytic Suzuki reactions with unreactive substrates such as aryl chlorides.



Scheme 1 Heck reaction in scCO₂

Both aryl iodides and bromides underwent the Suzuki reaction, although lower yields were obtained with the less reactive bromide

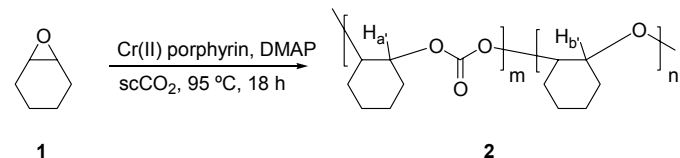
coupling partners. A variety of different bases were investigated and shown to be effective in scCO₂. Surprisingly these reactions proceeded effectively in the presence of solid tetra-alkylammonium acetate salts without addition of any other base. Jeffrey has reported the use of tetra-alkylammonium salts for the Heck reaction in conventional solvents.¹⁴ Herrman has also used the corresponding bromide salts as neat molten solvents.¹⁵



Scheme 2 Suzuki cross coupling reaction in scCO₂

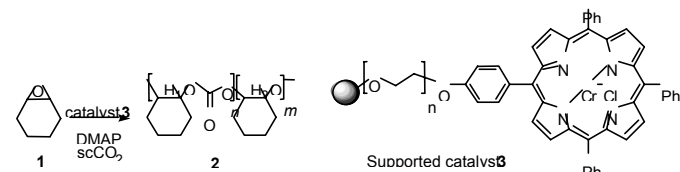
Supported catalysts have been extensively developed for use in organic synthesis¹⁶ and for palladium-mediated reactions on a solid phase support.¹⁷⁻¹⁸ We have also developed variants of the solid phase synthesis of cinnamate derivatives by carrying out Heck reactions on a REM resin in scCO₂.¹¹

Polycarbonate Synthesis. Another area of interest is the synthesis of polycarbonates in which carbon dioxide behaves as both solvent and reactant. This work was pioneered by Darensbourg¹⁹ and Beckman²⁰⁻²¹ and it shows the power of various catalysts for this process. We recently employed a Cr(III)-tetra(pentafluorophenyl)porphyrin catalyst which was soluble in scCO₂ as a catalyst for polycarbonate synthesis using cyclohexene epoxide as the monomer.²² This afforded low polydispersity polymer in excellent yields, but had the disadvantage that the porphyrin catalyst contaminated the final product (Scheme 3).



Scheme 3 Preparation of polycarbonate **2**

It is now shown that an Argogel[®] supported chromium porphyrin **3**²³ is effective in the copolymerization of 1,2-cyclohexene oxide (CHO) **1** and CO₂ (Scheme 4).



Scheme 4 Copolymerization of cyclohexene oxide and carbon dioxide in the presence of the Argogel catalyst **3** and dimethylaminopyridine

The ring opening copolymerization of cyclohexene oxide (CHO) **1** and CO₂ to form the copolymer poly(cyclohexenecarbonate-*co*-cyclohexene ether) **2** was investigated using catalyst **3** under various reaction conditions. Polymerizations were also carried out using an Irori Kan[™] reactor²⁵ to separate the porphyrin beads from

the product polymer. This technique offered the opportunity to stir the reaction mixture with a magnetic stir bar and to study the recyclability of the catalyst. In fact the catalyst could be used for several cycles without loss of activity, and produced the polymer with increased yield compared with the unsupported catalyst.

Conclusions

This work has demonstrated that palladium-mediated cross coupling reactions can be carried out with commercially available phosphines and on solid phase supports in scCO₂. In a second aspect of this work it has been demonstrated that copolymers of cyclohexene oxide and carbon dioxide can be prepared under supercritical conditions in the presence of a polymer-supported Cr(III) porphyrin catalyst.

Acknowledgement. We thank Astra Zeneca (T. R. Early, L. Stamp), the Engineering and Physical Sciences Research Council UK (Swansea Mass Spectrometry Service), the Isaac Newton Trust (R. Gordon), and the Commission of the EU (Brite-Euram BRRT-CT98-5089 'RUCADI') for generous financial support. We are grateful for the collaboration with K. Knights and Y. R. de Miguel (King's College, London).

References

- (1) Oakes, R. S.; Clifford, A. A.; Rayner, C. M. *J. Chem. Soc., Perkin Trans. 1* **2001**, 917.
- (2) Darr, J. A.; Poliakoff, M. *Chem. Rev.* **1999**, *99*, 495.
- (3) Jessop, P. G.; Leitner, W. *Chemical Synthesis Using Supercritical Fluids*; Wiley-VCH: Weinheim, 1999.
- (4) Beletskaya, I.; Cheprakov, A. V. *Chem. Rev.* **2000**, *100*, 3009.
- (5) Suzuki, A. *J. Organomet. Chem.* **1999**, *576*, 147.
- (6) Carroll, M. A.; Holmes, A. B. *Chem. Commun.* **1998**, 1395.
- (7) Morita, D. K.; Pesiri, D. R.; David, S. A.; Glaze, W. H.; Tumas, W. *Chem. Commun.* **1998**, 1397.
- (8) Shezad, N.; Oakes, R. S.; Clifford, A. A.; Rayner, C. M. *Tetrahedron Lett.* **1999**, *40*, 2221.
- (9) Bhanage, B. M.; Ikushima, Y.; Shirai, M.; Arai, M. *Tetrahedron Lett.* **1999**, *40*, 2221.
- (10) Osswald, T.; Schneider, S.; Wang, S.; Bannwarth, W. *Tetrahedron Lett.* **2001**, *42*, 2965.
- (11) Early, T. R.; Gordon, R. S.; Carroll, M. A.; Holmes, A. B.; Shute, R. E.; McConvey, I. *Chem. Commun.* **2001**, 1966.
- (12) Littke, A. F.; Fu, G. C. *J. Org. Chem.* **1999**, *64*, 10.
- (13) Littke, A. F.; Fu, G. C. *J. Am. Chem. Soc.* **2001**, *123*, 6989 and references cited therein.
- (14) Jeffrey, T. *Tetrahedron* **1996**, *30*, 10113.
- (15) Böhm, V. P. W.; Herrmann, W. A. *Chem. Eur. J.* **2000**, *6*, 1017.
- (16) Ley, S. V.; Baxendale, I. R.; Bream, R. N.; Jackson, P. S.; Leach, A. G.; Longbottom, D. A.; Nesi, M.; Scott, J. S.; Storer, R. I.; Taylor, S. J. *J. Chem. Soc., Perkin Trans. 1* **2000**, 3815.
- (17) Kingsbury, C. L.; Mehrman, S. J.; Takacs, J. M. *Curr. Org. Chem.* **1999**, *3*, 497.
- (18) Franzen, R. *Can. J. Chem.* **2000**, *78*, 957.
- (19) Darensbourg, D. J.; Stafford, N. W.; T. Katsurao, T. J. *J. Mol. Catal., A* **1995**, *104*, L1.
- (20) Super, M.; Berluche, E.; Costello, C.; Beckman, E. *Macromolecules* **1997**, *30*, 368.
- (21) Sarbu, T.; Styranec, T.; Beckman, E. J. *Nature* **2000**, *405*, 165.
- (22) Mang, S.; Cooper, A. I.; Colclough, M. E.; Chauhan, N.; Holmes, A. B. *Macromolecules* **2000**, *33*, 303.
- (23) This supported catalyst was prepared as part of a collaboration with Mr K. A. Knights and Dr Y. R. de Miguel (ref. 24).
- (24) Stamp, L. M.; Mang, S. A.; Holmes, A. B.; Knights, K. A.; de Miguel, Y. R.; McConvey, I. F. *Chem. Commun.* **2001**, *in press*.
- (25) Nicolaou, K. C.; Pfefferkorn, J. A.; Mitchell, H. J.; Roecker, A. J.; Barluenga, S.; Cao, G.-Q.; Affleck, R. L.; Lillig, J. E. *J. Am. Chem. Soc.* **2000**, *122*, 9954.

CARBON DIOXIDE REFORMING WITH METHANE IN LOW TEMPERATURE PLASMAS

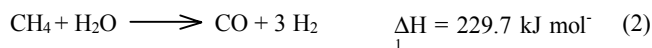
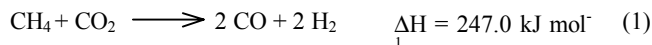
Korada Supat*, Sumaeth Chavadej*, Lance L. Lobban**
and Richard G. Mallinson**

*The Petroleum and Petrochemical College,
Chulalongkorn University
Bangkok 10330, Thailand

**Institute for Gas Utilization Technologies and
School of Chemical Engineering and Materials Science
University of Oklahoma,
100 E. Boyd St., Rm.T-335, Norman, OK 73019, USA

Introduction

With increasing population and rapid technology development, it is possible that we have begun to encounter alteration of the climate. Greenhouse gases, that include carbon dioxide, methane, ozone, halocarbons and nitrous oxide, to a significant extent come from the combustion of fossil fuels (coal, oil, and natural gas) for power generation and transportation. A potentially useful reaction for reducing the impact of carbon dioxide (reducing net emissions), a major component in many natural gas resources, especially in Asia, is carbon dioxide reforming with methane (reaction 1) for production of synthesis gas (carbon monoxide and hydrogen) at a lower H₂/CO ratio compared to steam reforming of methane (reaction 2), which is the conventional process for synthesis gas production. However, as with steam reforming, the highly endothermic reaction requires significant high temperature (ca. 800 °C) energy input that is usually provided by combustion that releases CO₂. Also, the 1:1 H₂/CO ratio produced from CO₂ reforming requires, for GTL applications, the use of the water gas shift reaction, in which much of the potential net consumption of CO₂ is lost. The alternative is to combine CO₂ reforming with steam reforming and its similar low net CO₂ reduction due to combustion to provide the required heat of reaction. Thus any net reduction of CO₂ impact from the process must be compared with the partial oxidation or combined/autothermal reforming which are exothermic or self heating, but require the production of oxygen that is itself energy intensive.



Therefore, rather than considering the net CO₂ reduction as the driver, other factors must be considered. For example, The previously mentioned high CO₂ natural gas resources may be stranded by the high cost of CO₂ removal, which may be reduced or eliminated by use of CO₂ reforming. Additionally, the possible lower capital investment and operating costs due to the elimination of the requirement for oxygen makes consideration of this technology worthwhile. However, a major problem with CO₂ reforming to this point in time is the deactivation of the catalyst due to carbon deposition (reaction 3 and 4) at the desired reaction conditions.



So far, no effective commercial catalyst exists which can operate without carbon formation [1]. Therefore, solving these problems to

find ways to operate this process at milder reaction conditions is of great interest.

In this work, a low temperature plasma reactor was used to facilitate this reaction by itself and in combination with steam, at low temperatures. This has been shown to be possible in other methane conversion studies without carbon dioxide, such as helping in the conversion of methane over Sr/La₂O₃ [2] and other materials. The disadvantage of using electrical energy, that at best may only be about 60 percent efficient, may be offset by process simplicity and cost, lower carbon formation and less excess energy that must be recovered and utilized only with considerable cost.

A plasma is a quasineutral gas consisting of charged and neutral gas molecules with a collective behavior in which the charged molecules follow the path of the electric field. It is in equilibrium when the kinetic energy of the charged particles and neutral species are the same. The non-thermal, also called cold, plasma, and its non-equilibrium properties, high electron temperature and low bulk gas temperature, provide the capability for initiating chemical reactions at low temperature and with lower energy input.

Corona discharge and dielectric barrier discharge (DBD) techniques are two of the commonly used methods for producing non-equilibrium plasmas at atmospheric pressure [3], [4], [5]. Because the corona is particularly easy to establish, it has had wide application in a variety of processes such as electrostatic precipitation, electro-photography and also synthesis of chemicals [3]. The electron energy, which corresponds to the electron temperature, is restricted to less than 6 eV in the corona discharge [6]. These relatively low-energy electrons have insufficient energy to ionize methane, which has an ionization potential greater than 12 eV [7], but high enough to dissociate CH₄ and CO₂ molecules with dissociation energies of 4.5 and 5.5 eV, respectively (reaction 5 and 6) [1].



The utilization of non-equilibrium plasma techniques for carbon dioxide reforming with methane has been studied in the dielectric barrier discharge. The combination of solid catalysts with a dielectric-barrier discharge was studied for carbon dioxide reforming of methane. It is shown that the use of a catalytic coating in the discharge can have a promoting effect on the plasma chemistry and the use of the ceramic foams improved the temperature and lowered the undesired temperature increase [4]. The dielectric barrier discharge has also been used to investigate the effect of a non-equilibrium discharge on the production of synthesis gas from two major greenhouse gases carbon dioxide and methane. A pronounced synergistic effect caused by free radical reactions was observed using these two gases simultaneously with a minimum required specific energy of 40 eV/molecule for the production of syngas and the highest energy efficiency (electric energy converted to chemical energy in the syngas) reached so far was about 7%[1]. The effect of a third body (helium) was also investigated in the DBD for carbon dioxide reforming [8].

Experimental

The flow rate of feed gases, methane and carbon dioxide, were controlled by a set of mass flow controllers supplied by Porter Instrument, Inc. All experiments were carried out at atmosphere pressure. The feed gases were introduced downward through the reactor and analyzed on-line by a Carle AGC 400 gas chromatograph, with thermal conductivity detector. To provide the water vapor in the feed, the feed gas was bubbled through a water

saturation system in a water bath maintained at the temperature needed to provide the desired vapor pressure of water. All inlet and exit lines were heat traced and the reactor tube was placed in a heater and maintained at 100°C. The exhaust gas from the reactor was introduced into a condenser cooled by a mixture of dry ice and acetone that was used to remove the condensable products. The power supply unit consisted of an AC power supply for converting domestic AC power 120V, 60 Hz, using a function generator for varying the frequency in the range of 300 to 600 Hz with a sinusoidal waveform. The output was then transmitted to a high voltage alternating current (HVAC) transformer. The HVAC could step up the low side voltage to the high side voltage by nominal factor of 125 at 60 Hz. This factor may not be constant with changes in frequency due to changes in power factor because of the capacitive nature of the reactor system. The discharge occurred in a quartz tube with an i.d. of 7 mm between two stainless steel electrodes. The upper wire electrode is centered axially within the reactor tube, while the lower electrode is a circular plate with four holes to allow gas to pass through the reactor and is positioned perpendicular to the reactor axis

For this system, the conversions are defined as:

Conversion of methane = (moles of CH₄ consumed/moles of CH₄ introduced) x 100 %

Conversion of carbon dioxide = (moles of CO₂ consumed/moles of CO₂ introduced) x 100 %

H₂/CO mole ratio = moles of H₂ produced/moles of CO produced

CO/C₂ mole ratio = moles of CO produced/moles of ethane, ethylene and acetylene produced

In some cases, at lower methane conversions, the product material balances could be below 80%, however in most cases the product carbon balance was in the 80-90% range. Water was not quantified.

Results and Discussion

In Table 1, It may be seen that in an excess of CO₂, without water, the methane conversion is low and little CO₂ is converted even as power is substantially increased. In the last column, with addition of water, much higher conversion of both CO₂ and methane is achieved at otherwise similar conditions. Power is somewhat higher, but eV/mol of carbon converted is lower despite a 50 percent dilution of CO₂ and CH₄ by the water. With the excess CO₂, little C₂ formation occurs and the H₂/CO is quite low.

At a CO₂:CH₄ ratio of 5:1, methane conversion is substantially increased with a more modest increase in CO₂ conversion. With less water, at 30 %, energy consumption per C converted is substantially reduced compared to 50 % water. Also noticeable is a substantial suppression of C₂ production with increased water content. At 30 percent water in the feed, are increases in both conversions but hydrogen production appears to be significantly reduced.

The results at the stoichiometric CO₂:CH₄ ratio of 1:1 and 50% water vapor are shown in Table 3. The conversions are similar to those at the 3:1 ratio with the same power and water content, but Energy consumption per C converted is lower due to decreased CO₂ dilution since methane conversion is the higher of the two. Increased power at 1:1 ratio shows increased conversion except when the frequency is increased. The increase in frequency essentially "detunes" the system, reducing the power factor and the power actually applied to the plasma. Power is actually measured on the low voltage side and therefore includes all high voltage system losses. A system designed to properly match impedances and operate at a high power could significantly lower the real power usage over that reported here. The lower CO₂:CH₄ ratio results in

greater C₂ production. C₂'s may be undesirable components of synthesis gas,

Table 1. Effect of Power and Water on CO₂ Reforming at a 3:1 CO₂: CH₄ Ratio

Flowrate (sccm)	100	100	100	100
CO ₂ :CH ₄	3	3	3	3
% vapor	0	0	0	50
Gas gap (cm)	1	1	1	1
Low side Voltage(V)	57	68	79	62
Frequency	300	400	500	400
Power (W)	11	11	11	14
Power Factor	0.56	0.48	0.42	0.78
Current (Amp)	0.35	0.34	0.33	0.29
X _{CH₄}	11.5	19.2	14.0	34.4
X _{CO₂}	1.5	4.1	2.0	13.0
S _{CO}	63.4	52.9	47.8	99.9
S _{H₂}	-	-	-	-
S _{C₂H₆}	13.8	5.9	11.6	1.0
S _{C₂H₄}	13.6	9.1	13.0	1.0
S _{C₂H₂}	18.8	17.6	14.9	4.5
S _{total}	109.6	85.5	87.3	106.3
eV/m _{C(CO₂+CH₄)}	41.4	21.0	33.0	23.3
H ₂ /CO	1.28	1.26	1.31	0.65
CO/C ₂	2.74	3.24	2.42	31.07

Table 2. Effect of Power and Water on CO₂ Reforming with Water at a 5:1 CO₂:CH₄ Ratio

Flowrate (sccm)	100	100	100
CO ₂ :CH ₄	5	5	5
% vapor	30	30	50
Gas gap (cm)	1	1	1
Low side Voltage(V)	62	75	79
Frequency	300	300	400
Power (W)	11	13	14
Power Factor	0.43	0.35	0.43
Current (Amp)	0.41	0.50	0.41
X _{CH₄}	51.1	57.4	58.1
X _{CO₂}	13.2	17.1	18.2
S _{CO}	85.3	86.4	100.2
S _{H₂}	-	-	-
S _{C₂H₆}	0.0	0.0	0.0
S _{C₂H₄}	2.3	1.6	0.0
S _{C₂H₂}	13.2	9.9	2.9

S _{total}	100.8	97.9	103.1
eV/m _{C(CO₂+CH₄)}	12.1	11.7	17.1
H ₂ /CO	5.00	0.44	0.41
CO/C ₂	11.05	14.97	68.83

but the olefinic nature of those produced here are reactive on Fischer Tropsch catalyst systems and therefore may be suitable for feeds to a Fischer Tropsch Synthesis Reactor. The H₂/CO ratio is close to that desired for Fischer Tropsch or methanol and may be controllable by altering the water content.

Table 3. Effect of Power on CO₂ Reforming with Water at a 1:1 CO₂: CH₄ Ratio

Flowrate (sccm)	100	100	100	100
CO ₂ :CH ₄	1	1	1	1
% vapor	50	50	50	50
Gas gap (cm)	1	1	1	1
Low side Voltage(V)	57	66	88	97
Frequency	300	300	400	600
Power (W)	11	13	14	14
Power Factor	0.54	0.45	0.34	0.40
Current (Amp)	0.36	0.43	0.47	0.36
X _{CH₄}	40.5	44.3	47	30
X _{CO₂}	19.6	20.9	21	12
S _{CO}	55.5	60.2	56	72
S _{H₂}	-	-	-	-
S _{C₂H₆}	1.5	1.4	1	3
S _{C₂H₄}	4.6	4.5	5	5
S _{C₂H₂}	22.7	23.8	26	21
S _{total}	84.3	89.9	88	101
eV/m _{C(CO₂+CH₄)}	11.0	12.0	12.3	19.7
H ₂ /CO	1.90	1.85	1.9	1.7
CO/C ₂	3.85	4.05	3.5	4.9

Table 4. Water Gas Shift Reaction Pathway

Flowrate (sccm)	100	100
CO ₂ :CH ₄	50%CO	50%CO ₂
% vapor	50	50
Gas gap (cm)	1	1
Low side Voltage(V)	63	85
Frequency	600	400
Power (W)	7	10
Power Factor	0.49	0.27
Current (Amp)	0.23	0.44
X _{CH₄}	X _{co} = 6.03	0
X _{CO₂}	0	1
S _{CO}	-	112
S _{H₂}	-	-

S _{C₂H₆}	0	0
S _{C₂H₄}	0	0
S _{C₂H₂}	S _{co} = 105.05	0
S _{total}	105	112
eV/m _{C(CO₂+CH₄)}	34.6	352.7
H ₂ /CO	H ₂ /CO ₂ = 0.87	0.0
CO/C ₂	-	-

Lastly, in Table 4, results of reacting with CO or CO₂ with water are shown. CO₂ and water are essentially unreactive under the conditions of this experiment, where of course both species are strongly favored by thermodynamics. CO and water or converted to some extent with the expected production of hydrogen and CO₂. Power consumption is high under these conditions, but a lower value might be feasible under optimal conditions.

Conclusions

CO₂ combined with steam reforming at moderate conversion levels has been demonstrated at near ambient conditions with moderate power consumption. Under most conditions, carbon formation was not an operational problem. If long term operation with high conversions can be demonstrated, a process can be envisaged wherein the cost and efficiency of using electricity to drive the reaction is counter-balanced by lower costs and simpler operation (without oxygen). For smaller resources and more remote locations, these tradeoffs may be highly advantageous. Whether there is a net reduction in CO₂ impact compared to more conventional reforming/partial oxidation syn gas generation processes can only be determined by a detailed life cycle analysis and not simply by the reaction equations.

Acknowledgements

ChevronTexaco, Inc. and The Thailand Research Fund are gratefully acknowledged for supporting this research. Helpful discussions with Terence A. Caldwell are also acknowledged.

References

- (1) Kogelschatz, U., Zhou, L.M., Xue, B., & Eliasson, B. (1998), 'Production of synthesis gas through plasma - assisted reforming of greenhouse gases', Proceedings of the 4th International conference on greenhouse gas control technologies, Interlaken, Switzerland, 385-390
- (2) Marafee, A., Liu, C., Xu, G., Mallinson, R., & Lobban, L. (1997), 'An Experimental Study on the Oxidative Coupling of Methane in a Direct Current Corona Discharge Reactor over Sr/La₂O₃ Catalyst', *Industrial and Engineering Chemistry Research*, **36**, 632-637
- (3) Chang, J., Lawless, P.A., Yamamoto, T. (1991), 'Corona Discharge Processes', *IEEE Transactions on plasma science*, **19**, 1152
- (4) Kraus, M., Eliasson, B., Kogelschatz, U., & Wokaun, A. (2001), 'CO₂ reforming of methane by the combination of dielectric-barrier discharge and catalysis' *Physical Chemistry & Chemical Physics*, **3**, 294-300
- (5) Lui, L., Marafee, A., Hill, B., Xu, G., Mallinson, R., & Lobban, L. (1996), 'Oxidative Coupling of Methane with ac and dc Corona Discharge', *Industrial and Engineering Chemistry Research*, **35**, 3295-3301
- (6) Eliasson, B., & Kogelschatz, U. (1991), 'Nonequilibrium Volume Plasma Chemical Processing', *IEEE Transactions on plasma science*, **19**, 1063

- (7) Sorensen, S. L., Karawajczyk, A., Stromholm, C., Kirm, M. (1995), 'Dissociative Photo excitation of CH₄ and CD₄', *Chemical Physics Letters*, **232**, 554
- (8) Larkin, D.W., Leethochawalit, M., Chavadej, S., Caldwell, T. A., Lobban, L.L., & Mallinson, R.G. (1998), 'Carbon Pathways, CO₂ Utilization, and In Situ Production Removal in Low Temperature Plasma Methane Conversion to Methanol', Proceedings of the 4th International conference on greenhouse gas control technologies, Interlaken, Switzerland, 397-402

CARBON DIOXIDE: AN EFFECTIVE SOURCE OF CARBON FOR THE CHEMICAL INDUSTRY

Michele Aresta

University of Bari and METEA Research Center
Department of Chemistry, Campus Universitario, 70126 - Bari, Italy,
fax +39 080 544 2083, e-mail:aresta@metea.uniba.it

Introduction

The overall CO₂ mass used in industrial (chemical and technological) applications is at present limited to ca. 100 Mt per year¹. Only four industrial processes based on carbon dioxide are on stream, two of which are more than one century old [synthesis of urea and salicylic acid] and do not require any catalyst. The two other processes are: the carboxylation of epoxides, and methanol synthesis, which require both metal catalysts.

However, the utilisation of carbon dioxide as a source of carbon in synthetic chemistry appears very attractive in view of the fact that, if recovery of carbon dioxide will be adopted as a technology for controlling its emission into the atmosphere, large amounts will be easily available. The products that can be conveniently obtained from carbon dioxide can be categorized as:

- i) *Fine or commodity chemicals*, i.e. molecules containing functionalities such as: -C(O)O- acids, esters, lactones; -O-C(O)O- organic carbonates; -N-C(O)O- carbamates; -N-C(O)-ureas, amides;
- ii) *Products for the energy industry*, i.e., energy-rich C1 molecules (HCOOH, CO, CH₃OH) and C_n hydrocarbons or their derivatives.

Developing industrial processes in these areas would produce the following advantages:

- i) replacement of multistep processes with more direct synthetic procedures with waste reduction at source and atom economy, ii) implementation of alternative ways to processes presently based on more toxic or expensive materials, iii) raw materials diversification, and iv) recycling of carbon.

A point that must be emphasized is that speaking of "avoided CO₂", one should consider not only the amount of CO₂ recycled through its fixation in chemicals, but also the amount of CO₂ not produced by implementing the atom efficiency and waste minimization principles.

Results and Discussion

The carbon dioxide-utilizing reactions mentioned so far, can be divided into two main categories from the energetic point of view.²

Class 1

Reactions in which the whole carbon dioxide molecule is used. The substrate (amines, unsaturated hydrocarbons) is the energy vector and the amount of extra energy, if required, is usually very low. These reactions include the carboxylation reactions with the formation of a C-C or C-heteroatom bond (C-E; E=O, N, P, other element).

Class 2

Reduction reactions to C1 or C_n species, using dihydrogen, electrons, or heat as energy source.

All these reactions are common to, and very important in, biological systems (plants and bacteria), in which several enzymes involved in carbon dioxide utilisation are metal enzymes with the metal acting as the active site.

A great emphasis has been put on elucidating the role of CO₂-metal complexes, in which CO₂ is either η²-C, O or μ-bonded to one or more metal centres, in carbon dioxide reduction or in its reaction with olefins to afford carboxylates. This issue is relevant to the more general question if the coordination of CO₂ to a metal is a necessary prerequisite for CO₂ fixation onto an organic substrate. Available data suggest that such co-ordination is necessary in the reduction to CO.

In carboxylation reactions either the olefin is activated first, or a concerted three-centre mechanism may operate. The carboxylation of unsaturated hydrocarbons (alkenes, alkynes, butadienes, allenes) has been recently developed with interesting yield and selectivity (>90%) using transition metal complexes as catalysts. In all cases the homo coupling of substrates is a concurrent process with the hetero-coupling substrate-CO₂. The solvent and the carbon dioxide concentration in solution play an important role in driving the reaction in either directions.

Methanol may have a large market as fuel or intermediate and its synthesis from carbon dioxide attracts the attention and interest of several research groups all over the world in order to define its potential. The use of carbon dioxide (Eq. 1) has as major draw-back the higher consumption of dihydrogen with respect to CO.



However, higher selectivity and better yields may counterbalance such apparent negative point.

The implementation of innovative synthetic technologies based on CO₂ can considerably contribute to the reduction of carbon dioxide emission. The avoided amount is not simply represented by the amount of fixed CO₂. New synthetic methodologies implementing the principles of atom economy, solvent shift, waste minimisation at source, use of less noxious materials and carbon recycling, contribute to CO₂ reduction in many different ways, which cannot be discovered and quantified by simply looking at the stoichiometry of a reaction.³

Acknowledgement. This work was supported by MURST, Project no. 9803026360 and MM03027791

References

- (1) Aresta, M.; Quaranta, E. - *ChemTech.*, **1997**, 32-40.
- (2) Aresta, M.; Dibenedetto, A. - *ACS Book on CO₂ Conversion and Utilisation*, **2001**
- (3) Aresta M.; Tommasi I.; Dibenedetto A. - *Energy&Fuels*, **2001**, 15, 2, 269-273.

CATALYTIC BEHAVIOR OF CALCIUM OXIDE FOR SYNTHESIS OF DIMETHYL CARBONATE FROM PROPYLENE CARBONATE AND METHANOL

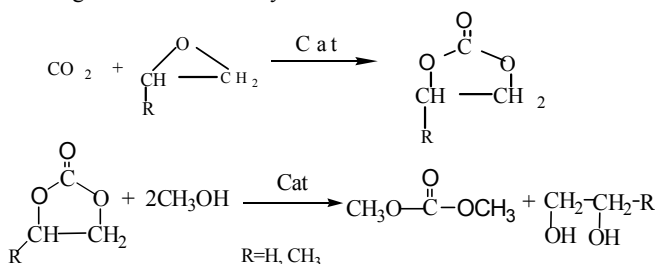
Tong Wei, Wei Wei*, Mouhua Wang, Yuhan Sun, Bing Zhong

State Key Laboratory of Coal Conversion Institute of Coal Chemistry Chinese Academic of Sciences, Taiyuan, 030001

*To whom corresponding should be addressed.
Fax: +86 351 4041153
E-Mail: yhsun@sxicc.ac.cn or weiwei@sxicc.ac.cn

Introduction

Dimethyl carbonate (DMC) is an important precursor of polycarbonate resins as well as a useful carbonylation and methylation agent [1]. Because of the negligible toxicity of DMC, it is promising as a substitute for phosgene, dimethyl sulfate, or methyl iodide. DMC can be prepared by the oxidative carbonylation of methanol, carbonylation of methyl nitrite or transesterification of cyclic carbonate with methanol [2]. Because of the moderate reaction conditions and the use of CO₂ as raw material, transesterification method, as shown follow, has gained increasing attention in recent years.



In present paper, CaO calcined from CaCO₃, which shows excellent catalytic activity, is used as solid base catalyst for the rudimental investigation of its catalytic behavior for synthesis of DMC from propylene carbonate (PC) and methanol (MeOH) as well as the mechanism of this reaction over CaO.

Experimental

CaO was prepared from CaCO₃ calcined at 1173K in N₂ atmosphere. The reaction was carried out in a 250mL flask equipped with reflux condenser, water bath and magnetic stirring. Except particular description, catalyst was added into the flask accompanied with violent magnetic stirring after the temperature reached to the expected one. Reaction product was analyzed by Gas Chromatograph after centrifugal separation of solid catalyst from liquid.

Result and discussion

Fig.1 and Fig.2 shows the effect of temperature on DMC yield and DMC selectivity. It can be seen that CaO shows excellent catalytic activity for synthesis of DMC from PC and MeOH so that the reaction even can reach equilibrium in 60 minutes at 10°C. With the increase of temperature, equilibrium DMC yields decrease gradually. As for DMC selectivity, while it increase firstly then decrease gradually at 10°C and 20°C, it decrease gradually all along at 30°C, 40°C and 50°C with the prolong of reaction time. This reaction is a little exothermic with $\Delta_r H = -7.092 \text{ kJ/mol}$ [3-6], therefore, the increase of temperature would result in equilibrium constant decrease and the consequent decrease of equilibrium

DMC yield. Since Knifton reported that hydroxyethyl methyl carbonate, which could be detected only at short reaction time and/or low temperature, was intermediate when MeOH reacted with ethylene carbonate to generate DMC and ethylene glycol, hydroxypropyl methyl carbonate (HMC) may be the intermediate of reaction in present paper. On the other hand, the intermediate can also react with PC continually to generate polymeric propylene carbonate (PPC) with the rate much slower than that of subject reaction. Thus the by-product is mainly intermediate--HMC before the reaction reach equilibrium, and is mainly PPC after reaction reach equilibrium, which is good explanation of white colloidal solid produced from MeOH and PC reacting 2hr at 120°C. The increase of temperature can promote the polymerization of PC and consequently result in the decrease of DMC selectivity.

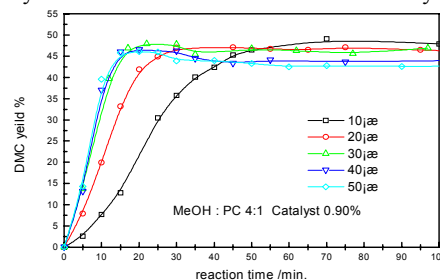


Fig.1 Effect of temperature on DMC yield

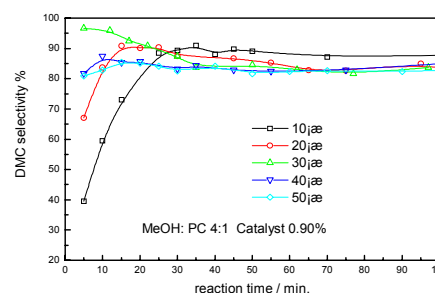


Fig.2 Effect of temperature on DMC selectivity

The effect of catalyst concentration on DMC yield and DMC selectivity is illustrated in Fig. 3 and Fig. 4. It can be seen that DMC equilibrium yield keep constant as catalyst concentration increase from 0.61% to 1.80%, which means that catalyst concentration have no effect on reaction equilibrium but can increase reaction rate. On the other hand, when catalyst concentration is 0.61% and 0.91, the variance of DMC selectivity with the prolong of reaction time like that at low temperature, which means that the decrease of catalyst concentration can decrease the reaction rate of HMC with MeOH and thus increase the concentration of HMC at short time. Furthermore, the increase of catalyst can promote the polymerization of PC and consequently result in the decrease of DMC selectivity.

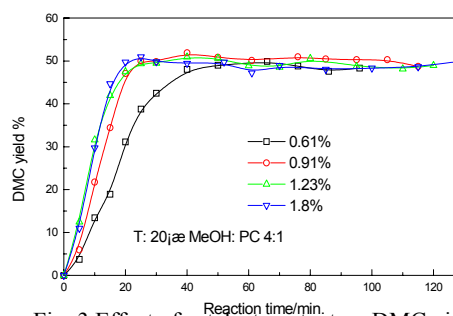


Fig. 3 Effect of catalyst content on DMC yield

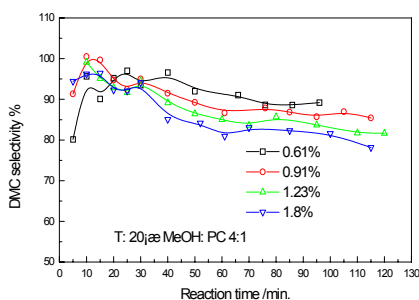


Fig. 4 Effect of catalyst content on DMC selectivity

The effect of the ratio of MeOH and PC on DMC yield and DMC selectivity is shown in Fig.5 and Fig. 6. It can be seen that equilibrium DMC yield increase gradually with the increase of the ratio of MeOH and PC. This reaction is reversible; therefore the increase of MeOH concentration can make equilibrium PC conversion increase and the subsequent increase of equilibrium DMC yield. From Fig. 6 we can see that on the one hand, DMC selectivity-time curve, liking that at low temperature, increase firstly then decrease gradually with low ratio of MeOH and PC, on the other hand, DMC selectivity increase gradually with the increase of the ratio of MeOH and PC after the reach of equilibrium. The decrease of the ratio of MeOH and PC means the decrease of MeOH concentration, which makes the reaction rate of HMC and MeOH decrease and consequent increase of HMC concentration at short time. At the same time the polymerization of PC is competitive with subject reaction. The increase of MeOH concentration can inhibit this side reaction and make DMC selectivity increase.

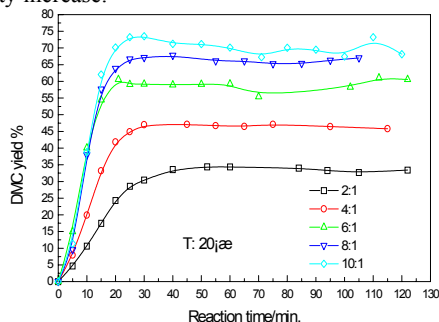


Fig. 5 Effect of MeOH to PC ratio on DMC yield

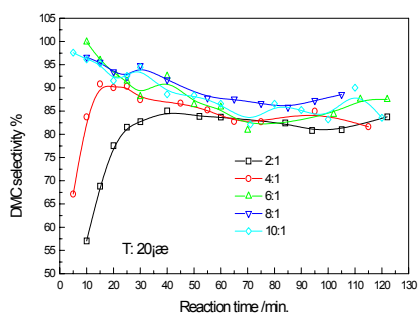


Fig 6. Effect of MeOH to PC ratio on DMC selectivity

In order to further understand the mechanism of this reaction on the catalyst, the effect of addition method, temperature, catalyst concentration and the ratio of MeOH and PC on reaction rate are studied. Fig. 7 shows that there is an induction period in rate-time curve when MeOH and PC was added first as well as the PC and catalyst was added first, which means that the induction period

comes from the activation of MeOH on solid base catalyst. On the other hand, the reaction rate is faster for MeOH and PC being added firstly than that of PC and catalyst being added firstly, which may be caused by activation of PC by H-bond between PC and MeOH. Therefore the catalytic mechanism of CaO may be as follow:.

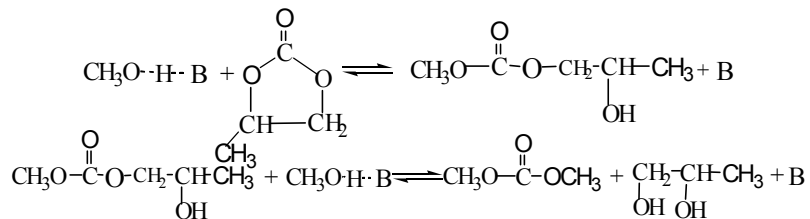
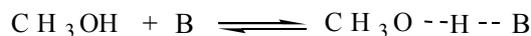


Fig. 8 shows the effect of temperature on reaction rate. The maximum rate increase and the induction period is shortened with the increase of temperature. At the beginning of the reaction, the concentration of activated MeOH is low, so the activation of MeOH has an important effect on DMC production rate, then after the activation step reach equilibrium, the surface reaction of activated MeOH with PC becomes an important factor that influence the rate of DMC production. The increase of temperature can promote the rate of all steps and consequently result in the maximum rate increase and the induction time shortened.

As for effect of catalyst concentration shown in Fig 9, the maximum rate increase and the induction period is shortened with catalyst concentration increase from 0.61% to 1.23%, but the rate-time curve almost unchanged when catalyst concentration increase from 1.23% to 1.84%. The increase of catalyst concentration can result in the increase of both MeOH activation rate and equilibrium activated MeOH concentration, so the maximum rate increase and the induction time is shortened with the increase of catalyst content. However, when the catalyst concentration reach certain amount, it is not an important factor that affect MeOH activation rate and equilibrium activated MeOH any more, therefore the reaction rate-time curve doesn't change with the continue increase of catalyst concentration.

As far as the effect of the ratio of MeOH and PC is concerned, the induction period is shortened with the increase of the ratio of MeOH and PC, but the maximum rate increase when the ratio of MeOH and PC increase from 2:1 to 6:1 first, and then decrease when MeOH to PC ratio continual increasing from 6:1 to 10:1. With the increase of MeOH to PC ratio both MeOH activation rate and equilibrium activated MeOH concentration increase, but PC concentration decrease, thus although the induction time was shorten due to the increase of the ratio of MeOH and PC ratio, but the surface reaction rate of activated MeOH with PC increase first then decrease with the increase of the ratio of MeOH and PC.

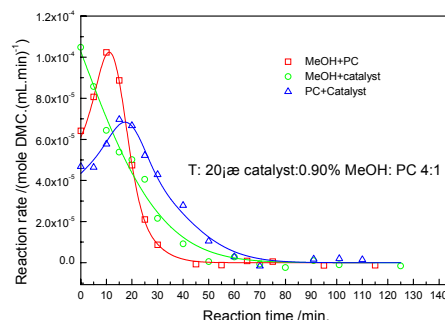


Fig. 7 Effect of addition method on reaction rate

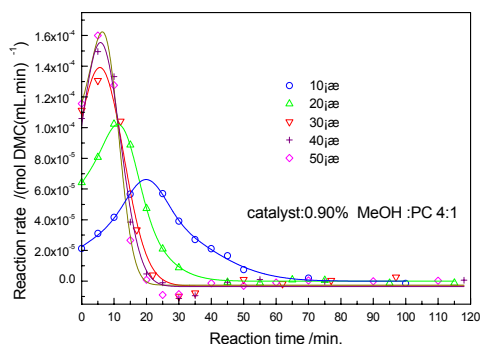


Fig 8 Effect of temperature on reaction rate

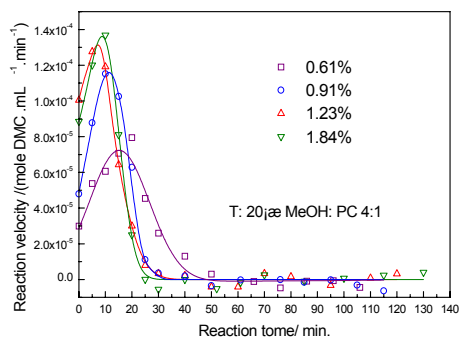


Fig. 9 Effect of catalyst content on reaction rate

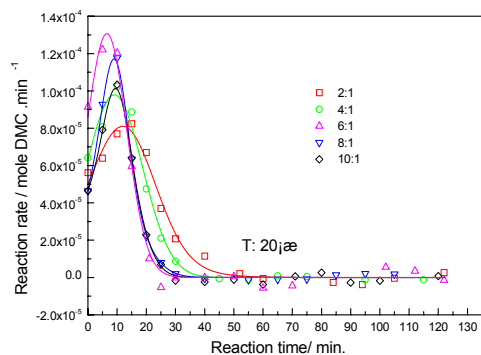


Fig.10 Effect of MeOH to PC ratio on reaction rate

Conclusion

- 1 CaO calcined from CaCO₃ shows excellent catalytic activity for synthesis of DMC from MeOH and PC. The reaction even can reach equilibrium in 60 minutes at 10 °C.
- 2 The main function of CaO is the activation of MeOH and the consequent promotion of MeOH and PC reaction. The H-bond between MeOH and PC can activate PC and make reaction rate increase.
- 3 Relative low temperature and high ratio of MeOH and PC is preferable for high DMC yield and selectivity. Increase of catalyst concentration has little effect on DMC yield but make DMC selectivity decrease.

Reference

- (1)Watanabe, Y.; Tatsumi, T. *Microporous and mesoporous materials* 1998, 22,399~407
- (2) Pacheco, M. A.; Marshall, C. L. *Energy & Fuels* 1991, 11, 2~29
- (3) Yin,Y.; Xi, Zh.; Li, D. *Physical Chemistry*. 3rd edition, Higher Education Press, Beijing, 1994, PP. 569
- (4) Dong, Z. *Hangzhou Chemical Engineering* 1979, 3, 39~96
- (5) Reid, R.C.; Prausnitz, J.M.; Poling, B.E. *The properties of Gases and*

CATALYTIC DEHYDROGENATION OF AROMATIC HYDROCARBON WITH CARBON DIOXIDE AS AN OXIDANT

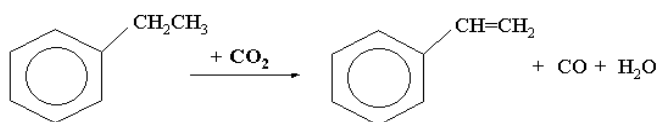
Jong-San Chang, Min Seok Park, Vladislav P. Vislovskiy,
Sang-Eon Park, and Jin S. Yoo

Catalysis Center for Molecular Engineering,
Korea Research Institute of Chemical Technology (KRICT),
P.O. Box 107, Yusong, Taejeon 305-600, Korea

Introduction

For the mitigation of global warming due to carbon dioxide, catalytic conversion of CO₂ has been extensively studied for last decade.¹ Most of studies on this field have been concentrated on the utilization of carbon dioxide as a carbon source through catalytic reduction processes with various kinds of reductants.¹ Particularly, hydrogen has long been used to abstract the oxygen atom of CO₂ for catalytic conversion into useful chemicals.² However, catalytic hydrogenation is confronted with some limitations to be commercialized because in most cases the cost of hydrogen from conventional sources such as steam reforming of hydrocarbons is not cheaper than that of chemicals obtained from catalytic hydrogenation. However, the utilization of CO₂ as a mild oxidant and an oxygen transfer agent is recently attracting considerable attention.³⁻⁵ This approach is expected to open new technology for CO₂ utilization. It has been proposed that the oxygen species of carbon dioxide is useful for oxidative conversions of hydrocarbons.⁶⁻⁸ Krylov and Mamedov have studied on the oxidative conversions of alkanes, alkenes, and alcohols with carbon dioxide over Mn oxide-based catalysts.⁹ Yoo *et al.* showed that Fe/Mo/borosilicate catalyst could activate CO₂ which could be functioning as a promoter and co-oxidant for the gas-phase oxidation of alkylaromatics with oxygen as well.²

Styrene is commercially produced by dehydrogenation of ethylbenzene (EB) using potassium-promoted iron oxide catalysts with a large excess of superheated steam. However, the use of steam has a drawback of losing latent heat of condensation during subsequent separation in the commercial process. The energy consumption required for the EB dehydrogenation using carbon dioxide is estimated to be much lower than that for the currently operating process using steam.¹⁰ In addition to energy saving, the use of CO₂ with replacement of steam can give a beneficial advantage for increase in equilibrium conversion. Considering these aspects, it is desirable to design a new catalytic system based on the use of carbon dioxide instead of steam. Some selected catalytic systems show promoting effects in the presence of carbon dioxide.^{4,6,11} In particular, we have reported that, in the case of zeolite-supported iron oxide catalysts, carbon dioxide exhibits beneficial effects on improving catalytic activity and preventing coke formation.⁶



This work deals with dehydrogenation of aromatic hydrocarbons, especially ethylbenzene using CO₂ as an oxidant. We suggest catalysts to exhibit high activity and excellent selectivity for styrene with the help of carbon dioxide as an oxidant.

Experimental

Catalyst Preparation. γ -Al₂O₃-supported iron oxide catalyst (Fe/ γ -Al₂O₃) was prepared by depositing iron(II) sulfate solution onto supports at the temperature range 60 - 70°C under nitrogen atmosphere to prevent the dissolution of oxygen.⁶ It was precipitated at pH = 10 - 11 with ammonia water. The precipitates were filtered, dried at 80°C in vacuum oven, and calcined under a nitrogen stream at 700°C for 4 h. Al₂O₃-supported vanadium oxide (V₂O₅/Al₂O₃) or vanadium-antimony binary oxide (V-SbO_x/Al₂O₃) catalysts were prepared by impregnation of aqueous solutions of ammonium metavanadate and antimony (III) chloride onto activated alumina. The impregnated sample was dried at 100°C and then calcined in air at 600°C for 4 h. For V₂O₅/Al₂O₃, the content of V₂O₅ was 20.0 wt%. For V-SbO_x/Al₂O₃, the content of V₂O₅ and Sb₂O₃ was 7.5 wt% and 15.5 wt%, respectively.

Catalytic Measurement. The EB dehydrogenation into styrene was carried out in a micro-activity test unit (Zeton, MAT 2000) with a fixed bed reactor at 600°C under atmospheric pressure. A sample of 1g was placed on a fritted metal disk in the reactor. Before reaction, the catalyst was treated in a nitrogen stream from RT to 600°C with a heating rate of 10°C/min. Ethylbenzene was introduced by syringe pump and supplied into the reactor by a carrier gas with flow rate of 20 ml/min. The liquid and gas products were analyzed by GC (Donam Corp., DS6200) equipped with FID and TCD, respectively. Effluent gases from the reactor were analyzed by a gas chromatograph (Chrompack CP9001) equipped with a thermal conductivity detector (TCD).

Results and Discussion

Steam is generally utilized as diluent in dehydrogenation of aromatic hydrocarbons and oxygen works as strong oxidant in oxidative reactions of aromatic hydrocarbons. However, carbon dioxide can be utilized as both oxidant and diluent since it can release oxygen as surface oxygen species upon activation on reduced or oxygen-deficient catalyst surface and it has high heat capacity. It can be confirmed that CO₂ plays a key roles as oxidant and diluent in EB dehydrogenation using carbon dioxide instead of steam. **Table 1** displays the effect of carrier gas in EB dehydrogenation over 5 wt% Fe/ γ -Al₂O₃ catalyst. It is clearly seen that carbon dioxide works very well in EB dehydrogenation as the soft oxidant and diluent to increase the conversion as well as selectivity. The order of catalytic activity and selectivity for styrene according to carrier gas was CO₂ > N₂ > H₂O. Such dependence of the activity on carrier gas is just contrary to that of commercial catalyst. Considering that conversion of CO₂ took place together with EB conversion, the enhancement of the dehydrogenation activity and the selectivity is certainly ascribed to the promotional effect of excess carbon dioxide to the oxidative process. This result implies that the initial hydrogen abstraction at benzylic C-H bond of EB was much facilitated by carbon dioxide.

Table 1. Effect of carrier gas in EB dehydrogenation over Fe/ γ -Al₂O₃ catalyst^a

Carrier Gas	X(EB), %	S(SM), %	X(CO ₂), %	H ₂ O/H ₂ ^b
N ₂	63.7	95.8	-	-
H ₂ O	25.0	88.8	-	-
CO ₂	68.5	97.2	47.4	1.7

^aReaction conditions: Temp. = 600°C, LHSV = 1.0 h⁻¹, CO₂(N₂ or H₂O)/EB = 10/1, Time-on-stream = 4 h. ^brelative concentration to EB.

Crystalline iron oxides have not been appeared on XRD pattern of Fe/ γ -Al₂O₃ catalyst, suggesting that iron oxide phase is amorphous and is well dispersed. Characterization results revealed that the oxidation state of iron oxide over γ -alumina is between γ -Fe₂O₃ and Fe₃O₄. These two phases in the catalyst seem to be interconvertible during EB dehydrogenation with CO₂. There may be optimal population of iron oxide phase between γ -Fe₂O₃ and Fe₃O₄ to show high activity. The surface basicity upon the introduction of iron oxide onto γ -Al₂O₃ support was not changed so much. It is known that a Fe₃O₄ spinel oxide, so-called magnetite is basically oxygen deficient enough to activate carbon dioxide at elevated temperature.¹² In our previous work, it has been considered that oxygen deficiency of iron oxide in the supported catalyst is one of the most important factors on promoting the catalytic activity in the presence of CO₂.⁶ Oxygen-deficient sites of the supported iron oxide catalyst seem to produce CO efficiently from the CO₂ dissociation, and the adsorbed oxygen on the catalyst surface can also play a role on hydrogen abstraction from EB. Dispersion of the oxygen-deficient sites or oxygen defects in the supported iron oxide catalysts appears to be more efficient for the CO₂ dissociation and thereby the oxidative dehydrogenation of EB. Therefore, it is assumed that high activity of Fe/ γ -Al₂O₃ in the presence of CO₂ is mainly due to the presence of Fe²⁺ species and its oxygen deficiency.

Figure 1 displays the catalytic results for EB dehydrogenation with CO₂ over V₂O₅/Al₂O₃ and V-SbO_x/Al₂O₃ catalysts at 600°C. These catalysts exhibited very high conversion (>75%) and high selectivity (>95%) at initial stage. However, catalytic activity of V-SbO_x/Al₂O₃ was higher than that of V₂O₅/Al₂O₃ and, moreover, its stability was much better than that of the unpromoted one. It has been proposed that redox behavior of vanadium oxide-based catalysts played a key role in accordance with Mars-van-Krevelen mechanism in oxidative dehydrogenation of alkylaromatics.¹³ Likewise, EB dehydrogenation with CO₂ is expected to follow the same mechanism. Vanadium oxide with V⁵⁺ is generally considered as an active component. Deactivation of supported vanadium oxide catalysts was

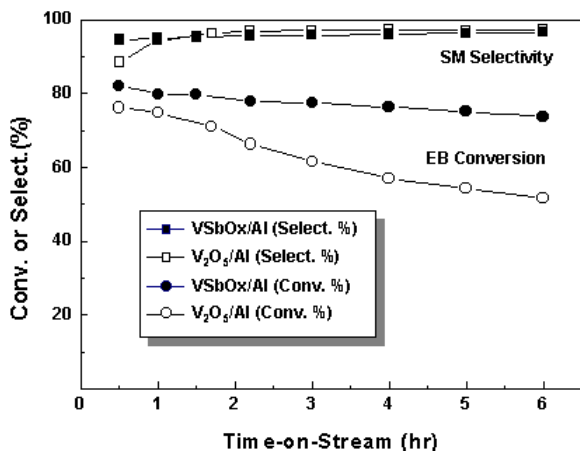


Figure 1. Comparison of catalytic activities of V₂O₅/Al₂O₃ and V-SbO_x/Al₂O₃ catalysts. Reaction conditions: Temp. = 600°C, LHSV = 1.0 h⁻¹, CO₂/EB = 1/1.

occurred by deep reduction of V⁵⁺ into V³⁺ and coke formation. The introduction of Sb oxide into V₂O₅/Al₂O₃ led to preventing the deep reduction of the oxidation state of vanadium and facilitating the redox cycle, resulting in enhancement of the catalyst stability as well as the

catalytic activity. Carbon dioxide for this reaction acted as the soft oxidant to provide oxygen species on reduced catalyst surface and, consequently, reoxidize the reduced vanadium species.

There are two possible pathways for EB dehydrogenation to styrene. The simple dehydrogenation of EB that produces styrene and hydrogen occurs under nitrogen or even carbon dioxide atmosphere, while the oxidative dehydrogenation of EB that produces styrene, carbon monoxide, and water occurs under carbon dioxide atmosphere. During the reaction, carbon monoxide and hydrogen in the gas phase were observed together with a trace of methane. Considering the gas product distribution, the ratio of H₂O/H₂ in the product stream is estimated to be 1.7 for Fe/ γ -Al₂O₃ and 1.4 for V-SbO_x/Al₂O₃, respectively, after 4 h on stream. The formation of water as well as carbon monoxide implies that CO₂ molecule over catalyst surface is dissociated with CO and surface oxygen, which can abstract hydrogen from EB and then results in the generation of water. Taking into account the formation of large amount of water, high activity for supported iron oxide and supported vanadium catalysts under CO₂ carrier may be mainly ascribed to oxygen species dissociated from carbon dioxide molecule, thus due to the promotion of the oxidative process by carbon dioxide. In other words, this indicates that carbon dioxide plays a role as an oxidant in EB dehydrogenation on supported iron oxide and vanadium oxide catalysts.

Conclusions

This work demonstrates that the utilization of carbon dioxide as an oxidant is very useful for oxidative dehydrogenation of aromatic hydrocarbon such as ethylbenzene. In dehydrogenation of ethylbenzene over supported iron oxide and vanadium oxide catalysts, carbon dioxide plays a key role as an oxidant to increase catalytic activity and selectivity to styrene.

Acknowledgment

This work was performed for the Greenhouse Gas Research Center, one of the Critical Technology-21 Programs, funded by the Ministry of Science and Technology of Korea (MOST). VPV thanks the MOST for the visiting scientist fellowship. We also thank Daebio Industries Co.(Korea) for financial support.

References

- Delmon, B., Yates, J.T., Advantages in Chemical Conversions for Mitigating Carbon Dioxide, Studies in Surface Science and Catalysis, Vol. 114, Elsevier: Amsterdam, 1998.
- Arakawa, H., *Stud. Surf. Sci. Catal.*, **1998**, 114, 19.
- Yoo, J.S., *Catal. Today*, **1998**, 41, 49.
- Park, S.-E., Yoo, J.S., Chang, J.-S., Environmental Challenges and Greenhouse Gas Control for Fossil Fuel Utilization in the 21st Century (eds. M.M. Maroto-Valer, Y. Song, C. Song), Chapter 33, Kluwer Academic/Plenum: New York, 2002.
- Aresta M., Tommasi I., Quaranta E., Fragale C., Mascetti J., Tranquille M., Galan F., Fouassier M., *Inorg. Chem.*, **1996**, 35, 4254.
- Chang, J.-S., Park, S.-E., Park, M.S., *Chem. Lett.*, **1997**, 1123.
- Choi, Y.-S., Park, Y.-K., Chang, J.-S., Park, S.-E., Cheetham, A.K., *Catal. Lett.*, **2000**, 69, 93.
- Ohtsuka, Y., *J. Catal.*, **1999**, 186, 160.
- Krylov, O.V., Mamedov, A. Kh., *Ind. Eng. Chem. Res.*, **1995**, 34, 474.
- Mimura, N., Takahara, I., Saito, M., Hattori, T., Ohkuma, K., Ando, M., *Catal. Today*, **1998**, 45, 61.
- Mimura, N., Saito, M., *Catal. Lett.*, **1999**, 58, 59.
- Tamura, Y., Tabata M., *Nature*, **1990**, 346, 255.

13. Rizayev, R.G., Mamedov, E.A., Vislovskii, V.P., Sheinin, V.E.,
Appl. Catal. A., **1992**, 83, 103.

CATALYTIC ESTERIFICATION OF CARBON DIOXIDE AND METHANOL FOR THE PREPARATION OF DIMETHYL CARBONATE

Fa-hai CAO⁺ Ding-ye FANG Dian-hua LIU and Wei-yong YING

Department of Chemical Engineering, East China University of Science and Technology, Shanghai 200237, China

Keywords: carbon dioxide; dimethyl carbonate; methanol; reaction on supercritical condition

1. Introduction

In the global warming imbroglio, carbon dioxide is number one enemy. It is mainly liberated from combustion of fossil fuels (coal, oil and natural gas). Conversely, carbon dioxide is also one of the cheapest and most abundant carbon source in the world. Carbon dioxide can be converted into a lot of useful organic compounds by effectively activation. Thus, the recycle and utilization of carbon dioxide seem to be a fundamental task from environmental protection and economics points of view. For these reasons, we proposed a process by which dimethyl carbonate could be prepared by catalytic esterification of carbon dioxide and methanol.

Dimethyl carbonate has attracted much attention in terms of a non-toxic substitute for dimethyl sulfate and phosgene, which are toxic and corrosive methylating or carbonylating agents. In addition, DMC is considered to be an option for meeting the oxygenate specification for transportation fuels.

The conventional synthesis of DMC is via the reaction of methanol and phosgene. Owing to the high toxicity of the raw material and severe corrosivity, this method has fallen out of use gradually. The other two widely used methods of synthesis of DMC are ester exchange process^[1-2] and the process of oxidative carbonylation of methanol^[3-5]. Recently, a more challenging method^[6-9] is the direct synthesis from carbon dioxide and methanol. Although metallic magnesium powder, Sn(IV) and Ti(IV) alkoxides have been used the catalysts, respectively, unfortunately, the yield of DMC was low even in the presence of chemical dehydrates because mainly of thermodynamic limit.

The near critical regions are considered as the most significant regions that have the supercritical characteristics that affect the reactions to the greatest extent. The supercritical conditions would play a crucial role in carbon dioxide effectively activation and conversion. In this paper, we studied the process for the continuous preparation of DMC near the critical regions of carbon dioxide, in which carbon dioxide acted not only as a medium of the supercritical fluid, but also as one of the reactants.

2. Experimental

Chemicals. Methanol (analytical grade purity, 99.5%), dimethyl carbonate (99.8% purity) and CH₃I and K₂CO₃ (analytical grade purity, 99.8%) were all made in China. Compressed carbon dioxide (used as a food agent, purity min. 99.9%) was used.

Apparatus and Analysis. The experimental configuration is shown in Figure 1. The reactor was a stainless steel autoclave (FYX-5A, made in Dalian, China) with an inner volume of 500mL, a magnetic stirrer and an electric heater. When a given amount of CH₃I and K₂CO₃ were mixed with methanol (150mL) in the autoclave, the autoclave was sealed. After flushing with nitrogen and then purging with CO₂+N₂ to a given pressure at room temperature, the autoclave was heated and stirred constantly at a specific temperature and pressure for a given period of time. The reaction products, which were collected to a proper volume from the tap hole, were cooled to the ambient temperature. The samples so obtained were analyzed by gas chromatograph and organic 402 was used as monomer columns (60-80 mesh). After condensation, gas-liquid separation, depressure, the reaction products are continuously monitored on-line by double-column GC-900B (made in Shanghai, china) with a thermal conductivity detector, a TDX-02 column (80-100 mesh) was for the analyzing of the gas phase.

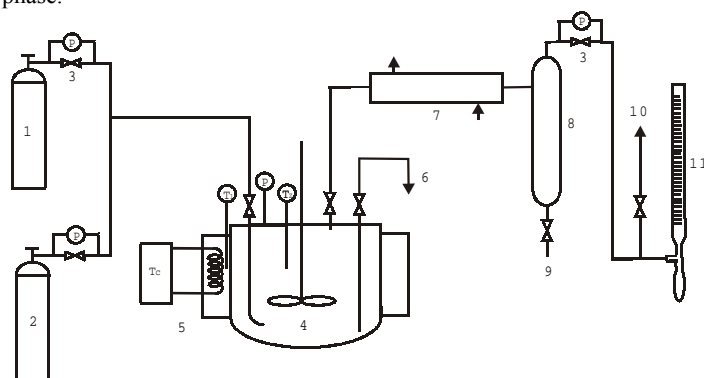


Fig. 1 The schematic diagram of the experimental apparatus

1—Cylinder of feed gas; 2—Cylinder of N₂; 3—Reducing pressure valve; 4—Autoclave; 5—Heater; 6—Tap hole; 7—Condenser; 8—Gas-liquid separator; 9—Gas chromatograph; 10—Vent; 11—Soap film flowmeter

3. Results and Discussions

In the all experiments, the constitute of feed gas is CO₂:N₂=3:5, the velocity of magnetic stirrer was controlled at 250 rpm. The preliminary tests showed that the dosages of CH₃I and K₂CO₃ were 10.0mL and 8.0g, respectively. If one of the two compounds was absence, the other compound had no activity for the catalytic reaction.

The x_D is defined as the mole fractional of DMC in liquid-phase product.

3.1 Reaction pressure and temperature

Figures 2 and 3 show the effects of the reaction pressure (P) and the temperature (T) on x_D , respectively. From Figure 2 it could be seen that x_D increases with increase of the reaction pressure. When the reaction pressure approaches about 7.3MPa, x_D reaches the maximum value. Then, x_D decreases. The change tendency of Figure 3 is similar to that of Figure 2, in which the peak value of x_D is at approximately 80~100°C. Obviously, it is near the critical regions of carbon dioxide that carbon dioxide can be converted effectively into DMC.

⁺ Author to whom correspondence should be addressed.

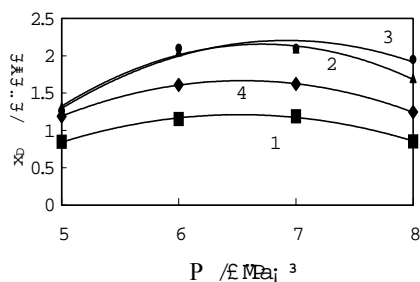


Fig.2 Effects of the reaction pressure on x_D

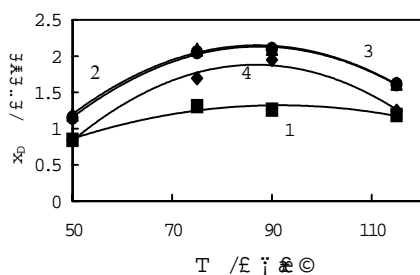


Fig.3 Effects of the reaction temperature on x_D

1—50.0°C; 2—75.0°C; 3—90.0°C; 4—115.0°C
1—5.0MPa; 2—6.0MPa; 3—7.0MPa; 4—8.0MPa

3.2 Supercritical phenomena and reaction pathway^[10-12]

There is a conjugated double bond in the molecule of carbon dioxide. Near the critical regions of carbon dioxide, the reaction rate varies with the change of the electric polarization of the conjugated system of the molecule, so that carbon dioxide can take part in an addition reaction. Furthermore, carbon dioxide has a Lewis -acid carbon atom and two weakly Lewis basic oxygen atoms, it is therefore not surprising that it can undergo various reactions, such as firstly bound "abnormally" to form the intermediate. The basic function is useful for the activation of methanol and formation of CH_3O^- , the nucleophilic attack of CH_3O^- upon CO_2 led to the formation of DMC. Methyl iodide is only involved in the catalytic cycle. Based on above analysis, near the critical point of carbon dioxide, x_D reaches the maximum value.

3.3 Tentative ideas for the commercial production of DMC

In the system of preparation DMC from carbon dioxide and methanol, besides the product such as DMC and water, there are large number of feed gas and a little of by-product like dimethyl ether. In order to obtain pure product of DMC, two-steps method can be utilized to separate dimethyl carbonate from reaction product. The first step is forerunning, it most fully used the azeotropic feature of methanol with dimethyl carbonate, the azeotropic mixture of $\text{CH}_3\text{OH} - \text{DMC}$ can be separated from by-product and feed gas in packed column. The second is refining step, extractive distillation method was adopted. Based on the feature, of which DMC is difficult to dissolve into water, water was used as an extraction reagent to extract and separate DMC from azeotrope, we put forward the tentative ideas for the commercial production of DMC.

Figure 4 showed the schematic diagram of the tentative ideas for the commercial production of DMC. After forerunning, the gasified azeotrope was added into extractive distillation column (3) at central section and water was sprayed from top of column. Distillate contained two layers, the upper layer was organic phase which contained 97% of DMC, the lower was aqueous phase which contained 5% of water and 0.05% of DMC, respectively. The water phase was discharged from bottom of separator (5) and mixed with first runnings.

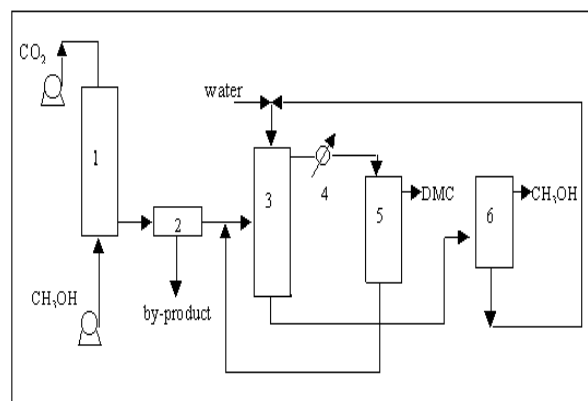


Fig. 4 The schematic diagram of the tentative ideas for the commercial production of DMC

1—reactor; 2—primary tower; 3—extractive distillation; 4—condenser; 5—separator; 6—fractionating town

The weak point of this preparation from methanol and CO_2 is that the conversion is limited by the reaction equilibrium at low level. But this limitation is avoidable by the removal of water from the reaction system, for example, by introducing trimethyl orthoformate. If it is possible to get a suitable method for the removal of water, DMC yield will be improved drastically.

4. Conclusions

The continuous catalytic synthesis of dimethyl carbonate from carbon dioxide and methanol in the presence of CH_3I and K_2CO_3 near the critical point of carbon dioxide was studied in an agitated reactor. The optimal x_D was obtained under the conditions of reaction temperature 80~100°C, reaction pressure 7.3MPa. The value of the reaction pressure was near the critical point of carbon dioxide. It could be concluded that under the supercritical condition carbon dioxide was effectively activated. A possible reaction pathway was suggested from the viewpoint of supercritical phenomena. Finally we put forward the tentative ideas for the commercial production of DMC, the results will be useful to the esterification of carbon dioxide and methanol.

Acknowledgments

Our work is supported by the Research Fund for the Doctoral Program of Higher Education (97025105) and the Basic Research Project of SINOPEC (598013).

References

- (1). Knifton, J. F. "Process for co-synthesis of ethylene glycol and DMC"; assigned to Texaco;1987, US Patent 4,661,609;

- (2). Duranleau, R. G.; Nieh, E. C. Y.; Knifton, J. F. "Process for production of ethylene glycol and dimethyl carbonate"; assigned to Texaco, 1986 US Patent 4,691,041;
- (3). Romano, U., et al. *Synthesis of DMC from methanol, CO, and O₂ catalyzed by copper compounds*. *Ind. Eng. Chem. Prod. Res. Dev.* 1980, **19**, 396-403
- (4). Fenton, D. M.; Steinward, P. J. *Noble Metal Catalysis, III: Preparation of dialkyl oxalates by oxidative carbonylation*; Union Oil. *J. Org. Chem.* 1974, **39**, 701-704
- (5). WO Patent 07601; Curnutt, G. L. "Catalytic Vapor Phase Process for Producing Dihydrocarbyl Carbonates"; assigned to Dow Chemical Company; 1987
- (6). Kizlink J. *Synthesis of dimethyl carbonate from carbon dioxide and methanol in the presence of organotin compounds*. *J Collect Czech Chem Commun*, 1993, **58**: 1399
- (7). Jiang Q, Lin Q H and Huang Z T. *A new catalytic process for the direct synthesis of dimethyl carbonate from carbon dioxide and methanol*. *Cuihua Xuebao*, 1996, **17** (2): 91 (in Chinese)
- (8). Fang S., Fujimoto K. *Direct synthesis of dimethyl carbonate from carbon dioxide and methanol catalyzed by base*. *Applied catalysis A: General*, 1996, **142**: L1-L3
- (9). Gui X S, Cao F H, Liu D H and Fang D Y. *Synthesis of dimethyl carbonate from methanol and carbon dioxide in the autoclave*. *Journal of east china university of science and technology*, 1998, **24** (1): 7 (in Chinese)
- (10). Savage P. E.; Gopalan S.; Mizan T. I.; Martino C. J. and Brock E. E. *Reactions at supercritical conditions: Applications and fundamental*. *AICHE Journal*, 1995, **41**(7): 1723
- (11). Xu X. D.; Moulijn J. A. *Mitigation of carbon dioxide by chemical conversion: Plausible chemical reactions and promising products*. *Energy & Fuels*. 1996, **10**: 305
- (12). Brounstein P, Matt D and Noble D. *Reactions of carbon dioxide with carbon-carbon bond formation catalyzed by transition-metal complexes*. *Chem Rev.* 1988, **88**: 747

CATALYTIC OXIDATION OF METHANE OVER Co/Mn MIXED OXIDES: THE WATER EFFECT

W. B. Li, Y. Lin, and Y. Zhang

Department of Environmental Science and Engineering
Tsinghua University
Beijing 100084, P. R. China

Introduction

Natural gas has been used as clean fuels in a variety of combustion processes, such as electrical utilities and motor vehicles. Catalytic combustion of methane without flame can not only improve the energy efficiency but also reduce the formation of thermal nitric oxide by lowering combustion temperatures.

Pd based noble metals have been reported as active catalysts for methane combustion. Besides high cost concerns, supported Pd catalysts usually deactivated by water vapor regardless of the type of the supports used, such as Pd/Al₂O₃,¹ Pd/SnO₂,² and Pd/ZrO₂.^{3,4} Most of the research works on metal oxides have been focussed on perovskite oxides⁵, only few studies have been devoted to single oxides such as Au, Ag, Fe, and Mn containing metal oxides partly because of their relatively easy deactivation by sintering. On the other hand, considering a great number of literatures on methane oxidation, inhibition by the reaction products, viz., CO₂ and water has not been given much attention.¹ It is recently found in our laboratory that the reaction activity of methane combustion on Co/Mn mixed oxides can be improved by the presence of water vapor at low temperatures.⁶

In this presentation, a series of Co/Mn Mixed Metal Oxides was prepared by a sol-gel process, and then the Ce modified Co-Mn oxides and the Co-Mn supported catalysts, Co-Mn/Al₂O₃-SiO₂, were prepared by homogeneous precipitation, respectively. The water effect on methane oxidation was investigated in an attempt to improve the thermal stability of these catalysts in the presence of water vapor.

Experimental

Synthesis of Co/Mn oxides. A citrate solution was added to a mixed aqueous solution of Mn(CH₃COO)₂·4H₂O and Co(NO₃)₂·6H₂O under strongly stirring conditions. 2M aqueous ammonia was slowly added to the above solution until the pH value reached 6.5-7.0. Subsequently, the above transparent solution was water bathed at 95 °C for 10 h and then dried at 120 °C for 12 h to obtain a gel powder, which was further calcined at 450 °C in nitrogen for 1 h and then in oxygen for next 2 h. The available powders were ready for the oxidation activity measurements after being crushed and sieved. The obtained metal oxide samples are denoted as MnOx, CoMn and CoMn₂, in which the subscript number stand for the molar ratio of Mn and Co in the samples.

Synthesis of cerium doped Co/Mn oxides and Co/Mn oxide supported catalysts. Cerium doped Co/Mn oxides were prepared in the similar procedure above except that urea was used to precipitate a mixed aqueous solution of Ce(NO₃)₃, Mn(CH₃COO)₂ and Co(NO₃)₂ at 120 °C in an autoclave. The resulting sample was then obtained after being washed by distilled water, dried at 120 °C and calcined at 450 °C or 850 °C for 2 h. The powder sample was denoted as Ce-CoMn, in which the molar ratio of Ce:Co:Mn is 0.1:0.9:1.

The Co/Mn supported catalyst was prepared from a mixed aqueous solution of Mn(CH₃COO)₂ and Co(NO₃)₂ and urea through adding an appropriate amount of Al₂O₃-SiO₂ (BET surface area is ca.

1000 m²/g) powders into the autoclave under the same procedure above. The obtained powder sample was denoted CoMn/SiAl, which contained 10 wt. % Co-Mn oxides with the molar ratio of Co to Mn as being 1:1.

Catalytic activity measurements Catalytic activities were measured in a fixed bed quartz tubular reactor. A gas mixture of CH₄ (0.5% by volume), O₂ (1.5% by volume) and argon was passed continuously through a 0.1 g catalyst sample bed with a total flow rate of 100 ml/min of argon. The inlet and outlet gas compositions were analyzed after stepwise changes in the reaction temperatures by on-line gas chromatograph.

Results and Discussion

Methane conversion was monitored between 300 °C and 800 °C. **Figure 1** shows methane conversion as a function of reaction temperature on the Co-Mn mixed oxides. It is observed that Co containing catalysts gave higher methane conversion than the bare Mn catalyst. The reaction activities at low temperatures followed the order of CoMn₂>CoMn>MnOx. For example, methane conversion at 400 °C in the absence of water vapor on CoMn₂, CoMn and MnOx was found to be 70%, 59% and 47%, respectively. When adding 5% water vapor into the reaction feed, methane conversion on MnOx was decreased in line with the previous report on Pd based catalysts. However, a remarkable increase in methane conversion was seen CoMn and CoMn₂ in presence of water vapor. It is shown that methane conversion at 500 °C on CoMn₂ was increased from 70% to 83% by the presence of 5% water vapor, and the value on CoMn was increased from 59% to 86% under the similar conditions. It was also noted that such a water enhancement effect became weak at high temperatures. The further work to understand the enhancement mechanism may help to develop a type of water-resistant catalysts for methane combustion.

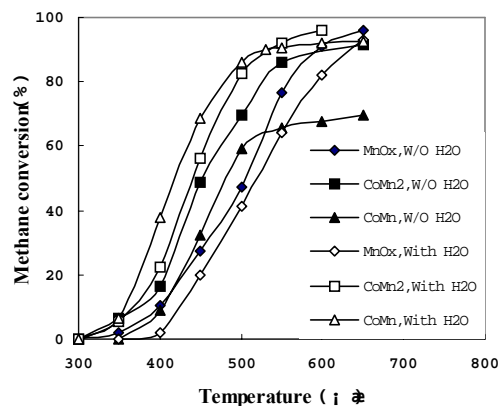


Figure 1. Methane conversion on Co/Mn mixed metal oxides calcined at 450 °C in the absence (solid symbols) and presence (open symbols) of water vapor.

In order to improve the thermal stability of the Co-Mn mixed oxides, cerium oxide was used to dope the catalyst. **Figure 2** shows methane conversion on Ce-CoMn calcined at 850 °C for 2 h. It was observed that a complete oxidation of methane occurred at 720 °C or higher on the cerium-doped catalyst as opposed to <10% of methane conversion on the catalyst without cerium, which indicates addition of cerium components can improve the thermal stability of the Co-Mn catalyst. Meanwhile, the enhancement of the reaction activity was also observed on Ce-CoMn in the presence of 5% water vapor.

A high surface area Al₂O₃-SiO₂ material was used as a

support for the Co-Mn oxide in an attempt to improve the thermal stability. The results were shown in **Figure 3**. As compared with the results on the CoMn sample in **Figure 1**, it can be seen that the reaction activities were improved on CoMn/SiAl in the absence or presence of water vapor, which might be related with the better dispersion of Co and Mn species on the support with a high specific surface area. Moreover, after the sample being calcined at 850 °C for 2 h, a similar water enhancement effect was still found on the CoMn/SiAl sample. For example, methane conversion at 700 °C reached ca. 100% in the presence of 5% water vapor as compared to the value of 74% in the absence of water vapor. Clearly, the thermal stability was improved after Co-Mn oxides being supported on an Al₂O₃-SiO₂ support.

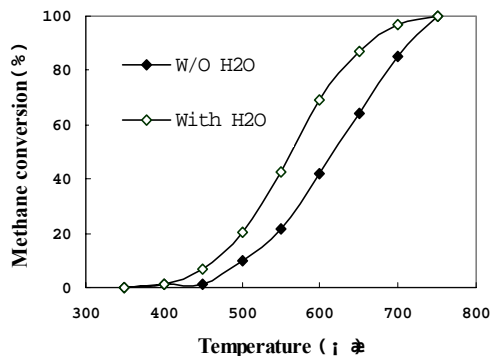


Figure 2. Methane conversion over Ce-CoMn calcined at 850°C.

Figure 4 shows the Changes in the catalyst activity of methane oxidation with time monitored at 500 °C in the presence of 5% water vapor over CoMn/SiAl calcined at 450 °C. It was demonstrated that methane conversion first slightly decreased from 96% to 89% after the reaction running for 1.5 h, and then the conversion was stabilized at ca. 85% for the next 24 h, which was indicating a better thermal stability in the presence of water vapor might be achieved by supporting Co-Mn components onto a support with a high surface area. An attempt to further improve thermal stability of the catalyst is in progress in our laboratory.

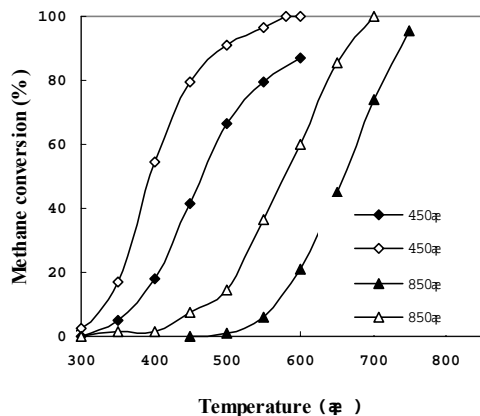


Figure 3. Methane conversion versus reaction temperature on CoMn/SiAl calcined at 450°C (diamonds) or 850°C (triangles) in the absence (solid symbols) or presence (open symbols) of water vapor.

In conclusion, a variety of Co/Mn mixed oxides has been

investigated in this presentation for catalytic oxidation of methane. The results showed that the catalytic activity was increased on Mn/Co mixed oxide catalysts by the presence of water vapor. The positive effect of water vapor was also observed after the Mn/Co oxide was doped with cerium oxide or supported on Al₂O₃-SiO₂, and the thermal stability of these catalysts was improved by these treatments to Mn/Co mixed oxides.

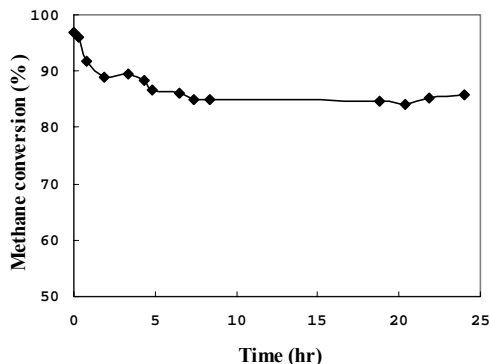


Figure 4. Methane conversion versus reaction time over CoMn/SiAl at 550 °C in presence of 5% water vapor.

Acknowledgment

This work was supported by the Basic Research Foundation of Tsinghua University (NO. JC1999009) and National Natural Science Foundation of China (NO. 29907003).

References

- 1 Van Giezen, J. C., Van den Berg, F. R., Kleinen, J., Van Dillen, L. A. J., Geus, J. W., *Catal. Today*, **1999**, *47*, 287.
- 2 Sekizawa, K., Widjaja, H., Machida, S., Ozawa, Y., Eguchi, K., *Appl. Catal. A: General*, **2000**, *200*, 211.
- 3 K. Nomura, K. Noro, Y. Nakamura, H. Yoshida, A. Satsuma, and T. Hattori, *Catal. Lett.*, **1999**, *58*.
- 4 K. Fujimoto, F. H. Ribeiro, M. Avalos-Borja, and E. Iglesia, *J. Catal.*, **1998**, *179*, 431.
- 5 T. Seiyama, *Catal. Review*, **1992**, *34*, 281.

CATALYTIC STABILITY OF NI CATALYST FOR PARTIAL OXIDATION OF METHANE TO SYNGAS

Li Zhenhua, Zhang Xiangyu, He Fei and Xu Genhui

State Key Lab of C₁ Chemistry and Technology, School of Chemical Engineering and Technology, Tianjin University, Tianjin 300072, P.R.China

Introduction

In recent years, catalytic partial oxidation of methane to synthesis gas (POM) attracted an extensive attention. Of the reported catalysts, supported Ni catalyst is a promising catalyst for POM industrial production since its high activity and low price^[1-4]. However, the catalytic stability of Ni catalyst is not so good as noble catalysts such as Rh or Pt. In this paper, 10% (wt%) Ni catalysts supported on 5 mm α -Al₂O₃, β -Al₂O₃ and γ -Al₂O₃ pellets were prepared by impregnation method. The catalytic activity and stability were measured in a continuous fixed bed reactor.

Experimental

A quartz tube of dimension of 5mm o.d.× 3 mm i.d. ×300mm length was used as a reactor. The catalyst loaded was 60 mg. High purity Argon was used as a carrier gas for GC analysis of inlet and outlet gas mixture. The conversion and selectivity were calculated from GC analysis results based on the C, H, O and N balance.

The specific surface area of the support and the catalyst before and after reaction were measured using a Pulse Chemisorption (CHEMBET-3000) Instrument. The catalyst amounts were 30 mg. The adsorption at liquid nitrogen and desorption at room temperature were recorded when partial pressure of N₂ in He is 0.1, 0.2 and 0.3 respectively.

XPS characterization has been done to analyze the carbon deposit and the dispersion of Ni on the support. XPS analyses employed a multi-pass analyzer (PHI 5600) with pass energy of 188 eV for survey spectra and 29 eV for high-resolution spectra. X-rays were generated using a Mg K α X-ray source.

Results and Discussion

Three catalysts were tested for POM process after reduced at 800 °C for 2 hours. As shown in Table 1, all catalysts exhibit good activity for POM process and 10% Ni/ β -Al₂O₃ catalyst shows the best activity. It can be seen that the catalytic activity and the product selectivity increase in the order of 10% Ni/ α -Al₂O₃< Ni/ γ -Al₂O₃< Ni/ β -Al₂O₃. The results were different from the reported results when the powder alumina was used. It was once reported^[5] that the 8% Ni/ α -Al₂O₃ is the best catalyst and the catalytic activity and the product selectivity increase in the order of 8% Ni/ γ -Al₂O₃<Ni/ β -Al₂O₃<Ni/ θ -Al₂O₃≈Ni/ α -Al₂O₃. It can be attributed to the differences of the support and the preparation method applied.

Table 1 Catalytic activities of 3 catalysts after reduced at 800 °C for POM process

Reaction condition Catalyst	O ₂ , N ₂ , CH ₄ flow rate: 19, 70, 38ml/min					O ₂ , N ₂ , CH ₄ flow rate: 37, 140, 74ml/min				
	X _{CH4} %	X _{O2} %	S _{CO} %	Y _{CO} %	H ₂ / CO	X _{CH4} %	X _{O2} %	S _{CO} %	Y _{CO} %	H ₂ / CO
10%Ni/ α -Al ₂ O ₃	50.64	98.80	75.72	38.30	2.03	62.42	98.59	82.75	51.67	2.02
10%Ni/ β -Al ₂ O ₃	69.33	98.59	82.85	57.45	2.08	73.57	98.59	87.21	64.18	2.05
10%Ni/ γ -Al ₂ O ₃	64.56	98.36	85.00	54.91	2.05	68.73	98.66	88.10	60.52	2.03

Note: reaction temperature: 650 °C, pressure: atmospheric pressure

Three catalysts were continuously tested for 100 hours at reaction temperature 700 °C and space velocity of 1.5×10⁵ hr⁻¹ with the molar ratio of CH₄:N₂:O₂=2:4:1. The results showed that the catalytic stability increases in the order of 10% Ni/ γ -Al₂O₃< Ni/ β -Al₂O₃< Ni/ α -Al₂O₃.

The above results indicated that the property of support alumina is a major factor of affecting the catalytic activity and stability. It is necessary to investigate this effect. The specific surface area of the

catalysts and the supports were measured and shown in Table 2. It was found that for 10% Ni/ β -Al₂O₃ and Ni/ γ -Al₂O₃ catalysts, the specific surface area decreased as the order of support>(the catalyst before reduced at 800 °C)>(the catalyst after reaction at 650 °C for 4 hrs). As for 10% Ni/ α -Al₂O₃ catalyst, its specific surface area has a little increase compared to that of the support.

Table 2 Specific surface area of the support and the 10% Ni catalysts

Catalyst	10% Ni/ α -Al ₂ O ₃			10% Ni/ β -Al ₂ O ₃			10%Ni/ γ -Al ₂ O ₃		
	1	2	3	1	2	3	1	2	3
specific surface area, m ² /g	8.6	11.9	10.8	71.3	47.0	43.8	251.1	107.6	66.2

Note: 1.support, 2.catalyst before reduction, 3.catalyst after reaction at 650 °C for 4 hrs

XPS characterization was done for three catalysts before reduction and after reaction at 700 °C for 100 hrs. The XPS spectra

for 10% Ni/ α -Al₂O₃ catalyst, which is similar with the spectra for the other two catalysts, was shown in Fig. 1.

The surface compositions for the three catalysts before reduction and after reaction at 700 °C for 100 hrs were determined by XPS and shown in Table 3. It was noted that the carbon on the 10%Ni/ α -Al₂O₃ and 10% Ni/ γ -Al₂O₃ catalysts before reduction are almost the same, which is about double the carbon on the 10% Ni/ β -Al₂O₃ catalyst. After these catalysts were reduced at 800 °C by hydrogen for 2 hrs and reacted at 700 °C for 100 hrs, the carbon deposits on the catalysts

all increased in the order of Ni/ α -Al₂O₃<Ni/ γ -Al₂O₃<10%Ni/ β -Al₂O₃. Combined with the 100 hrs POM reaction result, it is clear that the carbon deposit is a major factor resulting in the deactivation of Ni catalyst for POM process. The Ni atomic ratio data indicated that the dispersion of Ni on these three supports are different and may be another factor affecting the stability.

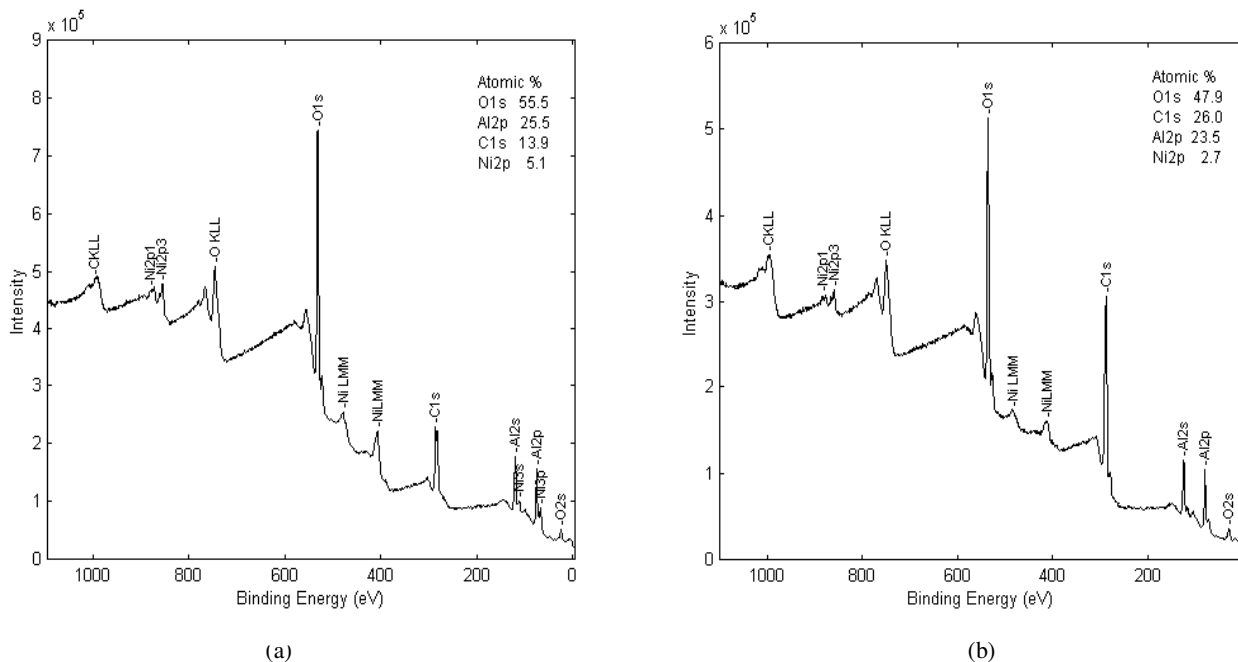


Figure.1 The XPS survey spectra for 10% Ni/ α -Al₂O₃ catalyst (a) before reduction; (b) after reaction at 700°C for 100 hrs.

Table 3 Surface compositions obtained from XPS for 3 catalysts

	Atomic ratio, %					
	10%Ni/ α -Al ₂ O ₃		10% Ni/ β -Al ₂ O ₃		10% Ni/ γ -Al ₂ O ₃	
	Before reduction	After reaction	Before reduction	After reaction	Before reduction	After reaction
O1s	55.5	47.9	59.7	49.2	56.3	44.1
Al2p	25.5	23.5	30.8	26.7	28.2	22.5
Ni2p	5.1	2.7	2.1	0.9	1.1	0.8
C1s	13.9	26.0	7.4	23.2	14.4	32.6

Conclusions

- (1) 10% Ni/ β -Al₂O₃ catalyst is better than 10%Ni/ α -Al₂O₃ and 10%Ni/ γ -Al₂O₃ catalysts considering both of the activity and stability.
- (2) The dispersion of Ni and the carbon deposit are the major factors affecting the catalytic activity and stability for POM process.

Acknowledgement. We appreciate the financial support from Chinese National Natural Science Foundation (No: 20106013) and State Key Laboratory of C₁ Chemical Technology of Tianjin University.

- (1) Ashcroft A T, Cheetham A K, Foord J S et al., *Nature(London)*, 1990, 344(6264)•319
- (2) Hickman D A, Schmidt L D, *J Catal*, 1992, 138(1)•267
- (3) Tornaiainen P M, Chu X, Schmidt L D, *J Catal.*, 1994, 146(1)•1
- (4) Zhenhua L., Xiangyu Zh., Xinbin M., *Huaxue Fanying Gongcheng Yu Gongyi(Chinese)*, In press
- (5) Lin Y., Shuhua Y., Jiuying T., et. al., *Chinese Journal of Catalysis*, 2001, 22(4)•383

References

Catalytic Tri-reforming of Methane Using Flue Gas from Fossil Fuel-based Power Plants

Wei Pan, Jian Zheng, Chunshan Song*

Clean Fuels and Catalysis Program, Energy Institute and
Department of Energy & Geo-Environmental Engineering,
The Pennsylvania State University, University Park, PA 16802
*Email: csong@psu.edu; Tel: 814-863-4466; Fax:814-865-3248

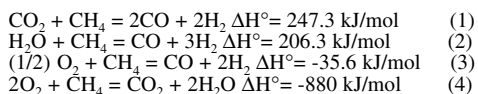
Introduction

The present work is an exploratory study on a new process for the production of synthesis gas ($\text{CO} + \text{H}_2$) using CO_2 in flue gas from fossil fuel-based electric power plants. The existing processes for synthesis gas production from methane or natural gas include steam reforming, CO_2 reforming, auto-thermal reforming, and partial oxidation, of methane or natural gas. The new process is called tri-reforming of methane, referring to simultaneous oxy- CO_2 -steam reforming.

Tri-reforming is a new process designed for the direct production of synthesis gas with desirable H_2/CO ratios by reforming methane or natural gas using flue gas from fossil fuel-based electric power plants without pre-separation of CO_2 . These flue gases are regarded as major source of CO_2 emission in the U.S. Generally the compositions of flue gases depend on the types of fossil fuels used in power plants. Flue gases from natural gas-fired power plants typically contain 8-10% CO_2 , 18-20% H_2O , 2-3% O_2 , and 67-72% N_2 ; flue gases from coal-fired boilers primarily contain 12-14% CO_2 , 8-10% H_2O , 3-5% O_2 , 72-77% N_2 , and trace amount of NO_x , SO_x , and particulates [1].

It is hypothesized that tri-reforming be a synergetic combination of CO_2 reforming (Eq.1), steam reforming (Eq. 2), and methane oxidation reactions (Eqs. 3 and 4). Therefore, tri-reforming is expected to encompass a number of unique features. One major feature is its ability to convert CO_2 in flue gas without CO_2 separation while avoiding the use of pure CO_2 and the severe problem of carbon deposition encountered in CO_2 reforming system [2-6]. Currently most of pure CO_2 is obtained from CO_2 separation processes (e.g. absorption, adsorption, and membrane separation) that are often energy-intensive and costly. Some separation processes could lower the power plant energy output as much as 20% [7].

Other features of tri-reforming include that there is no need to handle pure oxygen and it directly produces synthesis gas with a desirable H_2/CO ratio (e.g. $\text{H}_2/\text{CO} = 1.5 \sim 2$). Furthermore, oxygen in flue gas may help to ease the reaction energy requirement as encountered in CO_2 reforming alone or steam reforming alone. In general, the new tri-reforming process concept is consistent with the goals of DOE Vision 21 for power plants with respect to decreasing greenhouse gas emission, improving power generation efficiency and co-producing fuels and chemicals [8].



It should be pointed out that the H_2/CO ratio in synthesis gas is important since synthesis gas with different H_2/CO ratios has different applications in industry. The current major applications of synthesis gas (not hydrogen) include methanol synthesis and Fischer-Tropsch (F-T) synthesis that require synthesis gas with a H_2/CO ratio close to 2. However, synthesis gas directly produced from CO_2 reforming of methane has H_2/CO ratio close to 1. Hence this kind of synthesis gas (H_2/CO ratio ≤ 1) requires further treatment in order to be applied in methanol and F-T synthesis.

Similarly synthesis gas produced from steam reforming can not be directly applied in methanol or F-T synthesis either since the H_2/CO ratio of synthesis gas produced from steam reforming is usually larger than 3. Although methane partial oxidation produces synthesis gas with a H_2/CO ratio of 2, methane partial oxidation is difficult to control due to its exothermic feature and is dangerous and expensive due to the handling of pure oxygen. Tri-reforming, however, is expected to readily produce synthesis gas with the desired H_2/CO ratios of 1.5 ~ 2 by manipulating tri-reforming reactant compositions under relatively mild reaction conditions.

Unlike steam reforming, CO_2 reforming, or methane partial oxidation, tri-reforming has not been systematically studied. The concept of tri-reforming using power plant flue gas was first proposed by Song in 1999 [1,9]. Before 1999, several papers were published on the study of combined CO_2 reforming and partial oxidation reaction [10-12] and simultaneous steam and CO_2 reforming of methane in the presence of oxygen [13]. The results in these papers have indicated that combined reforming is feasible. However, the new tri-reforming process still faces a number of challenges. The future challenges include, for example, effective conversion of CO_2 in the presence of O_2 and H_2O ; the heat management; the minimization of the effect of SO_x and NO_x in flue gas on tri-reforming process; the management of inert gas N_2 in flue gas; and the integration of new process into power plants. The tasks in the current work of tri-reforming include the computational study of equilibrium properties of tri-reforming at various feedstock compositions and reaction conditions, the design of operation parameters, and the development of catalysts tailored for tri-reforming. In a real tri-reforming reaction, steam, CO_2 , and O_2 all compete to react with methane over catalysts. Improvement of CO_2 conversion in the presence of steam and O_2 would depend on the catalysts and reaction conditions.

Experimental

Computational Analysis. The theoretical analysis was based on thermodynamic calculations. The purpose of this analysis is to establish thermodynamic equilibrium conversions of reactants, equilibrium product distributions under different reaction conditions (such as feedstock compositions, temperatures, and pressures) in tri-reforming reaction system.

The equilibrium compositions were calculated based on the principle of atom and mass balance and Gibbs Energy Minimization Method (GEMM). Before calculation, it was critical to identify stable reactants and products in the reaction system. The calculation employed HSC Chemistry software developed by Outokumpu Research Oy, Finland.

Catalyst preparation. Catalysts studied in this work included 8 wt% Ni and 2 wt% Pt catalysts supported on Ce-Zr oxides with or without CaO or MgO promoters. Ce-Zr oxides were prepared according to the method of "soft chemistry" [14]. Zirconium n-propoxide ($\text{Zr}(\text{OC}_3\text{H}_7)_4$) dissolved in 20 ml of isopropyl alcohol was gradually added into an aqueous solution (20ml) of $\text{Ce}(\text{NO}_3)_2 \cdot 6\text{H}_2\text{O}$, leading to the immediate hydrolysis and the formation of a pseudo gel. The pseudo gel was dried at 60°C for 1 h and then at 120°C overnight. The dried sample was finally calcined in air at 870°C for 4 h and ready for use as a support.

Ni and Pt catalysts supported on Ce-Zr oxides were prepared by wet impregnation. $\text{Ni}(\text{NO}_3)_2 \cdot 6\text{H}_2\text{O}$ or $\text{Pt}(\text{NH}_3)_4\text{Cl}_2 \cdot x\text{H}_2\text{O}$ (MW = 334.12) was dissolved in 5 ml of H_2O . Ce-Zr oxide powder was then added into the solution under stirring. The mixture was dried at 60°C overnight, followed by calcination at 870°C for 4 h. The calcined sample was then pressed into disks and crushed and sieved. The particles between 18-35 meshes were collected for use

in reaction test. When preparing MgO or CaO promoted catalysts, $\text{Ca}(\text{NO}_3)_2 \cdot 4\text{H}_2\text{O}$ or $\text{Mg}(\text{NO}_3)_2 \cdot 6\text{H}_2\text{O}$ was dissolved in the same solution as $\text{Ni}(\text{NO}_3)_2$ or $\text{Pt}(\text{NH}_3)_4\text{Cl}_2$ and followed the same procedures as described above.

Tri-reforming experiments. The tri-reforming reaction was studied in a fixed-bed reactor at 850°C under 1 atm. The reactor was made of an Inconel 800H alloy tube with the dimension of 0.54" o.d., 0.375" i.d., and 16" in length. In each tri-reforming, about 0.1 g of catalyst sample was placed in the middle section of the reactor. The reactor was interfaced with GC by a ten-port gas sampling valve, which enables online product analysis. The GC included a packed silica gel column, a molecular sieve column, and a TCD detector. Before each reaction the catalyst was reduced in H_2 following the temperature program: keeping the reactor temperature at 100°C for 15 minutes, at 450°C for 75 minutes, and at 850°C for 10 minutes with a temperature ramp of 12°C/min. Then H_2 was stopped and the reactor temperature was kept at 850°C under Ar flow for another 20 minutes. Steam was first introduced into the reactor. After 20 minutes of steam flow (0.02ml(1)/min), CH_4 , CO_2 , and O_2 were then introduced into the reactor. The flow rates of CH_4 , CO_2 , and O_2 were maintained by mass flow controllers (Brooks Instruments Corporation, USA); steam flow was controlled by an ISCO liquid pump. The reaction effluent except steam was analyzed by an on-line GC in every 30 minutes during a time-on-stream (TOS) period of 300 minutes. Steam was condensed before the GC.

Results and Discussion

It is expected that steam reforming, CO_2 reforming, and methane oxidation take place simultaneously in tri-reforming system. Table 1 compares equilibrium methane conversions, CO_2 and steam conversions, and H_2/CO ratios in steam reforming, CO_2 reforming, and combined CO_2 and steam reforming with the $(\text{CO}_2+\text{H}_2\text{O})/\text{CH}_4$ ratio of 1. When steam is gradually replaced by CO_2 , H_2/CO ratios in products decrease monotonically from 3.06 in steam reforming to 1.03 in CO_2 reforming at 850°C and 1 atm while methane conversions and CO_2 conversions have only minor changes.

Table 1. Equilibrium H_2/CO Ratios and Equilibrium Conversions of Methane, Steam, and CO_2 at 850°C and 1 atm

	CH_4 Conv. (%)	CO_2 conv. (%)	Steam conv. (%)	H_2/CO ratio
$\text{CH}_4:\text{H}_2\text{O}:\text{CO}_2$ =1:1:0	94.0	-	95.4	3.06
$\text{CH}_4:\text{H}_2\text{O}:\text{CO}_2$ =1:0.75:0.25	94.9	91.3	93.1	2.25
$\text{CH}_4:\text{H}_2\text{O}:\text{CO}_2$ =1:0.5:0.5	95.8	93.7	88.7	1.66
$\text{CH}_4:\text{H}_2\text{O}:\text{CO}_2$ =1:0.25:0.75	96.6	94.3	76.4	1.32
$\text{CH}_4:\text{H}_2\text{O}:\text{CO}_2$ =1:0:1	97.4	95.0	-	1.03
$\text{CH}_4:\text{H}_2\text{O}:\text{CO}_2:\text{O}_2$ =1:0.475:0.475:0.1	97.9	87.0	77.0	1.67
$\text{CH}_4:\text{H}_2\text{O}:\text{CO}_2:\text{O}_2$ =1:0.45:0.45:0.2	99.0	75.2	56.0	1.69
$\text{CH}_4:\text{H}_2\text{O}:\text{CO}_2:\text{O}_2$ =1:0.375:0.375:0.5	99.8	28.4	-29.0	1.71
$\text{CH}_4:\text{H}_2\text{O}:\text{CO}_2:\text{O}_2$ =1:1:1:0.1	99.8	53.1	26.7	1.48

The calculation also predicts a decrease of steam conversions with increasing CO_2 and O_2 concentrations in the feed.

When O_2 is introduced, the ratio of $(\text{CO}_2+\text{H}_2\text{O}+0.5\text{O}_2)/\text{CH}_4$ is kept at 1 for comparison with steam reforming, CO_2 reforming,

and combined reforming (Table 1). Although both CO_2 and steam conversions decrease with O_2 concentrations in the tri-reforming system, steam conversions decrease more dramatically than CO_2 conversions. This may be contributed to the reverse water gas shift reaction at high temperatures. Methane conversions only have a slight increase (close to 100%) with the increase of O_2 and a constant H_2/CO ratio is predicted with the addition of O_2 .

When the same amount of CO_2 and H_2O is present in tri-reforming as in the cases of $\text{CH}_4:\text{CO}_2:\text{H}_2\text{O}:\text{O}_2=1:0.475:0.475:0.1$ and $\text{CH}_4:\text{CO}_2:\text{H}_2\text{O}:\text{O}_2=1:1:1:0.1$ (Table 1), CO_2 show higher equilibrium conversions (87% and 53.1%, respectively) than the steam conversions (77% and 26.7%, respectively).

Although thermodynamic analysis predicts CO_2 is more preferably converted than steam when same amounts of CO_2 and steam are present in tri-reforming system, one of the major challenges in the study of tri-reforming is the development of new catalysts that are able to efficiently convert CO_2 in the presence of H_2O and O_2 . We have prepared and tested a number of Ni and Pt-based catalysts. Some of the preliminary results are listed in Table 2.

Table 2. Experimental Results of Tri-reforming at 850°C and 1 atm ($\text{CH}_4:\text{CO}_2:\text{H}_2\text{O}:\text{O}_2=1:1:1:0.1$)

	CH_4 Conv. (%)	CO_2 conv. (%)	H_2/CO ratio
8%Ni/Ce-Zr-O	77.0	26.9	1.60
8%Ni/CaO/Ce-Zr-O	86.2	36.6	1.48
8%Ni/MgO/Ce-Zr-O	89.1	38.8	1.49
2%Pt/Ce-Zr-O	80.4	36.2	1.44
2%Pt/CaO/Ce-Zr-O	64.5	26.5	1.52
2%Pt/MgO/Ce-Zr-O	83.5	32.7	1.57
Equilibrium values	99.8	53.1	1.48

Note: all the experimental data in this table are average values during TOS of 300 minutes.

These experimental results show that CaO and MgO promote methane and CO_2 conversions over Ni-based catalysts although methane and CO_2 conversions over these catalysts are still lower than those predicted from thermodynamic analysis. On the contrary, CaO and MgO in Pt-based catalyst lower CO_2 conversions. These results indicate that catalysts still play an important role in tri-reforming. More catalysts are under investigation.

Conclusions

Equilibrium properties of tri-reforming under different conditions were analyzed by thermodynamics. O_2 in tri-reforming system could lead to the decrease of both CO_2 and steam conversions. CO_2 usually has a higher equilibrium conversion than steam when same amounts of steam and CO_2 co-exist in tri-reforming.

To achieve higher CO_2 conversions in catalytic tri-reforming of methane, a tailored catalyst for tri-reforming is desired.

Acknowledgement. The authors are grateful for the financial support from National Energy Technology Laboratory, US DOE (UCR Innovative Concepts Program, DE-FG26-00NT40829) and Department of Energy and Geo-Environmental Engineering (Graduate assistantship to WP) at Penn State University.

References

- (1) Song, C. Tri-reforming: A new process for reducing CO₂ emission. *Chemical Innovation*. **2001**, 31(1), 21-26.
- (2) Rostrup-Nielsen, J. R. Aspects of CO₂-reforming of Methane. *Studies in Surface Science and Catalysis - Natural Gas Conversion II*; Curry-Hyde, H. E. ; Howe, R.F. Elsevier: Amsterdam, **1994**; 81, 25-41.
- (3) Rostrup-Nielsen, J. R.; Bak Hansen, J. H. CO₂-reforming of methane over transition metals. *J. Catal.* **1993**, 144,38-49.
- (4) Wang, S.; Lu, G. Q. M. Carbon dioxide reforming of methane to produce synthesis gas over metal-supported catalysts: State of art. *Energy & Fuels* **1996**, 10(4), 896-904.
- (5) Bradford, M. C. J.; Vannice, M. A. CO₂ reforming of CH₄. *Catal. Rev.Sci. Eng.* **1999**, 40(1), 1-42.
- (6) Tomishige, K.; Himeno, Y.; Yamazaki, O.; Chen, Y.; Wakatsuki, T.; Fujimoto, K. Development of a New Generation Reforming Catalyst: Catalytic Performance and Carbon Deposition Behavior on Nickel-Magnesia Catalysts. *Kinet. and Catal.* **1999**, 40(3), 432-439.
- (7) DOE/FE . *Capturing Carbon Dioxide*. Office of Fossil Energy, U.S. Department of Energy, Washington, D.C., **1999**;
- (8) FETC (Federal Energy Technology Center). *Vision 21 Program Plan - Clean Energy Plants for the 21st Century*. Office of Fossil Energy, U.S. Department of Energy, Washington, D.C., **1999**;
- (9) Song, C. Chemicals, fuels and electricity from coal. A proposed tri-generation concept for utilization of CO₂ from power plants. *16th International Pittsburgh Coal Conference*, Pittsburgh, USA, **1999**; Paper No., 16-6.
- (10) Ashcroft, A. T.; Cheetham, A. K.; Green, M. L. H.; Vernon, P. D. F. Partial Oxidation of Methane to Synthesis Gas Using Carbon Dioxide. *Nature* **1991**, 352(6332), 225-226.
- (11) Inui, T.; Saigo, K.; Fujii, Y.; Fujioka, K. Catalytic combustion of natural gas as the role of one-site heat supply in rapid catalytic CO₂-H₂O reforming of methane. *Catal. Today* **1995**, 26(3/4), 295-302.
- (12) O' Connor, A. M.; Ross, J. R. H. The effect of O₂ addition on the carbon dioxide reforming of methane over Pt/ZrO₂ catalysts. *Catal. Today* **1998**, 46,203-210.
- (13) Choudhary, V. R.; Rajput, A. M.; Prabhakar, B. NiO/CaO-catalyzed formation of syngas by coupled exothermic oxidation conversion and endothermic CO₂ and steam reforming of methane. *Angewandte Chemie* **1994**, 33(20), 2104-2106.
- (14) Rossignonol, S.; Madier, Y.; Duprez, D. Preparation of zirconia-ceria materials by soft chemistry. *Catal. Today* **1999**, 50, 261-270.

CO₂ AND CO METHANATION OVER TWO DIFFERENT NICKEL LOADING Ni/TiO₂ CATALYSTS

Changwei Hu*, Dong-mei Tong

Faculty of Chemistry
Sichuan University
Chengdu, 610064, China

Introduction

Ni-based catalysts can catalyze the methanation of both CO and CO₂. Adsorbed carbon species C(a) and CO(a) formed in CO methanation on nickel can be transformed into CH₄ through the same way as those in CO₂ methanation¹. It is also found that different active phases which exhibit different methanation activities for CO with CO₂ can form on Ni/Al₂O₃ catalysts under different activation conditions². TiO₂ supported metal catalyst is typical to exhibit strong metal-support interaction, and the methanation of CO on Ni/TiO₂ is widely studied. However, the methanation of CO₂ on Ni/TiO₂ as well as the effect of treatment under reaction conditions on the structure and properties of Ni/TiO₂ has rarely been studied. In present work, two different nickel loading Ni/TiO₂ catalysts are used to study comparatively the methanation of CO and CO₂. The structure and properties changes of the samples under thermal treatment in CO+H₂ and CO₂+H₂ ambience are also studied.

Experimental Section

The catalysts were prepared by wet impregnation on which the amount of the nickel loading was controlled by concentration of nickel nitrate solution. The amount of nickel loading on the two catalysts was 3.53mass% and 9.31mass%, and named catalyst-1 and catalyst-2 respectively. Hydrogen adsorbance on reduced catalysts was detected by pulse chromatographic technique^{2,3}. Methanation experiments were carried out in a fixed-bed quartz reactor with the same method described previously². Catalysts were activated stepwisely at 523K, 573K, 673K and 723K under CO₂+H₂ mixture, and then switched to CO+H₂ mixture. Another cycle was carried out first in CO+H₂ mixture, and then in CO₂+H₂ mixture.

Results and Discussion

Catalyst-1 can be activated at 573K under CO₂+H₂ mixture to show CO₂ methanation activity. High temperature(723K) destroys the active phase formed at low temperature(523K) because CO₂ methanation activity at low temperature over the catalyst activated at 723K is lower than that when activated at 523K, as shown in **Figure 1(I)**. The active phase formed at 723K in CO₂+H₂ flow shows low activity of CO methanation. The same fresh sample does not show CO methanation activity (about 3.4μmol/min•g) until activated at 723K in CO+H₂ ambience, and the active phase thus formed cannot catalyze CO₂ to form CH₄. It suggests that the active phase formed in CO₂+H₂ ambience at 723K can catalyze CO methanation, but the active phase formed in CO+H₂ ambience at 723K cannot show CO₂ methanation activity. In another word, CO₂ and CO methanation can proceed on different active phases.

The results obtained over catalyst-2 for CO₂ and CO methanation are shown in **Figure 2**, they are similar to those on catalyst-1. Catalyst-2 can be activated at lower temperature(523K) to show methanation activity than catalyst-1 in CO₂+H₂ ambience. It is attributed to the high nickel loading. When the same sample is activated first under CO+H₂ ambience, then switched to CO₂+H₂

mixture, the similar phenomenon to catalyst-1 is observed. It also suggests that CO₂ and CO methanation can be catalyzed by different active phases formed on nickel loading Ni/TiO₂ catalyst.

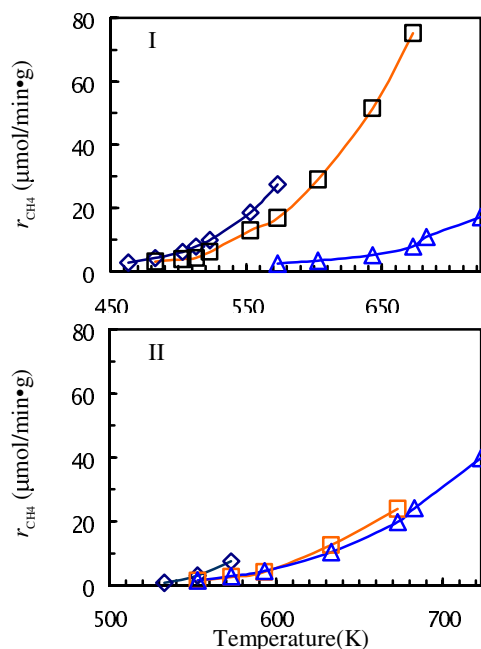


Figure 1. The methanation activity in terms of the formation of CH₄ on catalyst-1 activated under CO₂ +H₂ mixture(I), then switched to CO+H₂ mixture(II) at ◊573K, ◻673K, ◻723K.

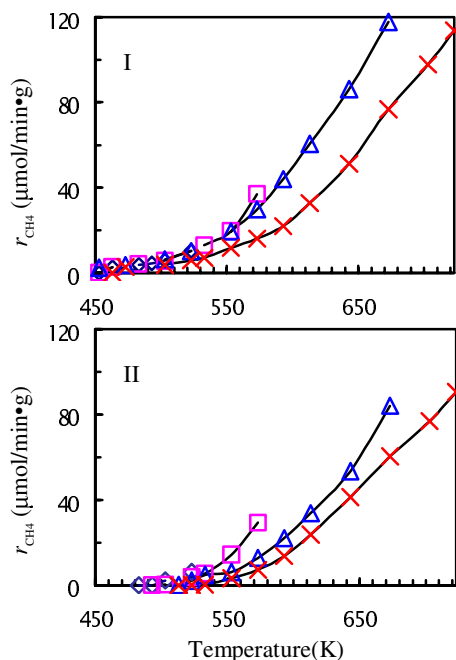


Figure 2. The methanation activity in terms of the formation of CH₄ on catalyst-2 activated under CO₂ +H₂ mixture(I), then switched to CO+H₂ mixture(II) at ◊523K, ◻573K, ◻673K, ◻723K.

* Corresponding author. E-mail:chewhu@mail.sc.cninfo.net

Hydrogen adsorbance at room temperature on catalyst-1 decreases with reduction temperature, while it increases with reduction temperature on catalyst-2, as shown in **Table 1**. It indicates that the initiation of strong metal-support interaction at low temperature(573K) on low nickel loading catalyst is more easier than on high nickel loading catalyst, and the SMSI is affected by the nickel loading. The results of the hydrogen adsorbance could be compared with the results of methanation, it is seen that SMSI is one of the reasons for the methanation activities to decrease when the catalysts are activated at high temperature. The phenomenon could be explained by electronic effect, the extent of electron transfer from support to a small metal particle is much easier than that to a large one⁴.

Table 1. The hydrogen adsorbance at room temperature over catalysts after reduction at different temperature.

reduction temperature (K)		523	573	673	723
H ₂ adsorbance (mol/gcatal.)	catalyst-1	0.0344	0.0333	0.0209	0.0081
	catalyst-2	0.0123	0.0172	0.0206	0.0215

Conclusion

The active phase formed in CO₂+H₂ ambience can catalyze CO methanation, but the active phase formed in CO+H₂ ambience cannot show CO₂ methanation activity on nickel loading Ni/TiO₂ catalyst. CO₂ and CO methanation can be catalyzed by different active phases. A Ni/TiO₂ catalyst with a low nickel loading can fall into SMSI state more easily than that with a higher one.

Acknowledgment

The authors are grateful for the financial support by the Special Research Foundation of Doctoral Education of China (No. 2000061028) and the Foundation of Science and Technology of Sichuan Province (No. 200018-16).

References

1. Shin-ichiro Fujita, Hiroyuki Terunuma, Masato Nakamura, and Nobutsune Takezawa, *Ind. Eng. Chem. Res.* 1991,30,1146-1151.
2. Chang-Wei Hu, Jie Yao, Hua-Qing Yang, Yu Chen, and An-Min Tian, *J.Catal.*,1997, 166,1
3. Wang Hua-Ming, Lu Quan-Jie, Zhou Xue-Kai, *Huaxue Tongbao*, 1987,(1),30-32.
4. Di Li, Nobuyuki Ichikuni, Shogo Shimazu, and Takayoshi Uematsu, *Appl.Catal.A:General*, 1999, (180), 227-235.

CO₂ hydrogenation over copper-based hybrid catalysts for the synthesis of oxygenates

Young-Kwon Park, Se-Won Baek and Son-Ki Ihm*

National Research Laboratory for Environmental Catalysis,
Dept. of Chem. Eng., Korea Advanced Institute of
Science and Technology
373-1 Kusong-dong, Yusong-gu, Taejeon 305-701, Korea
Tel : +82-42-869-3915, FAX : +82-42-869-5955
e-mail : skihm@mail.kaist.ac.kr

1. Introduction

Catalytic hydrogenation of CO₂ has been recently attracting considerable attention as one of the chemical fixation and recycling technologies for emitted CO₂. DME is a useful building block for making important chemicals, including dimethyl sulfate and high-valued oxygenated compounds. DME can easily be obtained through dehydration of methanol over solid acids[1], while methanol is commercially manufactured from syngas by using Cu-based catalysts. In this regard many investigations have been made on the combination of the methanol synthesis and methanol conversion process in a single step by using hybrid catalysts to obtain hydrocarbons or oxygenates directly either from syn-gas or from CO₂[2-5]. However, methanol synthesis from CO₂ hydrogenation has a severe limitation of thermodynamic equilibrium compared with that from CO hydrogenation. To overcome such a limitation, *in situ* transformation of methanol to dimethyl ether(DME) is a reasonable way to improve the total oxygenates yield (methanol + DME). However, very few studies were made on the direct synthesis of DME from CO₂ hydrogenation, while Dubois et al.[2] demonstrated that combination of Cu-based catalyst with a solid acid, which enhanced the DME formation, really provided a strong driving force for CO₂ conversion. In the present work, hybrid catalysts made of Cu-based methanol synthesis catalyst and a zeolite were used for the direct formation of oxygenates(methanol + DME) from CO₂ hydrogenation, and the catalytic behaviors were investigated in terms of their reducibility and oxygen coverage.

2. Experimental

Catalyst preparation Cu/ZnO based catalysts were prepared by co-precipitation. ZSM-5 was obtained through a three day hydrothermal synthesis at 170°C in a Teflon-lined 450ml Parr bomb by following the procedures in a US patent [3]. H-Ga-Silicate were synthesized according to the procedure similar to that of HZSM-5 except that Al source was substituted with Ga nitrate. SAPO-34 was hydrothermally prepared from reactive gels containing a silicon source (Ludox HS-30), an aluminum source (pseudoboehmite), phosphoric acid, morpholine and water [4]. Hybrid catalysts were prepared by physically mixing equal weight of a copper based catalyst and a zeolite.

Catalyst characterization The exposed copper surface area was measured by titration with nitrous oxide. The copper surface area (Cu_{react}) of used catalyst after 1hr of reaction was measured first, and the total copper surface area (Cu_{total}) was obtained from the same catalyst after complete reduction of copper. The oxygen coverage was calculated by the following equation [5] : $\theta_{\text{O}} = (\text{Cu}_{\text{total}} - \text{Cu}_{\text{react}}) / (\text{Cu}_{\text{total}} \times 2)$.

Temperature programmed reduction (TPR) was performed to determine the reduction temperature peak of catalyst. And Temperature programmed desorption(TPD) measurements by using ammonia as an adsorbate were carried out to determine the acidic properties of zeolites.

Catalytic activity for the synthesis of DME Carbon dioxide hydrogenation was performed in a continuous-flow fixed bed microreactor system made of a stainless-steel tube. In a typical experiment, 1.0g of hybrid catalyst was loaded in the reactor. It should be noted that the amount of Cu-based catalyst in the hybrid catalyst was 0.5g. After the catalyst bed was reduced with hydrogen at 280 °C, the reactor was pressurized to 28atm with helium, and CO₂ and H₂ were introduced into the reactor. CO₂ hydrogenation products were passed through a heated transfer line to a gas chromatograph with TCD and FID detectors.

3. Results and Discussion

In our previous work, it was found that Cu/ZnO/ZrO₂ and Cu/ZnO/Ga₂O₃ showed higher methanol yields. It was previously reported [5, 6] that ZrO₂ improved the dispersion of Cu, and that Ga₂O₃ increased the specific activity by optimizing the ratio of Cu¹⁺/Cu⁰ on the surface of Cu particles. Since it is believed that Cu¹⁺ species plays an important role in methanol synthesis [5], the optimization of the ratio Cu¹⁺/Cu⁰ should be made for high yield of methanol. Table 1 shows the results of oxygenates synthesis from CO₂ hydrogenation over different hybrid catalysts. It can be seen that the catalysts including different zeolites had different catalytic activities. The activity of hybrid catalyst with NaZSM-5 was the lowest among hybrid catalysts due to its weakest acidity. To convert methanol into DME, moderate acidity rather than weak acidity is preferable. The hybrid catalyst from Cu/ZnO/ZrO₂ and H-Ga-silicate showed the highest yield of oxygenates. Even if Cu/ZnO/Ga₂O₃ showed a good activity for methanol synthesis, its hybrid counterpart showed a lower activity for oxygenates and a higher selectivity for CO. The temperature at which the maximum of TPR curve is located (defined as peak temperature) could be a measure of reducibility or the degree of interaction, and the peak temperatures are listed in Table 2. It can be seen that the peak temperature of the original methanol synthesis catalysts changed through hybridization with zeolite. Some interactions between methanol synthesis catalyst and zeolite might modify the properties of each component in the hybrid catalyst such as the reducibility of methanol synthesis catalyst and the acidity of zeolite. The peak temperatures of hybrid catalysts were found to be higher than that of the original methanol synthesis catalysts such as Cu/ZnO/ZrO₂ or Cu/ZnO/Ga₂O₃. The increase in the peak temperature for the hybrid catalyst containing Cu/ZnO/ZrO₂ was rather small (about 20°C), while that for the hybrid catalyst with Cu/ZnO/Ga₂O₃ was quite large (about 60°C). This difference in the peak temperature seems to be related with the ability of oxygenate synthesis. Saito et al. [5] suggested that oxygen coverage is a measure of Cu¹⁺/Cu⁰ ratio and that the specific activity increased linearly with

Table 1. Comparison of different types of hybrid catalysts for oxygenates synthesis

Catalyst	Conv. (%)	Selectivities (wt%)			Yield of Oxygenates (wt%)
		CO	MeOH	DME	
A + NaZSM-5	15.4	50.6	19.5	29.9	7.6
A + HZSM-5	17.2	42.4	22.7	34.9	9.9
A + H-Ga-silicate	19.0	33.7	21.0	45.3	12.6
A + SAPO-34	17.5	44.0	21.1	34.9	9.8
B + NaZSM-5	18.2	73.0	10.5	16.5	4.9
B + HZSM-5	19.1	68.6	12.0	19.4	6.0
B + H-Ga-silicate	19.4	67.2	12.9	19.9	6.4
B + SAPO-34	19.6	67.9	12.7	19.4	6.3

Reaction conditions : 28 atm, 250°C, W/F = 20g-cat•hr/mol, H₂/CO₂ = 3
A : Cu/ZnO/ZrO₂(6:3:1), B : Cu/ZnO/Ga₂O₃(6:3:1)

Table 2. TPR peak temperatures and oxygen coverages

Catalyst	A	A + NaZSM-5	A + HZSM-5	A + H-Ga-silicate	A + SAPO-34
Peak temp. (°C)	280 (•0)	300 (•20)	300 (•20)	289 (•9)	300 (•20)
Oxygen coverage	0.21	0.24	0.24	0.19	0.24
Catalyst	B	B + NaZSM-5	B + HZSM-5	B + H-Ga-silicate	B + SAPO-34
Peak temp. (°C)	250 (•0)	310 (•60)	310 (•60)	310 (•60)	310 (•60)
Oxygen coverage	0.15	0.30	0.30	0.30	0.30

A : Cu/ZnO/ZrO₂(6:3:1), B : Cu/ZnO/Ga₂O₃(6:3:1)

the coverage below 0.16, reached a maximum at 0.17 and then decreased above 0.18. As shown in Figure 1, the oxygen coverage of hybrid catalysts with Cu/ZnO/Ga₂O₃ (data point 7,8,9 and 10) were much larger than that of original Cu/ZnO/Ga₂O₃ i.e., (0.15) and their oxygenate yields were smaller. If the optimum oxygen coverage is 0.15, the higher oxygen coverage of hybrid catalysts with Cu/ZnO/Ga₂O₃ may indicate that the hybridization made copper components less active and resulted in poor yield of oxygenates. Among hybrid catalysts with Cu/ZnO/ZrO₂, the hybrid catalyst containing H-Ga-silicate (data point 4) showed the highest yield of oxygenates probably due to weak interaction. Its oxygen coverage (0.19) was also not much different from that(0.15) of Cu/ZnO/Ga₂O₃. The Ga oxide inside the pore of H-Ga-silicate seems to make Cu species in the hybrid catalyst more active by balancing the ratio Cu¹⁺/Cu⁰. Table 3 shows that the increase of calcination temperature resulted in higher yield of oxygenates because the larger amount of Ga oxide, formed inside the pore, optimized the oxygen coverage. It is preferable to use H-Ga-silicate as a Ga source rather than Cu/ZnO/Ga₂O₃ to regulate the Cu ion state for a higher production of oxygenates. Another kind of interaction, i.e., acidity modification, seems to be more beneficial for hydrocarbon synthesis, while not good for oxygenates synthesis. The hybrid catalyst with SAPO-34 or HZSM-5 which had higher acid amount due to solid-solid interaction showed a poor yield of oxygenates but a higher yield of hydrocarbons than that with H-Ga-silicate [7]. It is believed that the reducibility should affect the synthesis of oxygenates and that the acidity should influence the hydrocarbon synthesis. The moderate acidity of H-Ga-silicate seems to be sufficient for oxygenate synthesis. Figure 2 shows the effect of mixing ratio on the yield of oxygenates over the hybrid catalyst from Cu/ZnO/ZrO₂ and H-Ga-silicate. It can be seen that the hybrid catalysts with low fraction of zeolite showed better yield for oxygenates. It was reported that for DME synthesis the rate limiting step is methanol formation [8], and accordingly it is desirable to increase the weight fraction of methanol synthesis catalyst. Relatively small amount of acid sites were sufficient to convert methanol into DME because the rate of dehydration due to H-Ga-silicate is much faster. Campbell et al. [9] showed that only a small active site concentration was necessary for HZSM-5 to be an efficient and effective methanol conversion catalyst.

Table 3. Effect of calcination temperature of H-Ga-silicate on oxygenates yield

Calcination temperature(°C)	550	600	650
Oxygenates yield* (Oxygen coverage)	12.6 (0.19)	13.4 (0.18)	13.8 (0.16)

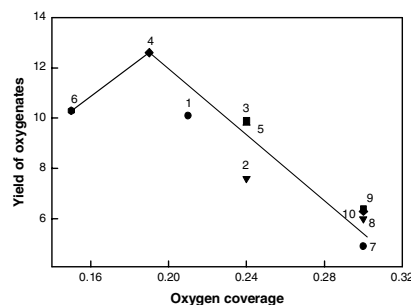


Figure 1. Yield of oxygenates vs. oxygen coverage; 1: CuO/ZnO/ZrO₂ (A), 2:A+NaZSM-5, 3:A+HZSM-5, 4:A+Ga-silicate, 5:A+SAPO-34, 6: CuO/ZnO/Ga₂O₃(B), 7:B+NaZSM-5, 8:B+HZSM-5, 9:B+Ga-silicate, 10:B+SAPO-34

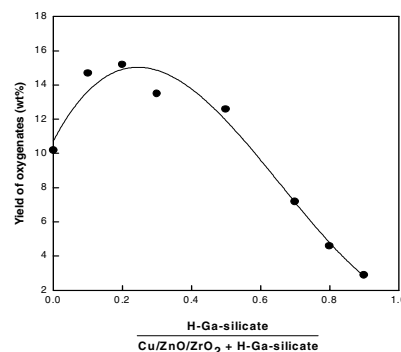


Figure 2. Effect of mixing ratio of hybrid catalyst on oxygenates yield

Conclusions

Since methanol synthesis from CO₂ hydrogenation has a severe limitation of thermodynamic equilibrium, *in situ* transformation of methanol to dimethyl ether (DME) was investigated by using hybrid catalyst composed of Cu-based methanol synthesis catalyst and a zeolite to improve the total oxygenates yield (methanol + DME).

Hybrid catalysts composed of Cu/ZnO/ZrO₂ showed higher yield of oxygenates than those of Cu/ZnO/Ga₂O₃. Among them the hybrid catalyst of Cu/ZnO/ZrO₂ and H-Ga-silicate showed the highest yield of oxygenates in CO₂ hydrogenation. The modification of reducibility or oxygen coverage due to the interactions between methanol synthesis catalyst and zeolite was believed to determine the ability of oxygenate synthesis.

References

- Spivey, J. J. *Chem. Eng. Commun.*, **1991**, 110, 123.
- Dubois, J.L.; Sayama, K.; and Arakawa, H. *Chem. Lett.* **1992**, 1115.
- Argauer, R.J.; and Landolt, G.R.; **U.S. Patent** 3 702 886.
- Ashtekar, S.; Chilukuri, S.V.V.; and Chakrabarty, D.K. *J. Phys. Chem.* **1994**, 98, 4878.
- Saito, M.; Fujitani, T.; Takeguchi, M.; and Watanabe, T. *Appl. Catal. A : General*, **1996**, 138, 311.
- Ihm, S.K.; Park, Y.K.; Jeon, J.K.; Park, K.C.; and Lee, D.K. *Stud. Surf. Sci. Catal.* **1998**, 114, 505.
- Park, Y.K.; Park, K.C.; and Ihm, S.K. *Catal. Today* **1998**, 44, 165.
- Fujimoto, K.; Asami, K.; Saima, H.; Shikada, T.; and Tominaga, H. *Ind. Eng. Chem. Prod. Res. Dev.*, **1986**, 25, 262.
- Campbell, S.M.; Bibby, D.M.; Coddington, J.M.; and Howe, R.F. *J. Catal.*, **1996**, 161, 350.

DE NOVO SIMULATION AND SPECTROSCOPIC STUDY OF IRON SPECIATION IN MICRO- AND MESOPOROUS BIOMIMETIC MATERIALS ACTIVE IN THE SELECTIVE OXIDATION OF METHANE

Peter-Paul H.J.M. Knops-Gerrits

Département de Chimie, Université Catholique de Louvain (UCL),
Batiment LAVOISIER, Place L. Pasteur n°1, B-1348 Louvain-la-
Neuve, Belgium

Introduction

Methane Mono-Oxygenase (MMO) and Deoxyhemerythrin are examples of diiron enzymes that catalyze the dissociative and non-dissociative binding of molecular oxygen [1-5]. Dissociative binding of oxygen via a peroxo intermediate to a diamond core structure leads to a reactive species active in the oxidation of alkanes [1-2]. Non-dissociative binding of oxygen via a side-on peroxo intermediate such as in the active site of deoxyhemerythrin does not allow the splitting and allows binding/release of oxygen as a function of the physiological conditions. Such active sites are among the growing list related to (hydr)oxo-bridged di- or poly-iron cores in biological systems. Methane mono-oxygenase has a binuclear active site in which two histidines and four glutarates are present. Both iron ions are coordinated by a histidine, an oxygen from a bridging carboxylate and a μ -oxo bridge [1]. Theoretical modeling of these enzyme active sites has been recently reported. Yoshizawa *et al.* studied the dioxygen cleavage and methane activation on diiron enzyme models with the extended Hückel method, an approximate molecular orbital method, the μ - η^1 : η^1 -O₂ or μ - η^2 : η^2 -O₂ binding modes are distorted to the corresponding dioxygen complex [4]. Shestakov and Shilov showed that the synchronous insertion of O atom mechanism is found to be significantly less contradictory (for example in methane) if it is supplemented by the stage of formation of the five-coordinate carbon intermediate complex of a hydrocarbon molecule via oxygen atom of an active center [5].

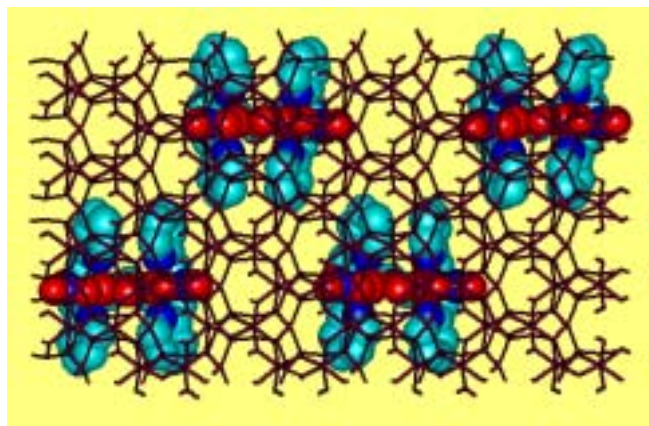


Figure 1. $[\text{Fe}_2(\text{HPTP})(\text{OH})(\text{NO}_3)_2]$ in montmorillonite clays.

Methane can be converted into methanol with binuclear iron(IV)-model complexes

To mimic the MMO active site with a finite cluster we chose to study the binuclear heptapodate coordinated iron (III)-complexes of *N,N,N',N'*-tetrakis(2-benzimidazolymethyl)-2-hydroxy-1,3-diaminopropane (HPTB) and *N,N,N',N'*-Tetrakis(2-pyridylmethyl)-2-hydroxy-1,3-diaminopropane (HPTP). These have active sites of the form $[\text{Fe}_2(\text{HPTP})(\mu\text{-OH})]^{4+}$ (1) and $[\text{Fe}_2(\text{HPTB})(\mu\text{-OH})]^{4+}$ (2). As supports for such complexes we use mesoporous materials such as

MCM-41, FSM-16, HMS (Hexagonal Molecular Sieve) [7-8] and clays (Fig 1) [9] since these materials have large surface areas and large pore sizes that can be tuned from 1.5 to 10 nm. We characterized these complexes using Quantum Mechanics (QM) and EXAFS, Mössbauer and Catalysis and studied the effect of the support.

The QM was at the *ab initio* and DFT (B3LYP) levels [3]. All chelating N-atoms and the ligand backbone were included in the QM determination of the geometry and electronic properties of the ground and excited states of the active site. The geometries of the supported complexes were determined with MD using the Universal FF (UFF) [6] supplemented with a FF based on the quantum mechanics. For the O₂ binding on the reduced active site the μ - η^1 : η^1 -O₂ mode seems to precede formation of the O=Fe-O-Fe=O bis-ferryl active site that reacts exothermally with methane by 50.56 kcal/mol. After the H splitting from methane, the methyl recombines with the FeO center via a weak Fe-OCH₃ bond in this model. The consecutive reaction with water protonates the methoxy group to form methanol and the substitution at the active site by a hydroxo group is endothermic by 7.50 kcal/mol. The regeneration of the active site with H₂O₂ is again endothermic by 3.24 kcal/mol. After the loss of methanol Fe^(III)-O-Fe^(III) is formed which is reduced to the Fe(II,II) form. Ferryl groups are reactive two center three electron bonds. The solvation calculations are very important to obtain good quantitative data. Siegbahn *et al.* [1] uses gas-phase values as the dielectric constant of an enzyme is low ($\epsilon = 4$) compared to this of water ($\epsilon = 80$). For the solvation of small model compounds in water such effects are not negligible. The solvation energies are about 150, 300 and 500 kcal/mol for the 2+, 3+ and 4+ complexes.

Mössbauer spectroscopy allows the oxidation and spin states of the iron atoms to be assessed. Thus the isomer shifts relative to metallic iron at 300 K in the range 0.35-0.60 mm/s are characteristic of 5- or 6-coordinate high-spin di-ferric μ -OH complexes, the smaller quadrupolar splitting < 1 mm/s, in the hydroxo-bridged complexes is due to the lengthening of the Fe-O bond upon protonation of the oxo bridge. The Mössbauer pattern of the supported complexes becomes more complex due to complex lattice interactions. The EXAFS shows lengthening of the Fe-Fe distances for benzimidazole compared to pyridine containing complexes. When the complexes are supported on mesoporous oxides, the EXAFS finds a lengthening of the Fe-Fe distances. The EXAFS data on the model compounds gives longer Fe-Fe distances than the QM. This may be due to neglecting in the QM the large counterbalancing anions associated with the structure of $[\text{Fe}_2(\text{HPTP})(\mu\text{-OH})(\text{NO}_3)_2](\text{ClO}_4)_2$ and $[\text{Fe}_2(\text{HPTB})(\mu\text{-OH})(\text{NO}_3)_2](\text{ClO}_4)_2$.

Methane can be converted into methanol with α -Oxygen on iron in ZSM5 type zeolites

α -Oxygen can be formed on such iron sites by nitrous oxide N₂O decomposition at elevated temperature. Nitrous oxides are formed in the industrial synthesis of adipic acid. In nitrous oxide decomposition several routes exist depending on pressure and temperature. In order to study the pretreatment, activation, reaction and extraction effects the Fe containing topologies such as CHA, MFI, MOR and CFI [10] are tested in the methane to methanol conversion. Pretreatment performed with O₂ at 550°C and vacuum at 800°C to 900°C is optimal. Activation with N₂O at 250°C is optimal and reaction with CH₄ occurs from 20°C, extraction is best with H₂O and quantification of methanol is performed by GC, GC-MS and NMR. Structure/activity effects require the notion of new structural parameters related to the introduction of iron in zeolite topologies such as CHA, MFI, MOR and CFI [10-11], performed via direct

synthesis and post-synthetic modification. When iron concentrations are kept low framework iron is seen (Fig 2).

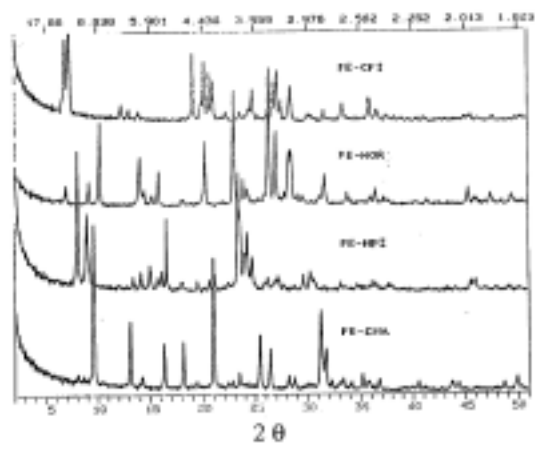


Figure 2. X-Ray Diffraction patterns of FeCIT-5, FeMOR, FeZSM-5 and FeCHA.

Extra-framework iron oxides are occluded after calcination of framework iron zeolites with high iron loading or physical mixtures of aluminum containing zeolites with iron salts or sublimation of iron by mixing zeolites with $\text{Fe}(\text{acac})_2$ followed by an oxygen calcination procedure. The recent structure of CIT-5 is composed of 1D, extra-large pores of nearly circular cross section (center of O to center of O distance $9.91\text{\AA} \times 9.87\text{\AA}$) circumscribed by 14 T-atoms. The asymmetric unit contains 10 T-atoms and 19 oxygen atoms resulting in a unit cell content of $[\text{Si}_{132}\text{O}_{64}]$, a framework density of $18.3\text{ T-atoms}/1000\text{\AA}^3$ and a density of 1.821 g/cm^3 . The topology consists of zigzag ladders of 4-rings with pendant 5-rings interconnected through single zigzag chains. For CIT-5 (CFI) all structural parameters are within reasonable ranges for silicate materials ($d(\text{Si}-\text{O})$ 1.591\AA with a range of $1.555\text{-}1.641\text{\AA}$, a Si-O-Si angle of 149.4° with a range of $168.7^\circ\text{-}140.6^\circ$, and an O-Si-O angle of 109.4° with a range of $113.8^\circ\text{-}104.2^\circ$. These values are appended to the molecular mechanics Universal Force Field (UFF) [3]. The UFF functional forms, parameters, and generating formulas for the full periodic table

Table 1. Partial oxidation of methane with α -Fe sites in ZSM-5 and other Zeolites.

Zeolite	%w t Fe in	Oxidation	μmol Fe in sample	μmol MeOH (oxygenate)
Fe-ZSM-5 Si/Al 11	0.5%	5 Torr $\text{N}_2\text{O}/250^\circ\text{C}$	75	-
Fe-ZSM-5 Si/Al 11	2.0%	5 Torr $\text{N}_2\text{O}/250^\circ\text{C}$	360	97
Fe-ZSM-5 Si/Al 11	5.0%	5 Torr $\text{N}_2\text{O}/250^\circ\text{C}$	800	163
Fe-ZSM-5 Si/Al 11	5.0%	10Torr $\text{N}_2\text{O}/250^\circ\text{C}$	800	208
Fe-CHA (0.1 μm)	5.0%	5 Torr $\text{N}_2\text{O}/250^\circ\text{C}$	800	10
Fe-MOR (1-3 μm)	5.0%	5 Torr $\text{N}_2\text{O}/250^\circ\text{C}$	800	10 (33)
Fe-CIT-5 (3-7 μm)	5.0%	5 Torr $\text{N}_2\text{O}/250^\circ\text{C}$	800	4 (39)

are used to model these structures. XRD, EXAFS, Mossbauer, DRS, magnetic measurements and EPR can resolve and attribute presence of lattice iron and extra-framework clusters. XRD for as made and calcined materials with iron in the lattice reveals $\alpha\text{-Fe}_2\text{O}_3$ particles are absent (no $\alpha\text{-Fe}_2\text{O}_3$ reflection, $d_{104} = 2.70\text{\AA}$). From EXAFS structural parameters obtained in the k^3 weighted optimization give $1.7, 2.7$ and 3.4\AA distances for $\text{Fe}^{(\text{III})}\text{-oxygen}$, $\text{Fe}^{(\text{III})}\text{-Fe}^{(\text{III})}$ and $\text{Fe}^{(\text{III})}\text{-Si}$ bonds. In the EPR spectra the ratio of octahedral/tetrahedral iron can be assumed from the presence of lines at $g=2/4.3$, and depends on sample hydration. In mononuclear iron complexes the Fe-O bond distances of 1.86\AA ($2+$, O_h) 6 coordinated and 1.90\AA ($3+$, T_d) 4 coordinated. For tetrahedral iron and silicon atoms bond distances of 1.65 for Si-O and 1.90\AA for Fe-O obtained from QM seen in the direction of the Fe-O-Si bridge, with Fe-O-Si angles close to the 131.2° and to a O-Fe-O angles of 109.47° .

CONCLUSION.

The reaction of the MMO binuclear heptapodate coordinated iron (III)-complexes of N,N,N',N' -tetrakis(iminomethyl)-2-hydroxy-1,3-diaminopropane model with methane is exothermic The σ - and π -bonds of the ferryl $\text{Fe}=\text{O}$ in the plane of the Fe-O-Fe bridge, have the properties of a two atom three electron bond. After the H splitting from methane, the methyl recombines with the FeO center via a weak Fe-OCH₃ bond in this model.

Methane can also be converted into methanol with α -Oxygen at room temperature using N_2O as a selective oxidant inside the pores of various zeolites. Extraction of the catalysts with water is preferred over acetonitrile-water mixtures. The dinuclear iron oxide clusters realize the sub-stoichiometric (based on a diiron sites) oxidation of methane after N_2O activation, the small dinuclear Fe sites favor oxygen insertion chemistry over coupling chemistry.

Acknowledgement.

PPKG thanks ESA, FNRS and FSR Belgium for financial support, A.Fukuoka & M.Ichikawa from the CRC, at Hokkaido University, Sapporo, Japan for a collaboration on EXAFS. PPKG thanks WAGoddard III from the Material & Process Simulation Center, Beckman Institute (139-74), California Inst. of Technology, Pasadena CA, USA, WAG thanks BP Amoco for financial support.

References

- (1) R.H. Crabtree, *Chem.Rev.*, **1995**, 95, 987.
- (2) P.E. Siegbahn, R.H.Crabtree, *J.Am.Chem.Soc.*, **1997**,119, 3103.
- (3) P.P. Knops-Gerrits , P.A. Jacobs, A.Fukuoka, M.Ichikawa, F.Faglinoni, W.A. Goddard III, *J.Mol.Cat., A*, 166 (2001) 3, P.P. Knops-Gerrits, M. Witko, W.A.Goddard III, R. Millini Eds.
- (4) K. Yoshizawa, K. Ohta, T. Yamabe, R. Hoffmann, *J. Am. Chem. Soc.*, **1997**, 119, 12311.
- (5) A.E.Shestakov, A.E.Shilov, *J.Mol.Cat., A*, 105 (1996) 1.
- (6) A.K. Rappe, C.J. Casewit, K.S. Colwell, W.A. Goddard, W.M. Skiff, *J. Am. Chem. Soc.*, 114 (1992) 10024.; A.K. Rappe, W.A. Goddard, *J. Chem. Phys.*, **1991**, 95, 3358.
- (7) P.P. Knops-Gerrits, A.M. Van Bavel, G. Langouche, P.A. Jacobs, NATO ASI, **1998**, Derouane Eds., 3.44, 215.
- (8) P.P. Knops-Gerrits, A. Verberckmoes, R.A. Schoonheydt, M. Ichikawa, P.A. Jacobs, *Micro- Mesop. Mat.*, **1998**, 21: 4-6, 475.
- (9) P.P. Knops-Gerrits, A. Weiss, S. Dick, P.A. Jacobs, *Stud.Surf.Sci.Catal.*, **1997**, 110, 1061.
- (10) P.P. Knops-Gerrits, W.A. Goddard III, *J.Mol.Cat., A*, **2001**, 166, 1 & 135.
- (11) Y. Oumi, M. Yamadaya, T. Kanougi, M. Kubo, A. Stirling, R. Vetrivel, E. Broclawik, A. Miyamoto, *Catal. Lett.*, **1997**,45, 21.
- (12) G.I., Panov, V.I., Sobolev, K.A. Dubkov, A.E., Parmon, N.S., Ovanyesan, A.E., Shilov, A.A., Shteinman, *React. Kinet. Catal.Lett.*, **1997**, 61, 251 .

DE NOVO SIMULATION AND SPECTROSCOPIC STUDY OF IRON SPECIATION IN MICRO- AND MESOPOROUS BIOMIMETIC MATERIALS ACTIVE IN THE SELECTIVE OXIDATION OF METHANE

Peter-Paul H.J.M. Knops-Gerrits

Département de Chimie, Université Catholique de Louvain (UCL),
Batiment LAVOISIER, Place L. Pasteur n°1, B-1348 Louvain-la-
Neuve, Belgium

Introduction

Methane Mono-Oxygenase (MMO) and Deoxyhemerythrin are examples of diiron enzymes that catalyze the dissociative and non-dissociative binding of molecular oxygen [1-5]. Dissociative binding of oxygen via a peroxo intermediate to a diamond core structure leads to a reactive species active in the oxidation of alkanes [1-2]. Non-dissociative binding of oxygen via a side-on peroxo intermediate such as in the active site of deoxyhemerythrin does not allow the splitting and allows binding/release of oxygen as a function of the physiological conditions. Such active sites are among the growing list related to (hydr)oxo-bridged di- or poly-iron cores in biological systems. Methane mono-oxygenase has a binuclear active site in which two histidines and four glutarates are present. Both iron ions are coordinated by a histidine, an oxygen from a bridging carboxylate and a μ -oxo bridge [1]. Theoretical modeling of these enzyme active sites has been recently reported. Yoshizawa *et al.* studied the dioxygen cleavage and methane activation on diiron enzyme models with the extended Hückel method, an approximate molecular orbital method, the μ - η^1 : η^1 -O₂ or μ - η^2 : η^2 -O₂ binding modes are distorted to the corresponding dioxygen complex [4]. Shestakov and Shilov showed that the synchronous insertion of O atom mechanism is found to be significantly less contradictory (for example in methane) if it is supplemented by the stage of formation of the five-coordinate carbon intermediate complex of a hydrocarbon molecule via oxygen atom of an active center [5].

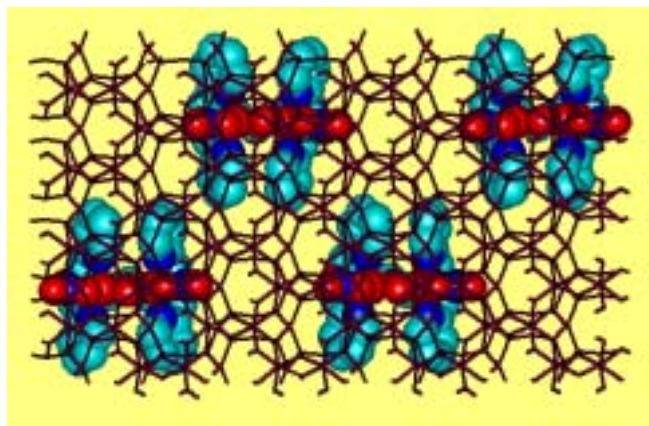


Figure 1. $[\text{Fe}_2(\text{HPTP})(\text{OH})(\text{NO}_3)_2]$ in montmorillonite clays.

Methane can be converted into methanol with binuclear iron(IV)-model complexes

To mimic the MMO active site with a finite cluster we chose to study the binuclear heptapodate coordinated iron (III)-complexes of *N,N,N',N'*-tetrakis(2-benzimidazolymethyl)-2-hydroxy-1,3-diaminopropane (HPTB) and *N,N,N',N'*-Tetrakis(2-pyridylmethyl)-2-hydroxy-1,3-diaminopropane (HPTP). These have active sites of the form $[\text{Fe}_2(\text{HPTP})(\mu\text{-OH})]^{4+}$ (1) and $[\text{Fe}_2(\text{HPTB})(\mu\text{-OH})]^{4+}$ (2). As supports for such complexes we use mesoporous materials such as

MCM-41, FSM-16, HMS (Hexagonal Molecular Sieve) [7-8] and clays (Fig 1) [9] since these materials have large surface areas and large pore sizes that can be tuned from 1.5 to 10 nm. We characterized these complexes using Quantum Mechanics (QM) and EXAFS, Mössbauer and Catalysis and studied the effect of the support.

The QM was at the *ab initio* and DFT (B3LYP) levels [3]. All chelating N-atoms and the ligand backbone were included in the QM determination of the geometry and electronic properties of the ground and excited states of the active site. The geometries of the supported complexes were determined with MD using the Universal FF (UFF) [6] supplemented with a FF based on the quantum mechanics. For the O₂ binding on the reduced active site the μ - η^1 : η^1 -O₂ mode seems to precede formation of the O=Fe-O-Fe=O bis-ferryl active site that reacts exothermally with methane by 50.56 kcal/mol. After the H splitting from methane, the methyl recombines with the FeO center via a weak Fe-OCH₃ bond in this model. The consecutive reaction with water protonates the methoxy group to form methanol and the substitution at the active site by a hydroxo group is endothermic by 7.50 kcal/mol. The regeneration of the active site with H₂O₂ is again endothermic by 3.24 kcal/mol. After the loss of methanol Fe^(III)-O-Fe^(III) is formed which is reduced to the Fe(II,II) form. Ferryl groups are reactive two center three electron bonds. The solvation calculations are very important to obtain good quantitative data. Siegbahn *et al.* [1] uses gas-phase values as the dielectric constant of an enzyme is low ($\epsilon = 4$) compared to this of water ($\epsilon = 80$). For the solvation of small model compounds in water such effects are not negligible. The solvation energies are about 150, 300 and 500 kcal/mol for the 2+, 3+ and 4+ complexes.

Mössbauer spectroscopy allows the oxidation and spin states of the iron atoms to be assessed. Thus the isomer shifts relative to metallic iron at 300 K in the range 0.35-0.60 mm/s are characteristic of 5- or 6-coordinate high-spin di-ferric μ -OH complexes, the smaller quadrupolar splitting < 1 mm/s, in the hydroxo-bridged complexes is due to the lengthening of the Fe-O bond upon protonation of the oxo bridge. The Mössbauer pattern of the supported complexes becomes more complex due to complex lattice interactions. The EXAFS shows lengthening of the Fe-Fe distances for benzimidazole compared to pyridine containing complexes. When the complexes are supported on mesoporous oxides, the EXAFS finds a lengthening of the Fe-Fe distances. The EXAFS data on the model compounds gives longer Fe-Fe distances than the QM. This may be due to neglecting in the QM the large counterbalancing anions associated with the structure of $[\text{Fe}_2(\text{HPTP})(\mu\text{-OH})(\text{NO}_3)_2](\text{ClO}_4)_2$ and $[\text{Fe}_2(\text{HPTB})(\mu\text{-OH})(\text{NO}_3)_2](\text{ClO}_4)_2$.

Methane can be converted into methanol with α -Oxygen on iron in ZSM5 type zeolites

α -Oxygen can be formed on such iron sites by nitrous oxide N₂O decomposition at elevated temperature. Nitrous oxides are formed in the industrial synthesis of adipic acid. In nitrous oxide decomposition several routes exist depending on pressure and temperature. In order to study the pretreatment, activation, reaction and extraction effects the Fe containing topologies such as CHA, MFI, MOR and CFI [10] are tested in the methane to methanol conversion. Pretreatment performed with O₂ at 550°C and vacuum at 800°C to 900°C is optimal. Activation with N₂O at 250°C is optimal and reaction with CH₄ occurs from 20°C, extraction is best with H₂O and quantification of methanol is performed by GC, GC-MS and NMR. Structure/activity effects require the notion of new structural parameters related to the introduction of iron in zeolite topologies such as CHA, MFI, MOR and CFI [10-11], performed via direct

DECOMPOSITION OF CF₄ BY MICROWAVE HEATING

Franz-Josef Spiess and Steven L. Suib

Department of Chemistry, University of Connecticut,
55 N.Eagleville Rd., Storrs, CT 06268

Introduction

Carbon tetrafluoride is an inert gas that is also a greenhouse gas with a very high global warming potential. It is a by-product in the aluminum production and used in the semiconductor industry. The exceptionally long atmospheric lifetime of carbon tetrafluoride makes it imperative to find solutions to destroy this potent greenhouse gas.

So far mostly catalytic and plasma discharge methods have been used to decompose CF₄.¹⁻³ Grytsinin et al. showed effective decomposition using a slipping surface discharge.¹ Whereas Takita et al. used AlPO₄-rare earth phosphate catalysts to decompose CF₄ at conversions of about 50%.² Several papers like Jacobsohn et al. describe the decomposition as a means to deposit fluorinated amorphous-carbon films.³

In this research, we studied the effective decomposition of carbon tetrafluoride using microwave heating at medium power (0-1200 W) using water as a supplement and activated carbon as a catalyst. The experiments were carried out using an ASTEK microwave unit.

Experimental

A simple setup was used as shown in Fig. 1. The feed is a mixture of carbon tetrafluoride, water (introduced by a bubbler), and nitrogen. The content of the feed gas is 4 % CF₄, 3 % water and balance nitrogen at a flow rate of 15 mL/min. The active carbon (100 mg) was placed in a quartz tube and secured with quartz wool. This tube was then placed into the ASTEK microwave cavity (Fig 2.). The reaction mixture was continuously monitored with a MKS-UTI PPT quadrupole residual gas analyzer mass spectrometer with a Faraday cup detector and a variable high-pressure sampling manifold. The system was equilibrated at the beginning and then the power was turned on to the desired level and continued until an equilibrium value was achieved. The catalysts used were either prepared in our research group or used as obtained from commercial vendors.

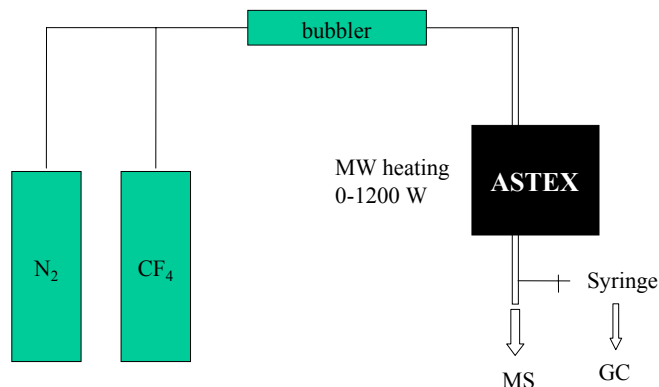


Figure 1. Schematic of the experimental setup for CF₄ decomposition.

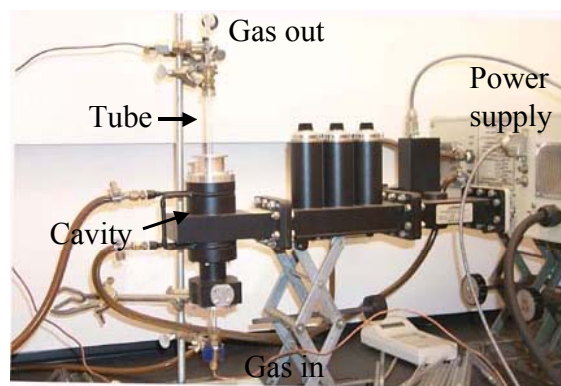


Figure 2. Photograph of the reaction setup

Results and Discussion

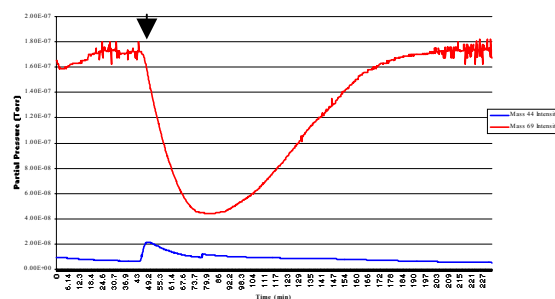
Initial studies using discharge plasmas yielded only low conversions (up to 12 %). Additionally, MS studies suggest that CF₄ alone or CF₄ and water are the most suited systems. Studies using microwave heating exhibited promising results under similar conditions and were therefore pursued.

The reactions were carried out with the setup presented before at a constant flow rate of 15 mL/min. Several catalysts were tested in this line of experiments. The catalysts tested were several different kinds of activated carbon, Ni filament type catalyst, V₂O₅ Supported on Al₂O₃, and a zeolite/active carbon mixture.

Of these catalysts, only the activated carbon exhibited any change in the CF₄ concentration in these experiments. It was furthermore observed that no reaction takes place without the presence of water vapor.

In the case of activated carbon, several kinds of activated carbon were used, but the results presented here are the ones for a commercial brand available from Sigma-Aldrich. A typical decomposition versus time plot is shown in Fig. 3 as obtained with the mass spectrometer.

Figure 3. Plot of CF₄ decomposition versus time, top plot is the CF₄ plot, bottom plot is the CO₂ plot, power was turned on to 480 W (arrow= time of power on)



- (3) Jacobsohn, L.G.; Franceschini, D.F.; Maia da Costa, M.E.H.; Freire Jr. F.L. *J. Vac. Sci. Technol. A* **18(5)**, Sept/Oct 2000, 2230-2238.

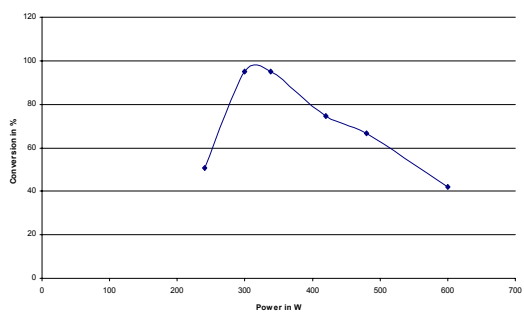


Figure 4. Plot of Conversion of CF_4 versus Power in Watts

The conversion was studied as a function of power. As shown in Fig. 4., the maximum conversion is achieved at medium power levels of 300-400 W (whole range 0-1200 W). The maximum conversion observed is 95 % measured as the disappearance of the CF_4 in the MS plot. As seen in the time versus conversion plot, the activated carbon deactivates rather quickly.

Furthermore, the reaction produces significant amounts of hydrogen, about 100,000 ppm. The extent of the reaction can also be seen on how the reaction tube looks after the reaction. The higher the extent of the reaction is, the more “decomposed” is the reaction tube due to the glow and HF production. The surface area of the activated carbon was determined to be $653 \text{ m}^2/\text{g}$. It consists of meso- and micropores. The surface area below 20 Angstrom is $349 \text{ m}^2/\text{g}$, and between 20 and 200 Angstrom, it is $280 \text{ m}^2/\text{g}$.

The role of the water in this reaction is twofold. It is the primary energy absorber for the microwave radiation, but also it is the hydrogen and oxygen source needed in this reaction. It is believed that the carbon tetrafluoride reacts with the water under the use of the supplied microwave energy to yield hydrogen fluoride and carbon dioxide (The formed hydrogen fluoride is absorbed by a scrubber before it enters the mass spectrometer.). The reaction mechanism is believed to include the attack of hydrogen radicals on the CF_4 molecule; this is indicated by the formation of hydrogen in the reaction. Furthermore, the catalyst deactivation is thought to be due to the formation of hydrogen fluoride.

Conclusions

The destruction of carbon tetrafluoride by microwave heating represents an efficient and easy means to get rid of this greenhouse gas. Carbon tetrafluoride is almost completely decomposed. The main products are hydrogen fluoride, carbon dioxide and hydrogen. The activated carbon catalyst deactivates after a short period of time. The deactivation time has to be prolonged. Furthermore it was found out that water is essential in these reaction and a reaction scheme was proposed.

Acknowledgement. The authors thank JFCC and Planet Japan for support of this research. We also thank Daniel Conde for assistance in the power measurements and reactor setup.

References

- (1) Grytsinin, S.I.; Korchagina, E.G.; Kossyi, I.A.; Misakyan, M.A.; Silakov, V.P.; Tarasov, N.M.; Temchin, S.M. *Plasma Sources Sci. Technol.* **10 (2001)**, 125-133.
- (2) Takita, Y.; Ninomiya, M.; Miyake, H.; Wakamatsu, H.; Yoshinaga, Y.; Ishihara, T. *Phys. Chem. Chem. Phys.* **1999**, **1**, 4501-4504.

synthesis and post-synthetic modification. When iron concentrations are kept low framework iron is seen (Fig 2).

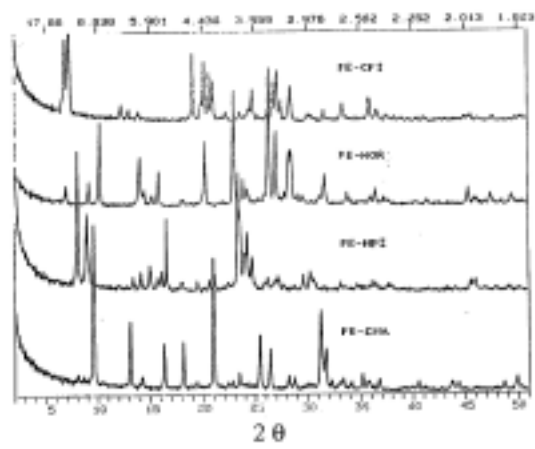


Figure 2. X-Ray Diffraction patterns of FeCIT-5, FeMOR, FeZSM-5 and FeCHA.

Extra-framework iron oxides are occluded after calcination of framework iron zeolites with high iron loading or physical mixtures of aluminum containing zeolites with iron salts or sublimation of iron by mixing zeolites with $\text{Fe}(\text{acac})_2$ followed by an oxygen calcination procedure. The recent structure of CIT-5 is composed of 1D, extra-large pores of nearly circular cross section (center of O to center of O distance $9.91\text{\AA} \times 9.87\text{\AA}$) circumscribed by 14 T-atoms. The asymmetric unit contains 10 T-atoms and 19 oxygen atoms resulting in a unit cell content of $[\text{Si}_{132}\text{O}_{64}]$, a framework density of $18.3\text{ T-atoms}/1000\text{ \AA}^3$ and a density of 1.821 g/cm^3 . The topology consists of zigzag ladders of 4-rings with pendant 5-rings interconnected through single zigzag chains. For CIT-5 (CFI) all structural parameters are within reasonable ranges for silicate materials ($d(\text{Si-O})$ 1.591 \AA with a range of $1.555\text{-}1.641\text{ \AA}$, a Si-O-Si angle of 149.4° with a range of $168.7^\circ\text{-}140.6^\circ$, and an O-Si-O angle of 109.4° with a range of $113.8^\circ\text{-}104.2^\circ$. These values are appended to the molecular mechanics Universal Force Field (UFF) [3]. The UFF functional forms, parameters, and generating formulas for the full periodic table

Table 1. Partial oxidation of methane with α -Fe sites in ZSM-5 and other Zeolites.

Zeolite	%w t Fe in	Oxidation	μmol Fe in sample	μmol MeOH (oxygenate)
Fe-ZSM-5 Si/Al 11	0.5%	5 Torr $\text{N}_2\text{O}/250^\circ\text{C}$	75	-
Fe-ZSM-5 Si/Al 11	2.0%	5 Torr $\text{N}_2\text{O}/250^\circ\text{C}$	360	97
Fe-ZSM-5 Si/Al 11	5.0%	5 Torr $\text{N}_2\text{O}/250^\circ\text{C}$	800	163
Fe-ZSM-5 Si/Al 11	5.0%	10Torr $\text{N}_2\text{O}/250^\circ\text{C}$	800	208
Fe-CHA (0.1 μm)	5.0%	5 Torr $\text{N}_2\text{O}/250^\circ\text{C}$	800	10
Fe-MOR (1-3 μm)	5.0%	5 Torr $\text{N}_2\text{O}/250^\circ\text{C}$	800	10 (33)
Fe-CIT-5 (3-7 μm)	5.0%	5 Torr $\text{N}_2\text{O}/250^\circ\text{C}$	800	4 (39)

are used to model these structures. XRD, EXAFS, Mossbauer, DRS, magnetic measurements and EPR can resolve and attribute presence of lattice iron and extra-framework clusters. XRD for as made and calcined materials with iron in the lattice reveals $\alpha\text{-Fe}_2\text{O}_3$ particles are absent (no $\alpha\text{-Fe}_2\text{O}_3$ reflection, $d_{104} = 2.70\text{ \AA}$). From EXAFS structural parameters obtained in the k^3 weighted optimization give $1.7, 2.7$ and 3.4 \AA distances for $\text{Fe}^{(\text{III})}\text{-oxygen}$, $\text{Fe}^{(\text{III})}\text{-Fe}^{(\text{III})}$ and $\text{Fe}^{(\text{III})}\text{-Si}$ bonds. In the EPR spectra the ratio of octahedral/tetrahedral iron can be assumed from the presence of lines at $g= 2/4.3$, and depends on sample hydration. In mononuclear iron complexes the Fe-O bond distances of 1.86 \AA ($2+$, O_h) 6 coordinated and 1.90 \AA ($3+$, T_d) 4 coordinated. For tetrahedral iron and silicon atoms bond distances of 1.65 for Si-O and 1.90 \AA for Fe-O obtained from QM seen in the direction of the Fe-O-Si bridge, with Fe-O-Si angles close to the 131.2° and to a O-Fe-O angles of 109.47° .

CONCLUSION.

The reaction of the MMO binuclear heptapodate coordinated iron (III)-complexes of N,N,N',N' -tetrakis(iminomethyl)-2-hydroxy-1,3-diaminopropane model with methane is exothermic The σ - and π -bonds of the ferryl $\text{Fe}=\text{O}$ in the plane of the Fe-O-Fe bridge, have the properties of a two atom three electron bond. After the H splitting from methane, the methyl recombines with the FeO center via a weak Fe-OCH₃ bond in this model.

Methane can also be converted into methanol with α -Oxygen at room temperature using N_2O as a selective oxidant inside the pores of various zeolites. Extraction of the catalysts with water is preferred over acetonitrile-water mixtures. The dinuclear iron oxide clusters realize the sub-stoichiometric (based on a diiron sites) oxidation of methane after N_2O activation, the small dinuclear Fe sites favor oxygen insertion chemistry over coupling chemistry.

Acknowledgement.

PPKG thanks ESA, FNRS and FSR Belgium for financial support, A.Fukuoka & M.Ichikawa from the CRC, at Hokkaido University, Sapporo, Japan for a collaboration on EXAFS. PPKG thanks WAGoddard III from the Material & Process Simulation Center, Beckman Institute (139-74), California Inst. of Technology, Pasadena CA, USA, WAG thanks BP Amoco for financial support.

References

- (1) R.H. Crabtree, *Chem.Rev.*, **1995**, 95, 987.
- (2) P.E. Siegbahn, R.H.Crabtree, *J.Am.Chem.Soc.*, **1997**,119, 3103.
- (3) P.P. Knops-Gerrits , P.A. Jacobs, A.Fukuoka, M.Ichikawa, F.Faglinoni, W.A. Goddard III, *J.Mol.Cat., A*, 166 (2001) 3, P.P. Knops-Gerrits, M. Witko, W.A.Goddard III, R. Millini Eds.
- (4) K. Yoshizawa, K. Ohta, T. Yamabe, R. Hoffmann, *J. Am. Chem. Soc.*, **1997**, 119, 12311.
- (5) A.E.Shestakov, A.E.Shilov, *J.Mol.Cat., A*, 105 (1996) 1.
- (6) A.K. Rappe, C.J. Casewit, K.S. Colwell, W.A. Goddard, W.M. Skiff, *J. Am. Chem. Soc.*, 114 (1992) 10024.; A.K. Rappe, W.A. Goddard, *J. Chem. Phys.*, **1991**, 95, 3358.
- (7) P.P. Knops-Gerrits, A.M. Van Bavel, G. Langouche, P.A. Jacobs, NATO ASI, **1998**, Derouane Eds., 3.44, 215.
- (8) P.P. Knops-Gerrits, A. Verberckmoes, R.A. Schoonheydt, M. Ichikawa, P.A. Jacobs, *Micro- Mesop. Mat.*, **1998**, 21: 4-6, 475.
- (9) P.P. Knops-Gerrits, A. Weiss, S. Dick, P.A. Jacobs, *Stud.Surf.Sci.Catal.*, **1997**, 110, 1061.
- (10) P.P. Knops-Gerrits, W.A. Goddard III, *J.Mol.Cat., A*, **2001**, 166, 1 & 135.
- (11) Y. Oumi, M. Yamadaya, T. Kanougi, M. Kubo, A. Stirling, R. Vetrivel, E. Broclawik, A. Miyamoto, *Catal. Lett.*, **1997**,45, 21.
- (12) G.I., Panov, V.I., Sobolev, K.A. Dubkov, A.E., Parmon, N.S., Ovanyesan, A.E., Shilov, A.A., Shteinman, *React. Kinet. Catal.Lett.*, **1997**, 61, 251 .

DEHYDRO-AROMATIZATION OF CH₄ OVER W/HZSM-5-BASED CATALYSTS

Youzhu Yuan, Zhitao Xiong, Jinlong Zeng, Guodong Lin, Hongbin Zhang

Department of Chemistry & State Key Lab of Physical Chemistry for the Solid Surfaces, Xiamen University, Xiamen 361005, CHINA

Introduction

Direct catalytic dehydrogenation and aromatization of methane to aromatics and H₂ (DHAM) in the absence of O₂ has drawn increasing attention in the recent years with the development of a series of new catalysts^[1-5]. For practical uses, W-loaded HZSM-5 zeolite is among the most promising DHAM catalysts^[6-7]. Recent studies in our lab have shown that, following an initial induction period, a methane conversion of ca.20% could be achieved at a benzene selectivity of ca.58% at 1073 K over Zn (or Mn, Li)-promoted W/HZSM-5-based catalysts. Compared to Mo-based catalyst, the W-based catalysts can operate at 1073 K, and gain a methane conversion approximately 2 times as high as that of the Mo(or W)-based catalyst operating at 973 K. It can also operate at 973 K and have about the same methane conversion as that of the Mo-based catalysts at the same temperature. Its main advantage is its highly heat-resistant performance; the high reaction temperature did not lead to loss of W-component by sublimation. The present results shed light on the design and development of the practical W-based catalysts for DHAM reaction.

Experimental

The W/HZSM-5 catalyst was prepared by conventional method of impregnation with H₂SO₄-acidified (NH₄)₂WO₄ aqueous solution (pH=2~3) as precursor. The Zn (or Mn, Li)-promoted catalyst was prepared by firstly impregnating a certain amount of the HZSM-5 zeolite carrier (with Si/Al molar ratio of 38) with a calculated amount of ZnSO₄ (or MnSO₄, or Li₂SO₄) in aqueous solutions, followed by drying at 393 K for 2 h and calcining at 673 K for 4 h, and subsequently impregnating with a calculated amount of H₂SO₄-acidified (NH₄)₂WO₄ aqueous solution (pH=2~3), and finally drying at 393 K for 2 h and calcining at 773 K in air for 5 h.

The activity evaluation of catalyst was carried out in a fixed-bed continuous flow reactor-GC combination system. DHAM reaction was conducted at 0.1 MPa and 973-1173 K, with a gaseous mixture of CH₄ (of 99.99 % purity) +10%Ar (served as internal standard for GC analysis, of 99.99 % purity) as feed-gas. Conversion of CH₄ and selectivities of hydrocarbon products were evaluated with an internal standard analyzing method. The amounts of coke formed on catalyst were determined by TG-DTA method. In most cases, the results of calculation for carbon equilibrium may reach approximately 85% after 1 h of reaction. XPS measurements were done on a VG ESCA LAB MK-2 system under UHV (1×10⁻⁷ Pa), calibrated internally by the Si(2p) (B. E.) at 103.3 eV.

Results and Discussion

DHAM Activity of W/HZSM-5-based catalysts The results of activity assay of a series of catalysts for DHAM reaction were shown in Table 1. Over the Mn (or Zn, or Li)-promoted W/HZSM-5 catalysts, a methane conversion of ca.21% and a benzene selectivity of a value of 52-61% could be achieved in the initial 2 h of reaction at 1073 K. Addition of a minor amount of CO₂ (≤ 2%) to the feed-gas was found to significantly enhance methane conversion and selectivity of benzene and to improve the performance of coke-resistance of W/HZSM-5-based catalysts. The results of monitoring the changes of methane conversion and selectivities to hydrocarbon

products with time on stream of the reaction over a 3%W-1.36%Zn/HZSM-5 catalyst is shown in Fig.1, from which it can be seen that, in the initial 2 h of reaction, ~22% conversion of methane and ~62% selectivity of benzene were reached, and after 6 h of reaction, methane conversion still maintained at ~10%, with the corresponding benzene selectivity at ~38%. The lifetime of the catalyst was thus prolonged to a great extent.

Table 1. DHAM Reactivity over Catalyst Systems with Different Promoters*

Catalyst	Convers. of CH ₄ (%)		Selectivity (%)			
			Ben.		C ₂ H ₄	
	105 th min.	300 th min.	105 th min.	300 th min.	105 th min.	300 th min.
3%W/HZSM-5	19.5	6.2	48.2	22.0	9.2	12.4
3%W-1.5%Zn/HZSM-5	21.5	11.0	52.0	25.0	8.0	12.8
3%W-0.1%Mg-1.5%Zn/HZSM-5	21.0	15.0	55.0	42.0	12.0	13.5
3%W-1.5%Mn/HZSM-5	21.5	12.5	59.5	40.0	10.0	13.0
3%W-1.5%Li/HZSM-5	21.0	17.0	61.5	50.0	9.0	12.5

* The activity data of each catalyst taken at the 105th min. and the 300th min. of the reaction, respectively, under reaction conditions: 0.1MPa, 1073 K, GHSV of feed-gas CH₄+10%Ar at 960 h⁻¹.

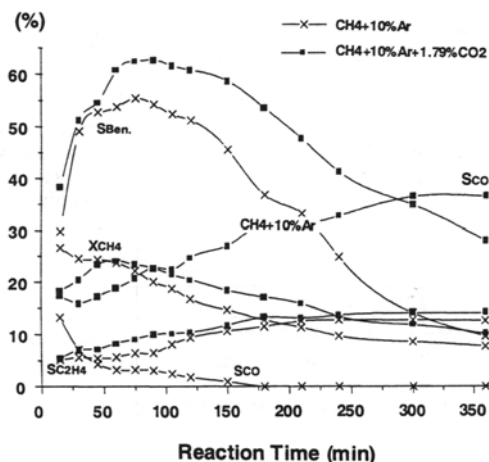


Fig. 3. Comparison between the assay results of DHAM reaction activity over the 3%W-1.36%Zn/HZSM-5 catalyst at 0.1 MPa, 1073 K, feed-gas: CH₄+10%Ar vs. CH₄+10%Ar+1.8%CO₂, both GHSV = 960 h⁻¹.

The promoting effect of the added CO₂ originated most probably from the role that it played as scavenger of functioning surface of the catalyst via Boudart reaction: CO₂ + C (deposited C at surface) →2CO, thus in favor of alleviating the deposition of carbon and inhibiting the formation of coke at the catalyst surface to a greater extent.

Carbon Deposition and Catalyst Regeneration Fig.2-I shows the changes of W(4f)-XPS spectrum of the 3%W/HZSM-5 catalyst with time on stream of the reaction. Detailed analysis and computer fitting of these W(4f)-XPS spectra revealed the existence of W-species in mixed valence-states at the surface of functioning catalyst, with the W(4f)_{7/2} binding energy of W⁶⁺, W⁵⁺, W⁴⁺, W²⁺ and WC at 36.0, 35.3, 34.5, 33.2 and 32.2 eV, respectively, and after the

reaction for 6 h, the WC had been the predominant W-containing species (See Table 2).

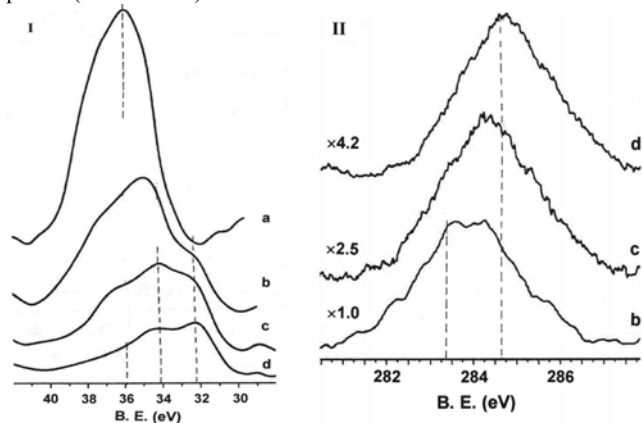


Fig.2 W(4f)-XPS spectra (I) and C(1s)-XPS spectra (II) of the 3%W/HZSM-5 catalyst with time on stream of the reaction.

Table 2 Composition of W-containing Species at the Surface of functioning 3%W/HZSM-5 Catalyst

Time (h) on stream of the reaction	Percentage of different W-Species in the total surface W (%)			
	W ⁶⁺	W ⁵⁺	W ⁴⁺	WC
1	19.1	13.5	28.8	18.6
3	12.5	24.2	32.1	31.2
6	7.5	18.2	20.1	54.2

Formation of the WC species was also evidenced from C(1s)-XPS spectra (Fig.2-II) taken on the functioning catalyst in different stages of the reaction; the dominant C-containing surface species was WC (B.E. of C(1s) at 283.3 eV) in the initial 1 h of reaction, while was amorphous carbon deposits (B.E. of C(1s) at 284.7 eV) after 6 h of reaction. By analysis and computer fitting of the XPS spectra taken on the catalyst samples with different time on stream of the reaction, it has been shown that the molar ratio of the component elements at the surface of 3%W/HZSM-5 catalyst was Al/C/O/Si/W= 1.2/~0/63.1/34.4/1.3 for the oxidation precursor, and 1.5/41.7/35.5/20.8/0.5 for the functioning catalyst after 1 h of reaction. It changed to Al/C/O/Si/W= 0.6/82.7/10/6.6/0.1 after 6 h of reaction, revealing that most portion of the surface of the functioning catalyst was covered by carbon deposits at that time.

NH₃-TPD measurements revealed that ca.80% of strong and medium-strong acidic sites were lost after 5 hours of reaction. N₂-BET measurements demonstrated that, after 1 h reaction, specific surface area of the functioning catalyst decreased to 302 m²g⁻¹ from 368 m²g⁻¹ for the oxidation precursor of catalyst. It further came down to 75 m²g⁻¹ after 5 h of reaction, implying that carbon deposits blocked most of the zeolite pores, thus resulting in the loss of a greater part of the surface. In fact, heavy deposition of carbon on the surface of functioning catalyst was the main reason leading to deactivation of the catalyst.

Reoxidation by air can regenerate the deactivated 3%W/HZSM-5 catalyst effectively, with the Al/C/O/Si/W molar ratio at the renewed surface recovered to 1.8/~0/64.7/31.7/1.9 and the X_{CH₄} and S_{C₆H₆} regained to 20-18% and ca.50%, respectively, after undergoing an induction period of 20 minutes. The results of activity evaluation of the 3%W-1.5%Mn/HZSM-5 catalyst for DHAM reaction after a series of operation/regeneration (by air-oxidation each time for 1 h at 873 K) showed that, it is not until after ten times of regeneration that a small decrease in the catalyst activity was observed (See Fig.3). It

seems that the reason leading to the decrease in the catalyst activity was probably due to dealumination to some degree of the framework structure of HZSM-5 zeolite caused by aqueous vapor resulting from the coke combustion in air-regeneration processes over and over again.

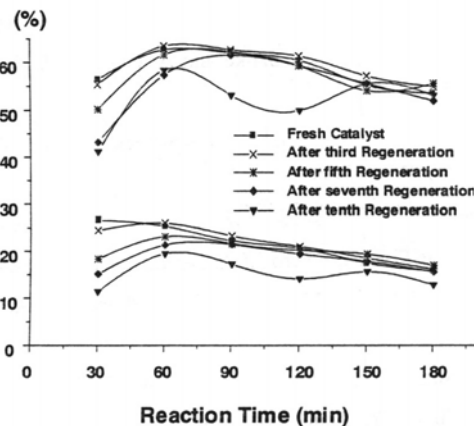


Fig.3 DHAM reactivity over the 3%W-1.5%Mn/HZSM-5 catalyst after undergoing a series of operation/air-regeneration; the below curves for CH₄ conversion and the upper curves for C₆H₆ selectivity.

Action of Promoters Zn, Mn and Li NH₃-TPD study of the W/HZSM-5-based catalysts confirmed that the intensity and concentration of the surface B-acid sites have pronounced effects on the catalyst performance for DHAM reaction. It was found experimentally that, by addition of a proper amount of Mg²⁺, the strong B-acid sites at the catalyst surface could be effectively eliminated, whereas the addition of a proper amount of Zn²⁺ or Li⁺ resulted not only in eliminating most of the strong surface B-acid sites but also in generating a kind of new medium-strong acid sites, mostly B-acid sites, simultaneously. The latter could serve as the catalytically active sites for DHAM reaction. On such medium-strong surface B-acid sites, the formation of coke would be also alleviated to a greater extent. By simultaneous addition of Mg²⁺ and Zn²⁺, optimized adjustment in surface acidity of the catalyst could be realized. On the other hand, it was indicated experimentally that the doping of the Zn²⁺ or Li⁺-component to WO_x matrix would facilitate inhibiting aggregation of the W-containing species and improving dispersion of the W-component at the surface of catalyst, thus bringing about decreasing in the reduction-temperature for the hard-to-be-reduced W⁶⁺-species and increasing in quantity of the reducible W⁶⁺-species, as has been evidenced by the results of H₂-TPR study on the reducibility of the Zn²⁺(or Li⁺, Mn²⁺)-promoted W/HZSM-5 system. The above two roles that Zn²⁺, Mn²⁺ and Li⁺ as promoters played both contributed to the persistence of high methane conversion and benzene selectivity, and the alleviation of coke deposition, as well as the prolongation of the catalyst lifetime.

Acknowledgment

This work was supported by the National Priority Fundamental Research Project (No: G1999022400) of China.

References

- [1] Wang, L.; Tao, L.; Xie, M.; *et al.*, *Catal. Lett.*, 1993, 21, 35.
- [2] Wang, D. J.; Lunsford, J. H.; Rosynek, M.P., *J. Catal.*, 1997, 169, 347.
- [3] Solymosi, F.; Szoke, A.; Cserenyi, J., *Catal. Lett.*, 1996, 39, 157.
- [4] Ohnishi, R.; Liu, S.; Ichikawa, M., *J. Catal.*, 1999, 182, 92.
- [5] Zeng, J.-L.; Xiong, Z.-T.; Zhang, H.-B.; *et al.*, *Catal. Lett.*, 1998, 53, 119.
- [6] Xiong, Z.-T.; Zhang, H.-B.; *et al.*, *Catal. Lett.*, 2001, 74(3-4), 227.
- [7] Xiong, Z.-T.; Zhang, H.-B.; *et al.*, *Catal. Lett.*, 2001, 74(3-4), 233.

Dry reforming of ethane on tri-metallic perovskites (LaCo_xFe_{1-x}O₃). Characterisations and reactivity.

G. Rodriguez^{1*}, A.C. Roger¹, L. Bedel¹, L. Udrón¹, L. Carballo^{*}, A. Kiennemann¹

¹LMSPC-ECPM, UMR 7515 25, rue Becquerel 67087 Strasbourg Cedex 2 France

*Universidad Nacional Colombia, Santa Fé de Bogota Colombia.

1. INTRODUCTION

The study of the catalytic dry reforming of light hydrocarbons (C₁, saturated C₂) is of interest for syngas (CO-H₂) production. The obtained CO-H₂ mixture can be used for hydroformylation, methanol or Fischer-Tropsch synthesis. The fast deactivation by excess of carbon deposits is the main drawback of metal supported systems (Ni, Co, Pt, Pd, Rh) [1]. Basic supports like MgO, La₂O₃ have been used to increase the catalyst life by lowering the rate of carbon deposition [2]. A second way has been explored through formation of well defined structure containing an active metal (nickel). For example, we have shown that the partial substitution of Ni by Fe in LaNiO₃ increases the Ni reduction temperature close to the reaction temperature. Strong Ni-tri-metallic perovskite interactions both improve lifetime and dispersion of nickel particles and decrease carbon formation and sintering of metal by formation of a Ni-Fe alloy [3,4,5]. Due to the good ability of perovskite-type oxides to be B-site substituted, Ni could be replaced by other metal such as Co.

The aim of the present study is to point out the interest of these defined Co-containing structures in reforming of ethane.

2. EXPERIMENTAL PART

2.1. Preparation. The mixed LaCo_xFe_{1-x}O₃ perovskites with x values varying from 0 to 1 (x = 0, 0.3, 0.5, 0.7, 1) were prepared from La acetate, Co acetate and Fe powder via a sol-gel related method [6]. The starting materials were separately dissolved in hot propionic acid under stirring and then mixed. After 30 minutes stirring, the boiling resulting solution was evaporated until a resin is obtained. This resin was heated 4 hours at 750°C with a ramping of 3°C.min⁻¹. BET surface areas were in the range of 3 (x=0) to 6 m².g⁻¹ (x=1).

2.2. Characterization The nature of the obtained phases and the lattice parameters were determined by powder X-Ray diffraction (XRD) recorded on a Siemens D-5000 diffractometer using the CuKα radiation.

Transmission electron microscopy (TEM) was performed on a TOPCON-EM002B apparatus coupled with an energy dispersive X-Ray device (EDS).

Temperature programmed reduction (TPR) was performed with a 50 mg sample placed in a U-shaped quartz tube (6.6 mm ID), the temperature was increased from 25 to 900°C with a slope of 15°C min⁻¹. The reducing mixture was 3 vol.% hydrogen in helium (50 mL min⁻¹). Hydrogen consumption was quantified by a TC detector after trapping on molecular sieve of the formed water.

2.3. Reaction conditions The operating conditions were the following : fixed bed quartz reactor (6.6 mm I.D.), inlet temperature : 400-800°C; feed flow rate : 0.15 L.h⁻¹ ethane, 0.3 L.h⁻¹ CO₂ and 2.55 L.h⁻¹ Ar; catalyst amount: 100 mg. The outlet gas was analyzed by two on line gas chromatographs: one for C₂H₆, CO and CO₂; and a second one for CO and H₂.

3. RESULTS

3.1. Characterization of LaCo_xFe_{1-x}O₃ systems before catalytic test

XRD pattern of LaCo_xFe_{1-x}O₃ (x=0.3, 0.5 and 0.7) shows that a solid solution is formed in all proportions. A split of the main reflection line for x ≥ 0.5 is characteristic of the rhombohedral system (R) of LaCoO₃ isomorphs. Compounds without split reflection crystallize in the orthorhombic (O) system such as LaFeO₃ [7].

The different catalysts have been analysed by TEM-EDS to confirm the initial composition of the structures and the homogeneity of the preparation (figure 1).

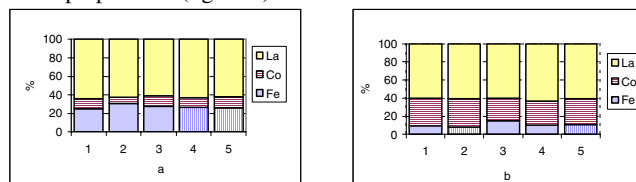


Figure 1. Elemental distribution observed by energy dispersive X-ray spectroscopy before catalytic test for: (a) LaCo_{0.3}Fe_{0.7}O₃ and (b) LaCo_{0.7}Fe_{0.3}O₃. (1) Broad focused beam 200nm (2-5) Narrow focused beam 14 nm.

The characterization (with broad and narrow focussed beam) shows a good homogeneity of each preparation which is formed of grains of around 50 nm each. The reducibility of the perovskites was studied by T.P.R.. The hydrogen consumption is given versus temperature for four different materials (figure 2).

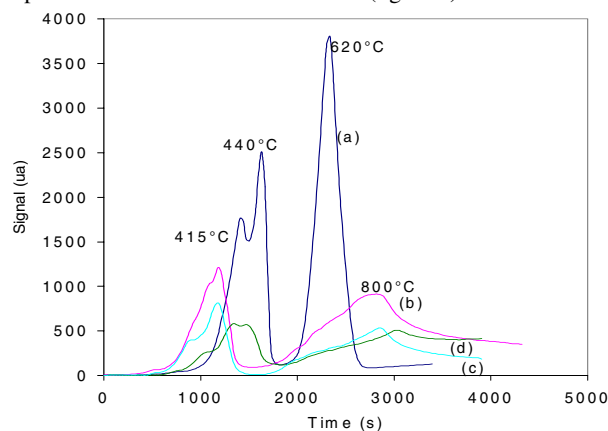


Figure 2. TPR before catalytic test for (a) LaCoO₃, (b) LaCo_{0.7}Fe_{0.3}O₃, (c) LaCo_{0.5}Fe_{0.5}O₃ and (d) LaCo_{0.3}Fe_{0.7}O₃.

The T.P.R. shape reveals two reduction areas. The first between 350°C and 500°C, the second with a maximum between 620°C (LaCoO₃) and 810°C (LaCo_{0.3}Fe_{0.7}O₃). The temperature of the second maximum increases with iron content. So it is possible to control the perovskite reduction temperature by varying the Co/Fe ratio, and to correlate it with the ethane reforming temperature.

3.2. Catalytic tests. Figures 3 and 4 show respectively the ethane conversion and the CO yield versus x for temperatures between 600°C and 800°C. Ethane conversion increases with increasing x values and temperatures. There is an important change in conversion and CO yield when x is equal or higher than 0.5. This value corresponds to a change of the structure from orthorhombic to rhombohedral. LaCoO₃ shows excellent results too, but deactivated very fast. On the other hand, catalysts containing cobalt and iron showed very good stability in addition to performance.

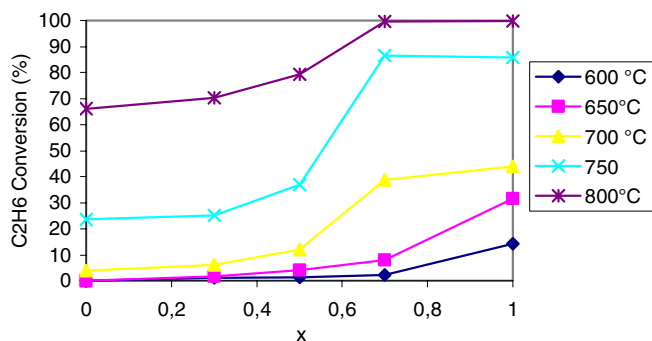


Figure 3. C₂H₆ Conversion at various temperatures versus x with a CO₂/C₂H₆=2 for LaCo_xFe_{1-x}O₃ perovskite.

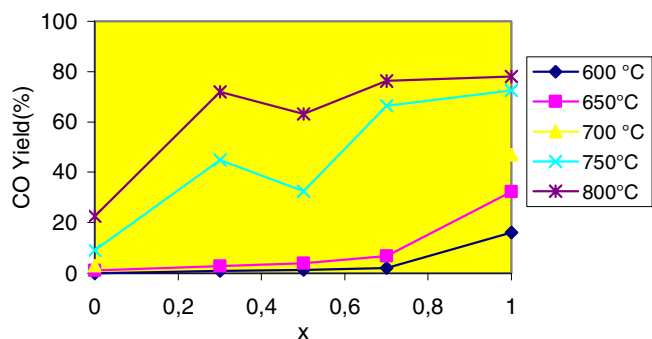


Figure 4. CO Yield (%) at various temperatures versus x with a CO₂/C₂H₆=2 for LaCo_xFe_{1-x}O₃ perovskite.

The interest of the tri-metallic perovskite La-Co-Fe compared to the bi-metallic La-Co is better understood by characterization of the catalysts after test.

3.3. Characterization after test. XRD diffraction patterns after test show different phases depending on x values as summarised in Table 1.

x	Crystalline phases detected by XRD after catalytic test
0	LaFeO ₃
0.3	LaCo _w Fe _{1-w} O ₃ La ₂ O ₃
0.5	LaCo _z Fe _{1-z} O ₃ La ₂ O ₃
0.7	La ₂ O ₃ LaFeO ₃ Co
1	La ₂ O ₃ Co CoO

Table 1. Crystalline phases detected by XRD after test for LaCo_xFe_{1-x}O₃ perovskite oxides.

For higher cobalt contents (x > 0.5) the three-metal perovskite structure is destroyed and the most stable LaFeO₃ perovskite is formed together with lanthanum oxide and cobalt. LaFeO₃ perovskite could also be characterised by FT-IR (555 cm⁻¹). For low cobalt content, the La-Co-Fe perovskite is preserved, although cobalt content is less than in the initial structure.

The LaCoFe elemental distributions (EDS) are given in figure 5 and the La/Fe ratios in figure 6 for x = 0.3 and 0.7. Figure 5 shows a higher heterogeneity of LaCo_{0.7}Fe_{0.3}O₃ compared to LaCo_{0.3}Fe_{0.7}O₃. For x = 0.3, almost the same ratio La/Co/Fe or La/Fe are observed in different parts of the sample, no free cobalt has been seen confirming that the tri-metallic structure was preserved. However, analyses show clearly that part of cobalt has left the perovskite and w and z (Table 1) are lower than the initial value of x. For x = 0.7, the tri-metallic perovskite is destroyed, free cobalt particles are evidenced and the La/Fe ratio changed. The change in La/Fe ratio indicates the presence of free lanthanum (as oxide or hydroxide). In the latter case, in

agreement with XRD results, it can be concluded that the LaFeO₃ perovskite behaves as a support for cobalt metal particles of 10 to 50 nm (TEM).

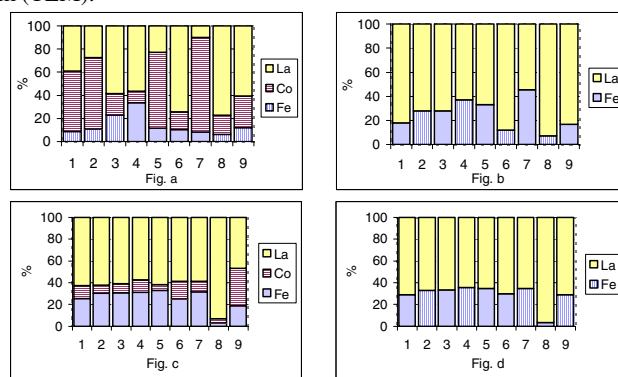


Figure 5. Elemental distribution observed by energy dispersive X-ray spectrometry after catalytic test for: LaCo_{0.7}Fe_{0.3}O₃ (a) La, Co and Fe. (b) La and Fe. LaCo_{0.3}Fe_{0.7}O₃ (c) La, Co and Fe. (d) La and Fe. (1) Broad focused beam 200nm (2-9) Narrow focused beam 14 nm.

4. DISCUSSION AND CONCLUSIONS

In the present study, we can see that whatever the x value (until 0.7), the perovskite structure is preserved : as LaCoFe for x ≤ 0.5 and as a LaFe system for x ~ 0.7.

The catalytic results have shown an increase of reactivity with the increase of the x value and of the reaction temperature. Moreover a gap of activity corresponds to a change of the perovskite structure from orthorhombic to rhombohedral. Such a change has also been seen in Fischer-Tropsch reaction (7). Good aging for the catalysts suggests that coke formation is limited as confirmed by elemental analyses. Different explanations could be given : formation of small Co metal particles in strong interaction with the perovskite support or formation of a Co-Fe alloy and dilution effect. With La-Fe-Co catalysts alloy formation was not seen. For 0.3 ≤ x ≤ 0.7, we suggest that the presence of cobalt inside the partially reduced perovskite network is in strong interaction with the free cobalt and then avoids an excessive coke formation, resulting in a good aging. This strong interaction is confirmed by the possibility of regeneration of the used catalyst by heating at high temperatures (900°C). Another contribution to decreasing coke formation is the performance of LaFeO₃ in total oxidation of hydrocarbons. Thus it is postulated that LaFeO₃ as well as La₂O₃ will participate in the oxidation of coke precursors.

Acknowledgement. The authors are deeply grateful to ECOS-NORD for providing fellowship to G. Rodriguez and to the European Community through the RUCADI program.

REFERENCES

- (1) J.R. Rostrup-Nielsen, *Catalysis Science and Technology* 5 **1984**, 1, J.R. Anderson, and M. Boudart (eds) Springer (Berlin).
- (2) F. Frusteri, F. Arena, G. Calogero, T. Torre, A. Parmaliana, *Catalysis Communications* **2001** 2 49.
- (3) H. Provendier, C. Petit, C. Estournes, S. Libs, A. Kiennemann, *Appl. Catal. A* **1999** 180 163.
- (4) C. Petit, A. Kiennemann, P. Chaumette, O. Clause, *U.S. Patent 5447705* **1995**.
- (5) H. Provendier, C. Petit, C. Estournes, A. Kiennemann, *Stud. Surf. Sci. Catal.* **1998** 119 741.
- (6) H. Provendier, C. Petit, J.L. Schmidt, A. Kiennemann, C. Chaumont, *J. Mater. Sci.* **1999** 34 4121.
- (7) L. Bedel, A.C. Roger, A. Kiennemann, C. Estournes, Prepr. Pap. ~ *Am. Chem. Soc., Div. Petroleum Chem.*, **2000**, 45, 236.

Effect of H₂S on the Reaction of CH₄ with CO₂ over Titania Supported Noble Metal Catalysts

András Erdőhelyi, Tamás Szailer and Éva Novák

Institute of Solid State and Radiochemistry, University of Szeged, P.O. Box 168, H-6701 Szeged, Hungary

Introduction

Great efforts are made in the last decade in the catalytic transformation of methane and carbon dioxide, the cheapest carbon containing materials, into more valuable compounds. One of the possibilities to achieve this goal is to react CH₄ with CO₂ to produce synthesis gas. All of the Group VIII metals on a variety of supports have been studied as a dry reforming catalyst [1]. The high efficiency of supported noble metals in this reaction was confirmed by our studies [2-4]. Relatively little attention was paid to the effect of sulphur on the CO₂ + CH₄ reaction although natural gases always contain more or less amount of sulphur compounds.

The present report gives an account of the effect of H₂S on the CO₂ + CH₄ reaction in the presence of different titania supported noble metal catalysts. This reaction can be described as the sum of different reactions, for example the steam reforming and the reverse water gas shift reactions. For comparison the CO₂ hydrogenation was also studied in the presence of H₂S. Great attention was paid to the formation of surface species during the reaction and to the effect of H₂S on it.

Experimental

Materials. The catalysts were prepared by impregnating the TiO₂ support (Degussa P25) with the solution of Pt metal salts to yield a nominal 1 % metal loading. The following salts were used: H₂PtCl₆·6H₂O, PdCl₂, RhCl₃·3H₂O and RuCl₃·3H₂O. The impregnated powders were dried at 383 K. Before any measurements the fragments of catalyst pellets were oxidized at 473 K for 30 min and reduced at 673 K in the catalytic reactor for 1 hour.

Methods. The adsorption and interaction of the reacting gas mixtures were studied by FTIR spectroscopy.

The catalytic reactions were carried out in a fixed bed continuous-flow reactor (100mm x 27 mm o.d.). The ratio of CH₄/CO₂ in the reacting gas mixture was 1:1 and that of CO₂/H₂ was 1:4. The inlet gas mixture contained 20 % of Ar or He as diluents and 22 ppm or 116 ppm of H₂S when the effect of H₂S was studied. The amount of catalysts used was usually 0.3 - 0.5 g. The flow rate of the reactants was 80 ml/min. Analyses of the gases were performed with gas chromatograph (Chrompack 9001) using Porapak QS column. The products were detected simultaneously by TCD and FID detectors. The amount and the reactivity of surface carbon formed in the catalytic reactions were determined by temperature-programmed reduction. After the catalytic run the reactor was flushed with Ar, the sample was cooled to room temperature, then the Ar flow was changed to H₂ and the sample was heated up to 1173 K with a 10 K/min heating rate and the hydrocarbons were determined.

Temperature programmed desorption experiments were carried out in a quartz reactor (8 mm o.d.) filled with 0.3 g of samples. The products were analysed by an online mass spectrometer (Balzers QMS 200).

The dispersions of the supported metals were determined by H₂-O₂ titration at 298 K using the pulse technique.

Results and Discussion

Infrared spectroscopy measurements revealed that CO is formed in the interaction of CH₄ + CO₂ and of CO₂ + H₂ far below the

reaction temperature. The CO spectra obtained in the interactions were compared with those of clean CO, adsorbed on the same catalyst after the same pre-treatment. In the presence of H₂S after the adsorption of CO nearly the same features were registered, only the intensity of the absorption bands decreased. Zhang et al. also found that the presence of S does not significantly influence the geometrical structure and chemisorption energy of CO adsorbed on Rh(111) surface [5]. In the interaction or in the reaction of CH₄ + CO₂ or CO₂ + H₂ the CO band appeared at significantly higher temperature on the spectra than in the absence of H₂S, although in the case of Rh/TiO₂ the gas phase spectra of CH₄, which was the main product in the H₂ + CO₂ reaction, were detectable with the same intensities.

The reaction between CO₂ and CH₄ proceeded rapidly above 673 K on TiO₂ supported noble metals to give CO and H₂ with different ratios. The reaction occurred at the highest rate (rates per unit surface area of metals) in the first minutes of the reaction on Ru followed by Pd, Rh and Pt. This is practically the same as the sequences for CH₄ + CO₂ reaction on alumina supported noble metals [2]. The conversion of CO₂ exceeded that of CH₄ for every catalyst sample. The CO/H₂ ratio was between 2 and 3 in the first minutes of the reaction (Table 1). In the presence of H₂S the initial rate of H₂ or CO formation and the conversion of the reactants decreased in time in all cases (Fig. 1 and Table 1). The deactivation rate was the highest on supported Rh catalyst, and the lowest on Ru/TiO₂.

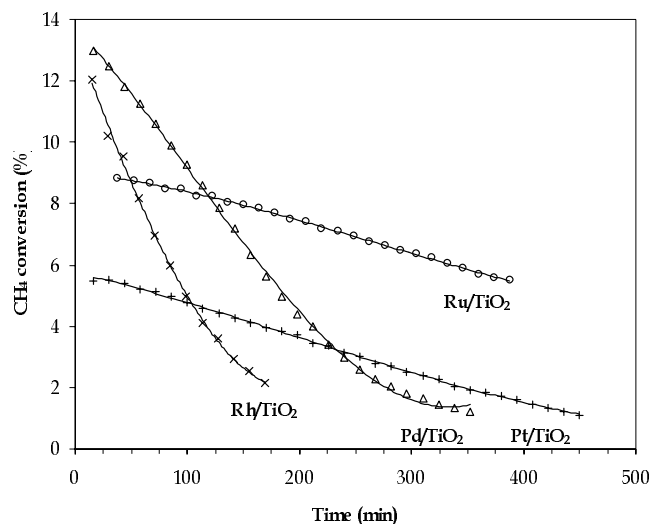


Figure 1. The conversion of methane in the CH₄ + CO₂ reaction on different TiO₂ supported catalysts at 773K in the presence of 22 ppm H₂S

The initial conversion of methane at 773 K was 12 % on Rh/TiO₂ but after 3 hours of the reaction it was only 2.1 %. On Ru/TiO₂ this value changed only from 8.8 % to 7.7 %. While the rate of products formation decreased, the CO/H₂ ratio surprisingly increased continuously in all cases (Fig. 2).

The enhancement of the CO/H₂ ratio at the beginning of the reaction was relatively low, but after a time lag it increased considerably. The length of this time depends on the metal; it was about 50 minutes on Rh/TiO₂ and more than 100 minutes on titania supported Pt catalyst. In the presence of Rh/TiO₂ after 180 minutes of the reaction the CO/H₂ ratio was more than 8 (Table 1). The most stable catalyst was Ru/TiO₂ on this sample the CO/H₂ was only 2.7 after 400 minutes.

When the H₂S concentration was increased in the reacting gas mixture (116 ppm) the conversion of CH₄ or CO₂ decreased more

rapidly. After 180 minutes the CH₄ conversion was less than the initial value by more than one order of magnitude in all cases. The CO/H₂ ratio increased as was observed earlier.

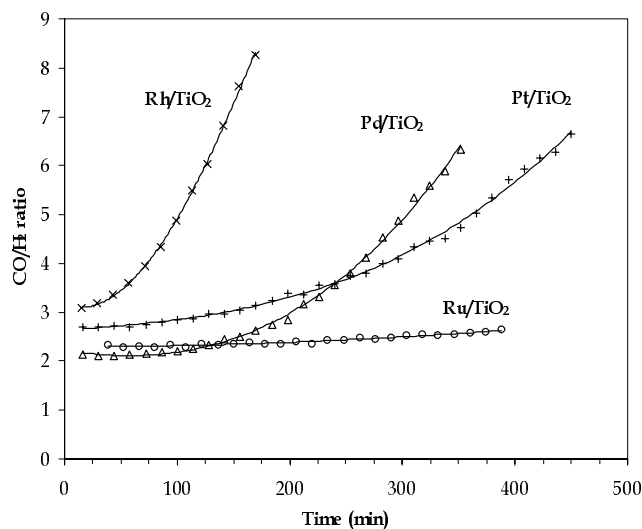


Figure 2. Changes of the CO/H₂ ratio in the CH₄ + CO₂ reaction on different TiO₂ supported catalysts at 773K in the presence 22 ppm of H₂S

The amount of surface carbon was determined after the catalytic reaction. In the case of Rh/TiO₂ in the presence of H₂S the amount of surface carbon was lower than the absence of it. The reactivity of this carbonaceous deposit did not change significantly. These results agree well with the observation found in the Sparg process [6] when the supported Ni catalyst was pre-sulphided to decrease the surface carbon formation.

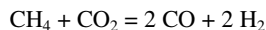
In the absence of H₂S on TiO₂ supported samples the CH₄, CO₂ conversion and the CO/H₂ ratio did not change significantly during the reaction. On silica-supported samples in the presence of H₂S although the conversion decreased as mentioned above, the CO/H₂ ratio remained nearly the same.

Table 1. Some Characteristic Data for CH₄ + CO₂ Reaction on Titania Supported Noble Metal Catalysts at 773 K in the Presence of 22 ppm H₂S.

Samples	D%	Conversion				CO/H ₂	
		CH ₄		CO ₂			
		15	360	15	360	15	360
		Minutes					
1%Ru/TiO ₂	9.4	8.8	5.5	14.9	10.8	2.32	2.65
1%Rh/TiO ₂	41	12.0	2.1*	17.9	4.9*	3.0	8.2*
1%Pd/TiO ₂	16	12.9	1.2	20.8	2.2	2.1	6.3
1%Pt/TiO ₂	38	5.5	1.7	10.4	4.2	2.7	5.0

* Data were obtained in the 180 minutes of the reaction

We found that CO₂ conversion was higher than that of methane in all cases and that the CO/H₂ ratio increased in time in the presence of H₂S. These observations indicated that the reaction



was followed by several secondary processes, including the hydrogenation of CO and CO₂, the water gas shift reaction and the Boudouard reaction.

CO₂ hydrogenation was studied in the presence of 22 ppm H₂S at 548 K. The main product of the reaction was methane on Ru and Rh catalysts; its selectivity was near 100%. On Pt and Pd samples mainly CO was formed. The methane selectivity was about 20% at the beginning of the reaction. These results agree well with our earlier results [7-9] obtained on different supported noble metal catalysts. In spite of the 22 ppm H₂S concentration of the reacting gas mixture the rate of product formation or the CO₂ conversion changed only slightly in all cases. The highest decrease was in the case of Pd catalyst when the initial conversion decreased from 10.0% to 6.54% during 6 hour of the reaction. It has to be mentioned that during the same time in the CO₂ + CH₄ reaction the CO₂ conversion decreased from 20.8 to 2.9%. When the reaction was studied at 773 K at the same temperature, where the CO₂ + CH₄ reaction was followed the same results were obtained. In this case the contact time was lower, so the conversion was in the same range.

These observations suggest that H₂S poisons the CO₂ + CH₄ reaction, while the CO₂ + H₂ reaction was only effected slightly by the same amount of H₂S. This finding results the changes of the CO/H₂ ratio. The rate of hydrogen formation in the CO₂ + CH₄ reaction decreased while the consumption rate of it in a secondary reaction remained the same. In some cases CO is also formed in this process so the CO/H₂ ratio has to increase during the CO₂ + CH₄ reaction.

On SiO₂ supported samples in the CO₂ + CH₄ reaction the CO/H₂ ratio does not change significantly, so the effect observed on TiO₂ supported metals depends on the support.

The interaction of H₂S with the titania supported metals was studied by temperature programmed desorption method. The adsorption was performed on the reduced samples by exposure to Ar flow containing 110 ppm of H₂S for 30 min at 373 K. Afterwards the reactor was flushed with Ar for 10 min, cooled down to room temperature and the sample was heated at a rate of 20 K/min up to 1073 K. The products were analysed by an online mass spectrometer. After H₂S adsorption on titania supported noble metals only SO₂ desorption was detected in two stages nearly at the same temperatures. H₂S evolution was not observed. Fig. 3 shows the TPD curve in the case of Pd/TiO₂ sample.

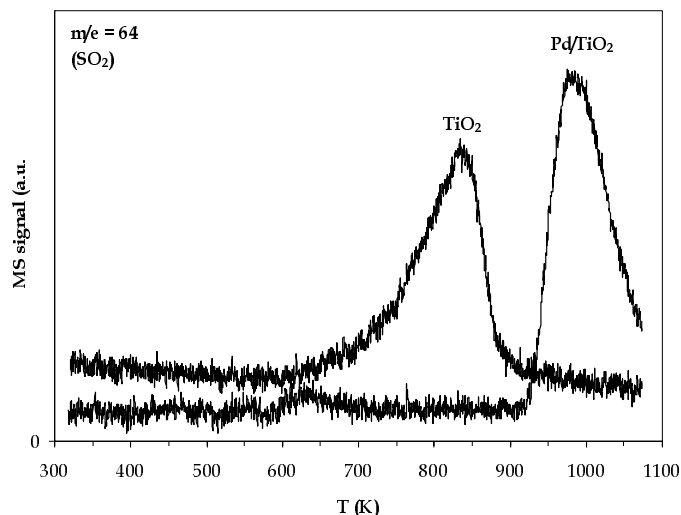


Figure 3. Temperature programmed desorption spectra of adsorbed H₂S at 373 K

A small peak was detected above 580 K ($T_{\text{Max}}=631$ K), but at higher temperature, above 920 K, great amount of SO_2 desorption was observed ($T_{\text{max}}= 988$ K). For comparison the TPD of adsorbed H_2S on clean TiO_2 is also presented on Fig. 3. In this case, too, only SO_2 was desorbed, but in one stage in the temperature range 630 – 910 K ($T_{\text{Max}}= 840$ K). Beck and White [10] and Chen et al. [11] found nearly the same picture on clean TiO_2 .

These results clearly show that the most part of the adsorbed H_2S desorbed from the TiO_2 and from the TiO_2 supported noble metals as SO_2 . From these results we may suppose that sulphur was built into the oxygen vacancies of the TiO_2 [11] and created new catalytic centres on the metal-support interface. These sites have different catalytic activities in the secondary reactions of the dry reforming of methane and this is the reason why the CO/H_2 ratio increased in the reaction in the presence of H_2S .

Acknowledgement.

Financial support of this work by OTKA (contract number T 034270) is gratefully acknowledged

References

- (1) Bradford, M.C.J., Vannice, M.A., *Catal. Rev.* **1999**, *41*, 1.
- (2) Solymosi, F., Kutsán, Gy., Erdőhelyi, A., *Catal. Letters* **1991**, *11*, 149.
- (3) Erdőhelyi, A., Cserényi, J., Solymosi, F., *J. Catal.* **1993**, *141*, 287.
- (4) Erdőhelyi, A., Cserényi, J., Papp, E., Solymosi, F., *Appl. Catal. A General* **1994**, *108*, 205.
- (5) Zhang, C.J., Hu, P., Lee, M.-H., *Surface Sci.* **1999**, *432*, 305.
- (6) Dibbern, H.C., Olesen, P., Rostrup-Nilsen, J.R., Toettrup, P.B., *Hydrocarbon Proc.* **1986**, *65*, 71.
- (7) Solymosi F., Erdőhelyi, A., *J. Mol. Catal.* **1980**, *8*, 471.
- (8) Solymosi F., Erdőhelyi, A., Bánsági, T., *J. Catal.* **1981**, *68*, 371.
- (9) Erdőhelyi, A., Pásztor, M., Solymosi, F., *J Catal.* **1986**, *98*, 166.
- (10) Beck, D.D., White, J.M., *J. Phys. Chem.* **1986**, *90*, 3123.
- (11) Chen, Y., Jiang, Y., Li, W., Jin, R., Tang, S., Hu, W., *Catal. Today*, **1999**, *50*,39.

ENZYMATIC CONVERSION OF CARBON DIOXIDE TO METHANOL BY DEHYDROGENASES ENCAPSULATED IN SOL-GEL MATRIX

Zhongyi JIANG, Hong WU, Songwei XU, Shufang HUANG

State Key Lab. of C1 Chemistry and Chemical Technology, School of Chemical Engineering and Technology, Tianjin University, Tianjin 300072, China

Introduction

Due to the abundance of CO₂ as the major greenhouse and the most oxidized form of carbon, the efficient utilization of CO₂ has aroused much interest from fundamental research to application application.

Herein, we report a novel and promising approach to convert carbon dioxide into methanol through consecutive reduction catalyzed by three different dehydrogenases. The whole process consists of three steps: reduction of CO₂ to formate catalyzed by formate dehydrogenase (F_{ate}DH), reduction of formate to formaldehyde by formaldehyde dehydrogenase (F_{ald}DH), and reduction of formaldehyde to methanol by alcohol dehydrogenase (ADH). Reduced nicotinamide adenine dinucleotide (NADH) acts as a terminal electron donor for each dehydrogenase-catalyzed reduction.

It is now well established that a wide variety of enzymes retain their characteristic reactivities and chemical functions when they are confined within the pores of the silica sol-gel derived matrix. The porosity of sol-gel glasses allows small molecules and ions to diffuse into the matrix while the enzymes remain physically trapped in the pores, and thus resulting in an enhanced probability of reaction due to an increase in local concentration of substrates within the nanopores. Our experiments demonstrated that when the above-mentioned three enzymes are encapsulated in the silica sol-gel matrix, the yield of methanol is considerably increased as compared to that in solution phase.

Experimental

The reaction was studied in the solution phase by using an enzyme stock solution that was comprised of 7mg/mL of F_{ate}DH, 2mg/mL of F_{ald}DH, 2mg/mL of ADH dissolved in 0.1M phosphate buffer at pH7. Add 1.0 mL of the enzyme stock solution to 1.0 mL of NADH solution in a polystyrene cuvette such that the final concentration of NADH varied from 0.025 to 0.1M. The cuvette was covered with Parafilm to prevent the evaporation loss of methanol produced, and CO₂ was then bubbled through the solution for 8 h to ensure that the reaction equilibrium was established.

The concentration of methanol was determined by gas chromatography. A calibration curve was established for methanol aqueous solutions with known concentration of methanol ranging from 0.001 to 0.005M. To evaluate the concentration of methanol produced as a result of the enzyme-catalyzed reaction. 1.0 μL of the final reaction solution was used for GC measurements. The concentration of methanol was calculated by using peak areas for the characteristic methanol band in the chromatogram.

The sol-gel encapsulated samples were prepared as follows:

Tetraethoxysilane (TEOS) was used as precursor for making the silica sol-gel. The initial sol was prepared by mixing 2.60g of TEOS, 1.10g of 3%(v/v) of HCl solution. The mixture was then vigorously mixed for 10 min to form sol. The gel were prepared by adding 1.0 mL of the stock enzyme solution to 1.0mL of the sol in a polystyrene cuvette. Typical gelation times are on the order of 10-30s. The cuvette was then covered with Parafilm and gel was allowed to age at 4°C for 24 h. The aged gel was then put into a dialysis membrane using 250 mL of 0.1M phosphate buffer at pH7 as dialysis solution, and placed in refrigerator at 4°C with frequent change of 0.1M phosphate buffer at pH7. The dialysis lasted 24-48 h to completely remove ethanol generated in the sol-gel process. 0.1 mL of NADH solution diffused into the gel by dialysis in the similar manner (the final concentration of NADH varied from 0.025 to 0.1M), the sample containing the gel and the NADH solution was left undisturbed for 48h. To this mixture, CO₂ was then bubbled for 8h for production of methanol. The concentration of methanol produced was determined using GC by taking a 1.0 μL aliquot of the solution.

Results and Discussion

Table 1 shows the preliminary methanol yields in solution and sol-gel matrix. The overall yield of the reaction in solution is near to 100%. In sol-gels, the production yield of methanol is substantially decreased due to the distribution effect, stereo hindrance, diffusion resistance.

Table1 Representative methanol yields in solution and sol-gel matrix

	Reaction Temperature °C	NADH (μ mol)	Methanol yield (%)
Solution	25	100	98.0
	37	100	100
	37	150	94.8
Sol-gel matrix	25	100	30.0
	37	100	91.9
	37	150	42.2

It is also found that all four species (i.e. F_{ate}DH, F_{ald} DH, ADH, NADH) must be present to generate methanol.

The introduction of chemical modification to the enzymes and the creation of mesoporous structure of gel by biomimetic synthesis is under investigation.

To sum up, the feasibility of enzymatic conversion of carbon dioxide to methanol is tentatively explored. The consecutive reduction of carbon dioxide by three different dehydrogenases encapsulated in sol-gel matrix results in enhanced yields for generation of methanol. This will open up a new avenue not only for on-site production of methanol from cheap raw material but also for efficient fixation of the greenhouse carbon dioxide.

Acknowledgment

This work was supported by the National Natural Science Foundation of China, under the contract 20176039

References

- (1). Obert R., Dave B.C.. *J. Am. Chem. Soc.*, 1999, 121, 12192-12193.
- (2). Gill I., Ballesteros A.. *Trends in Biotechnology*, 2000, 18: 282-296.
- (3). Ellerby L M, Nishida C R, Nishida F et al. *Science*, 1992, 255: 1113-1115

FREQUENCY EFFECTS IN THE CATALYTIC OLIGOMERIZATION OF METHANE VIA MICROWAVE HEATING

L. Daniel Conde, Carolina Marin, Steven L. Suib*, Zak Fathi

University of Connecticut
Department of Chemistry
55 North Eagleville Rd. U3060
Storrs, CT 06269-3060

Introduction

Many efforts have been focused on the activation of methane to more valuable products in the last two decades. Many studies have been done in order to produce more valuable products from natural gas, of which methane is the major constituent. Natural gas is an inexpensive and abundant energy resource. Therefore, effective and economic processes to obtain higher hydrocarbons, methanol and/or synthesis gas would be valuable.

Thermal,¹⁻³ homogeneous,⁴⁻⁶ and heterogeneous⁷⁻¹⁰ catalytic conversions of methane to higher hydrocarbons have been studied by many authors. Due to the high thermodynamic stability of methane compared with that of higher hydrocarbons, methane can only be thermally converted to C₂₊ hydrocarbons at temperatures higher than 1400 K. The products are unsaturated and unstable hydrocarbons such as acetylene. Therefore, appropriate temperature, residence time control, and rapid reaction quenching are necessary to achieve selectivity to desired products. Otherwise, carbon and hydrogen will be the only products.

The use of microwave heating to induce chemical reactions has been studied for several years. Over the past decade microwave heating has been employed extensively in organic³⁷⁻⁴¹ and inorganic synthesis.⁴¹⁻⁵⁵ Microwave-induced catalytic reactions have been studied extensively by Wan and coworkers.^{25,35,27-29,58-61} We have studied the oligomerization of methane to higher hydrocarbons using Ni powder, Fe powder, and activated carbon.⁶² Oligomers ranging from C₂ to C₆ hydrocarbons have been produced in a relatively high selectivity depending on the nature of the catalyst, power level, and the presence of He as a diluent gas.

Nickel catalysts have been shown to be highly selective and effective catalysts to lower the activation energy of breaking the carbon-hydrogen bond. Although microwave heating has been studied very systematically for the oligomerization of methane it is not clear yet what other factors might affect the activity and product distribution of this reaction. In this work, we studied the systematic effects of frequency and magnitude of the applied microwave radiation on the conversion and product distribution of methane oligomerization using nickel catalysts in the presence and absence of He as a diluent gas.

Experimental Section

Microwave Apparatus and Gas System. Oligomerization of methane was carried out in a flow reactor system. A Lambda Technologies variable frequency unit, Vari-Wave model VW-2750 was used for these experiments. The reactor, a straight 3/8 in-quartz tube, was mounted horizontally inside the cavity. Methane gas as well as He diluent gas was mixed in a panel when necessary and flowed into the quartz reactor. High Purity (HP) grade methane obtained from Matheson and Ultra High Purity (UHP) helium purchased from Airgas were used.

Various frequencies and modes were produced in the microwave cavity. This cavity allows TM_{01n} modes (n = 2 to 9) over a frequency

range of 2.400 to 5.056 GHz. The cavity was designed by Lambda Technologies to have different modes for each frequency. Our experiments were done with and without diluent at 2.40 GHz at TM₀₁₂ and also at 4.60 GHz at TM₀₁₈ for comparison. Thermal paper was inserted into the microwave cavity and used to map the heating patterns of the various modes.

The length of the aluminum cavity was 29.5 cm and the radius was 5.15 cm. In order to ensure microwave absorption for a specific frequency value and power level, the reflected power had to be minimized first by means of a tuning knob and the frequency tuning control on the main panel. Therefore, the working frequency is a result of the tuning process. Reflected power higher than 60 W makes the safety feature of the unit shut off. Thus, not all frequencies are possible for a particular system.

Catalyst. Nickel powder catalyst with morphology of branched filaments was used for these experiments. The diameters of the filaments were 2.5 μm as measured in a Scanning Electron Microscopy (SEM) photograph. Clusters of nickel metal particles were aggregated to form the filaments. The catalyst (100 mg) was placed inside the reactor with high purity quartz wool on either side of the catalyst bed. The reactor was placed in the center of the aluminum cavity. Helium was flushed for 30 min through the reactor to purge the atmosphere.

The experiments were run at two different flow rates: 3 mL/min of pure methane; and 12 mL/min of a 3:1 mixture of helium and pure methane respectively at atmospheric pressure. Samples for analyses were taken after 3 min of irradiation time for each power level (100, 130, 170, 210, 300, and 370 W).

Product Analysis. Products were trapped using a 4 way-gas sampling valve and analyzed by using an HP5890 Series II Chromatograph equipped with a mass detector. Details about the Gas Chromatograph/Mass Spectrometer (GC/MS) were published elsewhere.⁶²

Results

Microwave Induced-Oligomerization (MIO) of methane was performed at two different frequency levels (2.40 and 4.60 GHz). It was not possible to set the unit to operate under other frequencies. The effect of power and the presence of helium as diluent gas on conversion and product distribution were also studied at these two different frequency values. A summary of the results can be seen in **Table 1**.

Feed	Flowrate (mL/min)	Time (min)	Power ^(a) (W)	Astex Unit ^(b)		
				2.45 GHz	2.40 GHz	4.60 GHz
CH ₄	3	3	130	N.R.	N.R.	Y
			370	Y	N.R.	Y
CH ₄ :He	3:9	3	130	N.R.	N.R.	Y
			370	Y	Y	Y

Table 1. Summary Results. N.R. = no reaction; Y = see Fig. 4 - 7 for product distribution. ^(a) 100, 130, 170, 210, 300, 370 Watts of power level were used. Those not shown in the table were neither relevant nor reaction detected at any frequency. ^(b) It was not possible to set other frequency values with successful microwave absorption.

No visible arc formation was detected during these runs and the catalyst bed remained the same after reaction (checked by SEM photographs). Ethylene, acetylene and ethane were the major C₂ products observed for the oligomerization of methane via microwave

heating using Ni powder as a catalyst. Benzene was also formed with selectivities that ranged from 10 to 29%. In the case of 25% diluted methane as a feed and low frequencies (2.45 GHz), low selectivities of benzene were detected (2 to 5%).

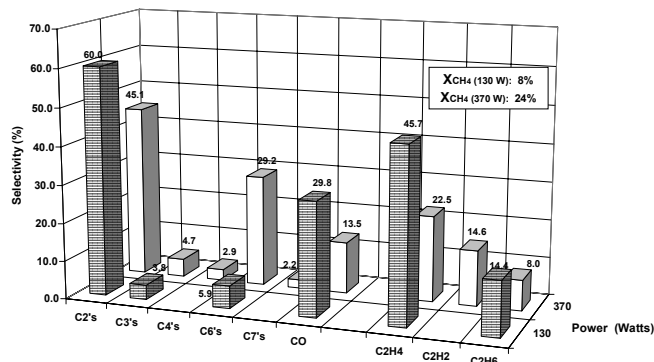


Figure 1. Effect of applied power on product distribution at 4.60 GHz using pure methane as a feed and nickel powder catalyst

Pure Methane as Reactant. When using pure methane as reactant, as power increased from 130 to 370 W at 4.60 GHz, conversion increased from 8 to 24%. Selectivities towards C_{2s} decreased from 60 to 45% and selectivities towards C_{6s} increased from 6 to 29% (Figure 1). Acetylene was not detected at low power (130 W). At 370 W, the relative proportions of C_2 products were ethylene > acetylene > ethane. At a low frequency (2.45GHz), when using pure methane as reactant, oligomerization was not achievable using the variable frequency unit. Therefore, for pure methane, the effect of frequency was compared using an ASTEX unit at the same conditions except at a fixed 2.45 GHz frequency (for more detail see previous publication).⁶² The selectivities towards C_{2s} decreased from 71 to 45% and the selectivities towards benzene (C_{6s}) increased from 20 to 29% when the frequency was increased from 2.45 to 4.60 GHz at 370 W. The selectivities towards ethylene, acetylene, and ethane decreased as frequency increased, maintaining their relative proportions (Figure 2).

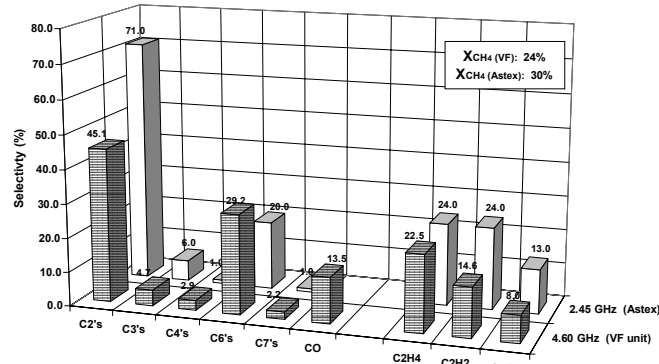


Figure 2. Frequency effect on product distribution at 370 W using pure methane as a feed and nickel powder catalyst

Methane Diluted in He (25%). When the feed was changed to 25% methane in helium, as power was increased from 130 to 370 W at 4.60 GHz, conversion increased from 6 to 8%, selectivities towards C_{2s} decreased from 83 to 72%, and selectivity towards benzene increased from 1 to 10%. Conversion levels were lower than those in the case of using pure methane as a feed (6 and 8% compared to 8 and 24%). Also, while increasing power, less drastic changes in

selectivity towards C_{2s} and C_{6s} were observed than those when using pure methane (See Figures 1 and 3).

Acetylene was not detected at 130 W and 4.60 GHz frequency. The relative proportion of C_{2s} changed from ethylene > ethane to ethane > ethylene > acetylene as power was increased from 130 to 370 W (Figure 3), which was different from the proportion of C_{2s} in the case of pure methane as a feed (ethylene > acetylene > ethane). The systematic effect of frequency was studied using the Lambda variable frequency unit and comparisons were also made when using the fixed frequency ASTEX unit in order to check for reproducibility of results at low frequency (2.45 GHz).

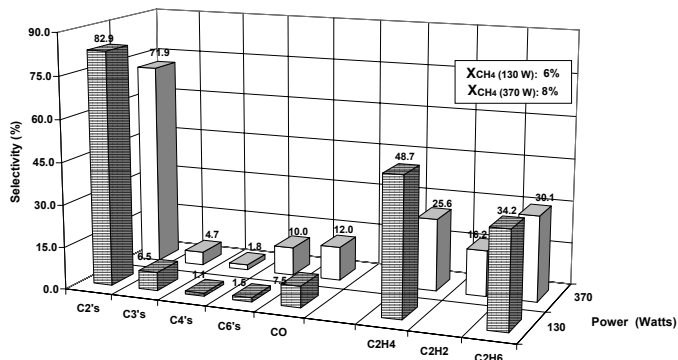


Figure 3. Effect of applied power on product distribution at 4.60 GHz using methane diluted in helium (25%) and nickel powder catalyst.

The data here show that both the ASTEX fixed frequency and the Lambda variable frequency systems behave almost the same when comparing data at low frequency (2.45 GHz) with respect to conversion levels (about 7%) and product distributions (Figure 7) at 370 W. As frequency was increased from 2.45 to 4.60 GHz, selectivities towards C_{2s} decreased from 81 to 72% and selectivity towards benzene increased from 5 to 10% (Figure 4). When using He as diluent at 370 W, the only C_2 detected was ethane at a low frequency value (2.45 GHz). As frequency was increased from 2.45 to 4.60 GHz, the proportion of C_2 products changed from ethane to ethane > ethylene > acetylene (Figure 4). The effect of frequency on product distribution among C_{2s} was different with respect to the case of pure methane in the feed as seen in Figures 5 and 7. The proportion of C_{2s} changed from ethylene > acetylene > ethane to ethane > ethylene > acetylene at 4.60 GHz. At 4.60 GHz and pure methane, selectivity of benzene was higher than that at 4.60 GHz and diluted methane (29 vs. 10% respectively).

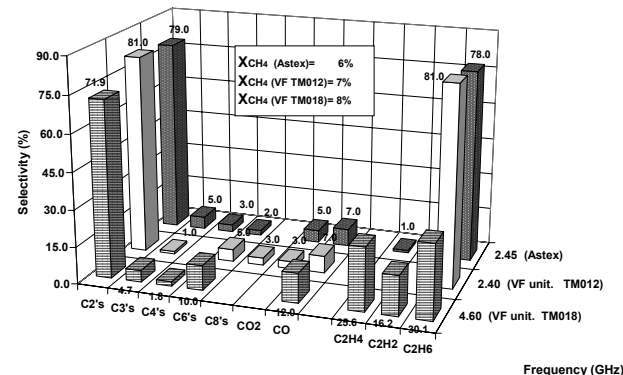


Figure 4. Frequency effect on product distribution at 370 W using methane diluted in helium (25%) and nickel powder catalyst

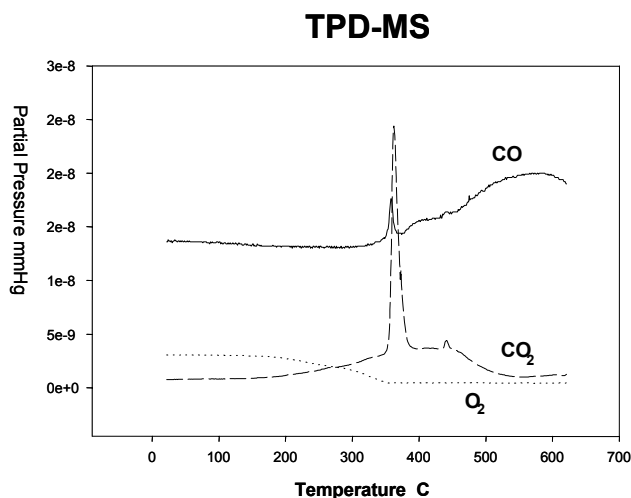
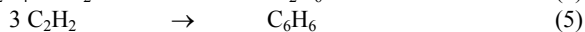
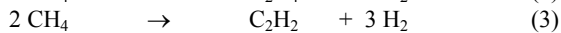
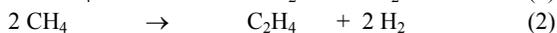
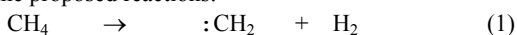


Figure 5. Fresh nickel catalyst Temperature-Programmed Desorption analysis

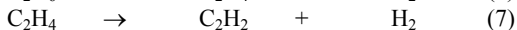
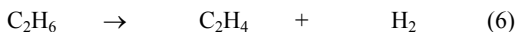
There are different sources of oxygen that account for the formation of carbon monoxide and carbon dioxide detected. Nickel catalyst was used as received for the experiments. Subsequent temperature-programmed desorption analysis revealed the presence of oxygenated species in the catalyst as seen in **Figure 5**.

Discussion

Microwave radiation does not have sufficient energy to cause any chemical changes, such as breaking bonds and transferring electrons. Nickel catalyst strongly absorbs microwave energy providing the necessary kinetic energy for the surface electrons to enhance the surface chemical reaction. The energy absorbed by the metallic sites is transformed from a rapid oscillating electric field into thermal energy. Since only the catalyst surface site is heated, there is a large temperature gradient between the surface and the bulk of the gas phase. The reaction pathway most likely proceeds via formation of free radical intermediates as shown by Wan et. al.⁵⁶ The primary decomposition fragment from methane is the methylene radical which recombines on very hot surfaces to yield acetylene, whereas on cooler surfaces it leads to the formation of ethylene. This finding is in agreement with our results as seen in Figures 4 and 6, which show formation of acetylene as power increased. Equations 1-7 summarize some of the proposed reactions:



The presence of H_2 from reaction (1) leads to hydrogenation of olefins and production of ethane as shown in reaction (4). The highly reactive methylene (:CH_2) intermediate can be used to elucidate the formation of ethylene and acetylene as indicated in reactions (2) and (3). The formation of benzene may be explained by the well-known cyclization reaction given in Equation (5). This is in agreement with the fact that selectivity of benzene increases as selectivity of acetylene also increases. Another viable mechanism for ethylene and acetylene formation could involve the dehydrogenation of secondary hydrocarbons:



The increase in the duration of the pulse in order to achieve a certain average power and therefore an increase in the surface temperature of the catalyst explains the general trend where conversion increases as power increases. Conversion levels were smaller when using He as a diluent in the feed due to the fact that the residence time was about four times smaller than that when using pure methane in the feed (0.08 vs. 0.33 min^{-1} respectively). Allowing the reactant to spend more time in the reaction zone will permit the methane molecules to find adequate sites for reaction to occur. Since the irradiation time of the catalyst was small (3 min), the bulk temperature was not completely homogeneous. That is, there were hot spots, cold spots, and intermediate temperature spots. Methane will only react on those sites that have reached the proper temperature. Thermodynamic analysis has indicated that a catalyst particle surface temperature on the order of 1400°C – 1600°C is required to yield C_2 products from methane.⁶⁷ The proportion of C_2 products changed from ethylene > acetylene > ethane when using pure methane to ethylene > ethane > acetylene when using methane and He in the feed. More benzene was also formed when using pure methane. These observable facts can be explained by both the difference in reagent residence time and the difference in concentration of methane. Wan found that sudden cooling of products would favor the formation of ethylene and ethane.⁶⁷ For the case of CH_4 :He feed, low concentration of active intermediates and products, relatively cold He molecules combined with low residence time, would give the molecules more likelihood for rapid quenching. As mentioned previously, benzene very likely comes from the trimerization of acetylene. High concentrations of methane will statistically favor the formation of acetylene and benzene. Including a diluent in the feed will help prevent the coupling of intermediates to these products.⁶³⁻⁶⁶

At present, the issue of microwave effects is very controversial. Unfortunately, many of the expected results from microwave processing such as rapid and uniform heating, more uniform microstructures, inverse temperature profiles, and selective heating are included in the general category of microwave effects. However, only those anomalies that cannot be predicted or easily explained based on our present understanding of differences between thermal and microwave heating should be referred to as microwave effects.^{44,68} “Microwave specific” activation has been a debated concept which actually refers to a unique interaction, reaction, or activation, specific to the microwave radiation. Two models of the chemical mechanisms in such reactions have emerged from research work done so far on microwave induced reaction chemistry. One model assumes that rate enhancement is simply due to thermal dielectric heating and the other assumes that there is a specific activation due to microwave radiation that occurs in addition to the dielectric heating mentioned earlier.⁶⁹

Our work is unique in the sense that systematic frequency effects have been found to markedly influence conversion and selectivity under microwave radiation in the oligomerization of methane. The effect of frequency on product distribution for the oligomerization of methane was studied with and without He as a diluent. It is a fact that when increasing microwave frequency, selectivities towards C_2s decreased and selectivity towards C_6 increased for both cases (with and without diluent).

All C_2 hydrocarbons decreased as frequency increased when using pure methane feed. When using He as a diluent, ethylene and acetylene increased as frequency increased while ethane decreased (see Figures 4 and 7). These effects on product distribution are related to the transverse magnetic modes at different frequencies that would generate diverse transient heating patterns. The two parameters that define the dielectric properties of materials and

concomitant heating patterns are dielectric constant and dielectric loss.

As quenching of intermediates has an important role in ethylene formation, different transient heating patterns would affect the environment in which the reaction is taking place, consequently affecting the selectivities of the final products. The dielectric constant, ϵ' , describes the ability of the molecules to be polarized by the electric field. At low frequencies this value will reach a maximum as the maximum amount of energy that can be stored in the material. As frequency increases ϵ' decreases as shown by Mingos et al.⁷⁰ The dielectric loss, ϵ'' , measures the efficiency at which microwave energy can be converted into heat and goes through a maximum as frequency increases.⁷⁰ The relationship between these two parameters ϵ''/ϵ' defines the dielectric loss tangent, $\tan \delta$, which measures the ability of a material to convert electromagnetic energy into heat at a given frequency and temperature. The dielectric loss also goes through a maximum as frequency increases. Therefore, higher formation of benzene-acetylene at higher frequency in our experiments can be explained by the increase of the dielectric loss as frequency increases before going through the maximum. Greater dielectric loss is directly related to greater temperatures, consequently related to acetylene formation.⁵⁶ Acetylene is later consumed in the trimerization reaction to obtain benzene, which is detected in the final products.

Conclusions

Systematic effects of power level, He as diluent, and microwave frequency were studied for the microwave oligomerization of methane using Ni powder catalyst with branched filament morphology. We are not aware of other heterogeneous catalysis studies where either direct or indirect frequency effects have been observed under microwave radiation. As frequency increased, selectivity towards benzene also increased. When using He as a diluent, as frequency increased, selectivities towards ethylene and acetylene also increased. When pure methane was used, the opposite result was observed. These changes in product distribution are most likely due to different transverse modes that generate different transient heating patterns and changes in dielectric constant and loss of the catalyst.

Acknowledgment

The authors thank the National Science Foundation and the Electrical Power Research Institute under Grant CTS-9413394 of the joint NSF/EPRI Initiative on Microwave Induced Reactions. We thank Lambda Technology Inc. for support of this research. We also thank Todd Ellis and Denise Tucker of Lambda Technology Inc. for their advice and technical support. We thank Professor G. Roussy of LSTM Université de NANCY 1, and Professor J.K.S Wan of Queen's University for helpful discussions.

References

- (1) Anderson, J. R., *Appl. Catal.* **47**, 177 (1989)
- (2) Mimoun, H., *New J. Chem.* **11**, 7, 513 (1987)
- (3) Pitchai, R., Klier, K., *Catal. Rev. -Sci. Eng.* **28**, 1, 13 (1986)
- (4) Janowicz, A. J., Periana, R. A., Buchanan, C. A., Kovac, C. A., Stryker, J. M., Wax, M. J., Bergman, R. G., *Pure Appl. Chem.* **56**, 13 (1984)
- (5) Hoyano, J. K., McMaster, A. D., Graham, W. A. G., *J. Am. Chem. Soc.* **105**, 7190 (1993)
- (6) Kao, L. C., Hutson, A. C., Sen, A., *J. Am. Chem. Soc.* **113**, 700 (1991)
- (7) Scurrrell, M. S., *App. Catal.* **32**, 1 (1987)
- (8) Lee, J. S., Oyama, S. T., *Catal. Rev. -Sci. Eng.* **30**, 2, 249 (1988)
- (9) Hutchings, G. J., Scurrrell, M. S., Woodhouse, J. R., *Chem. Soc. Rev.* **18**, 251 (1989)
- (10) Amenomiya, Y., Birss V. I., Goledzinowski, J., Galuszka, J., Sanger, A. R., *Catal. Rev. -Sci. Eng.* **32**, 163 (1990)
- (11) Shepelev S. S., Gesser H.D., Hunter N. R., *Plasma Chem. and Plasma Proc.* **13**, 3, 479 (1993)
- (12) Shilov A. E., "The Activation of Saturated Hydrocarbon by Transition Metal Complexes." Reidel D. and Dordrecht, The Netherlands, 1984.
- (13) Wada K., Yoshida K., Watanabe Y., Suzuki T., *J. Chem. Soc. Chem. Commun.* 726 (1991)
- (14) Otsuka K., Komatsu T., *J. Chem. Soc. Chem Commun.* 388 (1987)
- (15) Ogura K., Kataoka M., *J. Mol. Catal.* **43**, 371 (1988)
- (16) Sayyel B. A., Stair P. C., *J. Phys. Chem.* **94**, 409 (1990)
- (17) Hill C.L., "Activation and Functionalization of Alkanes." Wiley, New York, 1989.
- (18) Ryabov A. D., *Chem. Rev.* **90**, 403 (1990)
- (19) Wolf E. E., "Methane Conversion by Oxidative Process." Van Nostrand Reinhold: New York, 1992.
- (20) Huang J., Suib S. L., *J. Phys. Chem.* **97**, 37, 9403 (1993)
- (21) Huang J., Suib S. L., *Res. Chem. Intermed.* **20**, 1, 133 (1994)
- (22) Suib S. L., Zenger R.P., Zhang Z., "Proceedings, Symposium on Natural Gas Upgrading II", p 344, Petroleum Chem., ACS, Washington DC, 1992.
- (23) Suib S. L., Zenger R. P., *J. Catal.* **139**, 383 (1993)
- (24) Huang J., Badani M. V., Suib S. L., Harrinson J. B., Kablauoi M., *J. Phys. Chem.* **98**, 1, 206 (1994)
- (25) Tse, M. Y., Depew, M. C., Wan, J. K. S., *Res. Chem. Intermed.* **13**, 221 (1990)
- (26) Cameron K. L., Depew M. C., Wan J. K. S., *Res. Chem. Intermed.* **16**, 57 (1991)
- (27) Bamwenda, G., Moore, E., Wan, J. K. S., *Res. Chem. Intermed.* **17**, 243 (1992)
- (28) Bamwenda, G., Depew, M. C., Wan, J. K. S., *Res. Chem. Intermed.* **19**, 6, 553 (1993)
- (29) Ioffe, M. S., Pollington, S. D., Wan, J. K. S., *J. Catal.* **151**, 349 (1995)
- (30) Dinesen T. R. J., Tse M. Y., Depew M. C., Wan J. K. S., *Res. Chem. Intermed.* **15**, 113 (1991)
- (31) Cameron K. L., Depew M. C., Wan J. K. S., *Res. Chem. Intermed.* **16**, 57 (1991)
- (32) Depew M. C., Lem S., Wan J. K. S., *Res. Chem. Intermed.* **16**, 213 (1991)
- (33) Wan J. K. S., *Res. Chem. Intermed.* **16**, 147 (1991)
- (34) Wan J. K. S., Ioffe M. S., *Res. Chem. Intermed.* **20**, 1, 115 (1994)
- (35) Pollington, S. D., Ioffe, M. S., Westergaard, M., Wan, J. K. S., *Res. Chem. Intermed.* **21**, 1, 59 (1995)
- (36) G. Roussy, J. A. Pearce, "Foundations and Industrial Applications of Microwaves and Radiofrequency Fields." John Wiley, New York, 1995.
- (37) Caddick, S., *Tetrahedron* **51**, 38, 10401 (1995)
- (38) Strauss, C. R., Trainor, R. W., *Aust. J. Chem.* **48**, 1665 (1995)
- (39) Majetich, G., Hicks, R., *J. of Microwave Power and Electromagnetic Energy* **30**, 1, 27 (1995)
- (40) Bram, G., Loupy, A., Villemin, D., in "Solid Supports Catal. Org. Synth." Chapter 12, Microwave activation of reaction on inorganic solid supports Eds. Smith, K., p302, 1992
- (41) Whittaker, A. G., Mingos, D. M. P., *Journal of Microwave Power and Electromagnetic Energy* **29**, 4, 195 (1994)
- (42) Mingos, D. M. P., Baghurst, D. R., *British Ceramic Transactions and Journal* **91**, 4, 124 (1992)

- (43) Sutton, W., *Ceramic Bulletin* **68**, 2, 376 (1989)
- (44) Clark, D. E., Sutton, W. H., *Annu. Rev. Mater. Sci.* **26**, 299 (1996)
- (45) Rao, K. J., Ramesh, P. D., *Bull. Mater. Sci.* **18**, 4, 447 (1995)
- (46) Mingos, D. M. P., Baghurst, D. R., *Chem. Soc. Rev.* **20**, 1 (1991)
- (47) Baghurst, D. R., Chippindale, A. M., Mingos, D. M. P., *Nature* **332**, 311 (1988)
- (48) Baghurst, D. R., Mingos, D. M. P., *J. Chem. Soc. Chem. Comm.* 829 (1988)
- (49) Chatakondur, K., Green, M. L. H., Mingos, D. M. P., Reynolds, S. M., *J. Chem. Soc. Chem. Comm.* 1515 (1989)
- (50) Baghurst, D. R., Cooper, S. R., Greene, D. L., Mingos, D. M. P., Reynolds, S. M. *Polyhedr.* **9**, 893 (1990)
- (51) Baghurst, D. R., Mingos, D. M. P., *J. Chem. Soc. Dalton Trans.* 1151 (1992)
- (52) Baghurst, D. R., Mingos, D. M. P., Watson, M. J., *J. Organomet. Chem.* **368**, C43 (1989)
- (53) Baghurst, D. R., Mingos, D. M. P., *J. Organomet. Chem.* **384**, C57 (1990)
- (54) Whittaker, A. G., Mingos, D. M. P., *J. Chem. Soc. Dalton Trans.* 275 (1992)
- (55) Whittaker, A. G., Mingos, D. M. P., *J. Chem. Soc. Dalton Trans.* 2541 (1993)
- (56) Wan, J. K. S., Tse, M. Y., Husby, H., Depew, M. C., *J. of Microwave Power and Electromagnetic Energy* **25**, 1, 32 (1990)
- (57) Gourari, S., Roussy, G., Thiebaut, J. M., Zoulalian, A., *The Chemical Eng. J.* **49**, 79 (1992)
- (58) Roussy, G., Thiebaut, J. M., Souiri, M., Marchal, E., Kiennemann, A., Maire, G. *Catal. Today* **21**, 349 (1994)
- (59) Seyfried, L., Ganh, F., Maire, G., Thiebaut, J. M., Roussy, G., *J Catal.* **148**, 281 (1994)
- (60) Chen, C., Hong, D., Dai, S., Kan, J., *J. Chem. Soc. Faraday Frans.* **91**, 7, 1179 (1995)
- (61) Bond, G., Moyes, R. B., Whan, D. A., *Catal. Today* **17**, 427 (1993)
- (62) C. Marun, L. D. Conde, S. L. Suib., *J. Phys. Chem. A* **103**, 4332 (1999)
- (63) Maitlis, *J. Organomet. Chem.* **200**, 161 (1980)
- (64) Maitlis, *Acc. Chem. Res.* **9**, 93 (1976)
- (65) Vollhardt, *Acc. Chem. Res.* **10**, 1 (1977)
- (66) Reppe, Kutepow, and Magin, *Angew. Chem. Int. Ed. Engl.* **8**, 727 (1969)
- (67) Wan, J.K.S., US Patent 4574038 (1986)
- (68) Lewis D.A., *Microwave Processing of Materials III, Mater. Res. Soc. Symp. Proc., 269, Pittsburg: Mater. Res. Soc.* 21 (1992)
- (69) Jacob J, Chia L. H. L., Boey F. Y. C., *J. Mat. Soc.* **30**, 5321 (1995)
- (70) Mingos, D. M. P., Baghurst, D. R., in "Microwave-Enhance chemistry." Kingston, H. M. and Haswell, S. J. p. 1. Am. Chem. Soc., Washington, DC, 1997

HYDROGEN ABSTRACTION FROM ALKYLAROMATICS WITH CO₂

Sang-Eon Park

Catalysis Center for Molecular Engineering,
Korea Research Institute of Chemical Technology (KRICT),
P.O. Box 107, Yusung, Taejeon 305-600, Korea

Introduction

Catalytic conversion of CO₂ has been extensively studied as an important issue for last decade. However, utilization of carbon dioxide as an oxidant evokes emerging interest on new way of chemical fixation of CO₂.^{1,2} Several examples have proved that CO₂ can play as soft oxidant in the various catalytic oxidative reactions by CO₂ alone or together with O₂, resulting in improved activities and selectivities.³

Dehydrogenation of aromatic hydrocarbons with benzylic hydrogen leads easily to aromatic hydrocarbons with α -olefin group through the hydrogen abstraction of benzylic C-H bond by surface oxygen of heterogeneous catalyst. This step is considered to be a rate-determining one. A representative example of such reactions is the dehydrogenation of ethylbenzene to styrene. It has been already proposed that for this reaction CO₂ plays a role as the soft oxidant to abstract the hydrogen atom from ethylbenzene.^{4,5} It is worth verifying if carbon dioxide acts on dehydrogenation of other aromatic hydrocarbons.

The oxidation of alkylaromatics is an important commercial reaction. Discovery of bromide promoted metal catalysts in 1954⁶ for the oxidation in presence of molecular oxygen evolved into one of the major industrial processes. The cobalt-based catalysts have been developed with different promoters (Br, Mn, Zr, Mo, Hf, Ni, Cr etc.) for the last four decades.⁷ The promotional effects of several transition metal promoters have been reported for the oxidation reactions.⁷ On the other hand, the unexpected function of CO₂ as a co-oxidant and/or oxidation promoter was reported in the early 1990s for the vapor phase oxidation of aromatic compounds,⁸ and recently the similar effect has been found for the MC-type oxidation of xylenes to the corresponding dicarboxylic acids with Co/Mn/HBr in the liquid phase.⁹

Here, the effect of carbon dioxide as the soft oxidant is demonstrated in both oxidative dehydrogenation of alkylaromatics to corresponding olefins and oxidation of alkylaromatics to corresponding aldehydes and acids.

Experimental

For dehydrogenation of aromatic hydrocarbons with CO₂, Al₂O₃-supported vanadium-antimony binary oxide (V-SbO_x/Al₂O₃) catalyst was prepared by impregnation of aqueous solutions of ammonium metavanadate and antimony (III) chloride onto activated alumina. The impregnated sample was dried at 100°C and then calcined in air at 600°C for 4 h. The content of V₂O₅ and Sb₂O₃ was 7.5 wt% and 15.5 wt%, respectively. Dehydrogenation of alkylaromatics was carried out in a micro-activity test unit (Zeton, MAT 2000) with a fixed bed reactor at 600°C under atmospheric pressure. The liquid and gas products were analyzed by GC (Donam Corp., DS6200) equipped with FID and TCD, respectively. Effluent gases from the reactor were analyzed by a gas chromatograph (Chrompack CP9001) equipped with a thermal conductivity detector (TCD).

For oxidation of alkylaromatics, the required quantity of the catalyst and reaction mixture was taken in a 150 ml Teflon-lined reactor and pressurised either with CO₂ or N₂ and raised the temperature to its optimum level and the optimum pressure was balanced by N₂. The O₂ was admitted to the reactor and measured the O₂ consumption with the help of pressure transducer connected to the oxygen chamber. The products were analysed by GC using

DB-1 capillary column and FID. The solid products (carboxylic acids) were esterified and analysed as methyl esters. The products were confirmed by GC-MS. CoBr₂ (0.54mmol) / Mn(OAc)₂·4H₂O (0.65mmol) / *p*-xylene (48.6mmol) / AcOH (420.6mmol) was exposed to reaction conditions with and without CO₂ for ESR analysis. ESR measurements were conducted on Bruker ESR (EMX model) at 77K and DPPH was used as a g-marker.

Results and Discussion

Dehydrogenation of Alkylaromatics with CO₂. The effect of CO₂ in dehydrogenation of aromatic hydrocarbons such as ethylbenzene, 4-ethyltoluene, and cumene was examined at 500°C as shown in **Table 1**. Indeed, it is certain that carbon dioxide works very well in dehydrogenation of other aromatic hydrocarbons as the soft oxidant to increase the conversion as well as selectivity. Thus, CO₂ stream gave beneficial effect on dehydrogenation of aromatic hydrocarbons in terms of reactant conversion, indicating the oxidant role of CO₂ in abstraction of hydrogen atom from the benzylic C-H bond. The dehydrogenation of ethylbenzene showed very high selectivity even under nitrogen stream, but other two reactants exhibited the increased selectivity to their dehydrogenated products in the presence of CO₂. The enhancement of the dehydrogenation activity and the selectivity is certainly ascribed to the promotional effect to the oxidative process by excess carbon dioxide since high conversion of CO₂ comparable with the conversion values of aromatic reactants was obtained. This result implies that the initial hydrogen abstraction of aromatic hydrocarbons was much facilitated by carbon dioxide. Dehydrogenation of cumene to α -methyl styrene was easier than those of other reactants and, especially, this reaction was much accelerated by carbon dioxide.

Table 1. Effect of carbon dioxide for dehydrogenation of alkylaromatics^a

Reactant	Carrier	Conv. (%)	Selec. (%)	X(CO ₂) (%)	H ₂ O /H ₂ ^b
Ethylbenzene	N ₂	28.6	98.3	-	-
	CO ₂	38.3	98.1	30.2	2.8
4-Ethyltoluene	N ₂	23.1	89.7	-	-
	CO ₂	33.9	91.8	27.5	4.7
Cumene	N ₂	33.4	93.6	-	-
	CO ₂	50.7	95.8	42.2	3.8

^aReaction conditions: Catalyst: V-SbO_x/Al₂O₃, °Temp. = 500°C, LHSV = 1.0 h⁻¹, CO₂/reactant = 10/1, Time-on-stream = 2 h. ^bmolar ratio of H₂O/H₂ estimated in the gaseous products.

*Notation: Conv., reactant conversion; Selec., selectivity of target product; X(CO₂), CO₂ conversion based on the reactant.

In gas phase distribution of products, carbon monoxide, water, and hydrogen are observed together with a trace of methane. The ratio of H₂O/H₂ in the product stream is estimated to be 2.8, 4.8, and 3.8 for ethylbenzene, 4-ethyltoluene, and cumene, respectively, after 2 h on stream. The formation of water as well as carbon monoxide implies that on the V-SbO_x/Al₂O₃ catalyst CO₂ molecule dissociates CO and surface oxygen which can abstract hydrogen from aromatic hydrocarbons, and then results in the generation of water. Taking into account the formation of large amount of water, high activity for supported V-SbO_x catalyst under CO₂ carrier may be mainly ascribed to oxygen species dissociated from carbon dioxide molecule, thus due to the promotion of the oxidative process by carbon dioxide. In other words, this indicates that carbon dioxide plays a role as the soft oxidant in dehydrogenation

of alkylaromatics.

Oxidation of Alkylaromatics with O₂/CO₂. The effect of CO₂ in the liquid phase of alkylaromatics over Co/Mn catalyst has been shown in the Table 2. Initially the reaction was carried out with *p*-xylene which indicates that the yields of acids are considerably increased in the presence of CO₂ under the similar reaction conditions. The study has been extended to other aromatic hydrocarbons such as toluene, *p*-toluic acid and ethyl benzene. The promotional effect of CO₂ on toluene is shown in Figure 1, in each time interval the conversions are higher with CO₂ and in the case of 3h run the yield of benzoic acid is about 80% in the presence of CO₂ whereas in the absence of CO₂ it is about 60% - the yield enhancement by the CO₂ is about 20%. Further investigation of CO₂ promotional effect has been made on *p*-toluic acid and found that the yield of terephthalic acid is 65% with CO₂ but in the absence of CO₂ it is only 58%. The catalytic activity in the oxidation of toluene and *p*-toluic acid followed the similar trend of *p*-xylene but in the case of ethyl benzene we observed different trend regarding product distribution. In the presence of CO₂ acetophenone is the main product whereas in the absence of CO₂ it is benzoic acid. It is proposed that the abstraction of hydrogen (α -C-H bond fission) from the ethylbenzene produces acetophenone via ethyl benzene free radical. In the absence of CO₂ benzoic acid was produced by the C-C bond cleavage from the ethyl benzene. Aresta *et al.*¹⁰ observed the similar behavior in the oxidation of double carbon side chain alkylaromatics (styrene).

Table 2. Effect of CO₂ in the liquid phase oxidation of alkylaromatics with Co/Mn catalyst

Substrate	P _{CO2} (atm)	Temp. (°C)	Time (h)	Yield (mol %)
<i>p</i> -Xylene	4	170	3.0	TPA (34.8), <i>p</i> -TA (36.9), TPAL (2.4), <i>p</i> -TAL (1.7), others (24.2)
<i>p</i> -Xylene	0	170	3.0	TPA (17.7), <i>p</i> -TA (47.9), TPAL (1.7), <i>p</i> -TAL (2.8), others (29.2)
<i>p</i> -TA	4	190	3.0	TPA (64.9), others (10.6)
<i>p</i> -TA	0	190	3.0	TPA (58.1), others (3.7)
Toluene	4	150	3.0	BA (78.7), others (0.7)
Toluene	0	150	3.0	BA (58.6), others (13.7)
EB ^a	6	100	2.5	AP (52.6), BA (36.9), others (10.5)
EB ^a	0	100	2.5	AP (19.4), BA (56.5), others (9.6)

Conditions: Substrate = 48.6mmol, Acetic acid = 420.6mmol, Co = 0.54mmol, Mn = 0.65mmol, Br = 1.08mmol, P_{total} = 12atm (P_{O2} = 2atm, P_{N2} = Balance), ^aP_{total} = 10atm (P_{O2} = 2).

Abbreviations: TPA (Terephthalic acid), *p*-TA (*p*-Toluic acid), TPAL (Terephthaldehyde), *p*-TAL (*p*-Tolualdehyde), BA (Benzoic acid), EB (Ethyl benzene), AP (Acetophenone).

In conclusion, typical oxidative dehydrogenation catalysts were proved to be utilized under the CO₂ stream alone instead of O₂ to get alpha olefin substituted aromatics from alkylaromatics such as ethylbenzene, 4-ethyltoluene, and cumene. Carbon dioxide

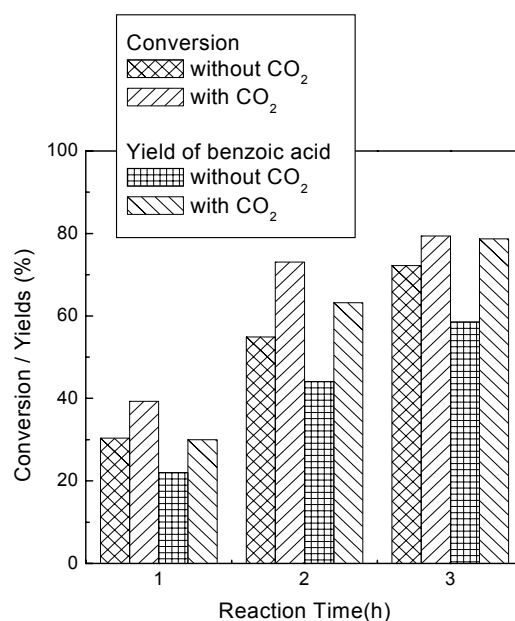


Figure 1. Effect of CO₂ in the liquid phase oxidation of toluene with Co/Mn catalyst. Conditions: Toluene = 48.6 mmol, Acetic acid = 420.6 mmol, CoBr₂ = 0.54 mmol, Mn(OAc)₂·4H₂O = 0.65 mmol, P_{total} = 12 atm (P_{CO2} = 0 or 4, P_{O2} = 2, N₂ = Balance), Temp. = 150°C.

contributes to highly improved activities together with selectivities on one hydrogen molecule abstracted aromatics. The conventional cobalt and manganese catalyst was utilized for the oxidation of alkylaromatic hydrocarbons with O₂/CO₂ as co-oxidants. Carbon dioxide co-fed with O₂ led to the selective control to produce the corresponding aldehydes and acids with the enhanced rates. Therefore, the main roles of CO₂ in these oxidative reactions are found to enhance the selective hydrogen abstraction with the improved activities.

Acknowledgment

This work was performed for the Greenhouse Gas Research Center, one of the Critical Technology-21 Programs, funded by the Ministry of Science and Technology of Korea (MOST). I also thank my colleagues including Dr. K.W. Jun for their contributions to this work.

References

1. Yoo, J.S., *Catal. Today*, **1998**, 41, 49.
2. Park, S.-E., Yoo, J.S., Chang, J.-S., Environmental Challenges and Greenhouse Gas Control for Fossil Fuel Utilization in the 21st Century (eds. M.M. Maroto-Valer, Y. Song, C. Song), Chapter 33, Kluwer Academic/Plenum: New York, 2002.
3. Park, S.-E., Yoo, J.S., Chang, J.-S., Lee, K.Y., Park, M.S., *Prep. ACS Fuel Chem. Div.*, **2001**, 46(1), 115.
4. Chang, J.-S., Park, S.-E., Park, M.S., *Chem. Lett.*, **1997**, 1123.
5. Mimura, N., Saito, M., *Catal. Lett.*, **1999**, 58, 59.
6. Landau, R., Saffer, A., *Chem. Eng. Proc.*, **1968**, 48, 20.
7. Partenheimer, W., *Catal. Today*, **1995**, 23, 69 and the references cited therein.
8. Yoo, J.S., Lin, P.S., Elfine, S.D., *Appl. Catal. A*, **1993**, 105, 259.
9. Jhung, S.-W., Lee, K.-W., Park, Y.-S., Yoo, J.S., US patent **2001**, 6,180,822.
10. Aresta, M., Tommasi, I., Quaranta, E., Fragale, C., Mascetti, J., Tranquille, M., Galan, F., Fouassier, M., *Inorg. Chem.*, **1966**, 35, 4254.

METHANE COUPLING AND REFORMING USING NON-EQUILIBRIUM PULSED DISCHARGE AT ROOM TEMPERATURE

Shigeru Kado[†], Kohei Urasaki[†], Yasushi Sekine[‡]

[†] Department of Applied Chemistry, School of Engineering, The University of Tokyo, Hongo, Bunkyo-ku, Tokyo 113-8656, Japan

[‡] Department of Applied Chemistry, School of Science and Engineering, Waseda University, Okubo, Shinjyuku, Tokyo 169-8555, Japan

Introduction

Methane, which is a major component of natural gas and one of the greenhouse gases, is so stable that high reaction temperature such as 1273 K or higher is required for its pyrolysis to ethylene or acetylene. Although high reaction temperature is favorable for high conversion, high reaction temperature promotes the consecutive decomposition of the products to carbon or complete combustion to CO₂ in the oxidative activation of methane. The utilization of natural gas as a chemical resource is limited in producing hydrogen and synthesis gas by steam reforming process, which requires higher operating temperature than 1073 K in the presence of catalysts.

Recently, methane conversion using non-equilibrium plasma technique has been studied at low temperature. For example, using 8 kPPS (pulse per second) high-frequency pulsed plasma produced acetylene selectively with relatively high energy efficiency.¹ A cogeneration of syngas and higher hydrocarbons can be achieved using a catalytic dielectric-barrier discharge (DBD).² In this study, selective formation of C₂ hydrocarbon and/or carbon monoxide was achieved using a periodic pulsed spark discharge^{3,4} with and without catalyst at room temperature.

Experimental

A schematic diagram of the experimental setup was almost the same as that reported previously.³ A flow type reaction apparatus composed of a Pyrex glass tube with 4.0 mm internal diameter was used as the reactor. All experiments were conducted under the conditions of ambient temperature and atmospheric pressure. Stainless steel electrodes of 1.0 mm diameter were inserted from each end of the reactor and fixed with a certain distance. In the catalytic reaction, a quartz tube with 6.0 mm internal diameter was used, and the gap distance was fixed at 10 mm. The catalyst bed was put between stainless meshes.

The discharge was initiated by supplying a negative high voltage with a DC power generator (MATSUSADA Precision Inc. HAR-30R10). Figure 1-a shows examples of the waveforms of discharge current and voltage measured by digital oscilloscope (LeCroy Japan Corp. 9314C, 400 MHz bandwidth) using a voltage probe (PMK-20kV, 100 MHz, LeCroy) and current transformer (AP015, 50 MHz, LeCroy). The current width of one pulse was far shorter than 1 μs as shown in Fig. 1-b, and the peak value of the pulse current reached about 40 A. The reason why the current pulses did not have the same frequency as the voltage oscillations in Fig. 2-a was the low sampling rate of the oscilloscope. Owing to the short width of current, the pulsed spark discharge belongs to the non-equilibrium plasma.

A catalyst of 1 wt% Pt/SiO₂ was prepared by the incipient wetness method using [Pt(C₅H₇O₂)₂] and CARIACT Q-15 SiO₂ (10-20 mesh, Fuji Silysia Chemical Ltd.), and Ni_{0.1}Mg_{0.9}O solid solution catalyst was prepared by the same method as Tomishige et al.⁵

All products were analyzed with two gas chromatographs of FID-GC-14A and TCD-GC-8A.

The conversions of the reactants were defined as follows.

Reactant conversion (%) = (moles of reactant consumed) / (moles of reactant introduced) * 100

The selectivities were defined as follows.
Product selectivity (%) = (carbon based moles of product derived from methane) / (moles of CH₄ consumed) * 100

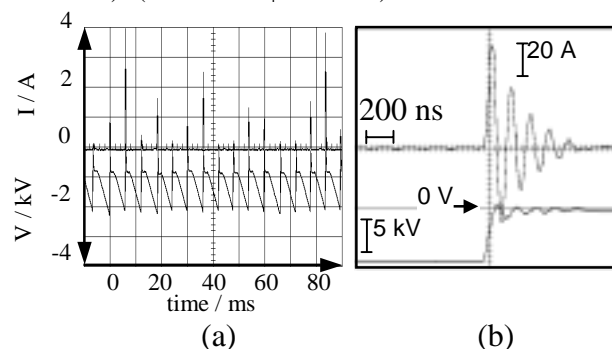


Figure 1. Typical waveform of pulsed spark discharge.

Results and Discussion

Selective Formation of C₂ hydrocarbon. Investigations of the activation of methane with the non-equilibrium pulsed spark discharge were made under the condition of feeding pure methane at the flow rate of 10 cm³min⁻¹ while increasing the pulse frequency. As shown in Fig. 2, methane was activated to form acetylene with a selectivity of more than 90% in the absence of a catalyst. Hydrogen was abstracted from methane directly by the collision between electrons and methane molecules. Even when methane conversion increased up to 52%, acetylene selectivity was very stable at about 95%, while the other C₂ products were ethane and ethylene (selectivity of ~ 4%). Other higher hydrocarbons such as prop-1-yne (C₃H₄) and buta-1,3-diyne (C₄H₂) were produced with a selectivity of less than 1%. These results are quite different from those of simple gas-phase reactions.

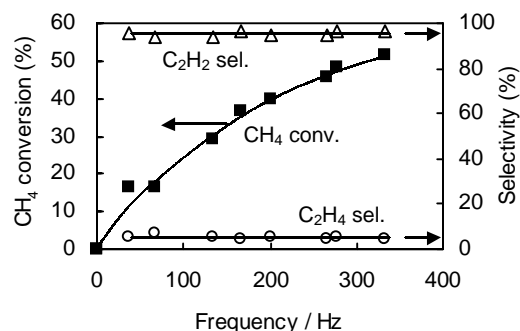


Figure 2. Effect of pulse frequency under the conditions of 10 cm³min⁻¹ total flow rate, CH₄ 100%, room temperature, 0.1 MPa, 1.5 mm gap distance.

To investigate the catalytic spark discharge reaction, 1 wt% Pt/SiO₂ was inserted between the electrodes. The height of catalyst bed from the downstream electrode was varied from 0 to 10 mm. The results are shown in Fig. 3. The height of 0 mm means non-catalytic reaction, and the discharge region was filled with the catalyst at 10 mm height (0.1 g-Cat.). Pt/SiO₂ was used without pretreatment like reduction by H₂. To prevent the carbon deposition, CH₄ was diluted with 80% H₂.

As compared with results in Fig. 2, to lengthen the gap distance and to dilute CH₄ with H₂ did not affect the selectivity so much. The selectivity to C₂H₂ in Fig. 3 was 87% in non-catalytic reaction. On the other hand, the use of Pt/SiO₂ had a great influence on the product composition, and the selectivity to C₂H₆ increased drastically, while the conversion decreased. Under the condition of CH₄/H₂=8/32 cm³min⁻¹, CH₄ conversion was 46% in non-catalytic reaction, which

decreased to 14.5% when the discharge region was filled with SiO₂ (void fraction: 65%). When the discharge region was filled with Pt/SiO₂, C₂H₆ was produced with the selectivity of 94% and the conversion of 10.5%. CH₄ conversion increased to 33% by decreasing the amount of the catalyst (2.5 mm height), and 25% yield of C₂H₆ was obtained.

Under the condition of CH₄/H₂=2/8 cm³min⁻¹, the decrease in the conversion by the insertion of catalyst was not so large compared with that under condition of higher flow rate. Although CH₄ conversion at 5 mm and 2.5 mm height were almost the same at 51%, the selectivity to C₂H₄ slightly increased to 15%. The highest C₂H₆ yield of 49% was obtained at 5 mm height of catalyst, much higher than 30% that is the upper limit in the conventional thermal chemistry.

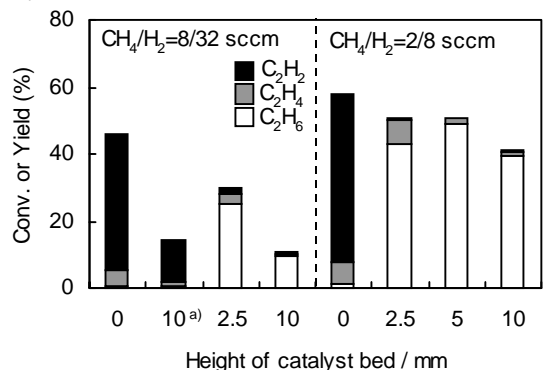


Figure 3. Effect of 1 wt% Pt/SiO₂ under the conditions of room temperature, 0.1 MPa, 10 mm gap distance, 100 Hz frequency. ^{a)}: SiO₂ without Pt.

Selective Formation of Synthesis Gas by CO₂ Reforming or Partial Oxidation of CH₄. Fig. 4 shows the effect of CO₂ content in the feed gas on the conversion, the selectivity and H₂/CO ratio. In the presence of CO₂, carbon deposition on the electrodes and the wall of the reactor was not observed. With increasing CO₂ content, CH₄ conversion rose and reached 76% at CH₄/CO₂=1/4 while CO₂ conversion remained almost stable with ca. 40%. The selectivity strongly depended on the feed gas composition. With the increase of CO₂ content, C₂ selectivity decreased sharply while CO selectivity increased drastically. Under the condition of high CH₄ concentration, the formation of C₂H₂ was predominant, whereas under the condition of high CO₂ concentration, CO became the main product. The feed gas composition also had a great influence on H₂/CO molar ratio, which was in inverse proportion to CO₂ content. Synthesis gas with H₂/CO ratio of 2 was obtained at 40% CO₂ content, which is suitable for the catalytic methanol synthesis.

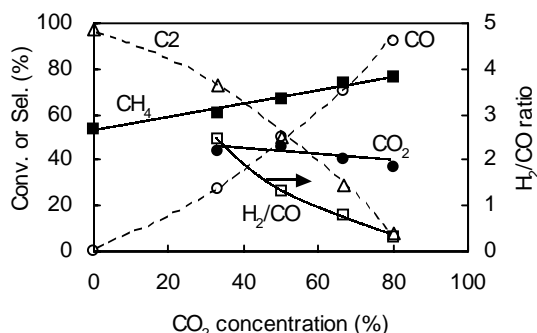


Figure 4. Effect of CO₂ concentration under the conditions of 10 cm³min⁻¹ total flow rate, room temperature, 0.1 MPa, 1.5 mm gap distance.

The use of pretreated NiMgO solid solution catalyst increased CO selectivity to 85% at CH₄/CO₂=1, while no remarkable effect was observed by using without pretreated one as shown in Table 1. The content of C₂H₄ in C₂ hydrocarbons was 78% with pretreated NiMgO, and that of C₂H₂ was 77% with non-pretreated one. NiMgO and discharge combined system promoted CO₂ reforming of CH₄ at room temperature without dilution.

Table 1. Effect of Ni_{0.1}Mg_{0.9}O with and without Pretreatment*

Catalyst	Frequency / Hz	Conv.(%)		Sel.(%)		H ₂ /CO ratio
		CH ₄	CO ₂	C ₂	CO	
non	50	62.8	50.0	44.1	55.9	1.1
NiMgO ^{a)}	200	29.6	23.9	37.0	63.0	1.1
NiMgO ^{b)}	91	29.5	26.2	15.5	84.5	1.0

* Reaction conditions: CH₄/CO₂=10/10 cm³min⁻¹, room temperature, 0.1 MPa, 10 mm gap distance. ^{a)}: without pretreatment, ^{b)}: pretreated by H₂ reduction at 1123 K.

The partial oxidation of CH₄ was examined by varying the partial pressure of O₂ as shown in Fig. 5. CH₄ conversion increased from 24% to 76% in proportion to an increase in the partial pressure of O₂. CO selectivity increased from 0% to 79% while C₂ compounds selectivity decreased from 99% to 7% with an increase in the O₂ content from 0% to 50%. The content of C₂H₂ in C₂ compounds, however, decreased slightly from 98% (CH₄/O₂=10) to 68% (CH₄/O₂=1). And CO₂ selectivity increased slightly by the consecutive oxidation of product. The pulsed spark discharge reaction of CH₄ in the presence of O₂ produced CO and C₂H₂ at room temperature while suppressing carbon deposition and CO₂ formation.

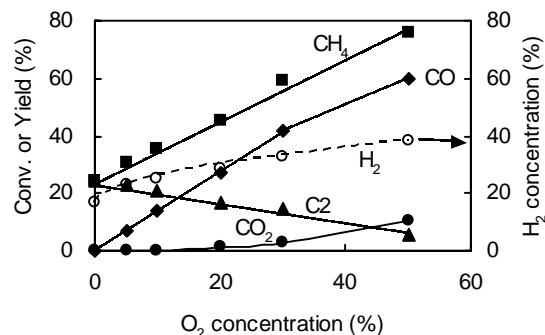


Figure 5. Effect of partial pressure of O₂ under the conditions of 50 cm³min⁻¹ total flow rate, 50% CH₄ concentration, balance gas of Ar, 45 Hz frequency, room temperature, 0.1 MPa, 10 mm gap distance.

Conclusion

The use of non-equilibrium pulsed spark discharge could activate CH₄ at room temperature. The selective formation of C₂H₂ with high conversion was achieved, and 49% yield of C₂H₆ was obtained in Pt/SiO₂ and discharge combined system. This method could be applied to the formation of synthesis gas, and has a possibility to be applied to the utilization of not only natural gas but also biogas, which is composed of CH₄ and CO₂.

References

- [1] Yao, S. L.; Nakayama, A.; Suzuki, E., *AIChE Journal*, **2001**, *47*, 419.
- [2] Eliasson, B.; Liu, C. J.; Kogelschatz, U., *Ind. Eng. Chem. Res.*, **2000**, *39*, 1221.
- [3] Kado, S.; Sekine, Y.; Fujimoto, K., *Chem. Commun.*, **1999**, *24*, 2485.
- [4] Kado, S.; Urasaki, K.; Sekine, Y.; Fujimoto, K., *Chem. Commun.*, **2001**, *5*, 415.
- [5] Tomishige, K.; Himeno, Y.; Matsuo, Y.; Yoshinaga, Y.; Fujimoto, K., *Ind. Eng. Chem. Res.*, **2000**, *39*, 1891.

METHANOL PRODUCTION FROM PARTIAL OXIDATION OF METHANE IN A SPECIALLY DESIGNED REACTOR

Qijian Zhang, Dehua He*, Xin Zhang and Qiming Zhu

State key Laboratory of C1 Chemistry and technology
Department of Chemistry, Tsinghua University, Beijing
100084, China

*Corresponding author. Email:

hedehe@mail.tsinghua.edu.cn

Fax: +86-10-6279-2122

Introduction

Research on direct partial oxidation of methane to methanol has last for a long time because of its great industrial potential. Unfortunately, in most literatures CH₃OH yield was always below 5%. The molecular of methanol is far more reactive than methane under similar condition. Methanol is easily oxidized to CO and/or CO₂. Therefore, the selectivity of methanol was always poor. Participation of catalyst has not improved methanol selectivity till now. The temperature and pressure for catalytic oxidation of methane were in the range of gas phase homogeneous oxidation. Then the gas phase homogeneous reaction was inevitable in the catalytic reaction. Therefore, it is necessary to continue the exploration on the gas phase homogeneous oxidation of methane.

Experimental

The gas phase partial oxidation of methane was investigated in a specially designed quartz lined tubular reactor. The quartz line was tightly fitted in the stainless steel line using an O-ring of fluoride rubber pressed by a locking nut to avoid contact of feed gas with metal wall so as to diminish the wall effect. And a spacer (quartz tube) was placed in the reactor to ensure the product mixture leave out the high temperature reaction zone rapidly so as to terminate the free radical reaction and minimize the deep oxidation of required product.

Results and discussion

In the specially designed reactor, a yield of CH₃OH about 7-8% (60-63% CH₃OH selectivity at 11-13% CH₄ conversion) could be obtained at 430-470°C, 5.0MPa and CH₄/O₂/N₂=100/10/10 (ml/min, STP), while O₂ was completely consumed. The selectivity of CO was about 30% and the selectivity of CO₂ was kept less than 5-10%. Production of H₂ was also observed, its concentration in the gas mixture was just less than that of CO. Since no HCHO was detected, it is believed that it decomposed quickly to CO and H₂ if it was formed in the reaction system.

In most literatures, high CH₃OH selectivity could be obtained when methane conversion was very low; however the selectivity would fall down quickly while increasing the methane conversion. The yield of methanol was always less than 5%. Comparison of the reaction conditions with that in our early work^[1] and other literatures^[2,3,4], the most difference lies in the reactor structure.

In order to verify what makes high methanol yield possible, some experiments were carried out by adjusting the structure of the reactor. Without O-ring for sealing the gap between quartz tube and stainless tube in the reactor, the methanol selectivity decreased

sharply from 62% to 31%, and methanol yield fell from 8% down to only 3%. Instead of quartz line with silicate glass line, the selectivity only decreased slightly. The spacer (quartz tube) in the reactor does have some effect on the reaction because the methanol selectivity decreased from 62% to 41% (Table 1).

Table 1 Effect of the varying of the reactor structure on the partial oxidation of methane

Case*	Methane Conversion/%	Selectivity /%			Methanol Yield/%
		CH ₃ OH	CO	CO ₂	
A	13.1	62.3	32.6	4.8	8.2
B	9.1	31.6	50.0	18.8	2.9
C	11.7	41.2	41.5	15.4	4.8
D	13.0	54.5	33.0	12.0	7.1

P=50atm, T=450°C, CH₄/O₂/N₂=100/10/10(ml/min)

*A-the original structure, B-without O-ring; C-without spacer; D-silicate glass line instead of quartz glass line

Conclusion

A yield of CH₃OH about 7-8% could be obtained in the specially designed reactor. It is supposed that the high CH₃OH yield should be attributed to the encapsulation of the ringed gap between the quartz line and the SS line. Higher CH₃OH selectivity could be achieved by improving the reactor design.

Acknowledgement

We acknowledge the financial support from the Key Project of National Fundamental Research and Development of China (973) and the Analytical Foundation of Tsinghua University.

References:

- [1] Han, Z.S.; Pan, W.; Li, J.L.; Zhu, Q.M. *Tsinghua Sci. Tech.* 1996, 1(4):420-424
- [2] Foulds, G.A.; Gray, B.F.; Miller, S.A.; Walker, G.S.; *Ind. Eng. Chem. Res.* 1993, 32:780-787
- [3] Omata, K.; Fukuoka, N.; Fujimoto, K.; *Ind. Eng. Chem. Res.* 1994, 33:784-789
- [4] Chellappa, A.S.; Fuangfoo, S.; Viswanath, D.S.; *Ind. Eng. Chem. Res.* 1997, 36:1401-1409

METHANOL SYNTHESIS FROM H₂/CO/CO₂ OVER CNTs-PROMOTED Cu-ZnO-Al₂O₃ CATALYST

Hongbin Zhang, Xin Dong, Guodong Lin, Youzhu Yuan, K. R. Tsai

Department of Chemistry & State Key Lab of Physical Chemistry for the Solid Surfaces, Xiamen University, Xiamen 361005, CHINA

Introduction

Among C₁ chemicals, methanol is the species most widely used in various chemical applications. More recently, it has been used as a clean synthetic fuel additive. Serious considerations have been given to it as an alternate fuel source^[1], including as a convenient hydrogen carrier for PEM fuel cells. More active catalysts and corresponding lower-temperature processes with high syngas single-pass conversion have been the objective for many research and development efforts.

Carbon-nanotubes (CNTs) are drawing increasing attention recently^[2]. This kind of new carbon material possesses a series of peculiarities, such as, its nanosize channel, the highly conductive graphite-like tube-wall, the *sp*²-carbons constructed surface, as well as its excellent performance of hydrogen adsorption, which make the CNTs full of promise to be a novel catalyst carrier^[3] or even promoter. In the present work, a CNTs-supported/promoted Cu-ZnO-Al₂O₃ catalyst was prepared. Its catalytic performance for CO/CO₂ hydrogenation to methanol was investigated and compared with those of the Cu-ZnO-Al₂O₃ systems supported by AC (active carbon) and γ -Al₂O₃. The results shed some light on the understanding the nature of promoter action by the CNTs and the prospect of developing highly active catalysts.

Experimental

The CNTs were synthesized by the catalytic method reported previously^[4]. The prepared CNTs were multi-walled carbon nanotubes, with O.D. of 15–45 nm and I.D. of ~3 nm. The N₂-BET surface area is ~130 m²g⁻¹. The supported catalyst, Cu-ZnO-Al₂O₃/CNTs (or AC or γ -Al₂O₃), symbolized as wt%Cu_iZn_jAl_k-O_x/CNTs (or /AC, γ -Al₂O₃), was prepared by impregnating a certain amount of CNTs (or AC, γ -Al₂O₃) with aqueous or ethanol solution containing a calculated amount of nitrates of Cu, Zn, and Al, followed by drying at 373 K for 6 h, and calcining at 473 K for 4 h.

The catalyst test for methanol synthesis was carried out in a continuous flow micro-reactor-GC combination system. 0.25 g of catalyst sample was used for each test. Prior to the reaction, catalyst sample was programmedly pre-reduced by 5% H₂+N₂ for 12 h. Methanol synthesis from H₂/CO/CO₂ over the catalysts was conducted at a stationary state with feedgas composition of H₂/CO/CO₂/N₂=62/30/5/3 (v/v) under 463–563 K and 2.0 MPa. The reactants and products were determined by an on-line GC (Model 102-GD) equipped with a TC detector and dual columns filled with 5A zeolite molecular sieve and 401-porous polymer, respectively. The former column was used for analysis of CO and N₂ (as internal standard), and the latter for CH₃OH, CO/N₂, CO₂, MF, and DMC. CO conversion was calculated by an internal standard analysis method, and space-time-yield (STY) of methanol evaluated by an external standard (i.e., working curve) method.

BET-surface area of catalyst carriers was measured by N₂ adsorption using a SORPTOMATIC-1900 (CARLO ERBA) system. H₂-TPR and H₂-TPD test of catalyst was conducted on a fixed-bed continuous flow micro-reactor or adsorption-desorption system. 20 mg of catalyst sample was used for each test. The rate of temperature increase was 10 K/min. Change of hydrogen-signal was monitored using an on-line GC with a TC detector.

Results and Discussion

Study of effect of the feedgas GHSV on the reactivity of methanol synthesis over the 40wt%Cu₆Zn₃Al₁-O_x/CNTs catalyst showed that, at a certain temperature (e.g. 503 K), CO conversion increased with increasing GHSV from zero to ~3000 ml (STP) h⁻¹ (g-catal.)⁻¹, and reached a maximum at GHSV close to 3000 ml (STP) h⁻¹ (g-catal.)⁻¹. It then started to decrease with further increasing GHSV. It was believed that, as the GHSV approached 3000 ml (STP) h⁻¹ (g-catal.)⁻¹, the reaction of methanol formation was in the kinetics-controlled region. In the present work, all reactivity tests of methanol synthesis were performed under the reaction condition of GHSV=3000 ml (STP) h⁻¹ (g-catal.)⁻¹.

It is well known that CO₂ in the feedgas is a participant component indispensable for continuous fast conversion of the syngas to methanol. Whereas the net-conversion of CO₂ indicated by GC analysis of the inlet and exit gases of the reactor was quite low, all assay results of the catalyst activity in the present work are shown with CO conversion and methanol STY. The reactivity of methanol synthesis over a series of wt%Cu_iZn_jAl_k-O_x/CNTs catalysts has been evaluated, and the results are shown in Table 1.

Table 1 Reactivity of CH₃OH Synthesis From H₂/CO/CO₂ Over A Series of Catalysts of wt%Cu_iZn_jAl_k-O_x/CNTs *

Catalyst sample	STY at initiating temperature		STY at the optimum working temp.	
	T/K	STY	T/K	STY
40%Cu ₅ Zn ₅ -O _x /CNTs	473	55.1	523	182
40%Cu ₆ Zn ₃ -O _x /CNTs	463	69.3	513	189
40%Cu _{4.5} Zn _{4.5} Al ₁ -O _x /CNTs	473	63.4	523	220
40%Cu ₅ Zn ₅ Al _{0.5} -O _x /CNTs	463	49.8	523	232
40%Cu ₆ Zn ₃ Al ₁ -O _x /CNTs	463	79.4	508	240
42%Cu ₆ Zn ₃ Al ₁ -O _x /CNTs	473	73.0	523	238
38%Cu ₆ Zn ₃ Al ₁ -O _x /CNTs	463	101	508	261
32%Cu ₆ Zn ₃ Al ₁ -O _x /CNTs	463	110.	508	287
24t%Cu ₆ Zn ₃ Al ₁ -O _x /CNTs	463	78.4	508	239
32%Cu ₆ Zn ₃ Al ₁ -O _x /CNTs**	463	100	513	307

*Reaction conditions: 2.0MPa, H₂/CO/CO₂/N₂=60/30/5/5(v/v), GHSV=3000ml(STP) h⁻¹ (g-catal.)⁻¹; and STY at mg-CH₃OH h⁻¹ (g-catal.)⁻¹. **Prepared from ethanol solution of the precursor.

It appears from the results shown in Table 1 that the optimum formula of catalyst composition is 32wt%Cu₆Zn₃Al₁-O_x/CNTs, i.e., with Cu/Zn/Al molar ratio at 6/3/1 and the corresponding loading amount of the Cu₆Zn₃Al₁ at 32wt%. On this catalyst, the STY of methanol reached 287 mg h⁻¹ (g-catal.)⁻¹, which is considerably superior to catalysts of other formulae, under the reaction conditions shown in Table 1.

Fig. 1 shows the results of activity evaluation of methanol synthesis over the catalysts of Cu-ZnO-Al₂O₃ supported by CNTs, AC, and γ -Al₂O₃, respectively. On all three catalysts, CO conversion and methanol STY both first went up with increasing temperature, reached a maximum at their respective optimum operating temperature, and then went down as temperature further increased. This could be understood considering that at the lower temperatures before the maximum, the methanol synthesis reaction was controlled by kinetics, and after the maximum, the reaction turned to be limited by thermodynamics equilibrium due to the high reaction temperature.

It is experimentally found that the support can significantly affect the activity of methanol synthesis. Over the 32wt%Cu₆Zn₃Al₁-O_x/CNTs catalyst, the methanol synthesis exhibited considerable reactivity at operating temperature as low as 463 K, and reached the highest STY, 287 mg-CH₃OH h⁻¹ (g-catal.)⁻¹, at 508 K, which was 1.9

and 2.5 times of those over the catalysts supported by AC and γ - Al_2O_3 (i.e., 150 and 114 $\text{mg h}^{-1} (\text{g-catal.})^{-1}$) obtained at the respective optimum operating temperatures, 523 and 543 K).

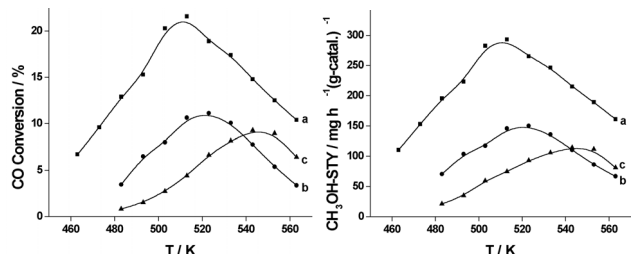


Fig. 1 Activity of CH_3OH synthesis on: a) 32% $\text{Cu}_6\text{Zn}_3\text{Al}_1\text{-O}_x/\text{CNTs}$; b) 32% $\text{Cu}_6\text{Zn}_3\text{Al}_1\text{-O}_x/\text{AC}$; c) 32% $\text{Cu}_6\text{Zn}_3\text{Al}_1\text{-O}_x/\gamma\text{-Al}_2\text{O}_3$.

It is conceivable that the dispersion of Cu-Zn-Al components on the hydrophobic surface of CNTs constructed by $sp^2\text{-C}$ could be improved by using proper organic solvent (e.g., ethanol), instead of water, for the preparation of the catalyst precursor solution, which would be conducive to enhancing the catalyst activity. That turned out to be the case. On the 32wt% $\text{Cu}_6\text{Zn}_3\text{Al}_1\text{-O}_x/\text{CNTs}$ catalyst prepared from the corresponding ethanol solution, the highest CO conversion and methanol STY attained were 23.1% and 307 $\text{mg h}^{-1} (\text{g-catal.})^{-1}$, ~7% higher as compared to that prepared from the corresponding aqueous solution.

Fig. 2 shows the H_2 -TPR spectra of the oxidation precursors of the three catalysts. For the 32wt% $\text{Cu}_6\text{Zn}_3\text{Al}_1\text{-O}_x/\text{CNTs}$, the H_2 started to react from ~463 K, with the main H_2 -TPR peak centred round 530 K. The two samples supported by AC and $\gamma\text{-Al}_2\text{O}_3$ were not reduced by H_2 until ~500 K, and each reached the reduction-peak round 578 K, which was ~48 degrees (K) higher than that of the CNTs-supported system. The observed reducibility sequence of the three samples was as follows: $\text{Cu}_6\text{Zn}_3\text{Al}_1\text{O}_x/\text{CNTs} \gg \text{Cu}_6\text{Zn}_3\text{Al}_1\text{O}_x/\text{AC} \cong \text{Cu}_6\text{Zn}_3\text{Al}_1\text{O}_x/\gamma\text{-Al}_2\text{O}_3$, in line with the sequence of their catalytic activity for the methanol synthesis.

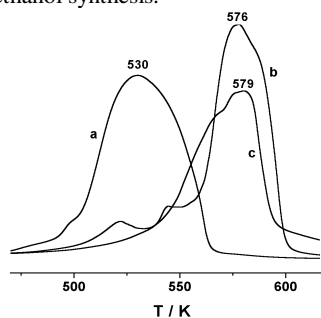


Fig. 2 H_2 -TPR spectra on the catalyst precursor: a) 32% $\text{Cu}_6\text{Zn}_3\text{Al}_1\text{-O}_x/\text{CNTs}$; b) 32% $\text{Cu}_6\text{Zn}_3\text{Al}_1\text{-O}_x/\text{AC}$; c) 32% $\text{Cu}_6\text{Zn}_3\text{Al}_1\text{-O}_x/\gamma\text{-Al}_2\text{O}_3$.

It is quite evident that the much better performance of the CNTs-supported catalyst for methanol synthesis from $\text{H}_2/\text{CO}/\text{CO}_2$ is closely related to the peculiar structure and properties of the CNTs carrier. Fig. 3 shows TEM image of the CNTs grown catalytically from CH_4 decomposition. The results of XRD measurements revealed that their main XRD feature at $2\theta = 26.1^\circ$ was close to that of graphite at $2\theta = 26.5^\circ$, but somewhat broadened, implying that the degree of long-range order of these nanostructures was relatively low compared to that of graphite. HRTEM observation revealed that they were constructed by superimposition of many layers of carbon with conical graphite-like platelets along a common central hollow.

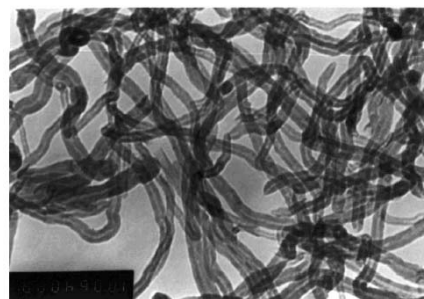


Fig. 3. TEM image of the CNTs grown catalytically from CH_4 decomposition.

From the viewpoint of chemical catalysis, in addition to its high mechanical strength, nanoscale channel, $sp^2\text{-C}$ constructed surface, and graphite-like tube-wall, the excellent performance of the CNTs in hydrogen-adsorption/storage and electron transportability is also very attractive. Fig. 4 displays H_2 -TPD spectrum of hydrogen adsorption on the CNTs. The main TPD peaks appeared at 400 K and 990 K. The lower-temperature peak was contributed from H_2 -desorption, while the higher-temperature peak involved desorption of CH_4 , C_2H_4 , C_2H_2 , and H_2 . Conceivably, there would exist a considerable amount of hydrogen-adspecies on the CNTs carrier under the condition of methanol-synthesis used in the present study. This would lead to higher stationary-state concentration of hydrogen-adspecies on the surface of the functioning catalyst, and would in turn favor a series of surface hydrogenation reactions in the process of CO/CO_2 hydrogenation to methanol. On the other hand, the operation temperature of the $\text{Cu}_6\text{Zn}_3\text{Al}_1\text{-O}_x/\text{CNTs}$ catalyst for methanol synthesis can be 20~30 K lower than those of the 32wt% $\text{Cu}_6\text{Zn}_3\text{Al}_1\text{-O}_x/\gamma\text{-Al}_2\text{O}_3$ (or /AC). That would contribute considerably to an increase in equilibrium conversion of CO and space-time-yield of CH_3OH . The results of the present study indicated that the CNTs served not only as carrier, but also as an excellent promoter, and that its peculiarity of adsorbing H_2 may play an important role in promoting the methanol synthesis activity more effectively.

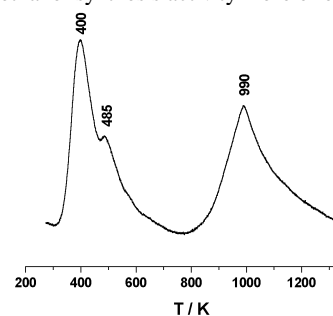


Fig. 4. TPD spectrum of hydrogen adsorbed on the CNTs material.

Acknowledgment

This work was supported by National Nat. Sci. Foundation (Project No. 50072021) and Fujian Provincial Nat. Sci. Foundation (Project No. 2001H017) of China.

References

- [1] MacDougall, L. V., *Catal. Today*, **1991**, 8, 337.
- [2] De Jong, K. P.; Geus, J. W., *Catal. Rev.-Sci. Eng.* **2000**, 42, 481.
- [3] Zhang, Y.; Zhang, H.-B.; Lin, G.-D.; Chen, P.; Yuan, Y.-Z.; Tsai, K.R., *Appl. Catal. A: General*, **1999**, 187, 213.
- [4] Chen, P.; Zhang, H.-B.; Lin, G.-D.; Hong, Q.; Tsai, K. R., *Carbon*, **1997**, 35 (10-11), 1495.

METHYL ACTIVATION BY NAKED Ni⁺ ATOM. THEORETICAL STUDY

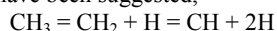
Chang-Wei Hu^{a*}, Hua-Qing Yang^a, Yao-Qiang Chen^a,
Mao-Chu Gong^a, An-Min Tian^a and Ning-Bew Wong^b

^a Faculty of Chemistry, Sichuan University, Chengdu, 610064, China

^b Department Of Biology and Chemistry, City University of
Hongkong, Kowloon, HK, China

Introduction

Methylidyne, methylene, and methyl fragments have been proposed to be key intermediates in the fuel reforming, methanation and the dissociation of methane processes.¹⁻³ Many transition metal catalysts have been synthesized, and Ni-based catalyst has been found to be one of the most active. In these processes, for example, the following steps have been suggested,^{4,5}



Due to the low concentration and relatively instability of CH_x fragments, direct experimental determinations have proved elusive. Information on stability and interaction of these intermediates, therefore, has to be taken from theoretical calculations. The main objective of the calculations presented in this study is to investigate the deliberate reaction mechanism between Ni⁺ and methyl.

Computational Details

The full-parametric geometry optimizations, the final energy evaluation and vibrational frequency analysis for all intermediates and transition states were calculated using two levels of theory, B3LYP with the 6-31G** basis sets for carbon and hydrogen and the SDD basis sets and the corresponding ECP for the nickel, and the larger 6-311+G(2d, 2p) basis set for all atoms, in the GAUSSIAN 98 programs.

Results and Discussion

For the intermediates and transition states, the calculated structures are displayed in Figure 1. The potential curve including both equilibria and transition states is shown in Figure 2. It is found that the calculated geometry structures, energies and vibrational frequencies of all compounds have little discrepancies using the two kinds of basis sets as mentioned above. For terseness, the results below are mainly at the B3LYP/6-311+G(2d, 2p) level. It should be emphasized that all transition states have been verified by IRC approach.

The initial interaction between Ni⁺ and CH₃· is the formation of NiCH₃⁺ species, with a stabilization energy of 129.4 kJ mol⁻¹. For NiCH₃⁺, with C_{3v} symmetry, the C-H distance (1.091 Å) is longer than that for free CH₃· (1.078 Å). The planar CH₃· has been bent by its interaction with Ni⁺. It is indicated that the C-H bond of -CH₃ moiety has been activated by Ni⁺ atom.

The second step is an oxidative addition from NiCH₃⁺ via TS1, yielding the insertion product HNiCH₂⁺. This step involves an activation energy of 112.0 kJ mol⁻¹, with an endothermicity of 112.7 kJ mol⁻¹.

For transition state TS1, the C-H(5) distance is notably longer than that for NiCH₃⁺, while their overlap population is remarkably smaller. Meanwhile, the Ni-H(5) distance is considerably shorter than that for NiCH₃⁺. These indicate that the C-H(5) bond has been activated and the interaction of Ni-H(5) has been strengthened.

For HNiCH₂⁺, the C-H(5) distance is longer than that for TS1,

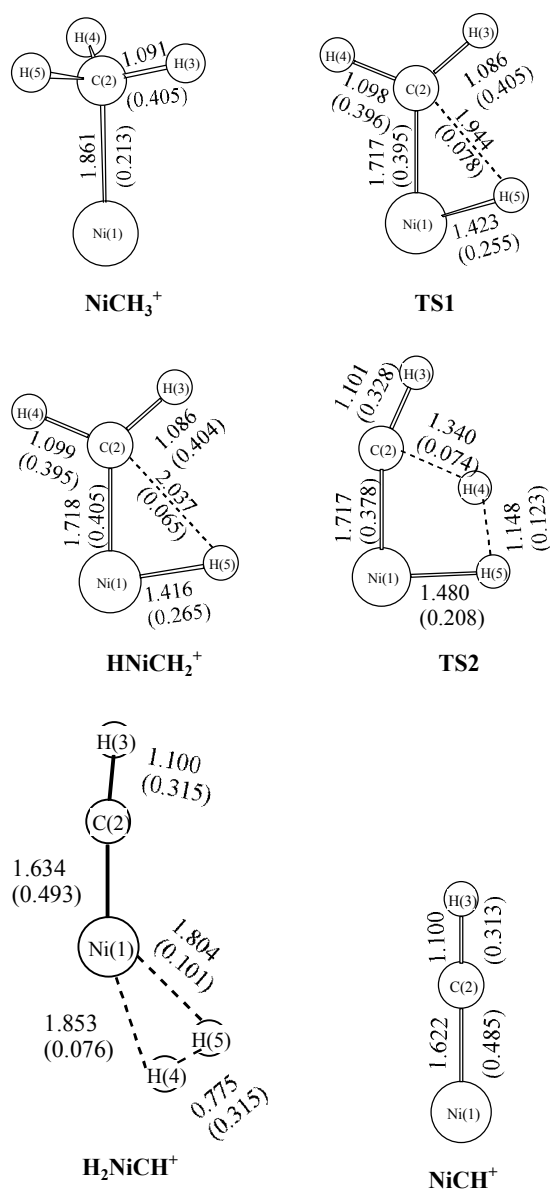


Figure 1. Calculated structures for intermediates and transition states on the potential energy surface at B3LYP/6-311+G(2d, 2p) level. Bond lengths are reported in Å and the overlap populations from the Mulliken Population are in parentheses.

while their overlap population is smaller. Meanwhile, the Ni-H(5) distance is shorter than that for TS1. This is characteristic of Ni-H(5) single bond. Obviously, the bond of C-H(5) has been completely cleaved and Ni⁺ atom has inserted into C-H bond of CH₃·.

The third step is the formation of molecular hydrogen complex of the nickel methylidyne H₂NiCH⁺, with an activation energy of 198.2 kJ mol⁻¹ and an endothermicity of 94.6 kJ mol⁻¹. From the whole potential energy curve, this barrier is the highest. It is indicated that this step is the rate-determination step in the whole reaction.

For transition state TS2, the C-H(4) distance is strikingly

* Corresponding author. E-mail: chwehu@mail.sc.cninfo.net

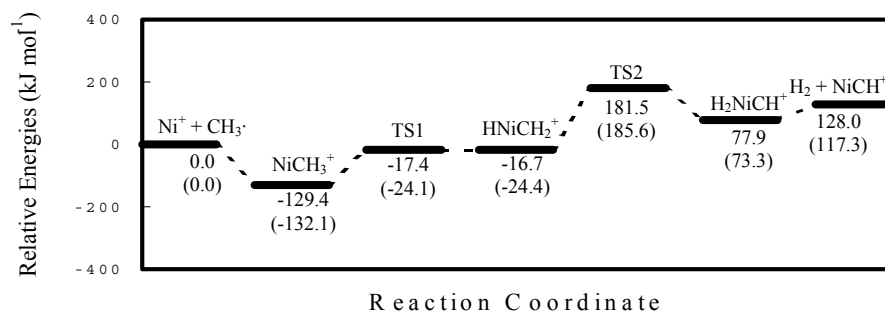


Figure 2. The singlet potential energy surface for the reaction $\text{Ni}^+ + \text{CH}_3\cdot \rightarrow \text{H}_2 + \text{NiCH}^+$ at 6-311+G(2d, 2p) level. The values in parentheses are the relative energies at the 6-31G** basis sets for carbon and hydrogen and the SDD basis sets and the corresponding ECP for the nickel.

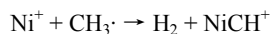
longer than that for H_2NiCH^+ , while their overlap population is clearly smaller. Meanwhile, the H(4)-H(5) distance is significantly shorter than that for H_2NiCH^+ . These indicate that the C-H(4) bond has been activated and the interaction of H(4)-H(5) has been increased.

For H_2NiCH^+ , the C-H(4), Ni-H(4) and Ni-H(5) distances are longer than those for TS2, while the H(4)-H(5) and Ni-C distances are shorter. These are representative of H(4)-H(5) single bond and Ni=C double bond. Furthermore, the H(4)-H(5) distance (0.775 Å) is slightly longer than that for free H_2 (0.743 Å), indicating that the H_2 molecularly adsorbed on NiCH^+ .

The final step is the release of H_2 molecule yielding nickel methylidyne NiCH^+ at cost of 50.1 kJ mol⁻¹.

Among all species on the potential energy curve, NiCH_3^+ has the lowest energy. On the other hand, HNiCH_2^+ does not appear to be a very stable entity, and is easily hydrogenated to NiCH_3^+ . This is in accordance with that obtained on Pd(111) surface by Paul et al.⁶

In general, our best estimate from the corrected calculations is that the reaction:



is endothermic by about 128.0 kJ mol⁻¹.

Conclusion

The initial interaction between Ni^+ and $\text{CH}_3\cdot$ is the formation of NiCH_3^+ species with C_{3v} symmetry. The second step is an oxidative addition, yielding the insertion product HNiCH_2^+ . The third step is the formation of molecular hydrogen complex of the nickel methylidyne H_2NiCH^+ . This step is predicted to be the rate-determining step in the whole reaction process. The final step is the release of hydrogen molecule yielding nickel methylidyne NiCH^+ . Subsequently, the overall reaction of $\text{Ni}^+ + \text{CH}_3\cdot \rightarrow \text{H}_2 + \text{NiCH}^+$ is endothermic by about 128.0 kJ mol⁻¹.

Acknowledgments

The authors are grateful for the financial support by the Key Project of National Fundamental Research and Development of China (973) (No. G1999022407), NNSF (No. 29873028), the Special Research Foundation of Doctoral Education of China (No. 2000061028) and the Foundation of Science and Technology of Sichuan Province (No. 200018-16).

References

1. Kaminsky M. P.; Winograd N.; Geoffroy G. L. *J. Am. Chem. Soc.* **1986**, *108*, 1315.
2. Koster A. D.; Santen R. A. V. *J. Catal.* **1991**, *127*, 141.
3. Yang H.; Whitten J. L. *J. Chem. Phys.* **1989**, *91*, 126.
4. Yang H. -Q.; Chen Y. -Q.; Hu C. -W.; Hu H. -R.; Gong M. -C.; Tian A. -M.; Wong N. -B. *J. Mol. Struct. (THEOCHEM)* **2001**, *574*, 57.
5. Michaelides A.; Hu P. *J. Chem. Phys.* **2000**, *112*, 6006.
6. Paul J. -F.; Sautet P. *J. Phys. Chem. B* **1998**, *102*, 1578.

A NEW ROUTE FOR CARBON DIOXIDE CYCLOADDITION TO PROPYLENE CARBONATE

Wei Wei Wei Tong Yuhua Sun*

State Key Laboratory of Coal Conversion, Institute of Coal Chemistry Chinese Academy of Sciences, Taiyuan, 030001, China

Introduction: The formation of five-cyclic carbonate (such as propylene carbonate) via cycloaddition between CO₂ and epoxides is not only one of the routes for CO₂ chemical fixation^[1], but also the cycloaddition of propylene oxide (PO) with CO₂ is the first step for synthesis of dimethyl carbonate (DMC) via transesterification^[2]. Furthermore, propylene carbonate (PC) itself was a nontoxic and versatile intermediates in environmentally benign organic synthesis. Hence, the green synthesis route of propylene carbonate has been expected in the half century.

Nemirovsky firstly reported the synthesis of alkyl carbonate by phosgenation method in a century ago^[3], but the method has gradually given up for using toxic and hazardous phosgene. After 1960s many methods have been published by patents, particularly, much attention has been paid attention to the cycloaddition between PO and CO₂, and the main catalytic systems included organometallic halides-Lewis base^[4], organotin halide-tetraalkylphosphonium halide^[5], alkali metal halide-crown ether^[6] or polyethylene glycol-400^[7]. But the catalytic performance and the severely reaction conditions limited their further utilization. In addition, a variety of solvents or promoters must be used, resulting in high separating cost or low purity of PC. Moreover, the reaction was carried out in a intermission autoclave, and leading to low production capacity. Thus, a new heterogeneous catalysts with high catalytic performance at moderate conditions (i.e. KI supported on different supports was firstly studied. In order to further improve the lifetime of the catalysts and productivity capability and avoid the hot spot of the catalysts, a new continual structural reactor was investigated. Combing the new heterogeneous catalysts and the new continual structural reactor, a new method for cycloaddition between PO and CO₂ in the heterogeneous process was developed in the present work.

Experimental: The purity of CO₂ was higher than 99.5%. Commercially available PO was used without further purification. Catalysts were prepared by impregnating the supports with an aqueous solution of KI, and then dried at 60°C for 10 h.

The catalysts were firstly evaluated in conventional intermission autoclave. For the cycloaddition between CO₂ and PO was intense exothermal reaction (≈30kcal/mol), this led to the difficult operation in heterogeneous catalytic process and the higher local temperature and the limitation of the lifetime of catalyst. Thus, a new structural reactor was designed. In this reactor the lifetime of the catalysts were further studied.

Results and discussion: In the heterogeneous process, KI supported on different supports was investigated (see Table 1). Firstly, the reaction conditions (reaction temperature, 120 °C, pressure, 4.0MPa) were very moderate, particularly, the pressure was lower than the saturate pressure of carbon dioxide at room temperature. Secondly, both PO conversion and PC selectivity were nearly 100% although neither solvents nor promoters in this catalytic synthesis were used. Thus, the product must not be

separated and simplified the production of PC. In addition, the space hour yield of PC was much higher than the conventional heterogeneous process (< 5g/(g(cat.) hr)), in particular, for KI supported activated carbon the space hour yield could reach to 12.0.

Table.1 Effect of several supports on catalytic activity of cycloaddition

Catalysts	PO Conv(%)	PC yield(%)	Space hour yield (kg/(kg(cat.) hr
KI/γ-Al ₂ O ₃ ^a	100.0	99.0	7.0
KI/activated carbon ^a	100.0	99.3	12.0
KI/SiO ₂ ^a	100.0	99.0	7.4

a-temperature, 120 °C, pressure, 4.0MPa

In 1L conventional intermission autoclave, both the conversion of PO and the selectivity of PC were shown in Fig. 1 in 100 hours. The catalytic performance sharply decreased in 100 hours. The BET surface area of fresh catalyst and after reaction catalyst was showed in table 2. Obviously, the fouling of the catalyst pore was very severe in reaction process in the conventional intermission autoclave. In addition, we also found that the product color was wine. This indicated that KI in the catalysts was partly oxidized in reaction process because reaction heat could not removed and existed local hot spot.

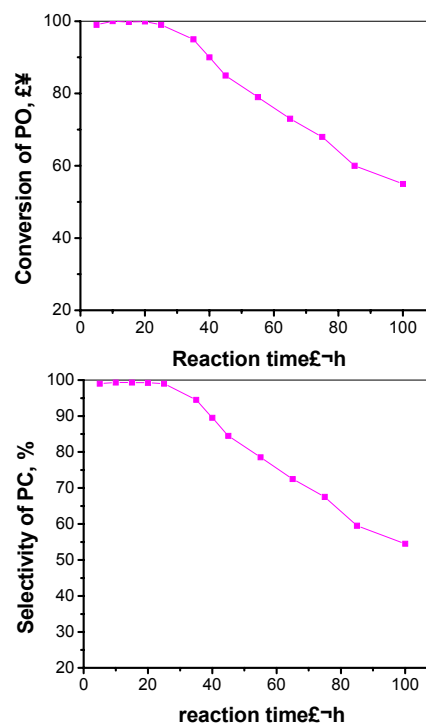


Fig. 1 Both the conversion of PO and the selectivity of PC in 1 L conventional intermission(autoclave in 100 hours)

Table 2 The characters of the fresh catalyst and after the reaction

catalyst	BET surface m ² /g	pore size ^a , Å	pore vol., cc/g
fresh catalyst	394.3	22.2	0.22
after reaction	40.7	56.8	0.06

a-average pore diameter

* To whom correspondence should be addressed: weiwei@sxicc.ac.cn or yhsun@sxicc.ac.cn

In order to further improve the lifetime of the catalysts and productivity capability and avoid the hot spot of the catalysts, a new continual structural reactor was designed^[8]. The advantages of the continual structural reactor included: (1) In this reactor the PC could be immediately removed from the surface of the catalysts as soon as it was produced, and avoided the deposition of the catalyst pore; (2) The catalysts were particularly loaded in this reactor and the reaction heat could be efficiently removed. Thus, the lifetime of catalyst could be improved; (3) The reaction was continual in this reactor, and improved its production capacity. Figure 2 demonstrated that in the new continual structural reactor both the PO conversion and PC selectivity hardly decreased in 400h. And the product was not color.

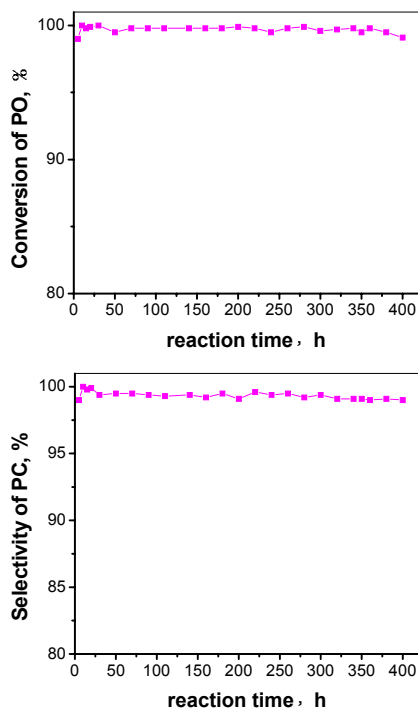


Fig. 2 Both the conversion of PO and the selectivity of PC in 20 L new continual structural(reactor in 400 hours)

Conclusion: For the new heterogeneous catalysts, both PO conversion and PC selectivity, especially, KI/A.C. catalyst, were nearly 100% at moderate conditions; the STY of PC was also very high. In the 1L intermission autoclave the fouling of the catalyst pore led to the deactivation of the catalysts, and the reaction heat could not be removed. Both the PO conversion and PC selectivity hardly decreased in 400h in the new continual structural reactor. In general, the new method provided an economically advantageous process for the production of propylene carbonate under milder reaction temperature and pressure condition in high yield.

Reference:

- [1] R. Nomura, M. Kimura, S. Teshima, etc., *Bull. Chem. Soc. Jpn.*, 1982. 55. 3200.
- [2] A. Baba, T. Nozaki, T.Miki, *Bull. Chem. Soc. Jpn.*, 1987. 60. 1552.
- [3] I. Nemirovsky, *J. Prakt Chem.*, 1883. 28. 439.
- [4] R. Nomura, M. Kimura, S. Teshima, etc., *Bull. Chem. Soc. Jpn.*, 1982. 55. 3200.
- [5] A. Baba, T. Nozaki, T.Miki, *Bull. Chem. Soc. Jpn.*, 1987. 60. 1552.
- [6] G.Rokicji and W. Kuran, *Bull. Chem. Soc. Jpn.*, 1984. 57. 1662.
- [7] Z.Z.Tang, Y.Chen, Z.J.Qu, etc, *J. Petrochem Technol.* (China), 1996.

A NOVEL HIGHLY ACTIVE REFORMING CATALYST SYSTEM AND PRODUCTION OF PURE HYDROGEN FROM THE GREENHOUSE GASES OF CH₄ AND CO₂ AT MILD TEMPERATURES WITH A MEMBRANE REACTOR

Linsheng Wang, Kazuhisa Murata, Megumu Inaba

Research Institute for Green Technology, National Institute of Advanced Industrial Science and Technology,
AIST Tsukuba Central 5, Tsukuba, Ibaraki 305, Japan
E-mail: linsheng.wang@aist.go.jp

Introduction

Conversion of methane and carbon dioxide into synthesis gas (CO/H₂) is an important route for reasonable utilization of natural gas resource. Carbon dioxide reforming reaction of methane was first studied by Fischer and Tropsch using Ni and Co based catalysts in 1928 [1]. Recently the reforming reaction of methane with carbon dioxide on supported Ru, Rh, Pd, Ir, Pt, Mo or W carbide based catalysts has been studied by many other authors [2-10]. SiO₂, Al₂O₃, TiO₂, MgO, ZrO₂, La₂O₃, NaY, NaZSM-5 were used as supporting materials of the catalysts for the reforming reaction. The Bronsted acid sites of the supports are not necessary for the reforming reaction on the traditional catalysts [8]. The reported traditional reforming catalysts are also active for the two-step homologation of methane [11-13]. It has recently been reported that Re/HZSM-5 is a promising catalyst for one-step activation of methane into aromatics and C₂ hydrocarbons [14,15]. However, the catalytic performance of Re/HZSM-5 for the reforming reaction of methane with carbon dioxide has not been studied so far. In the present paper, the reforming reaction of methane with carbon dioxide on the bifunctional Re/HZSM-5 and Mo/HZSM-5 catalysts has been studied. In addition, High pure hydrogen was directly produced from the two greenhouse gases of methane and carbon dioxide on the novel catalyst at mild temperatures by integration of the reforming reaction and H₂ separation with a Pd membrane reactor.

Experimental

Re/HZSM-5 and Rh/HZSM-5 were prepared by impregnating NH₄ZSM-5 • SiO₂/Al₂O₃=30 • with NH₄ReO₄ and RhCl₃ aqueous solution respectively, followed by drying at 383 K for 4 h and calcination at 773 K for 4 h. The sample was finally pressed, crushed and sorted into 20-40 meshes. Catalytic tests were carried out with about 200-2000 mg catalyst placed in a fixed bed continuous-flow membrane reactor. The catalysts were reduced by hydrogen at 623-673K for 2h. The membrane reactor is with 5/8" diameter and by 10" tall. It contains four membrane tubes with 1/8" diameter and by 7" tall. H₂ was permeated through the membrane into the tubes and removed by pump immediately after produced. The selectivity for hydrogen permeation through the membrane is 100% and ultra high pure H₂ was produced as a result. Conversion, selectivity and formation rate of products were calculated by an internal standard analyzing method described as previously. About 11.1% N₂ was added into ethane feed as internal standard. Catalytic conversion of ethane on Re/HZSM-5 was conducted at a reaction temperature range of 773-858K and a wide SV range.

Results and discussion

Catalytic performance of the novel Re based catalysts has been compared with traditional noble metal Rh based catalyst for the carbon dioxide reforming reaction of methane and results are listed in table 1. HZSM-5 supported Re catalyst exhibits a quite high activity

for the reforming reaction and even better than the traditional noble metal Rh based catalyst as shown in table 1.

Table 1. The bifunctional effect of catalysts in activation of CH₄ and CO₂

Catalyst	Conversion (%)		CH ₄ /CO ₂ consumed	H ₂ /CO ratio in product
	CH ₄	CO ₂		
Re/HZSM-5	83	80	1.07	0.81
Rh/HZSM-5	78	72	0.96	0.80
Re/KZSM-5	17	9	1.74	0.43
Mo/HZSM-5	22	15	0.68	0.38

Methane SV=5000 ml/h/g; Feed ratio (CH₄/CO₂)=1.05; Temperature=973K

The high methane and CO₂ conversions of 83% and 80% were attained on Re/HZSM-5 at 973K. Conversions of methane and carbon dioxide on Rh/HZSM-5 are 78% and 72% at the exactly same reaction conditions. The high activity of the novel bifunctional Re/HZSM-5 for the reforming reaction is due to its high activity for one-step activation of methane. It is also indicated in table 1 that both metal Re and Bronsted acid of ZSM-5 support are necessary for the high activity of Re/HZSM-5. The monofunctional Re/KZSM-5 (B acid sites of HZSM-5 support were poisoned by K) and bifunctional Mo/HZSM-5 give much lower activity for carbon dioxide reforming of methane although Mo/HZSM-5 is also an excellent catalyst for one step activation of pure methane. This is due to the active phase of Mo/HZSM-5 for methane active phase is unstable when it is exposure to CO₂. Table 2 gives the effect of feed ratio (CH₄/CO₂) on the conversions of CH₄ and CO₂. It is indicated in table 2 that the maximum methane conversion is obtained when the feed ratio (CH₄/CO₂) is near 1. However, CO₂ conversion increases with increasing the ratio of CH₄/CO₂ in feed. The H₂/CO ratio is near unity is at the higher CH₄/CO₂ ratio. In addition, the ratio of the consumption rates of methane and carbon dioxide is about 1 even at the different feed ratio (CH₄/CO₂).

Table 2. Dependence of CH₄ and CO₂ conversions on the feed ratio (CH₄/CO₂)

Feed ratio CH ₄ /CO ₂	Conversion (%)		CH ₄ /CO ₂ consumed	H ₂ /CO ratio in product
	CH ₄	CO ₂		
0.81	77	59	0.89	0.67
0.91	83	64	1.01	0.71
1.05	83	80	1.07	0.81
1.47	66	83	0.99	0.84
1.64	45	94	0.99	0.92

Methane SV=5000 ml/h/g; Temperature=973K

The low-temperature activity of Re/HZSM-5 catalyst for the dry reforming reaction is also evaluated and the result is listed in table 3.

Table 3. The lower temperature activity of Re/HZSM-5 for the reforming reaction CH₄ and CO₂

Temperature (K)	Conversion (%)		CH ₄ /CO ₂ consumed	H ₂ /CO ratio in product
	CH ₄	CO ₂		
773	15	26	0.61	0.15
818	30	44	0.70	0.60
858	41	49	0.85	0.66
973	83	80	1.07	0.81

Methane SV=5000 ml/h/g; Feed ratio (CH₄/CO₂)=1.05

It is indicated in table 3 that the Re/HZSM-5 exhibits a considerable activity even at as low as 773-858K and the conversions of methane and CO₂ are 41% and 49% at 858K. The excellent low temperature activity of Re/HZSM-5 makes it have many advantages for the integration of the catalytic reaction of the reforming and hydrogen separation because the Pd type membrane is limited to use only at relatively mild temperatures.

Although Re/HZSM-5 is quite active for the carbon dioxide reforming of methane even at the lower temperatures, the conversions of methane and carbon dioxide are constrained by thermodynamic equilibrium. To transform methane and CO₂ into pure hydrogen and CO at the conversions beyond the thermodynamic equilibrium, a Pd type membrane reactor was used for integration of the reforming reaction and hydrogen separation. The conversions of CH₄ and CO₂ when hydrogen is separated and not separated at 858K and different methane SV are compared in table 4. It is shown in table 4 that methane conversion for the dry reforming reaction is about 47-48% and it changes little with varying methane SV from 1300 to 325 ml/h/g when hydrogen was not separated from product. However, the much higher methane conversion of about 77% has been achieved at the low temperature of 858K as shown in table 4. CO₂ conversion is also enhanced by the hydrogen separation at the same time. In addition, the ratio of feed consumption rates (CH₄/CO₂) is more near unity when hydrogen is separated from product. This is because some side reaction such as reduction of CO₂ by H₂ in to CO is effectively suppressed by the continuously hydrogen separation from product with the membrane.

Table 4. Effect of H₂ separation on the conversions of CH₄ and CO₂ at different SV

SV of CH ₄ (ml/h/g)	Permeability of H ₂ (%)	Conv. (%)		CH ₄ /CO ₂ consumed	H ₂ /CO ratio
		CH ₄	CO ₂		
325	92	76.9	60.5	1.15	*
	0	48.3	48.0	0.91	0.63
650	92	69.2	45.6	0.98	*
	0	47.9	34.4	0.90	0.71
1300	90	62.7	42.6	0.95	*
	0	47.1	33.3	0.92	0.71

Feed ratio (CH₄/CO₂)=0.69; Temperature=858K; * H₂ separated

Conclusion

Re/HZSM-5 is a novel reforming catalyst for the conversion of methane and carbon dioxide into hydrogen and CO. The novel catalyst system exhibits a quite high activity for the carbon dioxide reforming reaction of methane even at mild temperatures and it is different from the traditional reforming catalysts because both Re metal and the Bronsted acid on the novel catalyst are contributed to the methane activation. On the novel catalyst system, high pure hydrogen are directly produced from the greenhouse gases of methane and carbon dioxide by integration of the reforming reaction and hydrogen separation with a Pd type membrane reactor. In addition, much higher conversions of methane and CO₂ beyond the thermodynamic equilibrium are attained because hydrogen is separated from the product.

References

1. F. Fischer and H. Tropsch, *Brennst. Chem.* 3 (1928) 39
2. F. Solymosi, Gy. Kutsan and A. Erdohelyi, *Catalysis Letters*, 11 (2000) 149
3. Z. L. Zhang, V. A. Tsipouriari, A. M. Efstathiou and X. E. Verykios, *Journal of Catalysis*, 158 (1996) 51
4. M. C. J. Bradford and M. A. Vannice, *Journal of Catalysis*, 173 (1998) 157
5. M. C. J. Bradford and M. A. Vannice, *Journal of Catalysis*, 183 (1999) 69
6. M. F. Mark and W. F. Maier, *Journal of Catalysis*, 164 (1996) 122
7. J. H. Bitter, K. Seshan and J. A. Lercher, *Journal of Catalysis*, 176 (1998) 93
8. R. N. Bhat and W. M. H. Sachtler, *Applied Catalysis A: General* 150 (1997) 279
9. M. Tsuji, T. Miyao and S. Naito, *Catalysis Letters*, 69 (2000) 195
10. A. J. Brungs, A. P. E. York, J. B. Claridge, C. Marquez-Alvarez and M. L. H. Green, *Catalysis Letters*, 70 (2000) 117
11. L. Guzzi, K. V. Sarma and L. Boriko, *Journal of Catalysis*, 167 (1997) 495
12. M. Belgued, A. Amariglio, L. Lefort, P. Pareja and H. Amariglio, *Journal of Catalysis*, 161 (1996) 282
13. T. Koerts, M. J. A. G. Deelen and R. A. Van Santen, *Journal of Catalysis*, 138 (1992) 101
14. L. Wang, R. Ohnishi and M. Ichikawa, *Journal of Catalysis*, 190 (2000) 276
15. L. Wang, K. Murata, A. Sayari, B. Grandjean and M. Inaba, *ChemComm.*, in press (2001)

OH RADICAL GENERATION BY ATMOSPHERIC PRESSURE PLASMA AND ITS QUANTITATIVE ANALYSIS BY MONITORING CO OXIDATION

Zhen-Zhou SU*, Kohei ITO**, Hyun-Ha KIM***, Kazunori TAKASHIMA*, and Akira MIZUNO*

*Department of Ecological Engineering, Toyohashi University of Technology, Tempaku-cho, Toyohashi, Aichi, 441-8580, Japan

**Department of Electrical Engineering, Toyohashi University of Technology, Tempaku-cho, Toyohashi, Aichi, 441-8580, Japan

***Japan Atomic Energy Research Institute, Takasaki, 370-1292, Japan

Introduction

Applications of non-thermal plasma for gaseous pollution control or methanol synthesis have been carried out by several researchers [1,2]. In these plasma chemical reactions, OH radicals play a very important role for their strong oxidation capability. In understanding the mechanism of plasma chemical reactions, the behavior of the OH radical in both formation process and the subsequent chemical reaction process is required to be known. The measurement of OH radicals in discharge plasma, however, is very difficult, especially under the atmospheric condition. There are several methods such as LIF (Laser-induced fluorescence) or OES (Optical emission spectroscopy). These methods require rather complicated measurement system.

In the atmospheric chemistry, the CO oxidation monitoring method has been used to measure OH radicals concentration [3]. In this paper, the application of CO oxidation monitoring method to the OH radicals measurement in a pulsed discharge plasma in argon and H₂O mixture at atmospheric pressure was examined.

When a pulsed discharge plasma is generated in H₂O/Ar, OH radicals are formed by the collisions of electrons or the excited Ar molecules with H₂O. If CO was added to H₂O/Ar, it will be rapidly oxidized by OH radicals as shown in reaction (1). According to this reaction, the concentration of OH radicals can be determined by the amount of produced CO₂.



In order to apply this method in the discharged plasma, it is necessary to consider both the dissociation of CO₂ due to the next pulse discharge and the loss reactions of OH radicals. Under a condition where these influences can be ignored, the concentration of OH radicals can be determined as CO₂ concentration. In this work, gas residence time and initial CO concentration necessary to ignore the dissociation of CO₂ was studied with experiment and calculation. On the basis of this method, the concentration of OH radicals in the H₂O/Ar plasma was measured to study the effect of H₂O content, SIE on the formation of OH radicals.

Experimental

The gas mixture of Ar (99.999%) and CO (99.95%) was adjusted using mass flow controllers (Estec Inc., SEC-410 and DS-3). The H₂O concentration was controlled by evaporating a constant rate of H₂O fed by a microfeeder. The gas temperature was controlled by a convection oven (SIBATA, SPF-600) and a ribbon heater. The gas-residence time was adjusted by changing the flow rate of gas. A square pulse high voltage (peak voltage 15-22kV, frequency 230-240Hz) was used to form non-thermal pulsed discharge plasma.

The reaction products were analyzed by FT-IR (BIO-RAD, FTS-30) and found to be CO and CO₂. A GC-FID (Shimadzu, GC-8A) equipped with a methanizer (GL Sciences, MT-221) was used for quantitative measurement of CO and CO₂. The voltage and current waveform were recorded with a digital oscilloscope (Tektronix, TDS-644A), a voltage divider (Tektronix, P6015) and

a current probe (Tektronix, P6021). The discharge power was calculated with voltage and current waveform.

Results and Discussion

A. Criteria of the method

Dissociation of CO₂ due to discharge. In the case of the pulsed discharge plasma, the dissociation of products is mainly caused when the products are exposed to the plasma. For the purpose of quantitative measurement of OH radicals, unless otherwise noted, experiments were carried out in a single pulse condition, to avoid the dissociation of products. The single pulsed discharge process was realized by adjusting the gas-residence time to the period of the applied voltage. Consequently, there will be no dissociation of CO₂ caused by the next pulse. The time evolution of CO₂ production of the reaction of CO and OH was calculated. **Fig. 1** indicates that 130μs was necessary for the reaction to reach an equilibrium state when the OH concentration was 50ppm and the CO concentration was 1%. Because the FWHM (Full width at half-maximum) of the pulse current was 40ns, the reaction of CO and OH ran at the interval term of two successive pulsed discharges. The oxidation of CO by OH can be considered as a chemical reaction, and it is not affected from discharge in the single pulsed discharge.

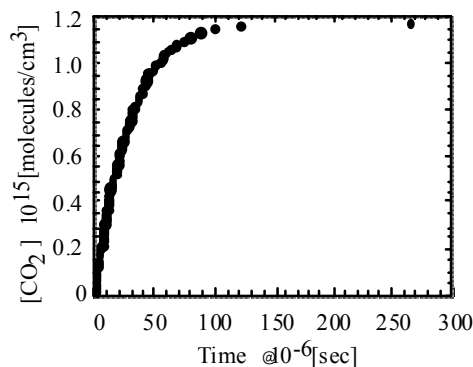


Fig. 1 Calculation for the reaction time of CO₂ production.

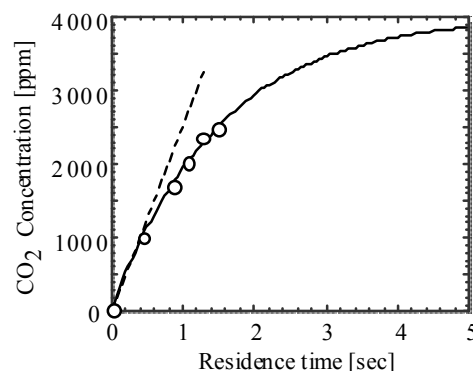
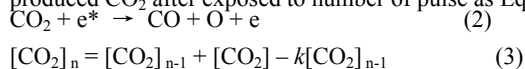


Fig. 2 Influences of the dissociation of CO₂ by discharge. (Discharge power=3.1W, H₂O/CO/Ar=1/1/98)

Under extended gas residence time, however, both processes of CO₂ formation and CO₂ dissociation take place at the same time. In this sense, we should consider these both processes to estimate the produced CO₂ concentration. Assuming that the production of CO₂ per each single pulse is constant and the dissociation of CO₂ is caused by reaction (2), then we can obtain the concentration of produced CO₂ after exposed to number of pulse as Eq. (3).



$$[\text{CO}_2]_n = [\text{CO}_2]_{n-1} + [\text{CO}_2] - k[\text{CO}_2]_{n-1} \quad (3)$$

Where

$[CO_2]$ = CO_2 production by a single pulse

$[CO_2]_{n-1}$ = CO_2 production by n-1 times of pulses

k = The rate of the dissociation of CO_2 by a single pulse discharge

Eq. (3) is transformed into Eq. (4).

$$[CO_2]_n = [CO_2] \times k^{-1} \times [1 - (1-k)^n] \quad (4)$$

It indicates that $[CO_2]_n$ increases with the number of pulse (the residence time) nonlinearly. Fig.2 shows the experimental results of the gas residence time up to 1.6sec. CO_2 production, $[CO_2]_n$, tends to increase linearly with the residence time up to 0.5sec, and then begin to saturate. The appearance of the linear increasing of CO_2 indicates that, the influence of the dissociation of CO_2 caused by succeeding discharges can be ignored when the residence time smaller than 0.5sec in this experimental condition.

The influences of loss reactions of OH radicals. Differing from the chemistry of atmospheric space, concentration of OH radical in the discharge plasma is very high. In the conditions where the concentration of OH radical is high, the loss-reaction mainly due to recombination may take place. Reactions (5)-(10) are regarded main reactions in the discharge space where H_2O exists. Reactions (5)-(8) are the loss-reactions of OH radicals. These reactions compete with the reaction (1), and affect the CO oxidation by OH radicals. OH radicals branching depends on the rate constants and initial concentrations of CO and OH. The variation of CO_2 production with the variation of the CO initial concentration was measured by the experiment. Calculation was also made using a simulation software (IBM, CKS version 1.0).

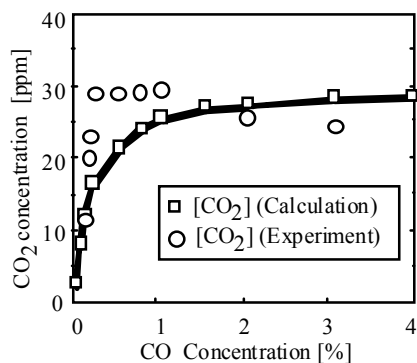
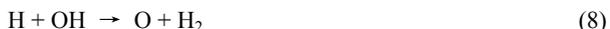


Fig.3 The influence of OH loss reactions. (Calculation condition: reaction (1), (5) -(10) were used. $[OH]_0=[H]_0=8.1 \times 10^{14}$ molecules/cm³, $[CO]_0=2.7 \times 10^{14}$ molecules/cm³, $[H_2O]_0=2.7 \times 10^{14}$ molecules/cm³, Experimental condition: Content of $H_2O=1\%$, Residence time=4.2ms, Discharge power=1.8W, T=50 degree)

Fig.3 shows the results of the experiment and the simulation. In the experiment, the CO_2 production was observed while the initial concentration of CO was varied from 800ppm to 4%. When $[CO]_0 < 2000$ ppm, the CO_2 production was increased with increasing $[CO]_0$. When $[CO]_0 \cong 2000$ ppm, the CO_2 concentration became constant. This result indicated that the influence of the loss-reactions of OH radicals could be ignored when initial CO concentration is higher than 2000ppm. However, when CO concentration exceeded 1%, the CO_2 concentration

began to decrease because the peak discharge current decreased.

The result shows the similar tendency in the variation of the CO_2 formation. It indicates that the influence of loss reactions much depends on the initial concentration of CO.

B. Influences of H_2O content and discharge power on OH formation

Fig.4 shows the relation between the H_2O content and the OH formation. It shows that production of OH radicals increased when the H_2O content increased under the same SIE (Specific Input Energy: energy to unit volume of gas, kJ/m³). The production of OH radical increased with the SIE value when the H_2O content was kept constant. These results agree with other measurements on spectroscopic analysis of OH formation in DBD (dielectric barrier discharges) of Ar/ O_2 / H_2O [4].

In our experiment, under the conditions with the SIE value of 9 kJ/m³ and H_2O content of 1.5%, the maximum OH production 30ppm (9.4×10^{14} cm⁻³) was obtained. The value is about the same as that observed in DBD [5]. In our experiment, the G value, which is defined as the number of OH produced per 100 eV, is 1.9. Penetrante calculated the G value for OH generation using DEGARD in the case of pure H_2O , and obtained 1.42[1]. It should be noted that a comparable OH yield-value has been obtained in our experiment using the simple equipment.

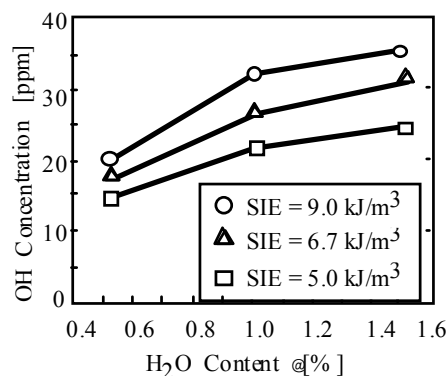


Fig.4 Influences of OH formation according to the variation of content of H_2O and discharge power. (CO/Ar=1%, T=50 degree)

Acknowledgment.

The authors are grateful to Professor H. Matsui, Professor K. Onda and Assistant T. Tatsuo of Toyohashi University of Technology for their valuable discussions.

References

- [1] B. M. Penetrante, *NATO ASI Series*, **1993**, G34, Part A, pp.65.
- [2] Liu, C. J., A. Marafee, R.G. Mallinson, and L.L. Loban, *Applied Catalysis A*, **1997**, 164, pp.21.
- [3] Campbell M J, Farmer J C, Fitzner C A, Heavy N M, Sheppard J C, Hardly R J, Hopper J F and Muralidhar V, *J. Atmos. Chem.*, **1986**, 4, pp.413.
- [4] Zoran Falkenstein, *J. Appl. Phys.*, **1997**, 81 (11), pp.7158.
- [5] C. Hibert, I. Gaurand, O. Motret, J.M. Pouvesle, *J. Appl. Phys.*, **1999**, 85 (10), pp.7070-7075.

OXYGENATE SYNTHESIS FROM METHANE AND CARBON DIOXIDE USING DIELECTRIC-BARRIER DISCHARGES

Ming-xia He,^{1,2} Ji-jun Zou,^{2,3} Yang Li^{2,3}, Baldur Eliasson^{2,4} and Chang-jun Liu^{2,3*}

¹ School of Chemical Engineering and Technology, ²Tianjin University-ABB Plasma Greenhouse Gas Chemistry Laboratory and ³ State Key Laboratory of C1 Chemical Technology, Tianjin University, Tianjin 300072, China

⁴ Energy and Global Change, ABB Corporate Research Ltd., Baden, CH5405, Switzerland

Introduction

Plasmas, including thermal and non-thermal plasmas, have been extensively investigated for methane conversion. The thermal plasma normally was used for the production of acetylene or carbon black from methane, with hydrogen as a by-product. There have been much more investigations on methane conversion using non-thermal plasmas recently. An important characteristic of non-thermal plasma is its high electron temperature (as high as 10^5 K) while the bulk gas temperature remains as low as room temperature. This characteristic makes it suitable for chemical synthesis of higher hydrocarbons and oxygenates. Most of products produced using corona, microwave, and radio frequency discharge are some little molecules, like ethylene, acetylene, hydrogen and carbon monoxide. Under the condition of dielectric-barrier discharge, product could be more complex for its large volume of discharges. Light hydrocarbons, liquid fuels, alcohols and acids can be produced. Furthermore, some operation parameters in dielectric-barrier discharges can be easily changed including dielectric material, length and distance of discharge gap and electrode configuration. The distribution of products will be different with the different parameters in dielectric-barrier discharges. Due to the poor understanding of plasma chemistry, the present status of plasma methane conversion is still in the laboratory test. More intensive fundamental investigations are required, esp., at the time when the direct catalytic methane conversion still remains as a challenge to the scientists all over the world.

On the other hand, the combination of utilizations of methane and carbon dioxide is very promising, even with the plasma methane conversion. As a co-reactant for methane conversion, CO_2 is a soft oxidant and can provide extra carbon atom for the conversion. Oxygenates can be generated including methanol, formic acid and others upon the operative conditions applied.[1-3] The metal electrode material has also an effect on the product distribution from methane and carbon dioxide.[4] The previous investigation focused on the formation of higher hydrocarbons (including liquid fuels) using the high voltage electrode covered by the dielectric material.[5] In this work, we investigated the synthesis of oxygenates directly from CH_4 and CO_2 under the conditions of dielectric-barrier discharges with the grounded electrode covered dielectric material layer. This means the high voltage electrode will expose directly to plasma phase. A big difference induced by this change in the electrode configuration is that only oxygenates are produced in the liquid products (no liquid hydrocarbons) in the present reactor design.

Experimental

The schematic configuration of the discharge reactor used in this investigation is shown in Figure 1. A quartz tube with the inner diameter of 14 mm served as the dielectric barrier. A transparent conductive (silver) film deposited on the quartz tube was used as the grounded electrode. The high voltage tubular electrode with the outer

diameter of 12 mm was made of aluminum foil and located in the center of quartz tube. The discharge zone was formed within a gap of 1 mm between the aluminum electrode and the quartz tube with the length of 200 mm. The feed gases passed through the gap and were converted within the discharge zone. The reaction was terminated at the end of discharge region. The high voltage generator supplied about 10 kV sinusoidal signals at frequency of 25 kHz to the discharge reactor. The voltage and current were measured with a high voltage probe (Tektronix P6015 A) and a pulse current transformer (Pearson Electronics 411) via a digital oscilloscope (Tektronix 2440). The discharge power was measured via a digital multimeter (Keithley 2000). The discharge power was fixed at 100 W in this investigation.

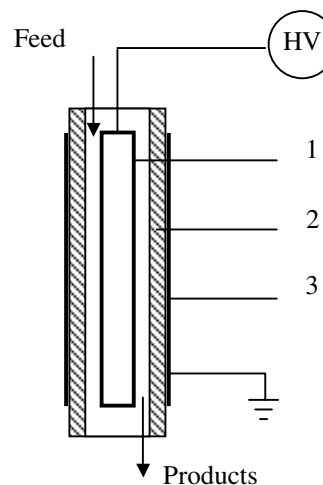


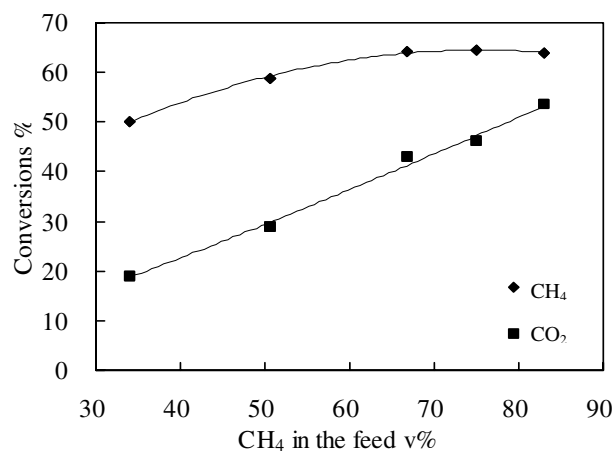
Figure 1. Schematic configuration of DBD reactor (1-HV electrode; 2-Quartz tube; 3-Grounded electrode)

The reactants, methane and carbon dioxide, were introduced into the reactor via mass flow controllers. The total flow rates were fixed at 60 ml/min with the retention time of about 12 second. The feed and products were analyzed with a GC (HP 5890) equipped with a thermal conductivity detector (TCD) and a flame ionization detector (FID) via a HP-PLOT Q (30 m \times 0.53 mm \times 40 μm) column. A mass selective detector (HP 5971) was used to identify the products. Liquid products were collected in a cold trap cooled with a mixture of ice and water. All the investigations were carried out at ambient conditions.

Results

Conversions of Methane and Carbon Dioxide. The conversions of CH_4 and CO_2 are shown in Figure 2. Conversion of carbon dioxide nearly proportionally increased with increasing of methane concentration in the feed. Methane conversion increased with the increasing of carbon dioxide conversion while methane concentration was less than 60 v% in the feed. However, the conversion of methane reached a saturated value when methane was more than 60 v% in the feed. The trend of the change of methane conversion is different from that reported previously.[5] It suggested that the conversion of methane is strongly affected by the conversion of carbon dioxide in this case, especially when carbon dioxide was the principal component in the feed.

Figure 2. Effect of composition of feed on conversions



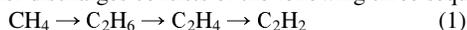
(Discharge power of 100 W; Flow rate of 60 ml/min)

Analysis of Gaseous Products. Gaseous products contain hydrocarbons (from C₂ to C₅) and CO. The selectivities of gaseous products are shown in Table 1. The selectivities of hydrocarbons were sharply decreased with the increasing carbon atom numbers in

Table 1. Selectivities of gaseous products
(Discharge power of 100 W; Flow rate of 60 ml/min)

CH ₄ in the feed v%	34.0	50.6	66.8	75.1	83.1
	Selectivity based on carbon atoms /%				
Ethene	0.4	0.5	0.6	0.8	1.1
Acetylene	0.5	0.8	0.9	1.1	1.3
Ethane	11.1	11.5	11.7	12.4	14.2
Propene	0.2	0.3	0.5	0.5	0.7
Propane	5.0	6.1	6.9	6.8	8.6
Isobutane	1.2	1.8	2.2	2.1	2.8
Butane	1.4	2.0	2.4	2.3	3.1
Neopentane	0.7	0.9	1.0	1.0	1.1
Isopentane	0.1	0.4	0.5	1.9	2.6
Pentane	0.2	0.3	0.4	0.8	1.1
CO	64.9	49.0	32.2	22.6	17.3

the molecules. The selectivities of unsaturated hydrocarbons were much less than those of paraffins. It was considered that the formation of C₂ hydrocarbons from plasma methane conversion using dielectric-barrier discharges consists of the following three sequential steps [6]:



As shown in Table 1, CO selectivity decreased with the increasing methane concentration in the feed. And there existed a nearly linear relationship between selectivity of CO and CH₄ concentration in the feed.

Distribution of Components of Liquid Products. Oxygenates, including methanol, ethanol, acetic acid and other alcohols and acids containing more than two carbon atoms, were the major products in the condensate as shown in Table 2. Acetic acid was the primary product in the condensate with the highest selectivity of 5.2% at 66.8

v% of methane in the feed. There existed an optimum component of feed for the selectivities of ethanol, 1-propanol and acids, respectively.

Table 2. Selectivities of liquid products
(Discharge power of 100 W; Flow rate of 60 ml/min)

CH ₄ in the feed v%	34.0	50.6	66.8	75.1	83.1
	Selectivity based on carbon atoms /%				
Methanol	1.1	1.0	0.3	0.3	0.1
Ethanol	2.6	4.9	1.8	1.7	0.8
Isopropyl alcohol	0.2	0.2	0.2	0.2	0.1
1-Propanol	0.2	0.3	0.1	0.1	0.1
Acetic acid	2.8	4.6	5.2	4.8	2.4
Propanoic acid	0.8	1.3	1.0	0.9	0.5
Isobutanoic acid	0.1	0.2	0.1	0.1	0.1
Butanoic acid	0.2	0.2	0.2	0.1	0.1

Conclusions

Direct synthesis of oxygenates, including acetic acid, propanoic acid, methanol and ethanol, from methane in the presence of carbon dioxide was conducted under the condition of dielectric-barrier discharges in this work. The present reactor design suggests the surface status of electrodes played an important role in the formation of oxygenates. The selectivities of acetic acid, propanoic acid, methanol and ethanol were 5.2%, 1.0%, 0.3% and 1.8%, respectively, with the conversions of methane and carbon dioxide of 64.3% and 43.1%, respectively, while methane of 66.8v% in the feed. From the obtained results, CO, gaseous and solid hydrocarbons are still the major product. To get a higher yield of oxygenates, it is better to remove the oxygenate product as soon as it is produced. Further investigation is being performed to achieve a better production of oxygenates directly from methane and carbon dioxide using plasmas (with special catalyst and typical reactor design).

Acknowledgement. Supports from the Key Foundation of Tianjin City Committee of Science and Technology and ABB Corporate Research Ltd., Switzerland are very appreciated.

References

- Larkin, D. W.; Lobban, L.L. and Mallinson, R.; *Ind. Eng. Chem. Res.*, **2001**, 40, 1594.
- Matsumoto, H.; Tanabe, S.; Okitsu, K.; Hayashi, Y. and Suib, S.L.; *J. Phys. Chem. A*, **2001**, 105, 5304.
- Okumoto, M.; Su, Z.; Katsura, S. and Mizuno, A.; *IEEE Tran. Ind. Appl.*, **1999**, 35, 1205.
- Li, Y.; Xu, G.-H.; Liu, C.-J.; Eliasson, B.; and Xue, B.; *Energy & Fuels*, **2001**, 15, 299.
- Liu, C.-J.; Xue, B.; Eliasson, B.; He, F.; Li, Y.; and Xu, G.-H.; *Plasma Chem. Plasma Process.*, **2001**, 21, 301.
- Kozlov, K. V.; Michel, P.; and Wagner, H.E.; *Plasmas and Polymers*, **2000**, 5, 129.

PLASMA CATALYTIC HYBRID REFORMING OF METHANE

Thomas Hammer, Thomas Kappes, Wolfgang Schiene

Siemens AG, Corporate Technology Department Plasma- and Switching Technology, POB 3220, 91050 Erlangen, Germany

Introduction

Hydrogen enriched fuel gases offer the potential for efficient low NO_x combustion processes. The reduction of NO_x-emission is caused by a reduction of the adiabatic flame temperature due to stable, lean combustion and in some cases due to steam addition or exhaust gas recirculation. In the past reduced NO_x-emissions both from gas turbines^{1,2} and internal combustion engines³ were reported. At the same time the energy efficiency of internal combustion engines³ was improved for 15-50 % compared to pure gasoline operation. In stationary applications there is an additional potential for the reduction of specific CO₂-emissions: If the hydrogen is generated by integrated reforming of fossil fuels, carbonaceous products of the reforming reaction like CO₂⁴, solid carbon⁵ or in the case of methane higher hydrocarbons⁶ may be separated prior to combustion and utilized as raw material e.g. in the chemical industry. For mobile application of PEM fuel cells requiring hydrogen as a fuel on-board generation of hydrogen is desirable because of the high energy storage density of gasoline or diesel fuel.

Large scale production of hydrogen is performed e.g. by catalytic steam reforming of methane. However, this process requires a temperature of about 900 °C. At lower temperatures catalyst coking and poisoning can get a problem. For the generation of hydrogen enriched fuel gases a low temperature reforming process which is not sensitive to coking or poisoning would be desirable.

Recently plasma reforming has been proposed for the efficient generation of hydrogen and higher hydrocarbons in a compact, light weight reactor. For large scale application arc based plasma torches heating the gas very rapidly to temperatures of several thousand degrees Celsius for complete fuel conversion are utilized. However, for small scale application and for incomplete fuel conversion non-thermal plasmas which avoid excessive gas heating are a much better choice. Non-thermal plasma (NTP) reforming induced by dielectric barrier discharges (DBD) has been shown to have the potential for the generation of hydrogen and higher hydrocarbons.

In facilities where waste heat can be utilized to support NTP-reforming an endothermic reforming process like methane steam reforming



rather than an exothermic one will be applied: However, neither the selectivity nor the energy efficiency of DBD induced methane steam reforming showed to be sufficient for practical application. For this reason plasma catalytic hybrid steam reforming of methane was investigated in the temperature range 200-600 °C.

Experiments on Plasma Induced Steam Reforming of Methane

The conversion of methane and water as well as the yields of hydrogen, carbon monoxide, carbon dioxide, methanol, and higher hydrocarbons up to C₄H_n were investigated as a function of the gas temperature, plasma input power, gas flow, and feed ratio of methane to water. Methane was fed from a pressurized gas cylinder using a mass flow controller, water was spray injected and evaporated at 250 °C. The gas mixture was heated to the desired temperature using a tubular heat exchanger.

For gas analysis a gas chromatograph (GC: Shimadzu GC 14B equipped with a combination of a HayeSep R/Q column and a mole sieve 13X column) and an FTIR-absorption spectrometer (FTIR:

Perkin Elmer System 2000 with a 1 m White cell heated to 190 °C) were applied. Prior to FTIR-analysis the gas was diluted for a factor 10 with pure nitrogen.

Dielectric Barrier Discharge Reactor. Reference measurements on NTP-induced steam reforming of methane were performed using a coaxial DBD-reactor (Figure 1) which was thermally isolated and thermostatically heated to the desired temperature. An alumina tube with an outer diameter of 25 mm and an inner diameter of 20 mm was applied as a dielectric barrier between the ground electrode and the high voltage electrode. The ground electrode was manufactured by flame coating the outer tube surface. The structured high voltage electrode consisted of sharp edged circular discs with a diameter of 16 mm fed on a stainless steel rod. The number and spacing of the discs was chosen such that the active region of the reactor had a length of 200 mm.

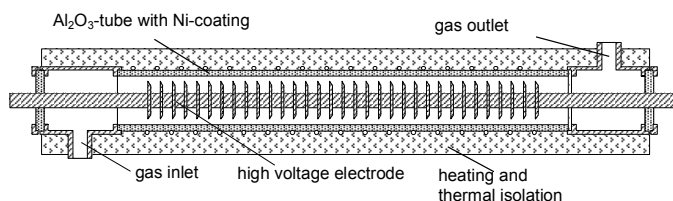


Figure 1. DBD-reactor set-up for methane steam reforming.

Dielectric Packed Bed Reactor. Plasma catalytic experiments were carried out in a thermostatically heated dielectric packed bed (DPB) reactor, which combines the features of a catalytic fixed bed tube reactor and of a DBD reactor (Figure 2). Its ground electrode and barrier were identical to those of the DBD-reactor. A stainless steel tube with an outer diameter of 10 mm was used as inner electrode. Thus a discharge gap 10 mm was obtained, which was filled with the catalyst packing consisting of nickel dispersed on ceramic pellets having diameters between 2 and 4 mm. For electrical discharge excitation a sinusoidal high voltage power supply with a maximum output power of 600 W was applied.

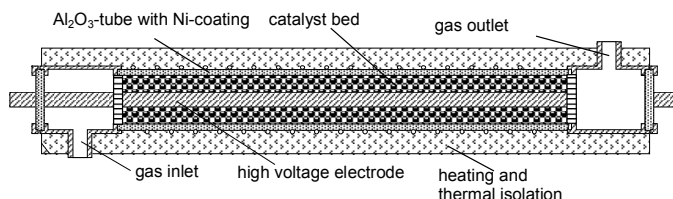


Figure 2. DPB-reactor set-up for methane steam reforming.

Experimental Results

DBD-Induced Reforming. We found that DBD-induced CH₄-conversion and product yields depended on all parameters under investigation. As a reference the dependencies on temperature and plasma input power are shown in Table 1 and Table 2, respectively.

Because the net water conversion was negligibly small, the hydrogen yield was calculated under the assumption that only CH₄ but not H₂O contributes to H₂-formation. It depends much stronger on power than on temperature. The conversion of CH₄ is roughly proportional both to temperature and plasma input power, however, the yields of H₂ and higher hydrocarbons (mainly C₂H₆) are not.

Increasing the CH₄:H₂O feed ratio from 1:3 to 1:1 reduced the yields, however, the molar flows of the reaction products remained nearly unchanged. When the flow rate was increased at constant specific plasma energy input (ratio of power to gas flow rate) both the CH₄-conversion rate and the product yields increased.

The energy requirements for H₂-generation did not depend substantially on the specific plasma energy input and decreased with increasing temperature. They ranged from 2 to 8 MJ/mole H₂.

Table 1. Dependence of Conversion and Product Yields on the Temperature

T [°C]	CH ₄ -conversion and product yields [%]									
	CH ₄	H ₂	CH ₃ OH	CO	CO ₂	C ₂ H ₆	C ₂ H ₄	C ₃ H ₈	C ₃ H ₆	C ₄ H ₁₀
200	2.3	1.3	0.23	0.43	0.02	1.4	0.03	0.39	0.00	0.45
400	4.9	1.7	0.11	0.31	0.05	2.6	0.11	0.68	0.01	0.37
600	7.9	2.7	0.00	0.21	0.19	4.1	0.71	0.73	0.12	0.26

Experimental conditions: Plasma input power 50 W, flow rate 1 Nlitter/min, feed ratio CH₄:H₂O = 1:2

Table 2. Dependence of Conversion and Product Yields on the Plasma Input Power

P [W]	CH ₄ -conversion and product yields [%]									
	CH ₄	H ₂	CH ₃ OH	CO	CO ₂	C ₂ H ₆	C ₂ H ₄	C ₃ H ₈	C ₃ H ₆	C ₄ H ₁₀
50	2.3	1.3	0.23	0.43	0.02	1.4	0.03	0.39	0.00	0.45
100	6.9	2.4	0.43	0.79	0.06	2.2	0.06	0.67	0.00	1.03
150	12.1	4.1	0.46	0.96	0.12	3.8	0.12	1.20	0.04	1.78
200	17.3	6.5	0.57	1.12	0.22	5.1	0.28	1.64	0.12	1.35

Experimental conditions: Temperature 200 °C, flow rate 1 Nlitter/min, feed ratio CH₄:H₂O = 1:2

Plasma-Catalytic Hybrid Reforming. In contrast, when plasma-catalytic hybrid treatment was applied both methane and water were converted (Figure 3). Therefore now the H₂-yield was calculated taking into account both the CH₄ and the H₂O-feed. At temperatures below 400 °C no catalytic conversion was observed when the plasma was switched off. In this temperature range mainly H₂, CO₂, and small amounts of C₂H₆ were formed by plasma-catalytic hybrid reforming. At temperatures above 400 °C substantial CO-yields were achieved, and the CO₂-yield dropped relative to the H₂-yield. In contrast to DBD-reforming the C₂H₆-yield gets negligible at higher temperatures.

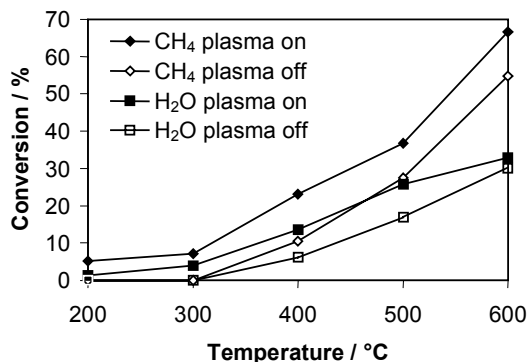


Figure 3. Plasma-catalytic hybrid reforming of methane – conversion as a function of the temperature (flow rate 1 Nlitter/min, plasma input power 150 W, feed ratio CH₄:H₂O = 1:2)

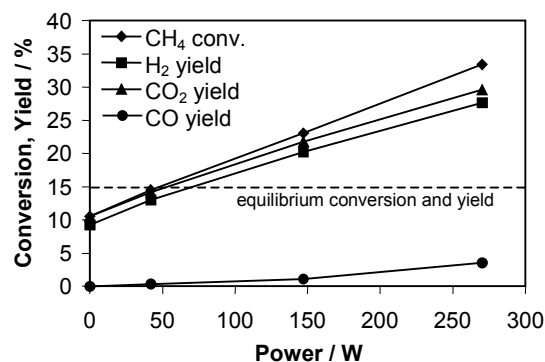


Figure 4. Plasma-catalytic hybrid reforming of methane – conversion as a function of the plasma input power (flow rate 1 Nlitter/min, temperature 400 °C, feed ratio CH₄:H₂O = 1:2)

Conversion and yields increased linearly with the plasma input power. At temperatures around 400 °C and input powers above 60 W the yields of H₂ and CO₂ exceeded the values calculated from thermodynamic equilibrium relations. With increasing power an increasing selectivity towards CO-formation was observed whereas the selectivity for CO₂-formation decreased.

The dependency of CO- and CO₂-concentrations on specific energy and temperature may be explained by the assumption that CO is formed by plasma induced gas phase processes and by catalytic processes, whereas CO₂ is mainly formed due to a low temperature catalytic water shift reaction converting CO to CO₂.

At temperatures above 200 °C by the combination of plasma and catalyst the energy requirements were reduced compared to DBD-treatment. Values as low as 315 kJ/mole H₂ were achieved at 600 °C.

Conclusions

NTP-reforming of methane in CH₄-H₂O-mixtures was investigated. Dielectric barrier discharges mainly induce formation of H₂ and C₂H₆ by decomposition of CH₄ at negligible H₂O-conversion. Numerical simulations of the DBD-induced chemical kinetics showed that 38 % and 7 % of the energy dissipated in discharge filaments are spent for CH₄- and H₂O-dissociation respectively.

By the combination of the DPB-plasma and a Ni-catalyst high H₂O-conversion rates and selectivities towards H₂- and CO₂-formation were achieved. For temperatures above 200 °C the energy requirements dropped for an order of magnitude down to values as low as 315 kJ/mole H₂ at 600 °C. Further improvements can be expected if thermal losses e.g. due to barrier heating could be avoided, which may be well above 60 % of the plasma input power.

References

- Phillips, J.N.; Roby, R.J. *Power Engineering* **2000**, May, 36-40.
- Maughan, J.R.; Bowen, J.H.; Cooke, D.H.; Tuzson, J.J. *Proc. ASME Co-gen-Turbo Conference*, **1994**, 381-390.
- Jamal, Y.; Wyszynski, M.L. *Int. J. Hydrogen Energy*, **1994**, 19(7), 557-572
- Nihous, G.C.; Mori, Y.; Masutani, S.M.; Vega, L.A.; Kinoshita, C.M. *Int. J. Hydrogen Energy*, **1994**, 19(4), 387-94.
- Fulcheri, L.; Schwob, Y. *Int. J. Hydrogen Energy*, **1995**, 20(3), 197-202.
- Kogelschatz, U.; Zhou, L. M.; Xue, B.; Eliasson, B. In *Greenhouse Gas Control Technologies*, Proc. 4th Int. Conf., Meeting Date 1998; Eliasson, Bal-dur; Riemer, Pierce; Wokaun, Alexander, Eds.; Elsevier, Oxford, UK, **1999**, pp. 385-390.

REFORMING OF METHANE INTO SYNGAS IN A PLASMA-ASSISTED REACTOR

Albin Czernichowski⁽¹⁾, Mieczyslaw Czernichowski⁽²⁾,
Piotr Czernichowski⁽¹⁾, and Thomas E. Cooley⁽¹⁾

(1) Synergy Technologies Corporation,
335 25th St. S.E., Calgary, Alberta, T2A 7H8

(2) Etudes Chimiques et Physiques
21 François Marchand, 45100 Orléans, France

Introduction

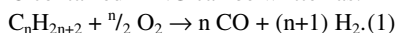
A mixture of H₂ + CO (called "synthesis gas" or "syngas") is an important bridge to several chemical syntheses like methanol or synthetic liquid fuels through the Fischer-Tropsch syntheses. Nowadays, syngas starts to be also considered as simple fuel that can be converted to electric energy in Solid Oxide or Molten Carbonate Fuel Cells (FC). These two kinds of FC use both H₂ and CO as fuel while other cells accept only pure hydrogen; in addition other cells are poisoned by traces of CO. Syngas is almost certain to play a major role in the massive production of pure hydrogen in the near- to medium-term future. This production, for exclusively H₂-based FC or other chemical, petrochemical, metallurgical or space applications, would go through hydrogen separation from the syngas, followed by the "water shift" in which remaining CO is converted to H₂ then polished using a less or more deep purification.

It also appears that in the near- to medium-term future most of syngas production will be based on fossil fuel reforming, mostly Natural Gas (NG). Small- and medium-scale reforming would allow using a pipeline distributed NG as well as numerous small NG sources. However, conventional reformers require careful attention to heat management, feed introduction, catalysts, etc., and entail solution of a set of difficult problems.

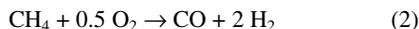
Our SynGen reformer based upon the gliding discharges (GlidArc) plasma principle solves many of these problems when using the electrically assisted Partial Oxidation (POX) of NG. For the sake of simplicity and economics, the unique oxidant (oxygen) source we use is atmospheric air. Although enriched oxygen up to and including "pure" oxygen can be used.

Thermodynamics and Energetics

The exothermic chemical reaction describing the POX of a mixture of HC contained in NG can be written as:



For pure methane the reaction is:



with a weak exothermic effect of $\Delta H^\circ = -36.1$ kJ per mol of converted methane. This heat of reaction is insufficient to keep moving it properly; it represents less than 5% of the methane full combustion heat so that extra heat and/or catalysts are necessary in classical technologies. For example, an O₂/CH₄ » 0.5 ratio could be used to burn a part of the methane feed. However, this adds steam and CO₂ into the syngas. As a compromise, we install gliding discharges directly in the reacting mixture; they add an active electric energy and catalytic species.

Experimental

A bench scale GlidArc stainless steel reactor, similar to those previously described^{1,2} was used as reformer; it is shown schematically on the Fig. 1.

The reactor /1/ uses six steel electrodes /2/ (only two electrodes are shown) that delimit a nozzle-shaped volume /3/ where gliding electric discharges /4/ may develop. This reactor contains a nozzle /5/

blowing the premixed NG + air mixture /6/ to be converted in the space /7/ between the electrodes arranged so that the mixture flows along the central part of these electrodes exposed to the discharges.

The discharges pre-ionize the gas at the point /9/, glide on the electrodes and disappear at the point /10/ near the end of the electrodes, to appear once again at the initial point. The process is sequential and the lifetime of a single discharge /4/ ranges from 1 to 20 ms, depending on the linear speed of the fluid in zones /7/, /9/, /13/ and /10/. Given the moderate temperature of the electrodes (not cooled) and a very short contact time of the discharge root /8/ with the electrodes, we do not observe any deterioration that may prevent the gliding of these current-limited discharges.

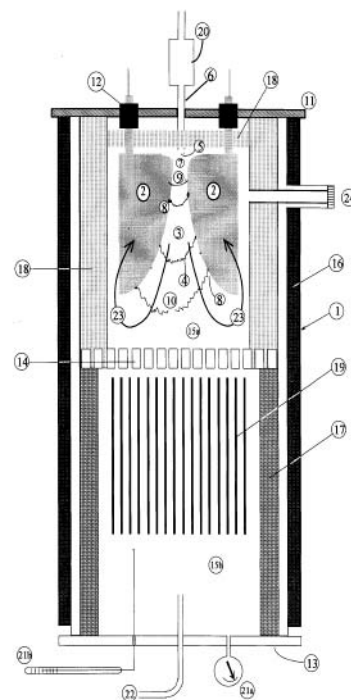


Figure 1. Schematic view of the GlidArc reformer.

Two flanges close the tubular reactor. One /11/ supports the electrodes through with high voltage connectors /12/. The other one /13/ closes the reactor on the other side and comprises a product output tube /22/. The entire structure is tight; it can support a pressure of 0.6 MPa (measured at point /21a/) but for the present tests we worked at slightly higher than atmospheric pressure.

A perforated plate /14/ separates a void plasma zone /15a/ and a post-plasma zone /15b/ which is partially filled with metallic Ni pads. The plate /14/ makes it possible to run products from the plasma treatment to the post-plasma zone. The reactor is insulated externally and internally by ceramic felts and tube /16/ and /17/ in order to keep it hot. The plasma zone is also insulated by a heat-resisting felt /18/. The total free volume (in terms of fluid) inside the reactor is about 2 L. No part of the reactor is cooled in a forced manner. Two holes in the flange /13/ provide for the connection of a pressure gauge /21a/ and for the insertion of a thermocouple /21b/ measuring the downstream temperature.

With almost punctual injection of the fluid between the electrodes we already provoke a phenomenon of re-circulation /23/ of the reactants in the gliding discharge zone. In order to reinforce this re-circulation, we also add this separating plate /14/, thus dividing the reactor in two parts. The perforated plate provides for the flow of

reactants (partially consumed) and "long-living" active species resulting from the excitation of the gases by the gliding discharges. In the post-plasma zone, the conversion is thus completed in the presence of that space filling. The luminous zone of the gliding electric discharges, as well as part of the wall of the zone, can be observed through a window /24/ in order to verify the proper operation of the reactor and to determine (through a pyrometer) the temperature in the compartment /15a/.

The reactor is fed by controlled (through mass flow meters) flows of compressed air and NG. Both flows were mixed together before their injection into the reactor.

A high voltage system provides both the pre-ionization of the medium and then the transfer of electric energy into the gliding discharges. The 6-phase system is composed of neon transformers. The time-averaged electric power of the reactor was measured using a 3-phase kWh-meter and a chronometer. We are taking into account a power consumption of the transformers themselves. The net GlidArc power during our tests was up to 0.85 kW.

The reforming products were flared. The flame spectrum gave us an important indication of the process. When the flame was satisfying we sucked a sample of the gas product through anhydrous CaCl₂ and analyzed immediately using gas chromatography methods. We use two chromatographs, each dedicated to individual dry gases: H₂, N₂, O₂, CO, CO₂ and CH₄ for the first, and all the HC for the second.

The gas from the town pipeline has the following composition (in vol. %) according to our analysis: CH₄ 84.5, C₂H₆ 10.4, C₃H₈ 2.2, C₄H₁₀ 0.7, C₅₊ 0.1, N₂ 1.6, and CO₂ 0.6. We sucked it from the low-pressure pipeline and than compressed it. The flow-rate from our "source" could be well stabilized at the levels from 19 to 25 L(n)/h.

Results and Discussion

Continuous run times for NG were 160 min and 560 min. During these two long runs we fully analyzed syngas samples as well as input air/NG and pure NG samples. Table 1 shows some parameters and results from these runs. For soot presence checking we installed a quartz filter at the stream of the produced syngas. Then, after a certain time, the filter was removed for appreciation. The mass increase of the filter was always less than 0.1 mg. A gray or white color of the filter indicated a very little or no soot presence.

Table 1. Results of completely non-sooting reforming of NG.

Flow rate input	air	L(n)/min	81
	NG	L(n)/min	23
O/C atomic ratio @ input		mol/mol	1.3
Electric power injected		kW _e	0.79
Output gas conc. (vol. %)	CH ₄		4.5
	C ₂ H ₆		0.02
	C ₂ H ₄		none
	CO ₂		4.0
	CO		13
		H ₂	
	N ₂		51
Output gas flow rate in m ³ (n)/h	Total		7.4
	H ₂ +CO		2.9
kWh _e spent to produce 1 m ³ (n) of H ₂ +CO			0.27

We observe a certain slippage of CH₄ while ethane, propane, and butane (all initially totalizing 13 vol. % in NG) are completely converted. No soot was observed for NG reforming at a sufficient

O/C ratio. We are not yet at the limits of possible optimization of the process; from the given reactor we can probably obtain a much higher flow of syngas when working at higher pressures... To increase the reactor throughput we can also preheat both air and NG (we have a heat available from the hot output syngas).

Conclusions

This contribution presents some of the experimental data from our work thus far in 2001. Pipeline grade natural gas is almost completely reformed in the SynGen reactor at atmospheric pressure and at quite low electric power GlidArc assistance. We have successfully engineered novel technologies in developing a fossil fuel reformer. Synergy Technologies Corporation's SynGen based on non-catalytic, plasma-assisted POX reforming offers the following competitive advantages:

- We produce syngas in quality and quantity that may be applied to an ideal 10-kW Solid Oxide or Molten Carbonate FC.
- For other applications, the reformer can also be a part of pure H₂ generators after a classical water-shift.
- It is a Sulfur-tolerant, non-catalytic reforming technology and can therefore process any acid NG.
- Any soot is produced.
- SynGen reformers are compact and easily scalable.
- No additional water or steam circuits, heaters, etc are necessary.
- Electrical consumption for process assistance is low.
- The process starts after only 15 min warm-up and can re-start after about 1 min.

Further developments are in progress. Our on-road development includes systems to generate 15 m³(n)/h of H₂+CO mix. A much bigger SynGen reformer for NG conversion is currently under development in Alberta as a part of Synergy's Gas-to-Ultra Clean Diesel and Gasoline advanced technology. Synergy's technology incorporates various proprietary and/or licensed components and is covered by appropriate US and PCT patents.

References

1. A. Czernichowski, P. Czernichowski, French Pat., No. 2,768,424, **1997**; see also US6007742, EP1012113 and WO9911572 patents.
2. A. Czernichowski, Oil & Gas Science and Technology - Revue de l'IFP, **2001**, 56(2) p. 181-98.

Acknowledgement

Participation of Michal Mlotek (Warsaw Technical University, Poland) in initial experiments is highly appreciated.

A REMARKABLE ENHANCEMENT OF FORMATION OF DIAMOND-LIKE CARBON FILM FROM METHANE USING DIELECTRIC-BARRIER DISCHARGES

Yue-ping Zhang¹, Hai-yan Du², Yang Li³, Baldur Eliasson^{3,4}, Fei He³ and Chang-jun Liu^{3*}

¹ Department of Chemistry, Tianjin University, Tianjin 300072, China; ² Analysis Center, Tianjin University, Tianjin 300072, China; ³ Tianjin Univ.-ABB Plasma Greenhouse Gas Chemistry Laboratory, State Key Laboratory of C1 Chemical Technology, Tianjin University, Tianjin 300072, China; ⁴ Energy and Global Change, ABB Corporate Research Center, Baden, CH5405, Switzerland

Introduction

Plasma can create polymer films or diamond like carbon film from monomers (e.g. methane) that do not form polymers by conventional chemical technologies [1,2]. Such plasma-polymerized films exhibit excellent properties and have a great potential as electronic, optical and biomedical materials. There is an increasing interest at plasma polymerization of methane. DC glow, low frequency (50 or 60 Hz), radio frequency (13.56 MHz) or microwave (2.45 GHz) radiation usually induces plasma for such plasma polymerization. Mostly, a vacuum or low-pressure condition is required. Recently, we have achieved a fabrication of diamond like carbon film from methane and carbon dioxide or methane and carbon monoxide feed using dielectric-barrier discharge at atmospheric pressure. We have also observed a remarkable enhancement of production of diamond like carbon film if methane and carbon monoxide were used as co-feeds under the condition of dielectric-barrier discharges.

Experimental

The experimental setup has been shown in Figure 1 and has been discussed in detail elsewhere [3-5].

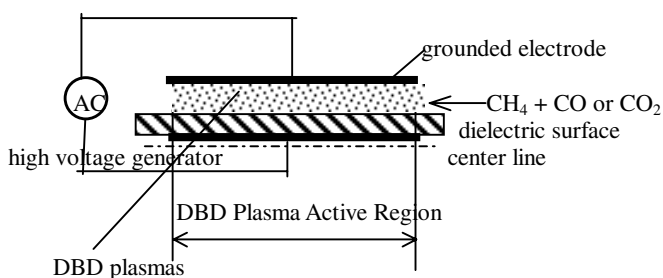


Figure 1. Schematic diagram of the DBD plasma polymerization reactor

Discharge zone lies between a dielectric-barrier made of quartz and a stainless steel tube serving as grounded electrode with a length of 250 mm and a gap width of 1.1 mm. An aluminum foil is connected with a high voltage generator, which output a sinuous signal at a frequency of 25 kHz. Methane and carbon monoxide or carbon dioxide were introduced into the discharge gap (between the grounded electrode and the quartz surface) both at 20 ml/min via two mass flow controllers. The voltage and current were measured with an on-line oscilloscope (Tektronix 2440) connecting a high voltage probe (Tektronix P6015 A) and a pulse current transformer (Pearson Electronics 411). The discharge power was read out with a multimeter

(Keithley 2000). The discharge power in this work was fixed at 100 W. The temperature of reaction was adjusted at about 338 K with circling oil. The experiments were operated at atmospheric pressure. The feed gases and gaseous products were analyzed with an on-line gas chromatograph (HP 5890 with TCD and FID) and mass selective detector (HP 5971). The plasma-polymerized film was formed first on the surface of the dielectric tube (quartz) close to the exit of plasma active region. Such formed film continues to grow up the dielectric tube with reactions. After reaction, a piece of quartz tube with plasma-polymerized film was cut as a sample for IR characteristics. The morphology of solid products on the quartz tube was analyzed using a scanning electron microscopy (SEM, PHILIPS XL-30). A FT-IR (VECTOR 22, Bruker Instrument Ltd.) was also used to characterize the functional groups of the plasma-polymerized film. The surface analysis of the chemical structure was performed by ESCA, also known as XPS with a Perkin Elmer PHI1600 system. The angle-resolved ESCA analysis was conducted using a monochromated Mg K α radiation at 250 w, by assuming a binding energy (BE) of adventitious carbon equal to 284.6 eV.

As discussed above, the reaction for the fabrication of carbon film occurs on the surface of dielectric material (quartz). A hard and dense uniform film has been observed after the reaction. It has been also observed that the hard carbon film was just formed within the discharge region. The formation of such carbon film was terminated right away out of the discharge region. It suggests that the gas discharge is a basic for the fabrication of carbon film. The hardness of the produced carbon film is 53.5 kgf/mm² (or 5.35 \times 10⁸ Pa) detected using a HVA-10A Vickers Hardness Measurement Instrument.

Results and Discussion

We have reported a production of plasma polymerized carbon film from methane and carbon dioxide using dielectric-barrier discharges [5]. The selectivity of such produced carbon film is from 30 to 40% upon the feed ratio of CH₄/CO₂. In this work, we feed carbon monoxide, instead of carbon dioxide, for the fabrication of plasma polymerized carbon film from methane. The selectivity of the carbon film was significantly increased. Table 1 shows the results of such a production.

Table 1. Conversions of Methane and CO and Selectivities (Temperature of reaction: 338K; flow rate of feed: 40 ml/min)

Ratio of CH ₄ /CO	2/1	2/1	1/1
Input power/W	50	100	100
Conversion of CH ₄	43.74	62.45	72.92
Conversion of CO	14.70	20.02	18.51
Selectivity of diamond like carbon film	60.14	65.88	72.99
Selectivity of gaseous hydrocarbons	38.33	32.31	23.38
Selectivity of liquid products	1.54	1.81	3.63

Table 1 shows more feed amount of carbon monoxide will lead to higher selectivity of diamond carbon film. This suggests the presence of carbon monoxide tends to induce the plasma polymerization from methane under the condition of dielectric-barrier discharges. The result of FT-IR characteristics of plasma-polymerized film from methane and carbon monoxide is shown in Figure 2. There are two

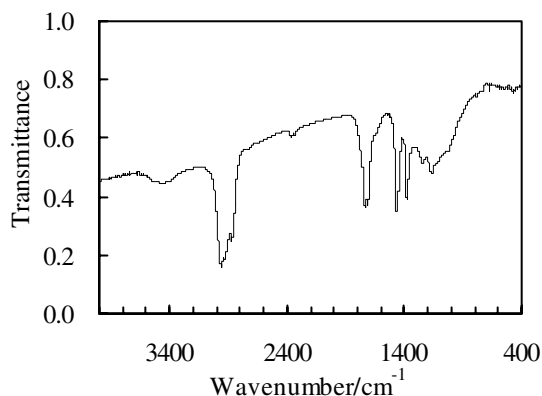


Figure 2. FTIR spectra of the carbon film sample

peaks at 1712 cm^{-1} and 1732 cm^{-1} , respectively, in the FT-IR spectrum. This splitting was assigned to the effect of coupling of α or β di-carbonyl. The presence of a band at nearly 3350 cm^{-1} was attributed to hydroxyl group. The bands at 2962 cm^{-1} , 2930 cm^{-1} and 2870 cm^{-1} were observed for CH_3 asymmetrical stretching vibration, CH_2 asymmetrical stretching vibration and CH_3 symmetrical stretching vibration, respectively. The bands at 1462 cm^{-1} and 1380 cm^{-1} were due to CH_3 asymmetrical bending or CH_2 scissoring vibration and CH_3 symmetrical bending vibration, respectively. The morphology of the polymer film on the quartz tube was studied by SEM microscope, as shown in Figure 3. Figure 3 shows the carbon film was consisted of small irregular units with the size from $5\text{ }\mu\text{m}$ to $10\text{ }\mu\text{m}$. All the units were closely aggregated to compose the dense film on the quartz tube. The polymer film produced from methane and carbon dioxide in Reference 5 was much more complex than the film produced in this work. It is considered that carbon monoxide is a better monomer for co-polymerization with methane using dielectric-barrier discharges. The plasma-polymerized film attained was also with relative simple structures that would lead many an application for coatings and others.

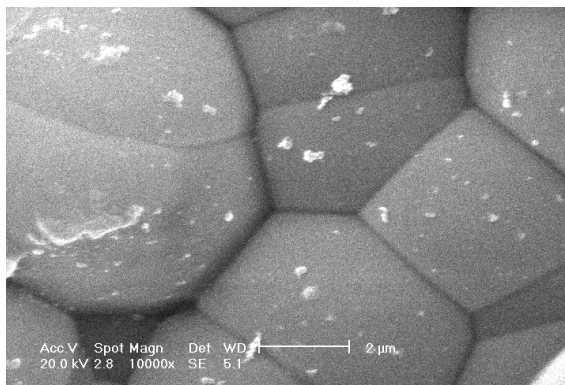


Figure 3. SEM images of polymer film on the quartz tube. (Discharge power of 100 W; the ratio of CH_4/CO : 1/1)

The angle-resolved ESCA allows an analyst to change the depth of analysis so that the depth information becomes available. The ESCA spectrum of plasma polymerized carbon film suggests another species in the binding energy of around 102.1 eV in addition to the Si species contributed from quartz (with a Binding Energy of 103.7 eV). This strange Si species could not be considered as a possible C-Si species in the polymerized film, upon the Angle-resolved ESCA analysis, since $\text{Si}_{102.1\text{eV}}/\text{Si}_{103.7\text{eV}}$ is very small at the small take-off angle

(close to the top layer of surface). The ratio of these two kinds of Si species reduces with the decrease in the take-off angle, as shown in Table 2. This suggests the quartz becomes electrically active under the condition of gas discharge plasmas and is reduced slightly. It has been considered that the electrically active quartz will provide active sites for plasma polymerization.

Table 2. $\text{Si}_{102.1\text{eV}}/\text{Si}_{103.7\text{eV}}$ Reduces with the Decrease in the Take-off Angle

$\text{Si}_{102.1\text{eV}}/\text{Si}_{103.7\text{eV}}$	Take-off angle θ
0.7	90
0.4	60
0.2	30

Conclusion

The co-feed of methane and carbon monoxide has led to a remarkable enhancement of the formation of diamond-like carbon film from methane using dielectric-barrier discharges, compared to that obtained from the co-feed of methane and carbon dioxide. Due to the easy operation of dielectric-barrier discharge at atmospheric pressure, the present method would lead to a significant improvement in the fabrication of diamond-like carbon film. The present investigation is also helpful for the understanding of the formation of plasma-polymerized carbon film from plasma methane conversion using dielectric-barrier discharge in the presence of carbon dioxide because carbon monoxide will present as a major by-product with it.

Acknowledgement The supports from The Research Fund for the Doctoral Program of Higher Education of China and ABB Corporate Research Ltd., Switzerland are very appreciated.

References

1. Suwa, T.; Jikei, M.; Kakimoto, M.-A.; Imai, Y.; Tanaka, A.; and Yoneda, Y. *Thin Solid Films*. **1996**, 273, 258.
2. Biederman, H.; and Osada, Y. *Plasma Polymerization Processes*, Elsevier, 1992.
3. Eliasson, B.; Liu, C.-J.; and Kogelschatz, U. *Ind. Eng. Chem. Res.* **2000**, 39, 1221.
4. Eliasson, B.; Kogelschatz, U.; Xue, B.; and Zhou, L.M. *Ind. Eng. Chem. Res.* **1998**, 37, 3350.
5. Liu, C.-J.; Xue, B.; Eliasson, B.; He, F.; Li, Y.; and Xu, G.-H. *Plasma Chem. Plasma Process.*, **2001**, 21, 301.

SUPPORTED Pd CATALYSTS FOR HIGH-TEMPERATURE METHANE COMBUSTION – EXAMINING THE COMBUSTION SYNTHESIS PREPARATION METHOD

M.A. Fraga, M.C. Greca, L.G. Appel

Instituto Nacional de Tecnologia – Laboratório de Catálise, Av. Venezuela, 82/sala509, CEP 20081-310 – Centro, Rio de Janeiro/RJ, Brazil – appel@uol.com.br

Introduction

Catalytic combustion of hydrocarbons, especially methane, has been widely investigated as an alternative technology for power generation (1). This process is also environmentally attractive as it produces less carbon dioxide, a greenhouse gas, per unit of power generated when compared to the combustion of other hydrocarbons. Furthermore, low amounts of NO_x emissions are formed as the combustion proceeds below 1400 °C (2). However, as far as the use of gas turbines is involved in the process, temperatures as high as 1200 °C can still be achieved and, therefore, the use of thermostable catalysts is compulsory.

Ceramic oxides obtained by a high temperature process arises as feasible materials to be used as catalysts supports. Indeed, the preparation of simple ceramic oxides via a route known as combustion synthesis has been gaining reputation as a straightforward process to produce homogeneous, very fine and crystalline powders (3,4). The synthesis explores an exothermic, generally very fast and self-sustaining chemical reaction between the desired metal salts and a suitable organic fuel, which is ignited at a temperature much lower than the actual phase formation one. The major drawback of such a route is that it leads to low surface area materials.

This work focuses on the preparation of Pd-based catalysts used on the methane combustion whose supports were obtained by combustion synthesis. Alumina was taken as the reference support and the effects brought about by the addition of different lanthanides, namely La and Ce, in the support texture and the catalytic activity are reported.

Experimental

In the combustion synthesis the appropriate amounts of the cations precursors (nitrates) and an organic fuel (urea) dissolved in water were heated in a wide-mouth vitreous silica basin up to boiling and self-ignition. The basin was then transferred to a muffle furnace preheated at 600 °C and kept for 30 min producing a fragile foam that easily crumbles into powder. The reactant proportions were calculated in order to obtain oxides with 4 and 12%wt. La or Ce. Different cerium precursors were used in order to evaluate the cerium oxidation influence, namely Ce(NO₃)₃ and (NH₄)₂Ce(NO₃)₆. These samples are denoted according to their chemical composition, lanthanide loading and cerium oxidation number, e.g. Al12Ce3 (alumina-ceria mixed oxide containing 12 %wt. Ce prepared from cerium nitrate III). Pure Al₂O₃, La₂O₃ and CeO₂ were also synthesized to be taken as reference.

The catalysts were prepared by contacting the supports and an aqueous solution of Pd(NO₃)₂ in a rotary evaporator for 8 h. The solvent was then slowly evaporated under vacuum at 80 °C; the powder obtained was dried overnight at 110 °C and lastly calcined at 500 °C for 4 h in air. These samples will be referred in the same way as their parent supports preceded by Pd, e.g. PdAl12Ce3.

X-ray diffraction (XRD) analyses were also carried out just after the powders synthesis in order to identify the oxides phases. The

diffractograms were collected in a Rigaku Denki, CuK_α/Ni, 2°/min from 15 to 75°/2θ. Specific surface area was determined by the BET method using nitrogen adsorption in a Micromeritics ASAP 2000 equipment.

UV-Vis diffuse reflectance (DRS) spectra in the range of 200 – 800 nm were recorded in a Varian Cary 5 spectrometer using a Harrick diffuse reflectance accessory. Spectra of the catalysts were obtained using pure alumina as a reference. In order to support the species identification, spectra of CeO₂, La₂O₃ and LaAlO₃ samples prepared by combustion synthesis were also recorded. Such spectra were collected from a 2% mixture in alumina to overcome specular reflectance.

Catalytic tests were performed at atmospheric pressure in a conventional system with fixed bed reactor, monitored by on-line chromatography. A gas mixture containing 2.5% methane and 10% oxygen (N₂ to balance) was fed at 100 ml/min on the catalyst bed (100 mg). Prior to reaction, the catalysts were reduced in situ at 300 °C for 2 h. The activity data were collected just after the catalysts have achieved the steady-state at 500 °C

Results and Discussion

The synthesized supports were first characterized by XRD. The lanthanides-containing supports diffractograms presented the same pattern as in α-Al₂O₃ although their peaks were less intense. On the lanthanum-based support (Al12La) the disturbance detected by XRD was even more pronounced as no α-Al₂O₃ could be detected. No phase related to Ce or La compounds were identified.

The UV-Vis spectra of La-containing samples presented two peaks at 210 and 300 nm. These absorbance bands are placed between those related to La₂O₃ and LaAlO₃ not allowing a faithful distinction between such compounds. The existence of both species, therefore, can not be ruled out.

The spectra of Ce-based supports were identical irrespective the loading or precursor used. The spectra exhibited basically two peaks centered at 240 and 300 nm, which can be associated with CeO₂. The absorbance at higher wavenumber is commonly attributed to three dimensional array of cerium and oxygen atoms while the peak at 240 nm is related to the presence of small crystallites (5). Therefore, it can be concluded that the cerium oxide crystallites on the prepared supports are rather small, which is consistent with the XRD results that were not able to detect the CeO₂ phase.

Table 1 collects the BET surface area data of both supports and catalysts as well as the crystallite average size calculated with the Scherrer equation (2θ = 43.4°). As previously referred, low surface area powder are typically obtained through combustion synthesis method. The values determined by alumina is quite consistent with those reported in the literature (3,4). It can be easily seen that textural changes were induced by adding low contents of lanthanides in the formulation as a dramatic surface area increase was detected. Such disturbance appears to be more significant when (NH₄)₂Ce(NO₃)₆ is used as cerium precursor. The results might suggest that the presence of small CeO₂ crystallites disturbs the crystallization process leading to a decrease in the alumina crystallite size and consequently improving the surface area. On the other hand, high Ce loading does not interfere the samples textural features, which might be related to the formation of CeO₂ agglomerates allowing phase segregation. As for La-based sample, a completely different behavior was observed; even at high loading the surface area was improved. As no alumina reflections were recorded by XRD it is reasonable to assume the formation of a mixed compound, LaAlO₃. Indeed, the formation of such aluminate has been reported in the literature under similar conditions (6).

Table 1. Surface Area and α -Al₂O₃ Crystallite Size

Sample	S _{BET} (m ² /g)		d (nm)
	Supports	Catalysts	
Al	3	3	36
Al4La	23	22	25
Al4Ce3	14	12	28
Al4Ce4	28	24	27
Al12La	20	18	-
Al12Ce3	5	5	37
Al12Ce4	7	6	42

Catalytic activity data for methane combustion are collected in Table 2. It was characterized by the temperatures at which methane conversion achieved 5 and 10% and is given as T₅ and T₁₀ respectively. It should be stressed that carbon dioxide and water were the only reaction products detected.

It can be seen that the catalytic activity markedly depend on the nature of the support. Pd/Al₂O₃ catalyst presents low activity which could be related to the specific features of such system, especially the rather low surface area, as mentioned above. Alongside the enhancement in the support texture, the addition of lanthanides appears to improve the catalyst performance especially when low contents is used. Ce revealed to be a better promoter than La irrespective its content. These results are in close agreement with the literature regarding the promoting effects of CeO₂ in noble metal-based combustion catalysts (7).

The catalytic activity of the La-based systems are dependent on the lanthanide concentration, being favored at low La loading. As a matter of fact, the difference in the temperature to reach methane conversion of 5% is quite significant, practically 30 °C.

Similar DRS spectra obtained for both samples suggested the presence of the same La species, which would be naturally associated with LaAlO₃ based on the XRD results. Nevertheless, the catalytic performance do not support such assignment. The activity data evidences a different La species distribution. At low concentration (PdAl4La) the promoting effect on the methane combustion may arise from the La-doped alumina support. On the other hand, the poor performance registered over PdAl12La might be ascribed to the nature of the support, that is, the intrinsic activity of the LaAlO₃-supported catalyst.

Table 2. Methane Combustion over Pd Catalysts Prepared by Combustion Synthesis Method

Catalyst	Catalytic Activity	
	T ₅ (°C)	T ₁₀ (°C)
PdAl	483	-
PdAl4La	441	473
PdAl4Ce3	415	447
PdAl4Ce4	429	460
PdAl12La	470	-
PdAl12Ce3	441	473
PdAl12Ce4	440	472

The different performance observed amongst the catalysts with low and high Ce content could be explained by the different distribution of CeO₂ crystallites on the alumina support as previously suggested. High concentration seems to lead to a CeO₂ and Al₂O₃ phase segregation which would allow the existence of different sites, namely Pd/Al₂O₃ and Pd/CeO₂. It is reasonable, thus, that the catalytic

activity diminishes due to the intrinsic behavior of Al₂O₃-supported catalyst. As the segregation occurs as a consequence of lanthanide loading, it may be expected that whatever the cerium precursor used, the prepared catalyst will present the same behavior. The results obtained over PdAl12Ce3 and PdAl12Ce4 indeed follow such a trend.

As for PdAl4Ce samples, a model of small CeO₂ crystallites uniformly spread on alumina could be accepted. Such a model is in line with the support textural modifications previously observed (Table 1). Nevertheless, differently from what is seen over PdAl12Ce3 sample, the catalytic performance is fairly distinct between samples with low Ce concentration prepared from different salt precursors (PdAl4Ce3 and PdAl4Ce4). Indeed it has been reported that the formation of CeO₂ aggregate crystallites on alumina surface is connected with the salt precursor (8). CeO₂ obtained from cerium (IV) ammonium nitrate allows the formation of small aggregate crystallites at concentrations as low as 1.7 %wt. Hence, taking into account the difference in CeO₂ dispersion, its promoting effects is softened on PdAl4Ce4 catalyst.

Conclusions

The texture of oxides prepared by combustion synthesis can be effectively enhanced by adding low contents of lanthanides, especially Ce. La does not seem to be a very suitable additive as it reacts with alumina forming LaAlO₃.

Low loading of cerium oxide well dispersed on alumina revealed to be the most effective promoter for the methane combustion.

Acknowledgement. The authors are indebted to Mr. F. Cano and IME for carrying out the BET measurements. The financial support from CTPETRO/FINEP is gratefully acknowledged.

References

- (1) Groppi, G.; Cristiani, C.; Lietti, L.; Ramella, C.; Valentini, M.; Forzatti, P.; *Catal. Today*, **1999**, *50*, 399.
- (2) Garten, R.L.; Dalla Betta, R.A.; Schlatter, J.C. In *Handbook of Heterogeneous Catalysis*; Ertl, G.; Knözinger, H.; Weitkamp, J.; Ed.; Wiley-VCH: New York, 1997; pp. 1668-1677.
- (3) Greca, M.C.; Moraes, C.; Morelli, M.R.; Segadães, A.M.; *Appl. Catal. A*, **1999**, *179*, 87.
- (4) Greca, M.C.; Moraes, C.; Segadães, A.M.; *Appl. Catal. A*, **2001**, *216*, 267.
- (5) Bensalem, A.; Muller, J.C.; Bozon-Verduraz, F.; *J. Chem. Soc. Faraday Trans.*, **1992**, *88*, 153.
- (6) Kingsley, J.J.; Patil, K.C.; *Mater. Lett.*, **1988**, *6*, 427.
- (7) Trovarelli, A.; *Catal. Ver.-Sci. Eng.*, **1996**, *38*, 439.
- (8) Appel, L.G.; Frydman, A.; Perez, C.A.C.; Eon, J.G.; Castner, D.G.; Campbell, C.T.; Schmal, M.; *Phys. Stat. Sol. B*, **1995**, *192*, 477.

SYNTHESIS AND EPR STUDY OF RU-MN DIMER COMPLEXES AS CATALYSTS FOR LIGHT-DRIVEN WATER OXIDATION: TOWARDS SOLAR ENERGY CONVERSION INTO FUELS

Licheng Sun^a, Anh Tran^a, Yunhua Xu^a, Reiner Lomoth^b, Ping Huang Kenéz^c, Ann Magnuson Styring^c, Björn Åkermark^a, Leif Hammarström^b, Stenbjörn Styring^c

^a Department of Organic Chemistry, Arrheniuslab, Stockholm University, SWEDEN

^b Department of Physical Chemistry, Uppsala University, Box 532, 751 21 Uppsala, SWEDEN

^c Department of Biochemistry, Center for Chemistry and Chemical Engineering, University of Lund, Box 124, S-221 00 Lund, SWEDEN

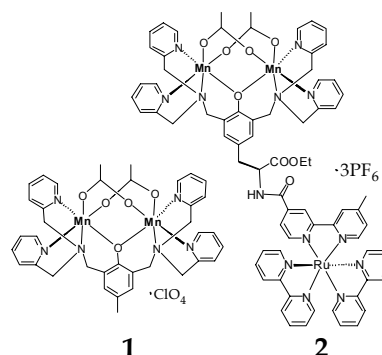


Figure 1. Structures of one Mn dimer complex **1** containing a $\text{Mn}_2^{\text{II,II}}$ moiety and one trinuclear complex **2** containing the same dimer covalently linked to a $\text{Ru}^{\text{II}}(\text{bpy})_3$ via an amide bond.

Introduction

In Photosystem II (PSII),¹ solar energy is used to extract the electrons needed to reduce CO_2 (the greenhouse gas) from water. Thereby, the biosphere is provided with an inexhaustible electron source, making water oxidation in PSII a key process in nature. Under illumination, the chlorophylls in the primary donor in PSII (P_{680}) are transiently excited to P_{680}^* which, within picoseconds, ejects an electron to a chain of protein-bound electron acceptors. The photo-oxidized P_{680}^+ has a potential of $E_m \text{P}_{680}^+/\text{P}_{680} \approx 1.18\text{V}$ vs. NHE, and retrieves its electron from a series of electron donors and ultimately from water.

Water oxidation is catalyzed by a domain within PSII called the water oxidizing complex (WOC), which involves a tyrosine residue, denoted Tyr_Z , and a cluster of four Mn ions functioning as a charge storing device for oxidizing equivalents. In each turnover of the enzyme, four electrons are extracted from two water molecules. The reaction is catalyzed by the manganese cluster in close conjunction with Tyr_Z .

In attempts to mimic the WOC and the redox reactions involved in photosynthetic water oxidation, we have incorporated principles from PSII into supramolecular complexes. Our strategy is to couple a photoactive Ru^{II} tris-bipyridine ($\text{Ru}^{\text{II}}(\text{bpy})_3$) center (which mimics P_{680}) to a redox active moiety containing manganese or tyrosine.² Others and we have synthesized several multinuclear Ru-Mn systems.^{3, 4} In all these systems, it has been possible to observe light induced electron transfer from the Mn ion(s) to the photo-oxidized Ru center when the molecules are exposed to laser flashes in the presence of an external electron acceptor. We have also shown that tyrosine can be coupled to the Ru-complex and function as a redox-active intermediate.³ However, to more completely mimic the reaction sequence, a higher degree of complexity is required.

To increase the similarities between our supramolecular complexes and the donor side of PSII, we have synthesized a triad system complex **2** (Figure 1) containing a $\text{Ru}^{\text{II}}(\text{bpy})_3$ center coupled via a modified *L*-tyrosine to a $\text{Mn}_2^{\text{II,II}}$ -bpmp dimer (**1**), (bpmp = 2,6-bis[[*N*, *N*-di(2-pyridylmethyl)amino]methyl]-4-methylphenol). In our first study of this complex,³ we described the synthesis and a few of the chemical and spectroscopic properties of **2**. We showed that under illumination, the excited $\text{Ru}^{\text{II}*}$ can reduce an external electron acceptor. The photo-generated Ru^{III} then retrieves an electron very rapidly ($k > 1 \times 10^7 \text{s}^{-1}$) via intramolecular electron transfer. In this paper we want to show the photo-induced multistep electron transfer in **1** and the synthesis of its derivatives **3** and **4**.

Experimental

Chemicals and Synthesis: Penta-aminechlorocobalt^{III} chloride (here denoted Co^{III}) was purchased from Aldrich. Ru^{II} tris-(2,2'-bipyridyl) dichloride ($[\text{Ru}^{\text{II}}(\text{bpy})_3]^{2+}$) was prepared according to Sullivan *et al.*⁵ Complex **1** in the $\text{Mn}_2^{\text{II,II}}$ and $\text{Mn}_2^{\text{II,III}}$ states was synthesized according to Diril *et al.*⁶ and complex **2** was prepared as described by Sun *et al.*⁷

EPR Spectroscopy: X-band EPR measurements were performed on a Bruker ESP 380E spectrometer equipped with a TE₁₀₂ cavity and an Oxford Instruments liquid helium flow system. EPR spectra were analyzed using the software package WinEPR. Laser flashes at 532 nm (6ns pulse width, ~250 mJ/flash) were given at room temperature from a Spectra Physics DCR 3G Nd:YAG laser. The incident laser light was adjusted with lenses to cover the entire EPR sample volume. In flash photolysis experiments, saturating laser flashes (1 Hz repetition rate) were applied to the EPR samples at room temperature. After the designated number of flashes, the sample was first frozen in a 200 K ethanol/dry ice bath within 2 seconds and then quickly transferred to liquid N_2 until further use. X-band EPR spectra were recorded before and after flashing of the EPR samples.

Electrochemistry: Electrochemical measurements were performed using a three-electrode system connected to a potentiostat from Eco Chimie with an Autolab/GPES electrochemical interface. The working electrode was a glassy carbon disc (diameter 2 mm, freshly polished) for voltammetry or a platinum grid for bulk electrolysis respectively. A platinum spiral was in a separate compartment was used as counter electrode. The reference electrode was an Ag/AgNO₃ electrode (10 mM AgNO₃ in acetonitrile). The electrolyte was prepared from dry acetonitrile (molecular sieves 3 Å) with 0.1 M tetrabutylammonium perchlorate (TBAClO₄, Aldrich) that had been dried at 413 K. For the aqueous electrolytes, 1% or 10% water (v/v%) was added. Before the measurements, oxygen was removed from the solution by purging for 10 minutes with solvent saturated nitrogen.

Results and discussions

Electrochemical Studies.

The redox potentials for the sequential oxidation of **1** and **2** were determined by cyclic voltammetry. Complex **1** was studied in both dry acetonitrile and mixtures of acetonitrile and water, whereas **2** was only studied in dry acetonitrile due to its low stability in water. The voltammogram of **1** in dry acetonitrile (Figure 2A) displays two reversible redox processes at $E_{1/2} = 0.50\text{V}$ and 1.06V vs. SCE. These potentials are in good agreement with the data previously reported by Chang *et al.*⁶ who assigned the first anodic peak to the $\text{Mn}_2^{\text{II,II/III}}$ redox couple and the second to the $\text{Mn}_2^{\text{II,III/III,III}}$ redox couple.

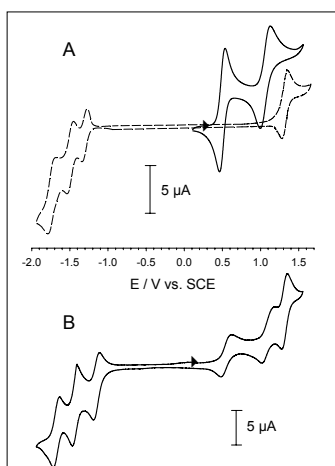


Figure 2. Cyclic voltammograms obtained in dry acetonitrile of **A**, 1.5 mM complex **1** (—) and 1 mM Ru^{II}(bpy)₃ (---) and **B**, 1 mM complex **2**. Conditions: scan rate 10mV/s. Otherwise, see experimental section.

The cyclic voltammogram of complex **2** in dry acetonitrile is shown in Figure 2B. The reversible anodic process at 1.35 V vs. SCE and the three cathodic peaks at negative potentials, are typical for Ru^{III/II} oxidation and ligand reduction in Ru^{II}(bpy)₃ complexes.²¹ By comparison with the voltammogram of complex **1** (Fig 2A) the additional quasi-reversible anodic processes can be assigned to the Mn moiety, i.e. to the Mn₂^{II,II/III,III} and Mn₂^{II,III/III,III} couples respectively. The peak potentials for these two processes are identical within 20 mV for **1** and **2**.

Photo-induced, Stepwise Oxidation of Mn₂^{II,II}.

Figures 3 and 4A demonstrate chemical reactions in complexes **1** and **2** when they are subject to flash illumination in the presence of Ru^{II}(bpy)₃ (in **1**) and Co^{III} in deaerated solution. The EPR spectrum of a mixture of complex **1** and Ru^{II}(bpy)₃ in buffered (20 mM MES, pH 7, saturated with Co^{III}) water solution containing 10% acetonitrile was recorded at 10 K. Previous to any illumination (Figure 4, top spectrum), **1** displays two spectroscopic species. The main part of the spectrum represents the Mn₂^{II,II} dimer, distinguishable by the broad peak at 2628 G (indicated by a bar) and by the broad trough at 3648 G (see above). However, because of the presence of 90% water a small fraction of the Mn dimers are destabilized to monomeric Mn^{II}. This fraction is visible as a set of 6 lines centered around 3384 G ($g \approx 2$), and was estimated to be less than 20%, measured from the peak-to-trough height. To steer clear of interference from this signal in our quantitative measurements of **1**, we have used the peak at 2628 G which only belongs to the coupled Mn₂^{II,II} spectrum.

The EPR spectrum of **2** prior to illumination is similar to that published earlier and is also dominated by the Mn₂^{II,II} dimer spectrum from two antiferromagnetically coupled Mn^{II} ions (top spectrum in Figure 4A). Notably, due to the lower water content (10%) in the measurement, there is no or negligible contamination from uncoupled Mn^{II} in the spectrum of **2**. Interestingly, there is an 11-line hyperfine pattern observable in **2** between ≈ 2400 to 2850 G with a splitting constant ≈ 40 to 45 G which is also typical for Mn₂^{II,II}⁸ but which was not observed in **1**.

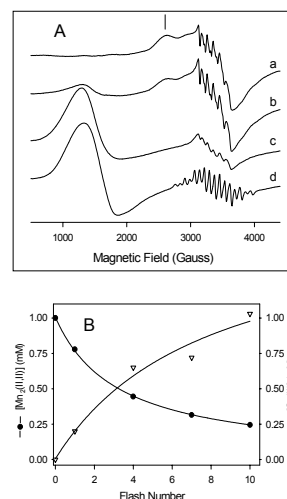


Figure 3. EPR spectra showing the flash dependent oxidation of **1** from the Mn₂^{II,II} to the Mn₂^{III,IV} oxidation state. Spectra **a**, **b**, **c** and **d** are recorded in samples that were exposed to 0, 1, 10 and 20 flashes respectively. EPR conditions: T= 10 K; microwave power, 3.3 mW; modulation amplitude, 10 G; microwave frequency, 9.47 GHz; modulation frequency, 100 kHz.

Spectra **b**, **c** and **d** in Figure 3 show the results of flash illumination at 532 nm of a mixture of complex **1**, Ru^{II}(bpy)₃ and Co^{III}. When one flash was applied (Figure 3 spectrum **b**) the maximum peak height of the Mn₂^{II,II} signal decreased compared to the spectrum recorded before flash illumination (Figure 3, **a**). Simultaneously a new signal at ≈ 1300 G, originating from Co^{II} arose. By increasing the number of flashes, the Co^{II} signal increased while the Mn₂^{II,II} signal amplitude decreased (Figure 3, **b** to **d**). The increase of the EPR signal from Co^{II} indicates that Co^{III} was reduced in a flash-dependent fashion. Spectra **c** and **d** in Figure 3 represent samples that were given 10 or 20 flashes respectively. It is clear that the EPR signal from Mn₂^{II,II} decreased, and already after 10 flashes most of the Mn₂^{II,II} features, as well as those from the uncoupled Mn^{II}, disappeared from the EPR spectrum (Figure 3 **c**). After 20 flashes (Figure 3, **d**), a well-resolved 16 line EPR signal appeared in the spectrum. The new signal is centered around $g \approx 2$ and has a width of approximately 1220 G, ranging from 2880 to 4100 G, with a hyperfine coupling constant of 78 to 80 G. This hyperfine pattern makes it clear that the signal originates from Mn, and EPR signals of this type with 16 lines are characteristic for a strongly spin coupled Mn₂^{III,IV} dimer.⁹

The photo-induced oxidation of **1** to the Mn₂^{III,IV} state is an interesting reaction, but it occurs *via* intermolecular electron transfer. We were therefore interested in whether a similar reaction could be achieved in **2**, where the Mn₂^{II,II} dimer is covalently linked to the Ru^{II}(bpy)₃ center. We have earlier described very rapid reduction of photo-oxidized Ru^{III} in **2** ($k > 1 \times 10^7 \text{ s}^{-1}$) and we proposed that the electron originated from the Mn-dimer in **2**¹⁴. Here, we expand these optical studies of Ru^{III} reduction with EPR studies aimed at following the redox chemistry in the Mn moiety of **2**.

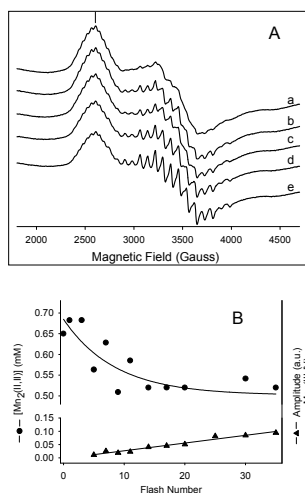


Figure 4. A, EPR spectra showing the oxidation of **2** from the $Mn_2^{II,II}$ to the $Mn_2^{III,IV}$ oxidation state. B, Decrease of the $Mn_2^{II,II}$ (●) and increase of the $Mn_2^{III,IV}$ (▲) signal amplitude from **2** as a function of flash number. Spectrum **a** was recorded in the dark. Spectra **b** through **e** were recorded after the sample was exposed to 7, 11, 20 and 25 flashes respectively. The EPR conditions as in Figure 3.

In the low temperature EPR spectrum of **2** (Figure 4A, spectrum a) the main spectral features from the $Mn_2^{II,II}$ dimer are clearly observable at 2605 G and 3680 G. Photo-oxidation experiments were carried out in the presence of 10% water. Figure 4A shows the results when **2** was exposed to laser flashes in the presence of Co^{III} as electron acceptor. A small, but significant, fraction of the signal amplitude from $Mn_2^{II,II}$ (indicated with a bar) disappeared as a function of number of flashes applied. After 10 and 35 flashes, about 15% and 25% respectively of the EPR signal amplitude had disappeared (Figure 4A,B). The spectra in Figure 4A also clearly reveal that continuous flashing results in the formation of a new dominating EPR feature centered around 3380 G ($g \approx 2$). This spectrum consists of 16 lines with a hyperfine coupling constant ≈ 78 to 80 G and is essentially identical to the $Mn_2^{III,IV}$ spectrum from **1**. We conclude that the $Mn_2^{II,II}$ moiety in **2** can also be photo-oxidized to the $Mn_2^{III,IV}$ state. Because of the rapid electron transfer to photo-generated Ru^{III} in **2** observed earlier, we propose that the photo-oxidation is an intramolecular electron transfer reaction.

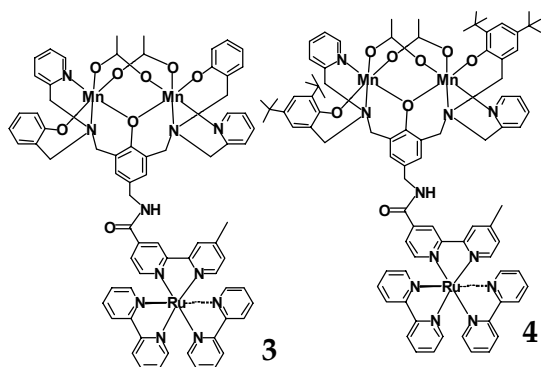


Figure 5. The structures of high valence Mn(III/III) dimer covalently linked to ruthenium tris-bipyridine complexes.

To drive the photo-oxidation of a Mn dimer to a higher oxidation state, such as $Mn_2^{IV,IV}$, complex **2** was modified. The complex **3** and **4** in Figure 5 have been synthesized recently. Two pyridine

groups were replaced by phenol groups. Preliminary measurements show that the new ligands can stabilize $Mn_2^{III,III}$ state from beginning. Photo-induced multi-step electron transfer study is underway.

Conclusions

The photochemistry and electrochemistry in two model complexes complex **1** and **2** were investigated. The EPR spectra revealed that both complexes underwent photo-induced, stepwise manganese oxidation by electron transfer to a photosensitizer. Figure 6 describes the reactions involved. The electron transfer is intermolecular for complex **1** and intramolecular in **2**. In the presence of water, the $Mn_2^{II,II}$ moiety was successively oxidized to the mixed-valence $Mn_2^{III,IV}$ state. Electrochemical studies indicate that ligand exchange in the $Mn_2^{III,III}$ state, e.g. substitution of the acetate bridges by water molecules, is most likely a prerequisite for oxidation to the $Mn_2^{III,IV}$ state.

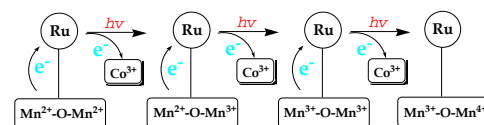


Figure 6. Photo-induced three step electron transfer in trinuclear complex **2**.

The light induced Ru oxidation to the highly oxidizing Ru^{III} species involves an oxidizing potential quite similar to that of P_{680}^+ in the PSII reaction center. The redox potentials of the different manganese oxidation states of **1** and **2** are also quite comparable to those involved in the donor side chemistry in PSII, with the potential of the highest oxidation state remarkably close to that which is necessary for oxidizing water. The successive recovery of Ru^{II} accompanied by stepwise Mn oxidation, possibly mediated by the tyrosine derivative in **2**, thereby highly resembles important steps in the function of the WOC in PSII.

Acknowledgements

This work was supported by grants from the Knut and Alice Wallenberg Foundation, the Swedish Natural Science Research Council, the Swedish Council for Engineering Science, the European TMR Program (TMR Network CT96-0031), and the Nordic Energy Research Program. We acknowledge valuable discussions with Prof. Jean-Jacques Girerd and colleagues, Orsay, France and Prof. Karl Wieghardt, Mulheim an der Ruhr, Germany.

References

- (a) Britt, R. D. *Oxygenic Photosynthesis: The Light Reactions*; Ort, D. R. and Yocum, C. F., Ed.; Kluwer Academic Publishers: Netherlands, **1996**, pp 137-164. (b) Diner, B. A.; Babcock, G. T. *Oxygenic Photosynthesis: The Light Reactions*; Ort, D. R. and Yocum, C. F., Ed.; Kluwer Academic Publishers: Netherlands, **1996**, pp 213-247. (c) Barber, J.; Kuhlbrandt, V. *Current Opinion in Structural Biology* **1999**, *9*, 469-475.
- Sun, L.; Hammarström, L.; Åkermark, B.; Styring, S., *Chem. Soc. Rev.* **2001**, *30*, 36-49.
- (a) Magnuson, A.; Berglund, H.; Korall, P.; Hammarström, L.; Åkermark, B.; Styring, S.; Sun, L. *J. Am. Chem. Soc.* **1997**, *119*, 10720-10725. (b) Magnuson, A.; Frapart, Y.; Abrahamsson, M.; Horner, O.; Åkermark, B.; Sun, L.; Girerd, J. J.; Hammarström, L. & Styring, S. *J. Am. Chem. Soc.* **1999**, *121*, 89-96. (c) Sjödin, M.; Styring, S.; Åkermark, B.; Sun, L.; Hammarström, L. *J. Am. Chem. Soc.* **2000**, in press (d) Sun, L.; Berglund, H.; Davydov, R.; Norrby, T.; Hammarström, L.; Korall, A.; Börje, A.; Philouze, C.; Berg, K.; Tran, A.; Andersson, M.; Stenhagen, G.; Mårtensson, J.; Almgren, M.; Styring, S.; Åkermark, B. *J. Am. Chem. Soc.* **1997**, *119*, 6996-7004. (e) Berglund-Baudin, H.; Sun, L.; Davidov, R.; Sundahl, M.;

-
- Styring, S.; Åkermark, B.; Almgren, M.; Hammarström, L. *J. Phys. Chem. A* **1998**, *102*, 2512-2518. (f) Sun, L.; Raymond, M.; Magnuson, A.; LeGourrierec, D.; Tamm, M.; Abrahamsson, M.; Huang Kenéz, P.; Mårtensson, J.; Stenhagen, G.; Hammarström, L.; Styring, S.; Åkermark, B. *J. Inorg. Biochem.* **2000**, *78*, 15-22.
- (4). (a) Burdinski, D.; Wieghardt, K.; Steenken, S. *J. Am. Chem. Soc.* **1999**, 10781-10787. (b) Burdinski, D.; Bothe, E.; Wieghardt, K. *Inorg. Chem.* **2000**, 105-116
- (5). Sullivan, D. J.; Meyer, T. J. *Inorg. Chem* **1978**, *17*, 3334.
- (6). (a) Diril, H.; Chang, H.-R.; Zhang, X.; Larsen, S. K.; Potenza, J. A.; Piepont, C. G.; Schugar, H. J.; Isied, S. S.; Hendrickson, D. N. *J. Am. Chem. Soc.* **1987**, *109*, 6207-6208. (b) Chang, H.-R.; Larsen, S. K.; Boyd, P. D. W.; Pierpont, C. G.; Hendrickson, D. N. *J. Am. Chem. Soc.* **1988**, *110*, 4565-4576.
- (7). Sun, L.; Burkitt, M.; Tamm, M.; Raymond, M. K.; Abrahamsson, M.; LeGourrierec, D.; Frapart, Y.; Magnuson, A.; Huang Kenéz, P.; Brandt, P.; Tran, A.; Hammarström, L.; Styring, S.; Åkermark, B. *J. Am. Chem. Soc.* **1999**, *121*, 6834-6842.
- (8). Khangulov, S. V.; Pessiki, P. J.; Barynin, V. V.; Ash, D. E.; Dismukes, G. C. *Biochemistry* **1995**, *34*, 2015-2025.
- (9). (a) Dismukes, G. C.; Siderer, Y. *Proc. Natl. Acad. Sci. USA* **1981**, *78*, 274-278. (b) Zheng, M.; Khangulov, S. V.; Dismukes, G. C.; Barynin, V. V. *Inorg. Chem.* **1994**, *33*, 382-387. (c) Schäfer, K.-O.; Bittl, R.; Zweggart, W.; Lenzian, F.; Haselhorst, G.; Weyhermüller, T.; Wieghardt, K.; Lubitz, W. *J. Am. Chem. Soc.* **1998**, *120*, 13104-13120.

SYNTHESIS OF DIMETHYL CARBONATE BY SUPERCRITICAL CO₂-FEEDING METHANOL AND DIMETHYL ETHER

Tian Yiling*, Qin Ying, Chen Li, Fang Jingang and Wang Li

Department of Chemistry, Tianjin University, Tianjin, 300072, China

Albert S.C. Chan

Department of applied Biology and Chemical Technology,

Polytechnic University, Hong Kong, China

1. Introduction

Dimethyl carbonate is an important methylating agent which replaces former toxic methylating agent (Me)₂SO₄ in the synthesis of medicines. It is also an intermediate of synthesis of higher carbonates and fuel oil additive. Many authors reported the synthetic methods of DMC⁽¹⁻⁵⁾, most of them used organometal compounds as catalysts. It would be difficult to separate product mixture, then it was spreaded difficultly in industry. Our technological process is a heterogeneous catalysis. This method has many obvious advantages. The product fractionation and purification are then easier and more economical.

There are many CO₂ resources in China, for example, Victory Oil Field has about ten billions m³ of CO₂ deposits, which is a nature carbon resource and is yet not exploited and used. The super-critical CO₂ (SC-CO₂) is non-toxic, nonflammable and cheap solvent. The high diffusivity, low viscosity and low surface tension of SC CO₂ is expected to speed up mass-transfer controlled reactions. In¹ this work, SC CO₂ is both reactant and solvent.

2. Experimental

2.1 Chemicals

CO₂, with a minimum purity 99.99%, was obtained from Tianjin Special Gas Limited Company, China.

Absolute alcohols was obtained from Tianjin Reagent company, China, with a stated purity of 99.8%. It was used as received without further purification.

The carbonylation catalyst of MeOH is a mechanical mixture of CuI, MgO and other addend powders, the purities of them are all C.P. Before use they were dried and activated.

The hydrolyst of DME, HZMS molecular sieve, was obtained from Nankai University, China. The specific surface of HZMS is 30 ± 2 m²/g. Before use it was activated for 4h at temperature of 280°C.

DME with purity of 99.9% was obtained from Shanxi Institute of Coal Chemistry, China. It was used without further purification.

2.2 Procedure

The experiments were carried out in a high-pressure autoclave of 0.5 dm³ equipped with stirring. The temperature of the autoclave was adjusted by a heating jacket and was measured directly by a shielded chromel-to-alumel thermocouple inside the autoclave. The chemical equilibrium, indicated by reaching a constant pressure (changed with

the added amounts of chemicals), was reached typically 4h after terminating stirring.

After feeding catalysts, MeOH was introduced into the evacuated autoclave from tared sample bottle and the mass determined by weighing. DME and CO₂ were pressured respectively into the autoclave from two little light-alloy flask, which were cooled before falling CO₂ and DME in the presence of ice and salt. The reactant mixture was stirred at established temperature for 4h. After that, the autoclave was cooled to room temperature and let the left gases out of the autoclave. The product mixture was analyzed by a gas chromatography equipped with integrator. All analysis were carried out under the same conditions: hydrogen (99.99%) as carrier gas, flowing rate 35 cm³ min⁻¹, FID detector, 2m column (i.d 3mm) packed with silicone elastomer. Column temperature 80°C, injection port temperature 220°C, n-butanol was used as internal standard. The bridge current was 100mA, The amount of injected sample was 2 μ dm³ for each.

3. Results and discussion

The total reaction can written as



Owing to the present of reaction (2), the water produced by reaction

$$y = \frac{n(\text{DMC}) \text{ in product mixture}}{n(\text{MeOH}) \text{ in reactant mixture}}$$

(1) was consumed and then equilibrium of (1) was removed to right hand. The yield of DMC was increased. In this paper the yield of DMC was defined as

3.1 The effect of temperature on the yield of DMC

The reaction(2) is an endothermic but reaction(1) is exothermic reaction. We selected temperature range was from 100°C to 150°C. Table 1 gives this effect. The reaction conditions were: MeOH, 160cm³(4mol); DME, 115g(2.5mol). CO₂, 44g(2.0mol), HZMS+CuI+MgO+other, 100g. Here the "other" is a kind of solid initiator.

Table 1 Effect of temperature on the yield of DMC

t/°C	yield of DMC /%	t/°C	yield of DMC /%
100	11.26	130	28.58
110	19.83	140	21.74
120	24.17	150	17.36

Table 1 shows that along with increasing temperature the yield of DMC was changed. Initially it was increased and then decreased. At temperature of 130°C shows a maximum of 28.58%. Two reasons account for the occurrence. Higher temperature is favorable to (2) and could increase reaction rate of (1). Since (1) is an endothermic reaction. The higher temperature is unfavorable to equilibrium of (1).

3.2 The effect of the ratio of reactants on the yield of DMC

Table 2 gives this effect. The reaction conditions were: 130°C, HZMS+CuI+MgO+other, 100g, reaction period 4h.

¹ To whom correspondence should be addressed. Email: tianyiling@eyou.com

Table 2 The effect of the ratio of reactants on the yield of DMC

<i>n</i> (of reactants)/mol yield of				<i>n</i> (of reactants)/mol yield of			
MeOH	DME		DMC/%	MeOH	DME	CO ₂	DMC/%
4	0	4	1.07	4	2	2	26.52
4	1	3	9.41	4	2.5	2	28.58
4	1.5	2.5	14.34	4	3	2	22.73

The main problem for the synthesis of DMC is the removal of product water. DME has proved to be aid to this synthesis. When the amount of DME was excess, then concentrations of CO₂ and MeOH would be diluted, so that reaction rate of (1) would be decreased. If the amount of DME was too few, the hydrolysis reaction (2) would not be successful. Therefore the decided optimal ratio is $n(\text{MeOH}):n(\text{DME}):n(\text{CO}_2)=4:2.5:2$

3.3 The effect of catalysts on the yield of DMC

Changing the amounts and ratios of catalysts would affect the yield of DMC. The results are gives in Table 3. The experimental conditions were:

the temperature 130 °C

$n(\text{MeOH}):n(\text{DME}):n(\text{CO}_2)=4:2.5:2$. The reaction period was 4h.

Table 3 The effect of catalysts on the yield of DMC

<i>m</i> (catalysts)/g Yield of			<i>m</i> (catalysts)/g Yield of		
CuI+MgO	HZMS	DMC/%	CuI+MgO	HZMS	DMC/%
+other			+other		
10	90	9.09	60	40	28.58
20	80	19.43	80	20	21.23
40	60	22.89	90	10	21.47
50	50	24.79	100	0	7.29

Table 3 shows that yield of DMC were initially increased with increasing amounts of (CuI+MgO+other) and then decreased. The optimum ratio is 60:40.

We have found during the analysis that besides DMC was formed, the by-products present in reaction mixture. They are methy carbamate and other unknown substances. Their total content was about 5%. The little amounts of solved DME and CO₂ in producted mixture were analyzed out.

References

- (1). Bolton [J]. Chem. Eng. **1992**,517,13
- (2). Yamazaki N, Nakahama S. , Ind. Chem. Prod. Res. Dev. **1979**,18,249
- (3). Kizlink J, Pastucha I, Collect. Czech. Chem. Commun. **1994**,59,2116
- (4). U.S.Patent 5902894
- (5). Kizlink J, and Pastucha I, Collect. Czech. Chem.Comun. **1995**,2,687

THEORETICAL STUDY OF THE CO-INTERACTION OF CO₂ AND H₂ WITH NICKEL

Changwei Hu*, Song Qin, Huaqing Yang,
Dongmei Tong, Anmin Tian
Faculty of Chemistry, Sichuan University,
Chengdu, 610064, China

Ning-Bew Wong
Department of Biology and Chemistry,
City University of Hong Kong,
Kowloon, HK

Introduction

The activation of carbon dioxide is a very active research area by experimental and theoretical approaches.¹⁻³ The reactions of nickel atom with carbon dioxide have been widely investigated.⁴⁻⁶ The hydrogenation of CO₂ is one of the most important ways for the effective use of CO₂. However, up to now, to our knowledge no studies of the co-interaction of carbon dioxide and H₂ with nickel have been performed theoretically. The ab initio calculation reported in this paper is intended to study the possible reaction path of carbon dioxide and hydrogen on nickel, including their reliable structures of the intermediates and transition states.

Computational Details

Full-parametric geometry optimizations and the final energy evaluation for all structures are performed at B3LYP level. The 6-311+G(2d,2p) basis set is employed for carbon, hydrogen and oxygen, and the SDD basis set and the corresponding ECP are used for nickel. The intrinsic reaction coordinate IRC method was used to track minimum energy paths from transition states to corresponding intermediates. All the ab initio calculations are performed using the Gaussian 98 programs.

Results and Discussion

The calculated energy profile is shown in **Figure 1**. The optimized geometry of various intermediates and transition states along the predicted pathway of this reaction and their corresponding ZPE corrected relative energies are shown in **Figure 2**.

As seen in **Figure 1** and **Figure 2**, when CO₂ molecule and H₂ molecule attaches to Ni atom, intermediate A of C₁ geometry forms, the calculated OCO angle is 178.1° and the distances between carbon atom and oxygen atoms are 1.171Å(C1-O3) and 1.152Å(C1-O4), respectively, which are similar to those of free CO₂ molecule(1.160 Å). In addition, the distance between Ni atom and O(3) of CO₂ molecule is 2.094Å which is close to the Ni-O distance(2.09Å) in NiO crystal,⁷ indicating the interaction of CO₂ molecule with Ni atom.

From the non-planer complex A, the reaction proceeds via transition state TS1 to form an intermediate B of C₁ geometry. The OCO angle in TS1 is slightly bend to 169.0° and the Ni-O(2) bond length is shortened to 2.022Å. Meanwhile C-O bonds in TS1 are larger than those in intermediate A, which indicates that the C-O bonds are weakened. However, there is little difference in structure between intermediate A and TS1. The calculated activation energy is 0.28 kJ mol⁻¹. IRC confirmed that TS1 connects intermediate A and intermediate B.

Compared with intermediate A, the structure of intermediate B is much different. The O(3)-Ni distance is 1.853Å which is obviously

shorter than that of intermediate A. Furthermore, the C-Ni bond forms (1.903Å). The calculated its relative energy is -49.1 kJ mol⁻¹. From those data, we may say the reaction proceeds via a formation of co-adsorption of CO₂ and H₂ on nickel atom. Since the activation energy of this step is so small, it may occur easily.

From intermediate B, the reaction proceeds via the transition state TS2 to form another intermediate C of C_s geometry. Compared with intermediate B, the central Ni-C and C-O(4) bonds (1.827Å and 1.266Å) in TS2 are slightly larger and the distance between Ni atom and H(6)(1.567Å) becomes larger, meanwhile O(4)-H(5) bond (1.351Å) becomes shorter, indicating the H(6)H(5)NiCO(4) five-members ring structure is formed. The calculated energy places the transition state TS2 156.1 kJ mol⁻¹ higher than intermediate B, it may stem from the congested structure of TS2. IRC calculation confirmed that TS2 does connect the intermediate B and intermediate C.

The differences in structure between TS2 and intermediate C are also obvious. The most distinct change is H(5) has transferred from Ni to O(5). The distance between Ni-H(5) is 2.924Å and the distance between O(4) and H(5) is 0.966 Å in intermediate C, revealing the Ni-H(5) bond is broken and the O(4)-H(5) bond is formed.

The overall endothermic of this reaction is calculated to be about 6.42 kJ mol⁻¹. Because the calculated energy between intermediate B and TS2 is much larger than that between intermediate A and TS1, we can consider the step from intermediate B to TS2 as the rate-determining-step (RDS) of the reaction.

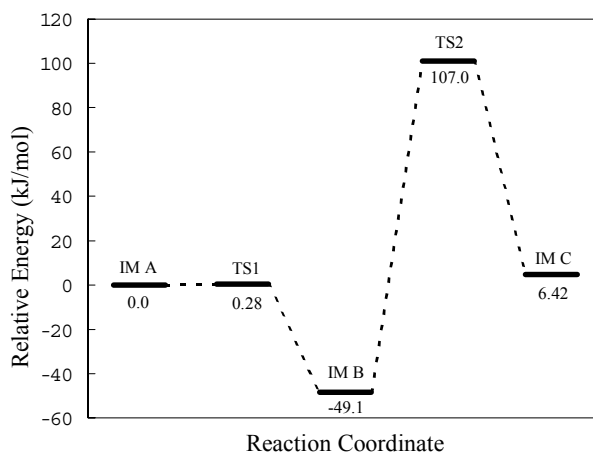


Figure 1. Potential energy diagram for the reaction calculated at the B3LYP level. All energies are given in kJ mol⁻¹ with respect to intermediate A.

Conclusion

The co-interaction of CO₂ and H₂ on Ni atom and then the reaction H₂NiOCO→HNiCOOH are studied by DFT method. The reaction of Ni with CO₂ and H₂ proceeds by forming co-adsorption complex of CO₂ and H₂ on Ni at the first stage. Reaction continues by forming the H(6)H(5)NiCO(4) five-members ring in TS2. Ab initio B3LYP method calculation reveals that overall endothermic of this reaction is calculated to be about 6.42 kJ mol⁻¹ and the activation of intermediate B is RDS of it.

Acknowledgments

This work has been financially supported by the Key Project of National Fundamental Research and Development of China (973) (No. G1999022407), NNSF (No. 29873028), the Special Research Foundation of Doctoral Education of China (No. 2000061028) and

* Corresponding author. E-mail:chewhu@mail.sc.cninfo.net

the Foundation of Science and Technology of Sichuan Province (No. 200018-16).

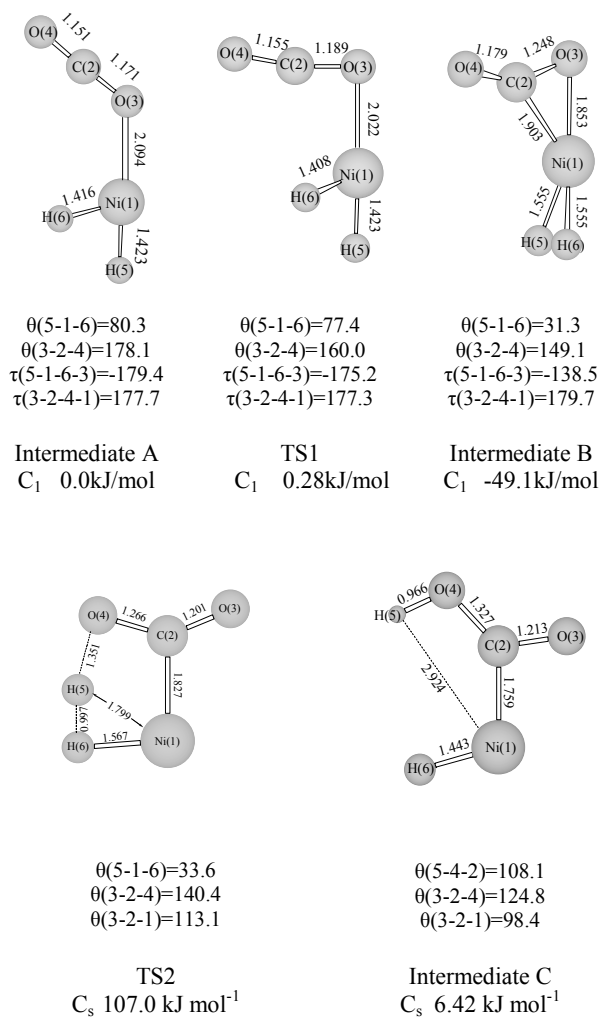


Figure 2. Geometries of intermediates and transition states in the reaction. Bond lengths are in Å and angles are in degrees.

Reference

1. F.Galan, M.Fourssier, M.Tranquille, and J.Mascetti., *J. Phys. Chem. A.* **1997**, 101, 2626
2. Gorge C.Schatz.,*J.Chem.Phys.***1980**, 72(2), 3929
3. Luis Rodriguez-Sanatiago, Mariona Sodupe, and Vicenc Branchadell.,*J.Chem.Phys.* **1996**, 105(22), 9966
4. Alexander M. Mebel and Der-Yan Hwang., *J. Phys. Chem. A.* **2000**, 101, 11622
5. Der-Yan Hwang, Alexander M. Medel., *Chemical Physics Letter.* **2000**, 325, 639
6. D.E.Peebles,D.W.Goodman., *J. Phys. Chem.* **1983**, 87, 4378
7. Hu Changwei, Chen Yu, Wang Wenzuo, Lu Guang, Ma Lidun, Shen Xiaoling., *J. Mol. Catal (China)* **1992**, 6(4),263

TOWARDS AN UNDERSTANDING OF CATALYSIS FOR THE SIMULTANEOUS CONVERSION OF GREENHOUSE GASES

Yuan Kou

College of Chemistry and Molecular Engineering, Peking
University, Beijing 100871, China

1. NO_x-catalyzed homogeneous partial oxidation of CH₄ to syngas

Our recent studies show that under both weak and strong oxidizing conditions (O₂/CH₄ = 1.5-5.0), NO_x can act as a good catalyst for the partial oxidation of methane to CO without the use of any solid catalyst. Under weak oxidizing conditions (O₂/CH₄ = 1.5) in the absence of NO_x, the oxidation of CH₄ requires temperatures higher than 850 °C. Addition of NO initiates the reaction at a much lower temperature around 550 °C, and the selectivity to CO is about 40% at a temperature of 650 °C.

Table 1 CH₄ conversion and CO selectivity in the partial oxidation of methane^a

NO /ppm	Flow rate /ml min ⁻¹	Temperature range of CO formation /°C	CO selectivity (maximum) ^b (%)	CH ₄ conversion at CO maximum (%)	Temperature of CO maximum /°C	T _{50%} /°C	TOF ^d /s ⁻¹
/	20	800-880	16	79	868	866	/
/	40	840-920	25	42	910	911	/
/	80	875-	30 ^c	54 ^c	>950	950	/
200	40	540-760	66	88	630	595	5
600	20	520-760	68	83	610	590	9
600	40	560-780	69	90	645	612	9
600	80	570-840	67	94	680	635	13

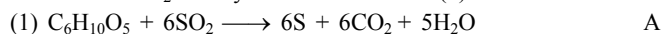
^a Reaction conditions: CH₄ : 0.4 mol%; O₂ : 2 mol%; temperatures: 200-950 °C. ^b CO selectivity: mol CO · (mol CO + mol CO₂ + mol CH₄)⁻¹ ^c Values measured at 950 °C ^d Values measured at 650 °C

Under strong oxidizing conditions (O₂/CH₄ = 5.0), NO_x also exhibits considerable catalytic activities and selectivities for the conversion of methane to CO. The results are summarized in Table 1. It can be seen that, in the absence of NO, the initial temperatures required for the activation of CH₄ are higher than 800 °C. In the presence of NO, however, the temperatures required are reduced to below 570 °C. The lowest temperature for the activation of CH₄ is only 520 °C. In all the experiments shown in Table 1, no decrease in NO/NO₂ concentration (based on the area of infrared absorption peak) is observed up to 950 °C, indicating that NO₂ and other possible nitrogen oxides cannot be reduced by CH₄ without a solid catalyst. NO-catalyzed partial oxidation of methane is a highly selective reaction for production of CO (68%). The highest TOF value (40 methane molecules converted per second per NO) is obtained at an NO concentration of 100 ppm, suggesting that the reactions described here are a gas-phase homogeneous catalytic reaction.

2. Biomass-based partial reduction of SO₂

Na₂CO₃/γ-Al₂O₃ has been employed as a regeneratable sorbent for SO₂ removal. Utilization of biomaterials or abandoned biomaterials (BIOM), treatments of which usually produces a great amount of CO₂, to take the place of alumina is a creative new approach to this problem. The BIOM includes farmland straw, rice husks and stalks, dried branches and leaves, waste paper and

similar materials. The breakthrough and stoichiometric SO₂ adsorption efficiencies of a biomass supported Na₂CO₃ system (80wt%Na₂CO₃/straw) reached 48.9% and 80.6% respectively at a desulfurization temperature of 80 °C. It should be noted that the reduction properties of cellulose-based materials like BIOM have been reported previously. Based on previous work and this study, a more efficient and complete flue gas desulfurization (FGD) process can be proposed. The key steps in the proposed process are the enrichment of SO₂ by Na₂CO₃/BIOM, and the subsequent reduction of SO₂ to S by BIOM via reaction (1):



A suitable catalyst will be needed for this reaction, and further studies are being carried out in this laboratory.

3. CO₂-related aromatization of lower alkanes including methane

Conversion of C₁-C₃ alkanes in the presence of CO₂ has been investigated for years. What role the CO₂ plays under the reaction conditions and what products may be obtained from the reaction is still unclear however. Thermodynamic analyses as well as reaction studies have shown that both SAMCA (simultaneous activation of methane and carbon dioxide to aromatics) and

SCACA (simultaneous conversion of alkanes and carbon dioxide to aromatics) are more thermodynamically favorable than other reactions reported to occur in the CH₄ (C₂H₆/C₃H₈)-CO₂ co-feed. For example, in comparison with aromatization of CH₄ without free-oxygen or oxidation of CH₄ by CO₂ to produce C₂H₄, reactions (2) and (3) are more thermodynamically feasible, suggesting that all studies of the conversion of lower alkanes in the presence of CO₂ as either an additive or a by-product should carefully check whether some aromatics are formed in the product mixture.

